An investigation of the magnetic properties of high tensile steels

Simon Nicolas Murray Willcock

AN INVESTIGATION OF THE MAGNETIC PROPERTIES OF HIGH TENSILE STEELS

SIMON NICOLAS MURRAY WILLCOCK,

B.Sc., A.R.C.S., C. Phys., M.Inst.P.

Thesis submitted to the University of Durham in Candidature for the Degree of Doctor of Philosophy, September, 1985.

To my Family

ABSTRACT

This thesis describes an investigation of the magnetic properties of high tensile steels typical of those produced for the high pressure gas pipe-line industry. Results are presented for both bulk and small section samples, and the observed variations in magnetic behaviour as a function of orientation and position within the steel are described qualitatively by changes in steel metallography. The development of an automated double-crank Vibrating Sample Magnetometer, required for determining the magnetic characteristics of small samples, is also described which, without signal amplification, has a moment detectability limit of 10^{-4} e.m.u.

The representation of the full magnetization loop by a Fourier series is investigated and the variations in harmonic amplitudes found for the range of steels considered here are compared to those predicted by theoretical models. The successful parameterization of the initial magnetization curve is also reported using a two parameter model ($LnB = (k - H^{-1})LnA$)), and linear relationships between the coercive field (H_c) and these parameters (k,LnA) are presented which permit the prediction of the initial magnetization curve of any similar steel from a knowledge of H_c. Although the latter may be determined accurately by direct measurements of small samples, further linear relationships are indicated which allow the determination of the coercive field from a knowledge of either the steel chemistry or metallography.

The compatibility of the observed ferrite grain size dependent contribution to the coercive field with grain boundary domain wall pinning models is also investigated.

ACKNOWLEDGEMENTS

Acknowledgement is made to the Science and Engineering Research Council and the British Gas Corporation whose financial support made this research possible.

It is my pleasure also to acknowledge the help and assistance given to me by the following people during the course of this work.

Firstly, I would like to thank Professor A.W. Wolfendale, F.R.S., for making available to me the facilities of the Department of Physics at the University of Durham.

Thanks are due also to Dr. B.K. Tanner for his excellent supervision, continuous enthusiasm and help over the three years, to Dr. W.D. Corner for many useful discussions and to Dr. S.R. Hoon for his willingness to share his expertise when dealing with problems of an experimental nature and for the many invaluable hours of discussion and help throughout the development of the Vibrating Sample Magnetometer.

I would also like to thank all the members of the Physics group of the British Gas On-Line Inspection Centre, Cramlington, Northumberland, and Dr. L.L. Morgan, Dr. J. Burd, Dr. P.A. Mundell and Mr. W. Warnes, in particular, for their collaboration throughout the research.

Finally, I wish to express my sincere thanks to Mr. D. Jobling, Mr. P. Armstrong and Mr. G. Teasdale for expert technical help, advice and the meticulous care with which they constructed apparatus and prepared samples, to Mr. T. Jackson and his staff of the Electronics Workshop for help and advice, to Mr. T.W. Hogg and his

staff of the main departmental workshop for the preparation of samples, to Mr. P. Foley for his invaluable assistance, to Mr. M. Lee for the preparation of photographs contained in this thesis, to Miss K.L. Gittins for the excellent diagrams and to Ms. M.A. Chipchase for the care with which she typed this manuscript.

LIST OF PUBLICATIONS

WILLCOCK, S.N.M., and TANNER, B.K., "Harmonic Analysis of B-H loops", IEEE Trans. Magn. MAG-19, 2265, (1983).

WILLCOCK, S.N.M., and TANNER, B.K., "Harmonic Analysis of B-H loops of Constructional Steel", IEEE Trans. Magn. MAG-19, 2145, (1983).

CONTENTS

CHAPTER 4 : THE DURHAM VIBRATING SAMPLE MAGNETOMETER

CHAPTER 5 : AUTOMATION OF THE VSM

CHAPTER 1

INTRODUCTIONS TO MAGNETISM AND THE METALLURGY, MANUFACTURE AND NON-DESTRUCTIVE INSPECTION OF HIGH PRESSURE GAS PIPE-LINE STEEL SYSTEMS

1.1 OVERVIEW

Brief introductions to magnetism, the metallurgy and manufacture of steels used in high pressure gas pipe-lines, and the magnetic non-destructive on-line inspection of such pipe-lines are given here. It is intended to familiarize the reader, not cognisant in these fields, with most of the concepts and terms which will be used throughout this thesis. A rigorous treatment of these subjects will not, therefore, be presented and, where relevant, the interested reader will be directed to sources which provide a much greater body of information than that summarized below.

1.2 MAGNETISM

1.2(i) Introduction

The magnetic force of attraction between lodestone (magnetite, $FeO.Fe_2O_3$) and iron was observed in ancient Greek times, but it was not until the advent of quantum theory earlier this century that it could be explained at an atomic level. Classical physics does not predict the existence of magnetic order.

The existence of a magnetic field which surrounds magnetized materials was postulated to explain such forces

and discoveries made in the eighteenth century showed that similar fields were generated by the passage of circulating electric currents. The magnetic field can be quantified, therefore, by considering the field inside a long solenoid. Here we have:

$$\underline{H} = NI\underline{n} \qquad (1.1)$$

where $\underline{n}$ is the axial unit vector, N is number of turns per unit length, and I is the coil current. In S.I units, therefore, the field strength $\underline{H}$ is measured in ampère per metre (Am^{-1}). It is impossible to determine directly the value of $\underline{H}$ using an experimental measuring device (e.g. search coil or Hall effect probe) because all such devices measure the induction ($\underline{B}$) in a medium arising from the field. The induction is measured in tesla (T) and is often represented by flux lines whose density is indicative of the magnitude of $\underline{B}$. The quantity of flux is measured in weber (Wb) and consequently 1 Wbm^{-2} is equivalent to 1T.

Magnetized materials possess a magnetic moment, $\underline{\mu}$, which can be quantified by comparison with a current loop. The moment of a circulating current, I, which encloses an area a is given by:

$$\underline{\mu} = Ia\underline{n} \qquad (1.2)$$

where $\underline{n}$ is the unit vector perpendicular to the area. Magnetic moment is measured, therefore, in ampère $metre^2$ (Am^2). The magnetic moment per unit volume of material is defined as the magnetization, $\underline{M}$, and has units of

ampère per metre in the S.I system. Thus we have the following expression for the induction in a magnetized material:

$$\underline{B} = \mu_o \underline{H} + \mu_o \underline{M} \qquad (1.3(a))$$

$$= \underline{B}_o + \mu_o \underline{M} \qquad (1.3(b))$$

$$= \mu_o \mu_r \underline{H} \qquad (1.3(c))$$

where $\mu_r = (1 + \frac{M}{H})$. μ_o is a constant called the permeability of free space ($4\pi x\ 10^{-7}$ henry metre^{-1} (Hm^{-1})) and μ_r is a dimensionless quantity referred to as the relative permeability of the material.

The relation between the magnetization of a material and the field strength to which it is subjected is normally represented by the volume susceptibility K.

$$K = \frac{M}{H} = \mu_r - 1. \qquad (1.4)$$

Hence K is also dimensionless. The susceptibility can, however, be defined in other ways (see, for example, Bozorth (1951) and Hawkins (1982)).

The occurrence of magnetization in a material can only be explained by quantum mechanical theory in which the magnetic moment of an individual atom is considered to originate from three potential sources; the quantized electron spin, the quantized orbital angular momentum of the electron, and the change in the orbital moment induced by a magnetic field. Paramagnetism is the result of the first two sources where finite atomic moments

orientate independently in an applied field to create a positive susceptibility. In certain materials (ferromagnets, anti-ferromagnets and ferrimagnets) a spontaneous ordering of the finite atomic moments occurs and a non-zero magnetization may then result in zero field. The last source produces a negative susceptibility referred to as diamagnetism and, although it is always present, the effect of a simultaneous occurrence of paramagnetism or ferromagnetism is so large as to render the diamagnetic contribution negligible. Excellent basic treatments of all three types of magnetism are given in the texts by Chikazumi (1964), Morrish (1965) and Kittel (1976).

1.2(ii) Ferromagnetism

The term ferromagnetism is given to the type of spontaneous magnetic ordering observed most commonly in the element iron. All internal moments in ferromagnetic materials are aligned in exactly the same direction at zero Kelvin. An increase in temperature results in a distribution of the moments about the magnetization direction until thermal agitation overcomes the ordering mechanism at a critical temperature known as the Curie temperature (T_c). The material then becomes paramagnetic and its behaviour is governed by the Curie-Weiss law:

$$K = \frac{C}{T - T_c} \qquad (1.5)$$

C is the Curie constant.

The other types of spontaneous order (antiferromagnetism and ferrimagnetism) show alignment of adjacent moments in opposite directions, but the moments at adjacent sites are unequal for the ferrimagnetic case. Zero nett magnetization is observed for antiferromagnetic materials, therefore, while ferrimagnetic materials still show a bulk magnetization although it is usually small compared to the ferromagnetic case.

The best known examples of ferromagnets are the transition metals iron, cobalt and nickel which are all ferromagnetic at room temperature. Other elements and alloys involving transition or rare-earth elements (e.g. gadolinium and dysprosium) also show ferromagnetism and these, together with many other materials, are discussed in the excellent text on ferromagnetism by Bozorth (1951). The relevance of ferromagnetism to steel, therefore, justifies a more detailed description of the origin of this phenomenon.

1.2(iii) Microscopic origins of ferromagnetism in the transition metals

Just as the paramagnetic alignment of independent atomic moments occurs in an external magnetic field, Weiss (1907) postulated the existence of an intrinsic internal field to explain the alignment of the moments in ferromagnetic materials and developed a fine theory of the temperature dependence of the saturation magnetization (see Figure 1.1). This field was assumed to originate from interactions between the molecules and was labelled

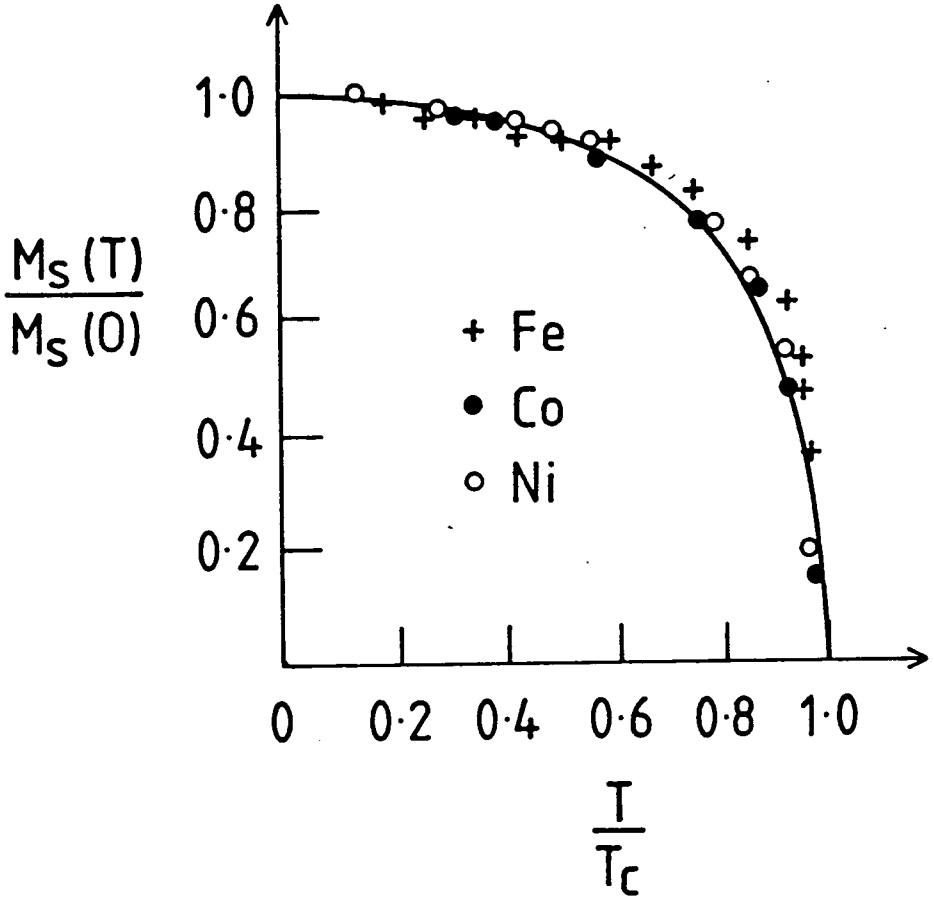

Figure 1.1

Ratio of saturation magnetization at temperature T to that at $0^{o}K$ for iron, cobalt and nickel. Solid curve is obtained from Weiss theory (after Omar (1975)).

the Weiss molecular or mean field but, in order to explain the degree of alignment observed in ferromagnets, the magnitude of the Weiss field would have to be of the order of 10^3 tesla. This field is much greater than that of the combined aligned moments and the origin of the Weiss molecular field remained obscure until the advent of quantum mechanics. Heisenberg (1928) then showed that this field is the result of the quantum mechanical 'exchange interaction' or "exchange force" which has no classical analogue.

Although it is impossible to understand the nature of the exchange force classically, a glimpse of it can be obtained in the following way: The electrons in the atomic structure, being fermions, are governed by Pauli's exclusion principle and must be described, therefore, by antisymmetric wave functions (i.e. functions which change sign when the coordinates, including spin coordinates, of any identical pair are interchanged). Thus for two electrons having the same spin state the spin part of the wave function will be symmetric and the exclusion principle dictates that, for overall antisymmetry, the spatial part will have to be antisymmetric. The only possible combination of spatial wave functions is;

$$\Psi_A = \psi_a(1)\psi_b(2) - \psi_a(2)\psi_b(1) \qquad (1.6)$$

where $\psi_a(1)$ is the single spatial wave function for an electron labelled "a" at coordinate (1) and Ψ_A is the combined antisymmetric function. It can be seen that,

as the electrons approach each other (i.e. coordinate (1) approaches (2)) the combined wave function tends to zero and the probability of finding the electrons in this state is, therefore, small. There is thus an apparent force of repulsion between two electrons of similar spin and, by the same argument, it can be shown that there is a force of attraction between two electrons of opposite spin. Thus the fermion exclusion principle is seen to be the origin of the exchange force and, although it is different from the Coulomb electrostatic interaction, its strength is of the same order as the Coulomb force.

A Hamiltonian, $\mathcal{H}$, may be written for the electron-electron interaction for two electrons experiencing a potential due to an atomic nucleus (or several nuclei) and an exchange integral defined,

$$J = \tfrac{1}{2}\iint \psi_a(1)^* \psi_b(2)^* \mathcal{H} \psi_b(1)\psi_a(2) d\tau_1 \, d\tau_2 \qquad (1.7)$$

The potential energy or exchange energy between two atoms (i,j) with unpaired spins is then given by:

$$V_{ex} = -2J_{ij} \, \underline{S}_i \cdot \underline{S}_j \qquad (1.8)$$

where $\underline{S}_i$ is the total spin quantum number of ith atom.

If the exchange integral, J, is positive it is energetically favourable for the spins to align and ferromagnetism can occur. This condition is best met if the interatomic spacing (r) is large compared to the radii of the orbitals (r_a) and J is most likely to be positive for d and f wave functions for the atoms of some transition

and rare earth metals (Slater (1937), Morrish (1965)). Figure 1.2 shows, for example, the variation in exchange integral with interatomic spacing for the transition elements. It can be seen that, although manganese and chromium are not ferromagnetic, a small increase in interatomic spacing would induce ferromagnetism. This does, in fact, occur with some compounds/alloys of manganese (MnSb, for example, is ferromagnetic, with a lattice spacing of 2.89Å compared to 2.58Å for pure Mn).

Quite apart from positive values for the exchange integral, the occurrence of ferromagnetism also requires the existence of unfilled electron shells. It is fortuitous, therefore, that the 3d shell is unfilled for the transition metals. The itinerant or collective electron model for ferromagnetism, first proposed and calculated by Stoner (Stoner (1933), (1938a,b), (1939) and (1947)) and Slater (Slater (1936a,b), (1937)), is invoked here because the non-localized nature of the 3d electrons result in the failure of the localized model to account for the observed magnetic moments per atom in these metals. This band model theory of ferromagnetism divides the 3d band (shown schematically in Figure 1.3(a) and (b)) into two sub-bands, representing the two possible orientations, up and down. In the absence of the exchange interaction the sub-bands are equally populated, resulting in zero magnetization. The presence of the exchange force and exchange energy, however, lowers the energy of the up sub-band and raises that of the down sub-band (Figure 1.3(b)) with the result that electrons transfer from

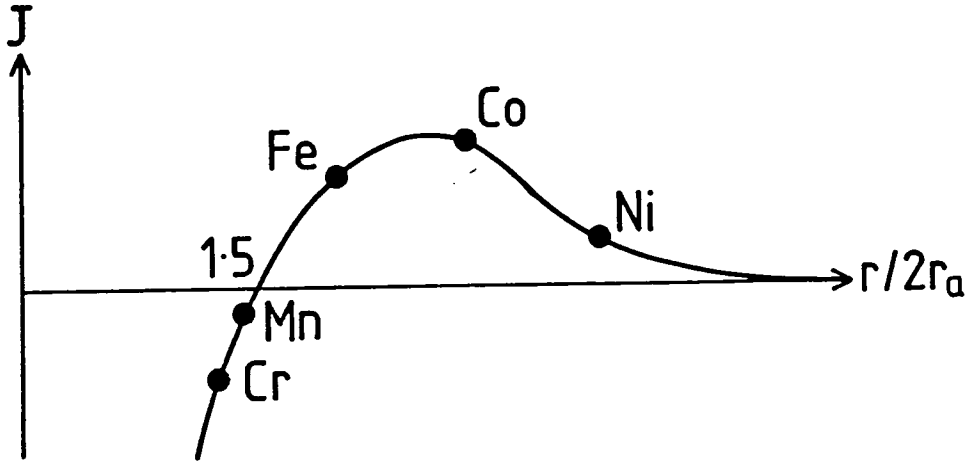

Figure 1.2

Exchange integral J versus interatomic distance for transition elements (after Omar (1975)).

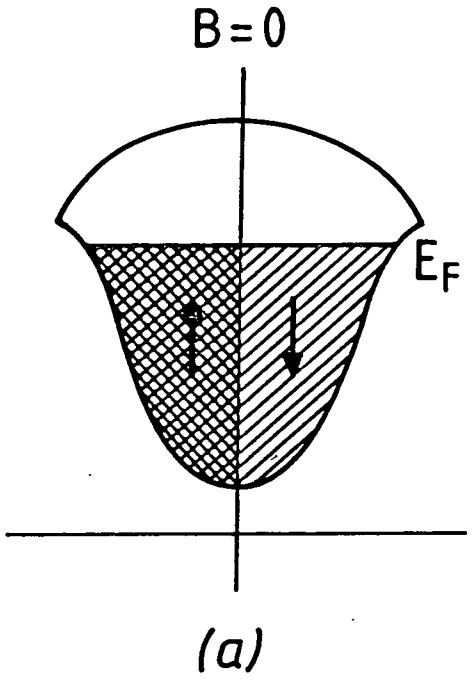

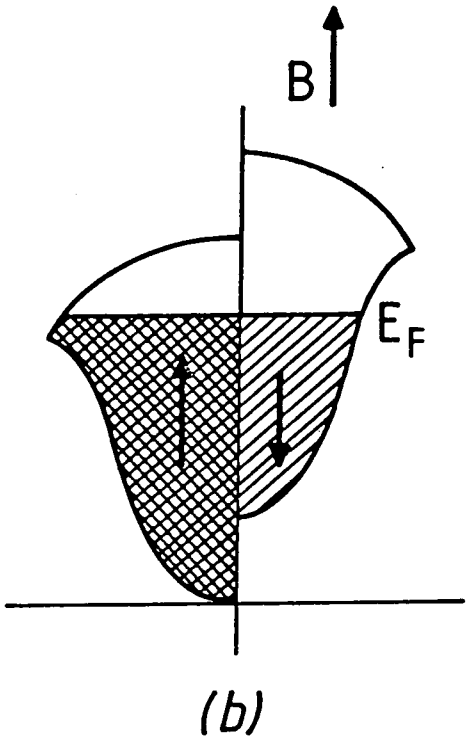

Figure 1.3

Magnetization process in the itinerant model (after Omar (1975)).

the down to up direction. A net magnetization, equal to the saturation magnetization (M_s), is then observed. The value of M_s is, therefore, determined by the strength of the exchange interaction and the shape of the band. Indeed, the density of states at the Fermi level must be large for ferromagnetism to occur otherwise the gain in kinetic energy occasioned by the electron flipping its moment may be greater than the reduction in exchange energy achieved in doing so. Figure 1.4(a) shows, by way of example, the density of states as a function of energy for the 4s and 3d bands of iron, nickel and copper. Figure 1.4(b) shows the same information for copper more accurately. It can be seen that the density of states for the 3d band is much greater than that of the 4s band which is essentially flat. The exchange integral for such a band would, therefore, have to be very large indeed for ferromagnetism to occur.

1.2(iv) Macroscopic ferromagnetism

It is well known that in spite of the spontaneous magnetization property a ferromagnetic specimen may exhibit no magnetic moment when the applied field is zero. The application of even a small field, however, usually produces a magnetic moment which is many orders of magnitude larger than that produced in a paramagnetic substance. In order to explain these results and the form of the observed hysteresis curve for such materials, Weiss (1907) postulated the existence of small regions, called domains, each spontaneously magnetized. In the bulk demagnetized state

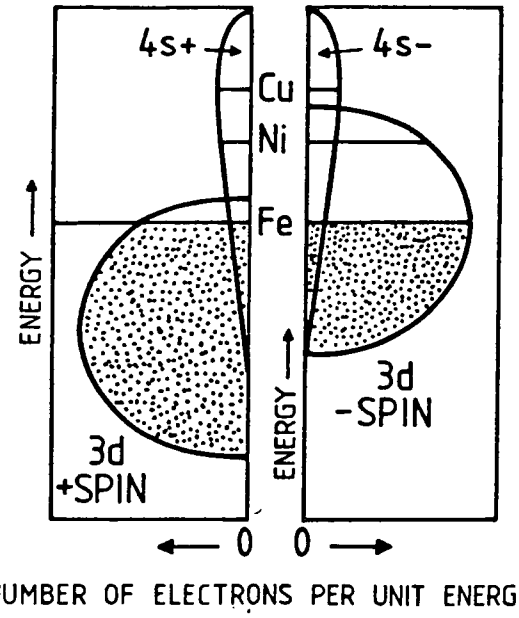

(a) Distribution of electrons in the 3d and 4s shells in iron, nickel and copper (after Bozorth (1951)).

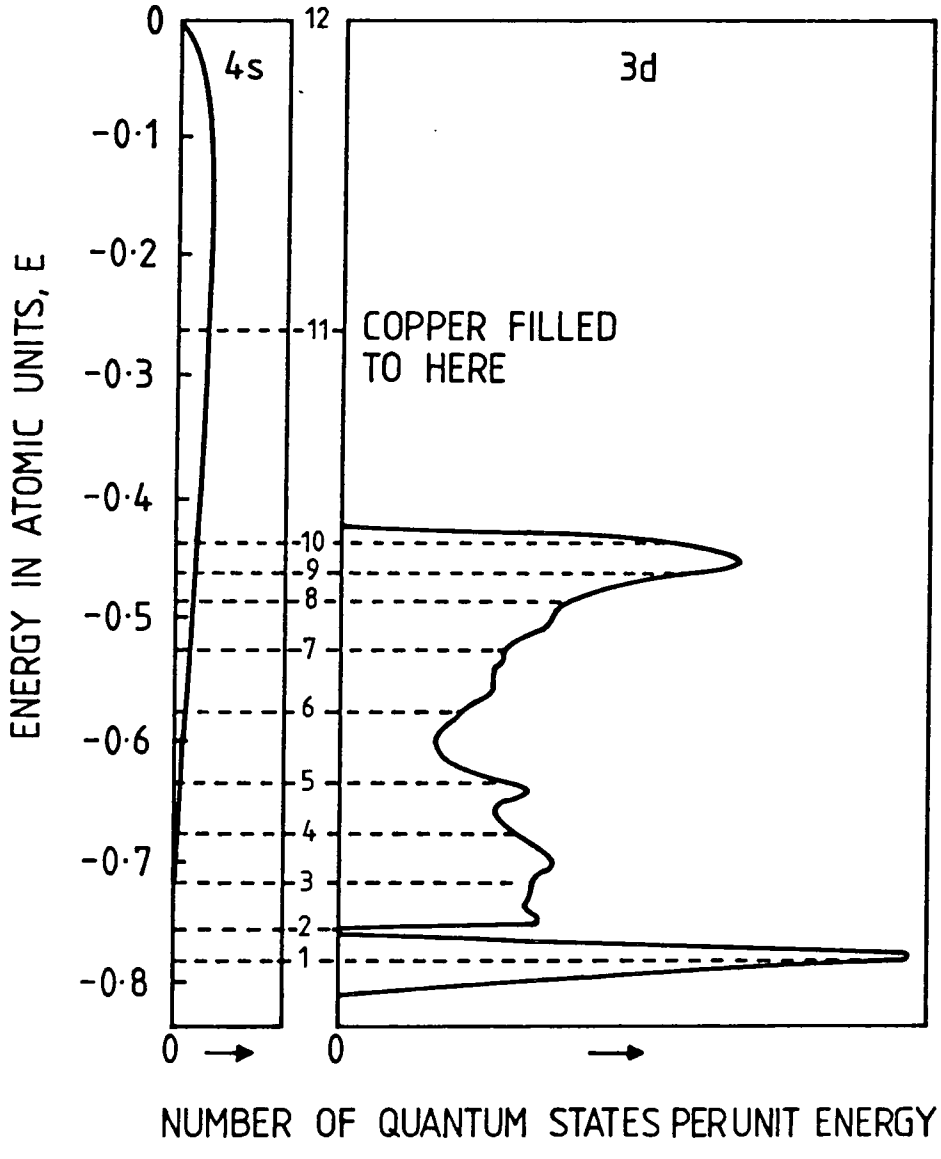

(b) Energy levels in the 3d and 4s bands of copper (after Bozorth (1951)).

Figure 1.4

these domains are randomly orientated (in a purely isotropic system), and the application of a magnetic field causes movement of the domain boundaries/walls, often called Bloch walls (Bloch (1932)), such that domains orientated in the field direction increase in volume at the expense of the other domains.

A theoretical treatment of ferromagnetic domain structure was first tried by Landau and Lifshitz (1935) and a good theory for a perfect single crystal should minimize the energy terms from magnetostatic, magneto-crystalline and magnetostrictive energy sources in order to calculate the size and orientation of the domains. The domain structures are usually complex, as they are modified by defects and impurities in the material, but they have been observed directly, for example Williams et al. (1949), using various imaging techniques, such as the Bitter method (Bitter (1931)), to show good agreement with the predictions of the theoretical models.

The macroscopic magnetization of a ferromagnetic material occurs, as stated above, through the growth in number and size of these domains which are favoured by the applied field. Starting with a demagnetized specimen, the application of a field causes initial reversible domain wall movement (see Figure 1.5) which, at higher fields, is followed by irreversible and reversible domain rotation processes, until eventually a single domain exists whose magnetization direction is coincident with the field direction. The presence of defects and impurities in the material causes secondary minima to appear in

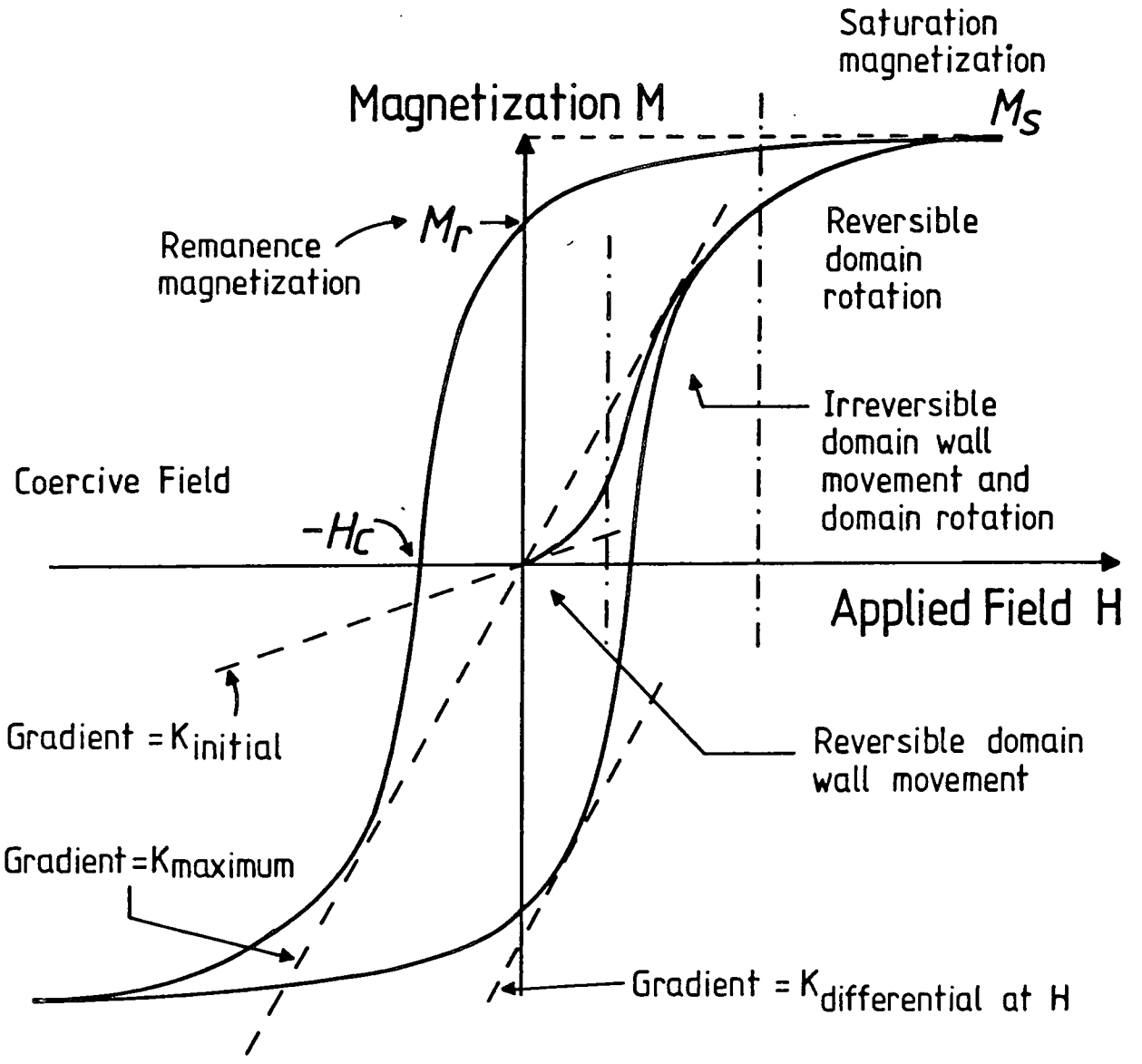

Figure 1.5

Initial magnetization curve and hysteresis loop of a typical ferromagnetic material.

the total wall energy as a function of displacement (Figure 1.6) which present extra energy barriers to the motion of the Bloch walls. The result is an increased coercive field and a reduced value for the initial permeability of the material.

The magnitude, large or small, of the energy lost during field-cycling associated with the above processes determines whether a material is magnetically "hard" or "soft". In this context, pipe-line steel can be regarded as a reasonably soft magnetic material. A knowledge of the hysteresis loss, together with the parameters obtained from the hysteresis curve, is essential, therefore, before defining the engineering applications of a material.

1.3 THE MANUFACTURE AND METALLURGY OF STEEL FOR HIGH PRESSURE GAS PIPE-LINES

1.3(i) Pig Iron

The material of greatest importance in many steel-making processes is pig-iron. The raw material used in its manufacture in the conventional blast furnace are:

(a) Ore - either magnetite ($FeO.Fe_2O_3$), hematite (Fe_2O_3), limonite and other hydroxides ($2Fe_2O_3\ H_2O$ to $Fe_2O_3\ 3H_2O$) or siderite ($FeCO_3$) and other types of carbonate ore.

(b) Limestone - a flux to combine with the non-metallic portion of the ore to form a fluid slag, mainly calcium silicate.

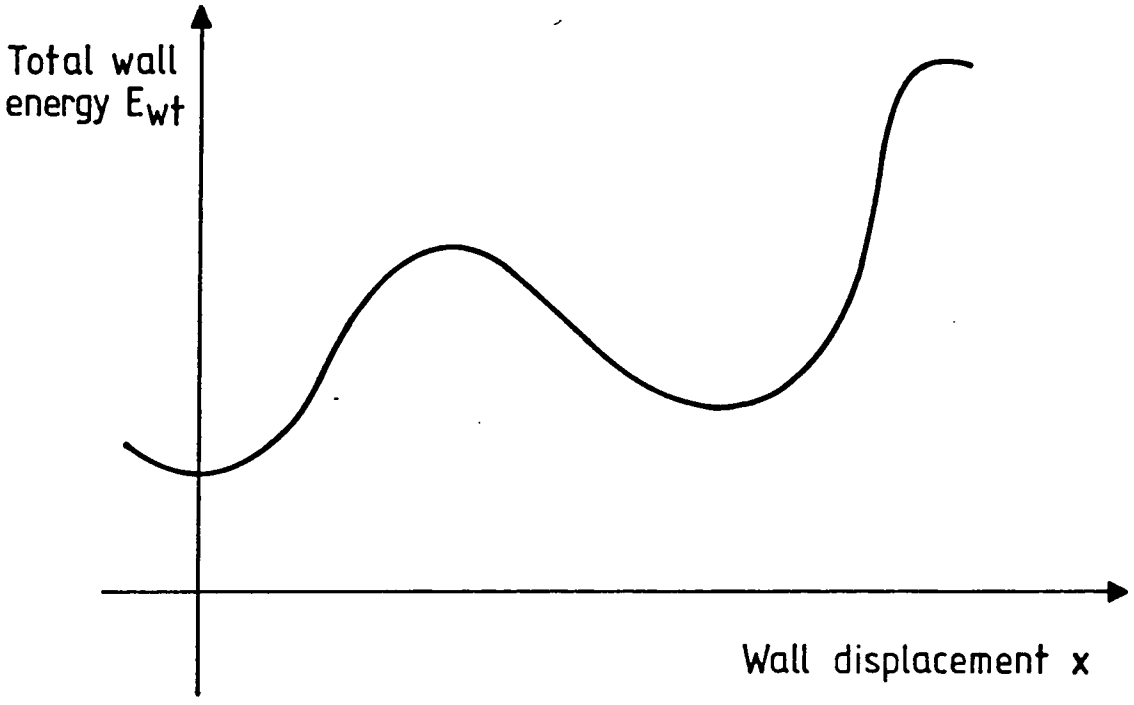

Figure 1.6

Plot of wall energy as a function of displacement (after Morrish (1965)).

(c) Coke - to reduce the iron oxides and provide heat for melting both metal and slag.

Throughout the operation of the blast furnace the molten iron accumulates at the bottom of the furnace from where it is tapped and transferred to the various steel furnaces or cast into sand or chill moulds to give "pigs".

While in the blast furnace the iron absorbs carbon, silicon, manganese, sulphur and the whole of the phosphorus in the charge. The iron thus produced is classed according to its phosphorus content and each class is graded according to its silicon content. A typical composition of pig iron is 3.5% carbon, 1.9% silicon, 0.06% sulphur, 1.0% phosphorus and 0.7% manganese.

The process required for steel production needs to remove most, if not all, of these impurities and to reduce the carbon content in order to produce steel with the required mechanical properties (see Figure 1.7). Excellent treatments of the production of pig iron (and all aspects of steel manufacture and structure) are given in the texts by Rollason (1964), Kirkaldy and Ward (1964), Johnson and Weeks (1964), Higgins (1965), Hume-Rothery (1966), Bailey (1973), and Kempster (1976).

The affect of these impurities on the mechanical properties of steel may be summarized as follows:

(a) Sulphur - this is the most deleterious impurity present in steel. It forms a brittle sulphide (FeS) which precipitates at grain boundaries and forms thin film coatings around the grains. It renders the steel

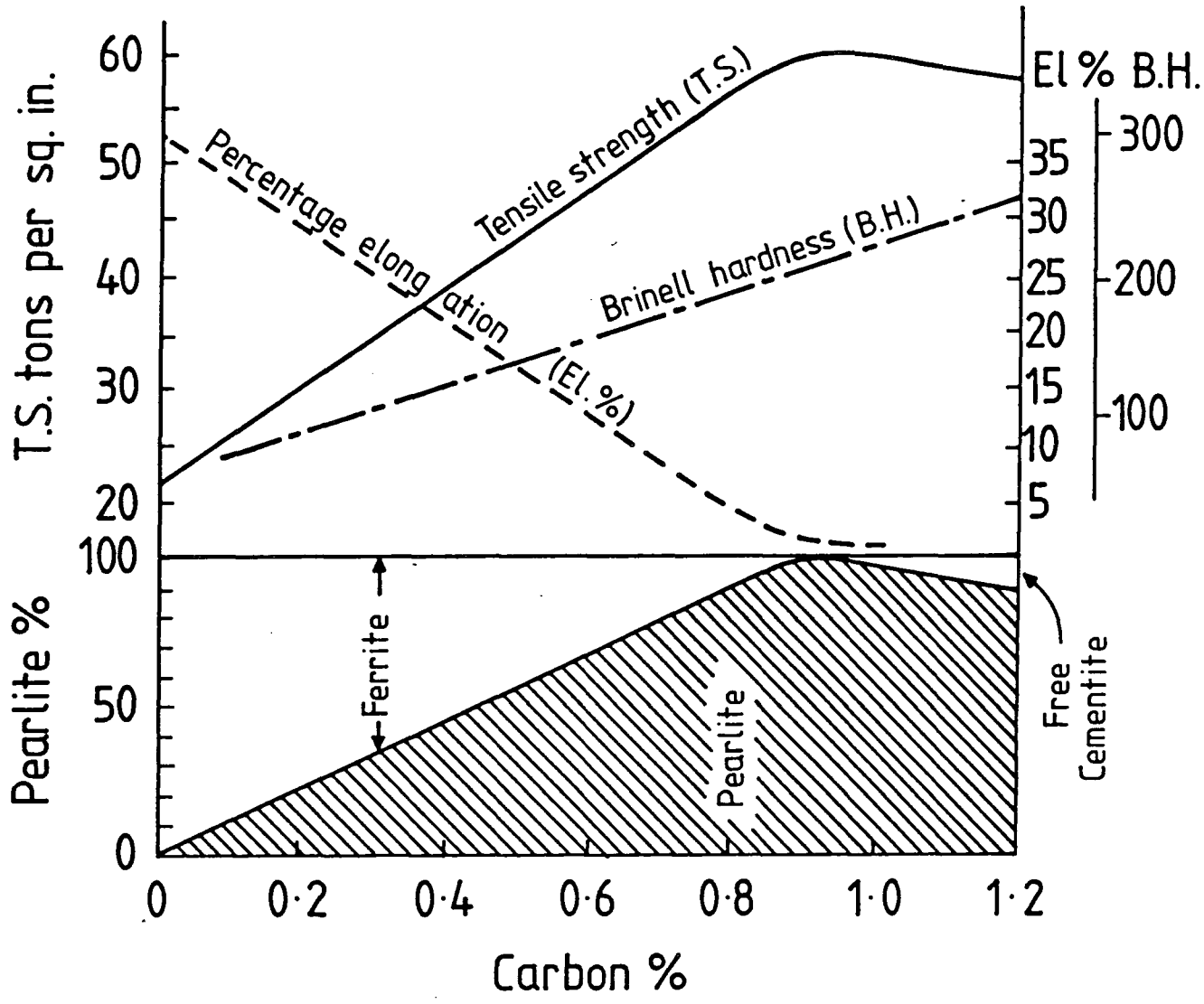

Figure 1.7

Effect of carbon content on mechanical properties of iron (after Rollason (1964)).

unsuitable for both hot and cold work.

(b) Manganese - a beneficial impurity. It increases the depth of hardening but can cause cracking during quenching processes. Mn is soluble in both austenite and ferrite and forms the stable carbide Mn_3C. It also combines readily with any sulphur in the steel to produce MnS which is less harmful than free sulphur. Provided that about five times the theoretical manganese requirement is added the insoluble MnS accounts for all the sulphur and forms large globules throughout the steel. These are readily deformable and become elongated into threads during subsequent rolling operations. As a result the presence of Mn improves both strength and toughness.

(c) Silicon - also beneficial. It is added as a deoxidant but in high-carbon steels it must be kept at low levels because of its tendency to render cementite (Fe_3C) unstable (giving free ferrite (Fe) and graphite).

(d) Phosphorus - forms iron - phosphide which is brittle and has a dangerous tendency to aggregate thus making the steel locally brittle. Levels must, therefore, be kept below 0.05%.

1.3(ii) Pipe Steel production - the Basic oxygen furnace

Most pipe-line steel made in this country and Europe is produced in the Basic oxygen furnace by the Linz-Donawitz (LD) process (Starratt (1960), McMulkin (1955)) because of its low cost, high production rates and particular

suitability for low-carbon steel. The vessel is usually pear shaped with an opening at the top for charging and slag removal (Figure 1.8). It consists of a steel shell with a basic lining of tar-bonded brick. Basic lining (normally burnt dolomite (CaOMgO) or magnesite (MgO)) is necessary to refine pig irons rich in phosphorous as only lime (CaO) will do this, resulting in the production of a basic slag. Historically the more conventional Acid process was preferred because of the better quality steel it produced, but modern techniques have ensured this quality can be matched by the Basic process.

A water-cooled lance supplying pure oxygen is gradually lowered into the molten pig iron in the vessel causing the impurities present to oxidize. Those impurities with the greater affinities for oxygen, namely silicon and manganese, oxidize first, and when the bulk of these have been converted to slag the carbon and then the phosphorus are oxidized to CO/CO_2 and P_2O_5 respectively. The recombination of the phosphorus pentoxide with some of the iron oxide in the slag is prevented by the addition of powdered lime via the lance at this stage. The calcium phosphate thus formed is stable and joins the slag:

$$P_2O_5 + 3CaO = Ca_3(PO_4)_2 \qquad (1.9)$$

At the end of this process (the "blow") additions of carbon, manganese and silicon are made to bring the carbon content to the specified percentage, counteract the influence of sulphur and deoxidize the melt respectively. The latter process, referred to as "killing" the steel

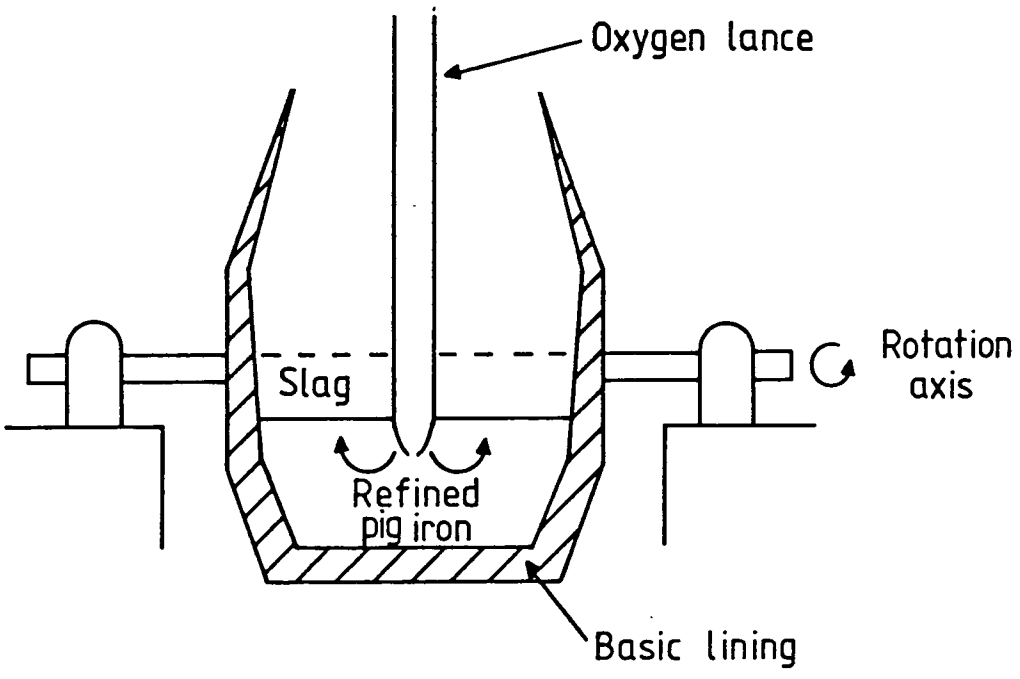

Figure 1.8

The Basic Oxygen furnace - the L.D. converter.

(see section 1.3(vii)), involves the reduction of iron oxide by either Mn or Si:

$$FeO + Mn = Fe + MnO \qquad (1.10)$$

The oxidized manganese or silicon then joins the slag.

The vessel is rotated to pour away as much slag as possible before the finished steel is poured into a ladle and then into ingot moulds for subsequent rolling.

1.3(iii) The Microstructure of Plain Carbon Steels

The essential difference between ordinary steel and pure iron is the presence of carbon in the former, which reduces the ductility but increases the strength and susceptibility to hardening when rapidly cooled from elevated temperatures. The latter effect will be considered later and the discussion of microstructure presented here is limited to steels which have been cooled slowly from 1760^{o} - $900^{o}C$.

Pure iron contains no carbon, but small quantities of impurity (e.g. P, Si and Mn) are dissolved in the metal. Its structure is built up of a number of crystals (grains) of the same composition, given the name "ferrite" in metallography (Brinell hardness 80[#]).

The addition of carbon to pure iron results in a considerable difference in the structure, as revealed by a suitable etching process, which now consists of two

---

#For a definition of Brinell hardness see Bailey (1973) and also BS.240.1962.

constituents, the white one being the ferrite, and the dark parts being the carbon bearing constituent (Figure 1.9). Carbon is present as a compound of iron and carbon (6.67%) called "cementite" (Fe_3C) which is very hard (Brinell hardness 600), brittle and has an orthorhombic structure (Lipson and Petch (1940)). A closer examination of the dark areas reveals that they also consist of two components occurring as wavy or parallel plates alternately dark and light. These two phases are ferrite and cementite which form a eutectoid mixture, containing 0.87% carbon, known as Pearlite. The areas containing either phase are, therefore, referred to as ferrite or pearlite grains.

Since the pearlite contains 0.87% carbon it is evident that the % Pearlite present in the microstructure is given by:

$$\% \text{ Pearlite} = \frac{\% \text{ Carbon} \times 100}{0.87} \qquad (1.11)$$

for % Carbon $\leq$ 0.87%. Any further increase in carbon gives rise to free cementite at the grain boundaries. The highest strength is obtained when the structure consists entirely of pearlite as the presence of free cementite, while increasing the hardness, reduces the strength (see Figure 1.7).

The formation of the lamellar Pearlite structure has been studied in some detail (Hickley and Woodhead (1954), Cahn (1956, 1957) and Mehl and Hagel (1956)) and an insight into the mechanism can be gained by an inspection of the iron-carbon partial equilibrium diagram (Figure 1.10).

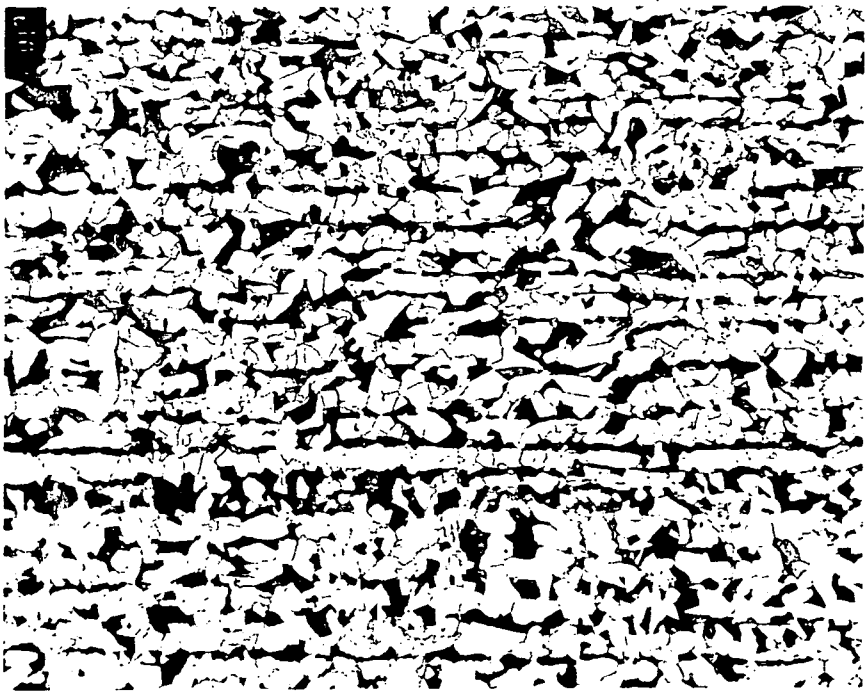

Figure 1.9 Metallograph which reveals the ferrite (white) and pearlite (black) grains in the microstructure of a typical pipe steel (fully killed). Magnification is 200 times.
(Photograph by courtesy of Dr. C.L. Jones, ERS, Killingworth).

This diagram is complicated by the allotropy of iron which can exist in four forms known as α, β, γ and δ. Of these the α, β and δ forms are all body centred cubic (b.c.c.) while γ iron has a face centred cubic structure (f.c.c.). The transition from α to β iron occurs at the Curie point (769°C) and the β - γ and γ - δ transitions take place at 937 and 1400°C respectively. The b.c.c. forms are all referred to as ferrite and have only slight solubility for carbon (e.g. 0.006% for α ferrite at room temperature) whereas up to 1.7% of carbon dissolves in δ -iron to form an interstitial solid solution called "Austenite". The complex diagram can, however, be divided into several more simple diagrams:

(a) Peritectic transformation CDB - δ -iron transforms to austenite

(b) Eutectic at E - austenite and cementite

(c) Solid solution D to F - primary dendrites of austenite form

(d) Eutectoid point at P - formation of pearlite.

In order to explain the observed microstructure of pipe steel (0.1 - 0.2% carbon), consider the freezing of such an alloy under slow cooling conditions:-

Dendrites of δ iron form initially whose composition is eventually represented by C (0.07% carbon) and the liquid, which is slightly enriched in carbon, by B. The majority of the solid crystals then react with all the liquid to form austenite of composition D. On further cooling the remaining δ -iron transforms

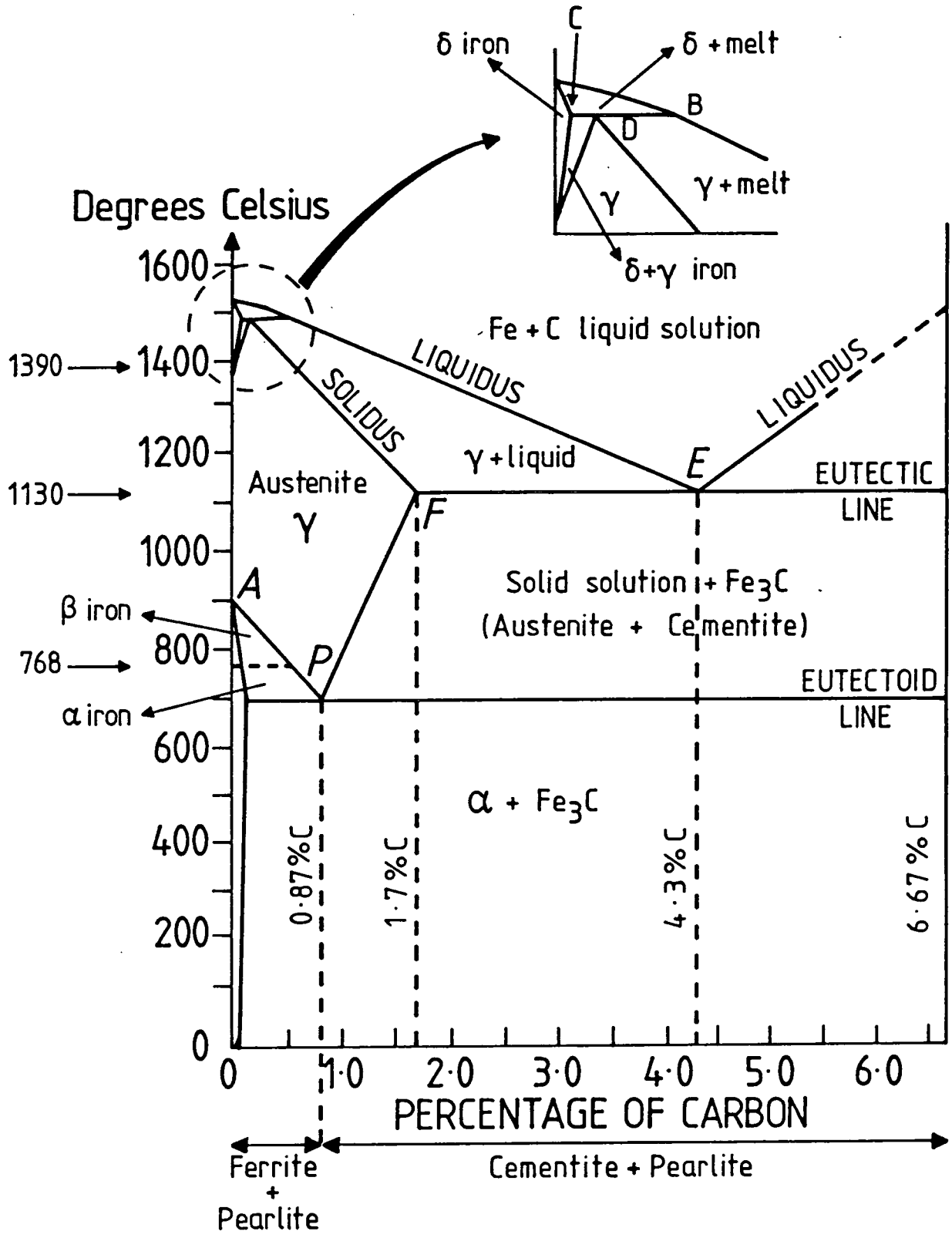

Figure 1.10

Partial Equilibrium Diagram of Iron-Carbon Alloys (after Rollason (1964) and Johnson and Weeks (1964)).

to austenite with the simultaneous diffusion of carbon within the austenite to form an austenitic composition identical to the original melt. Cooling proceeds with the development of an austenite grain structure until the ferrite solubility line (AP) is reached whereupon the precipitation of ferrite begins with the nucleation of ferrite grains at the austenite grain boundaries (Hume-Rothery (1966)). The remaining solid solution is enriched in carbon, therefore, until the point P is reached at which cementite can also be precipitated. The alternate precipitation of ferrite and cementite occurs at this temperature (695^{o}C) and results in the formation of lamellar pearlite. When all the austenite has been transformed in this way, cooling proceeds and the total structure consists of masses of pearlite (pearlite grains) embedded in the ferrite grain structure.

1.3(iv) The Rolling Process

A similar, but reversed, process takes place during the subsequent reheating of the steel (see Figure 1.11) which is necessary prior to rolling the steel ingot into plate of the required thickness. Conventional hot rolling occurs in the temperature range 1250 - 1050^{o}C and the degree of hot work involved helps inhibit the growth of the austenite grains which would otherwise occur at these elevated temperatures. As a result the ferrite grain size before and after the rolling process is not dissimilar.

The deformation of the plate during rolling also

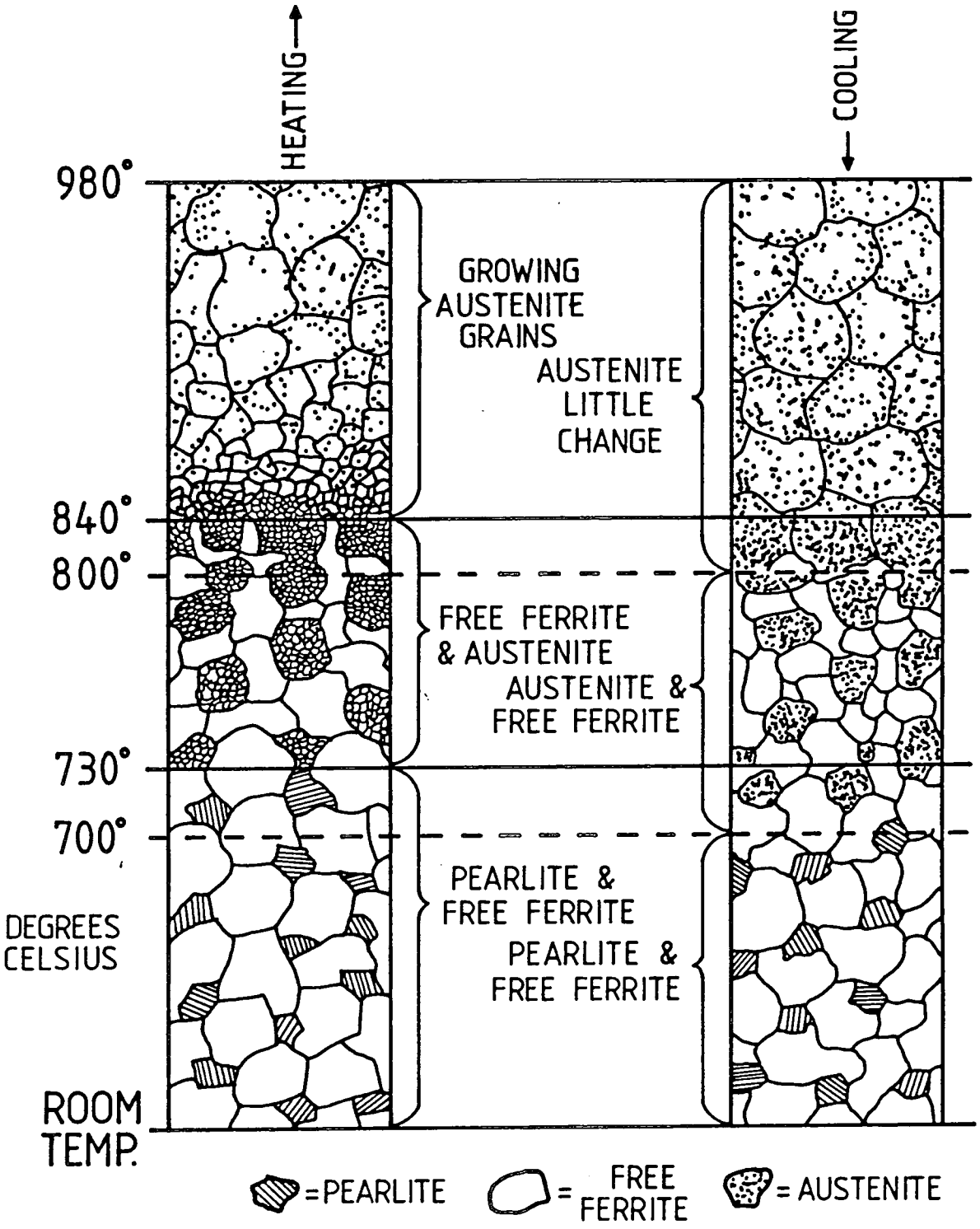

Figure 1.11

Changes in grain structure during heating and cooling processes (after Johnson and Weeks (1964)).

causes elongation of the ferrite and pearlite grains along the rolling direction either directly or by the inducement of preferential grain growth in this direction (Hume-Rothery (1966)). Such effects have been observed in pipe steels (Szpunar and Tanner (1984)) as has the related phenomenon of an anisotropic orientation distribution function of the crystallographic axes within the total assembly of grains. The latter is more usually referred to as texture (Bunge (1982), Szpunar (1984)). Both these effects (and the inevitable presence of internal strain which may also be anisotropic) give rise to anisotropy in the magnetic properties of the steel, and results are presented in Chapter 6 of this thesis which indicate such behaviour in pipe steels.

1.3(v) Other forms of carbon steels

The partial equilibrium diagram presented in section 1.3(iii) (Figure 1.10) is only valid for slow cooling rates and several different steel structures can be formed by a rapid cooling (quenching) of the melt (see Figures 1.12(a), (b)). It can be seen that a relatively slow quench results in the formation of sorbitic or troostitic pearlite. Both these forms of steel have been shown to be progressively finer pearlite structures (Hume-Rothery (1966), Zener (1946)) which are barely resolvable under the ordinary microscope. Troostitic pearlite, also referred to as Bainite, consists of nodules of radial lamellae of ferrite and cementite and differs from pearlite only in the degree of fineness and carbon content, which is

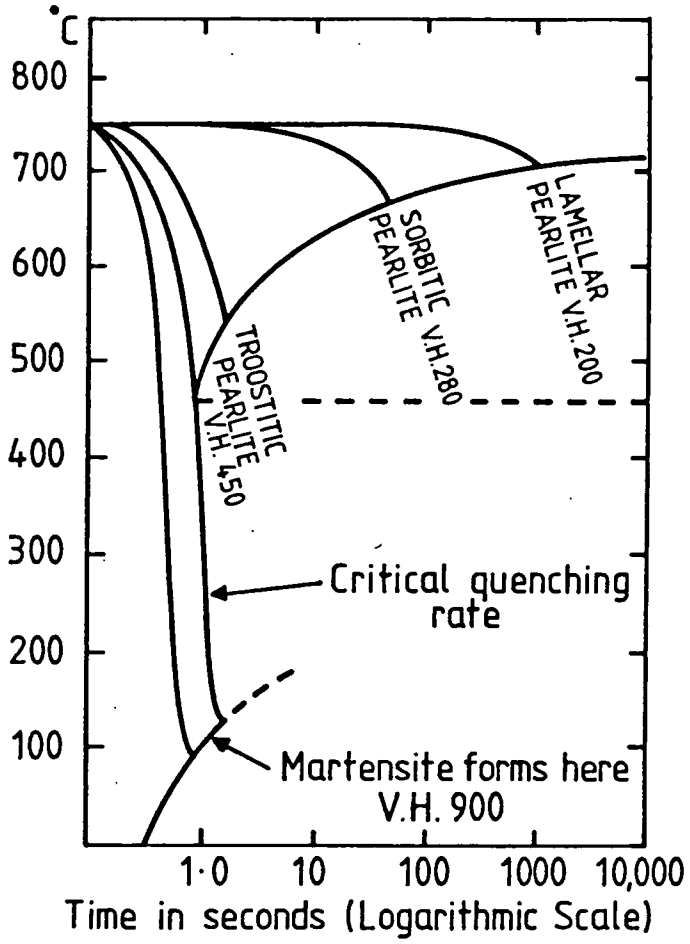

(a) Effect of Cooling Rate on the Transformation of a Eutectoid Steel (after Johnson and Weeks (1964)).

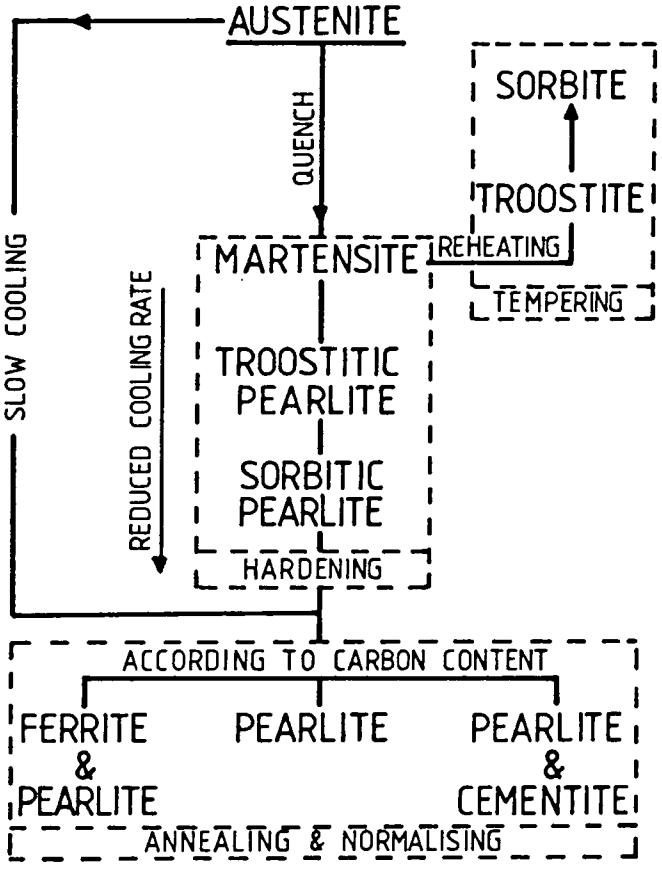

(b) Structures produced when Carbon Steel is cooled from an Austenitic Condition (after Kempster (1976)).

Figure 1.12

the same as that in the austenite from which it is formed. A much more rapid quench results in the formation of Martensite, the hardest structure in a given steel, which is seen as a needle-like structure under the microscope and has a body centred tetragonal crystallographic structure (Kurdjumow (1960), Kelly and Nutting (1960)). All three forms of steel are increasingly brittle and their presence in pipe steel is unwanted because their low ductility and toughness increases the susceptibility of these steels to crack formation and propagation. Martensite is, in fact, normally reheated (tempered) to a sub-critical temperature after hardening to transform it to troostite or sorbite which have improved toughness (see Figure 1.12(b)). These steels consist of fine dispersions of carbide in a ferrite matrix and must not be confused with the sorbitic and troostitic pearlite steels obtained from austenite.

Austenite itself can also be formed at room temperature by quenching, but it is always accompanied by martensite and is not stable. Large additions ($\sim$ 15%) of alloying elements (e.g. Cr, Mo, Ni) however, lower the critical points in the phase diagram (Rollason (1964)) and ensure stability for this steel type at room temperature. Stainless steels (> 11% Cr) are sometimes used for the production of pipe fittings but the large cost of the alloying elements prohibits the extensive use of such steels in pipe-line systems.

1.3(vi) Pipe Manufacture

The majority of steel pipe used in high pressure gas pipe-lines is fabricated from rolled plate as longitudinally seam welded pipe. The sequence of operations required for the manufacture of this pipe type are shown in Figure 1.13 and are usually referred to as the U-ing and O-ing method.

The first operation is to shear the plate to the correct size for the diameter of pipe required, machine the edges parallel and cut weld preparations. The longitudinal edges are then crimped, using a large press, to provide the correct curvature in the region of the weld and the crimped plate is further deformed into a "U" shape and finally into a complete circle by additional presses and dies. The pipe is welded along the seam, completing the inner weld first, after which a thorough inspection is carried out using both radiation and magnetic particle inspection techniques.

The final pipe diameter is obtained by hydraulically expanding the welded pipe using a high pressure water system until the limits provided by external retaining jackets are reached. The pressure is then reduced and held steady for a period to serve as a hydrostatic test for the weld. The additional advantage of this process, apart from testing the weld and achieving the sizing, rounding and straightening of the pipe, is that the degree of cold work involved serves to increase the mechanical properties of the steel.

(a)

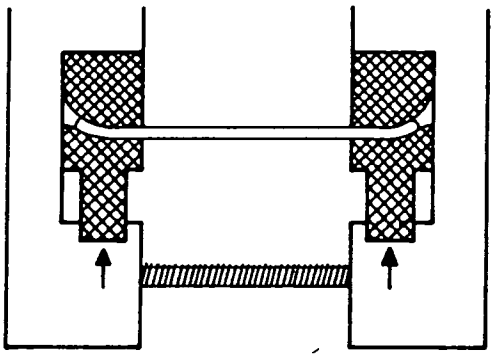

(b)

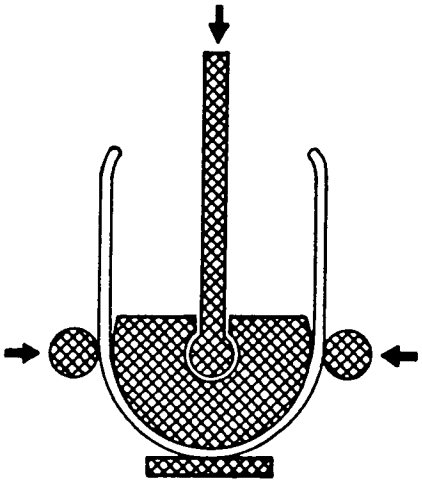

(c)

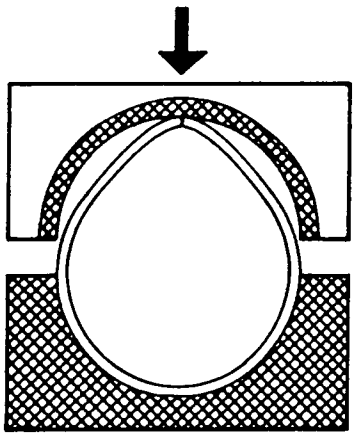

Figure 1.13 Illustration of the (a) crimping, (b) U-ing, and (c) O-ing processes involved in pipe manufacture.

The final process involves accurately finishing the pipe ends and machining the weld preparations in readiness for the girth welding to be done in the field.

1.3(vii) Steels used in British Gas high pressure transmission pipe-lines

Gas transmission pipe-lines in the British system operate at high pressure (up to a maximum of 70 bar (1000 p.s.i.)) and, in order to ensure the economic construction and safe operation of the system, it is essential that the pipe material has adequate strength, toughness and weldability. To this end British Gas only purchase material which meets well established specifications (BGC/PS/LX1) covering all three areas (Jones 1982)).

Since the first British Gas pipe-line was constructed in 1963 there has been a steady trend towards increasing the yield strength of the steels used. This has been a direct result of the economic advantages to be gained from constructing and operating pipe-lines of larger diameters as the quantity of gas to be transmitted has increased. The first transmission pipe-line was 456 mm (18") diameter with a specificed minimum yield stress (MSYS-defined as the stress to give 0.5% total strain) of 240 MNm^{-2} (35 k.s.i.), but there is now a range of pipe-lines within the system with diameters of up to 1067 mm (42"). The specification currently stipulates a MSYS of 414 MNm^{-2} (60 k.s.i.) with wall thickness $\leq$ 19 mm although occasionally pipe of 448 MNm^{-2} (65 k.s.i.) yield strength is required for certain projects.

MSYS values of this order are required to cope with hoop stress (circumferential) in the pipe wall for the largest diameter pipes. It is easily shown that

$$\sigma = \frac{PD}{2t} \qquad (1.12)$$

where σ = hoop stress (MNm^{-2})

P = operating pressure (MNm^{-2})

D = pipe diameter (m)

t = wall thickness (m)

and when the maximum stress level permitted is 72% of the MSYS a value of σ = 414 MNm^{-2} (60 k.s.i.) is required for a 42" (1067 mm) diameter pipe of ½" (12.7 mm) wall thickness, operating at 7 MNm^{-2} (1 k.s.i.).

The class of pipe-steel originally used in the transmission system was semi-killed steel. Dissolved oxygen is removed from the steel in the "killing" process by controlled additions of Si and Mn (see Section 1.3(ii)). In semi-killed steels sufficient oxygen is left in the melt for the gas evolution during solidification to offset the shrinkage of the ingot. A typical steel chemistry for a semi-killed steel is:

C	Mn	Si	S	P	Al	V	Nb
0.20%	0.9%	0.03%	0.04%	0.03%			

The largest MSYS value obtained with these steels was 386 MNm^{-2} (56 k.s.i.) and a new steel-making process was necessary, therefore, to produce an improved microstructure for the larger diameter pipes.

Petch (1953, 1954) had showed empirically that the yield stress σ_y could be represented by:

$$\sigma_y = \sigma_i + Kd^{-\frac{1}{2}} \qquad (1.13)$$

where σ_i is the lattice friction stress,

d is the ferrite grain size

and K is a constant.

Equation (1.13) indicates that, in order to increase the yield strength, either the smooth sliding of the atom planes must be disturbed (increase σ_i) or the ferrite grain size must be refined (or both).

Slip or plastic deformation occurs in metal crystals by a process whereby planes of atoms slide over one another under the action of an applied stress. In alloy systems such slip can be made more difficult by the replacement of atoms of one element by atoms of a second element of different size. This substitutional solid solution is, therefore, harder and the process described above is known as "solid solution hardening". In steels the elements used to produce such hardening are normally manganese and silicon. These were originally added as deoxidants (see above) but when added in excess they produce an extra increment of strength.

A second means of increasing the lattice friction stress (σ_i) is the use of small particles (20 - 40Å) of vanadium carbonitride or niobium carbide (or both) spread evenly throughout the lattice. These precipitates are very hard and prevent local distortion of the alloy's lattice hence increasing yield strength. This process is called "precipitation hardening".

The complete killing of steel by excess Mn and Si addition to produce a fully-killed steel now permits grain refinement by small additions of aluminium (0.04%). In the absence of oxygen, aluminium nitride particles are formed during the solidification of the steel or during the subsequent normalizing treatment which prevent austenite grain growth by pinning the austenite grain boundaries. The fine grained austenite transforms to a fine grained ferrite and hence produces a steel of enhanced yield strength which meets the MSYS requirement of 414 MNm^{-2}. As a result, a typical steel chemistry for a fully-killed steel is:

C	Mn	Si	S	P	Al	V	Nb
0.18%	1.4%	0.4%	0.03%	0.03%	0.04%	0.09%	0.04%

(Note that a silicon content > 0.1% indicates a fully-killed steel).

Another reason for the development of a fully-killed steel was the introduction of the Drop Weight Tear Test (DWTT) into BGC/ PS/LX1, which assesses the materials toughness - its ability to tolerate defects (e.g. propagating brittle cracks) (Rodgerson and Jones (1980)). The occurrence of a propagating brittle crack in high pressure gas pipelines is undesirable because the velocity of the crack tip is often greater than that of the decompression wave, with the result that the crack propagates for many miles. (An 8 mile long crack has been recorded in the U.S.A.).

All ferritic steels show a transition from brittle to ductile behaviour with increasing temperature and the DWTT requirement stipulates that this transition

should be below $0^{o}C$. The transition temperature for semi-killed steels was found to be in the range 10 - $30^{o}C$ (Rodgerson and Jones (1980)) and does not, therefore, meet this requirement. Consequently all semi-killed pipe in British Gas systems is operated well below the MSYS (Fearnehough et al. (1971)).

The same factors which were discussed above in connection with the relation between structure and strength also affect the brittle/ductile transition temperature and hence the toughness. Unfortunately their effect on toughness is not entirely analogous. Solution and precipitation hardening increase yield strength but are found to raise the transition temperature thus making the material more brittle. In contrast to this, however, a finer grain size increases yield strength and reduces (improves) the ductile/brittle transition temperature. Hence a greater emphasis is placed on ferrite grain size refinement than solution or precipitation hardening.

Fully-killed steels have transition temperatures in the range -50 to $-10^{o}C$ and it appeared that the use of these materials would totally eliminate the possibility of fracture propagation. Two long propagating fractures then occurred in the U.S.A., however, in which the fracture appearance was fully ductile. Extensive research into this problem revealed that, although the fractures were ductile, insufficient energy was absorbed by the ductile fracture to arrest the crack. This resulted in the introduction of the Charpy upper shelf energy (USE) criterion into pipe-lines specifications (Rodgerson and Jones (1980),

Jones (1982) and Poynton et al. (1974)). The higher Charpy USE value steels are selected, therefore, because they have lower ductile fracture speeds.

The metallurgical parameters important in producing high values of Charpy USE are non-metallic inclusions, with sulphur being the most deleterious (see Section 1.3(i)). The sulphur is present as MnS (if excess Mn has been added) which is highly deformable and becomes considerably elongated during the rolling operations. The resulting ribbons of MnS represent planes of weakness in the final product and are mainly responsible for low Charpy USE values. There are two remedies; (a) remove the sulphur in the melt by adding calcium carbide, and/or (b) made the sulphides less deformable.

This is normally achieved by adding rare-earth metals to the melt to form REM sulphides which have low relative deformability with respect to the steel matrix.

Steels present in gas pipe-lines in Britain before the Charpy USE criterion was added to the specification have USE values typically of $\sim$30 joules, whereas modern pipe-lines steels have USE values between 100 and 200 joules.

The third requirement for good pipe steel, apart from strength and toughness, is weldability. This term refers to the ease by which individual pipes can be joined end-to-end in the field (and its resistance to hydrogen induced cracking). It is defined quantitatively by a carbon equivalent (CE) given by

$$CE = C\% + \frac{Mn\%}{6} + \frac{(Cr\% + Mo\% + V\%)}{5} + \frac{(Ni\% + Cu\%)}{15} \qquad (1.14)$$

A lower CE value results in improved weldability and it was considered desirable to reduce the CE value from that prevalent for fully-killed steels. This was most easily achieved by a reduction in carbon levels, but in order to maintain the strength of the steel a simultaneous refinement of the ferrite grain size was required. This was achieved by a continuation of the rolling process down to temperatures as low as 800°C (i.e. lower than the austenite / ferrite transition temperature). This process, referred to as controlled-rolling, introduces controlled deformation into the steel which "breaks down" the austenite grains giving a finer structure. This, combined with the addition of niobium to provide extra austenite grain refinement (Meyer et al. (1975)) permits the intense refinement of ferrite grain size and allows reduction in the carbon levels required to produce adequate strength. A typical steel chemistry of controlled-rolled steel, therefore, would be

C	Mn	Si	S	P	Al	V	Nb
0.10%	1.4%	0.3%	0.02%	0.03%	0.04%	-	0.04%

The microstructures for all three steel types (semi-killed, fully-killed and controlled rolled) are compared in Figure 1.14. Together they form the vast majority of pipe-steel that currently forms the British Gas high

(a)

(b)

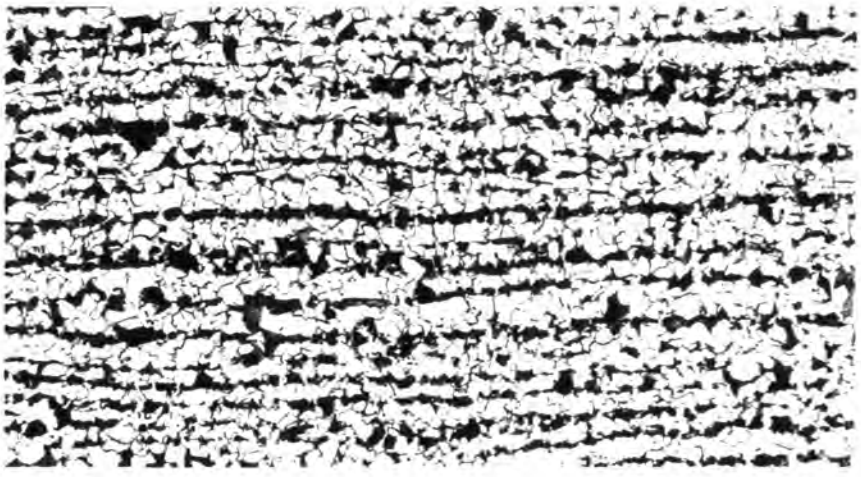

(c)

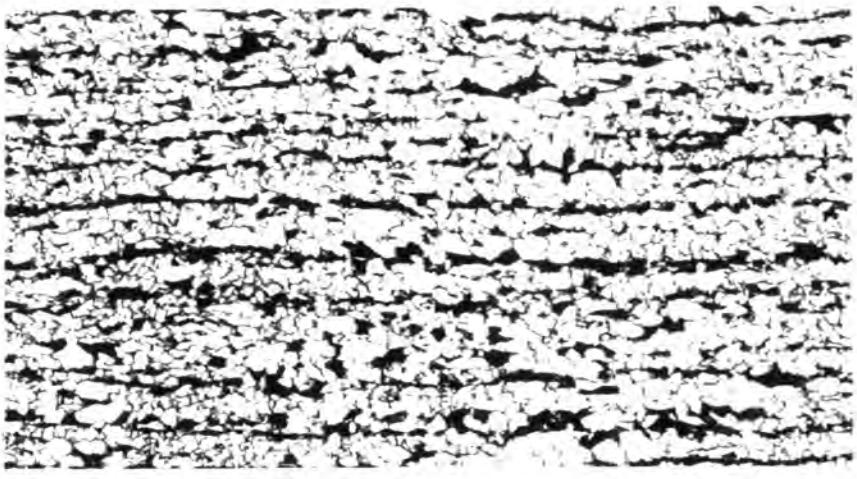

Figure 1.14 Comparison of the microstructures of typical (a) semi-killed, (b) fully-killed, and (c) controlled rolled pipe steels. Magnification is 200 times. (Photograph by courtesy of Dr. C.L. Jones, ERS, Killingworth).

pressure gas transmission pipe-line network and all the steels considered in this thesis can be categorized in this way.

1.4 ON-LINE NON-DESTRUCTIVE PIPE-LINE INSPECTION

1.4(i) British Gas pipe-line inspection philosophy

Britain is served by a national network of high-pressure gas transmission pipe-lines some 15,000 km long (see Figure 1.15) and, although the system has been constructed using materials and techniques which meet the stringent requirements outlined above, the inevitability of subsequent defect occurrence has been recognized. To imply that lines become defective does not detract from the structural integrity of the pipe-line so long as some system is available which permits early detection and eradication of defects before they lead to failure.

In the past this has been achieved using a combination of periodic but infrequent hydrostatic overload testing and above ground surveillance techniques which is both costly and inconvenient. It is costly because additional pipe-lines have to be provided to maintain the supply to customers during the test, and inconvenient because the lines have to be decommissioned, filled with water, tested, dried out and recommissioned. The advantage of such an operation is that it guarantees to remove all defects that exceed the pressure test level of structural significance, but the location and repair of small defects is often difficult.

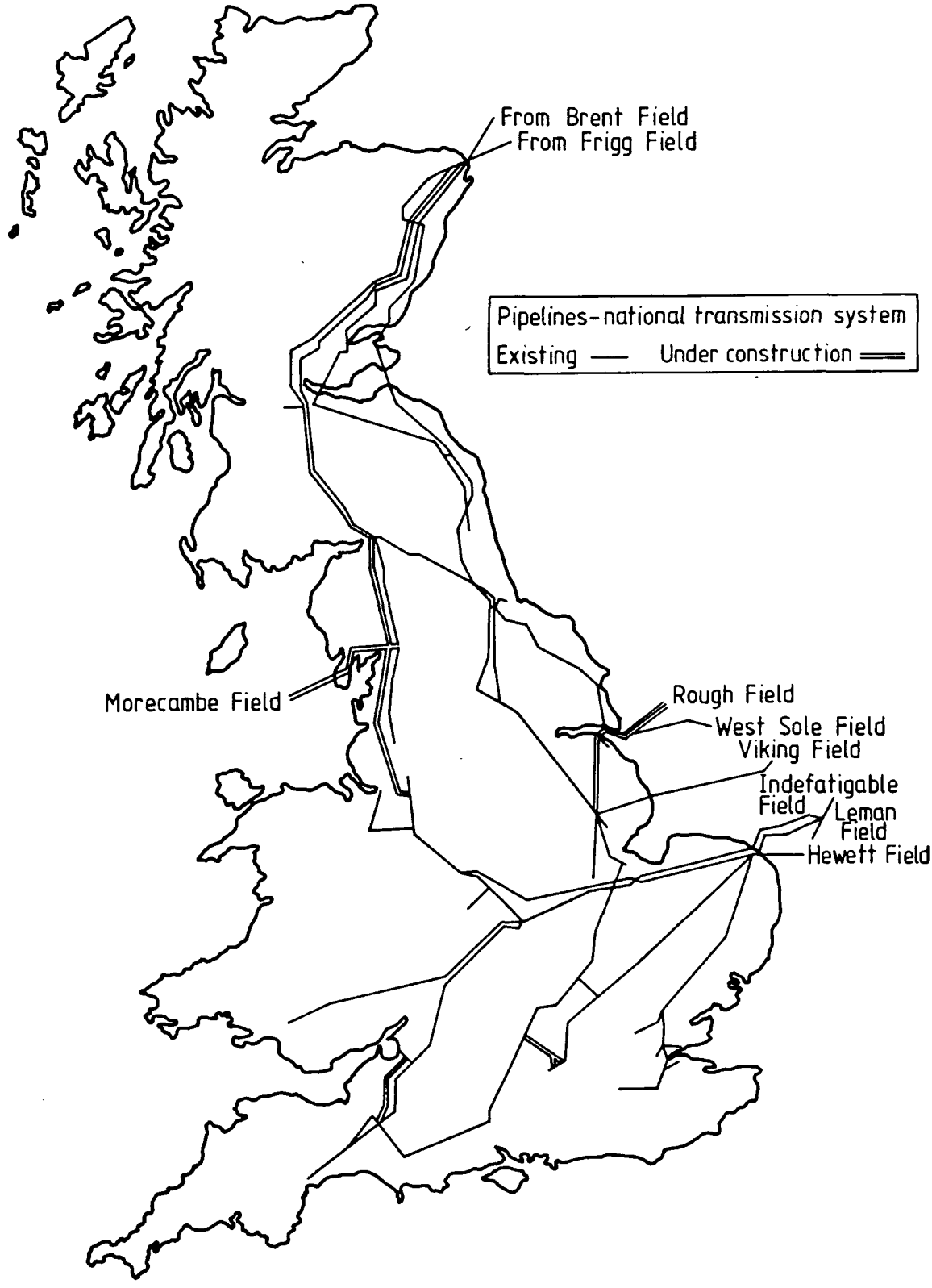

Figure 1.15 The British Gas National Transmission System.

In recent years British gas have developed an on-line inspection vehicle (called the "intelligent PIG") at the On-line Inspection Centre (OLIC), Cramlington, Northumberland, which has overcome these drawbacks. The use of the PIG has permitted detection of both structurally significant and insignificant defects, as well as allowing the defects subject to growth mechanisms to be monitored by data comparison from consecutive inspections. Long lengths of pipe-line can be surveyed in this way without the interruption of the supply and, as a result, the level of safety that can be maintained during the operational life of the system has been greatly enhanced.

1.4(ii) Design aims of the PIG

The development of the PIG followed the five major requirements of an on-line inspection vehicle:

(a) No interference with pipe-line operation.

(b) Detect all significant defects.

(c) Determine defect size accurately.

(d) Determine defect position accurately.

(e) No spurious indications.

The first aim was met by choosing a gas-blown vehicle, which fits inside the pipe, to carry the inspection equipment. The driving force is provided by the gas flow pushing against cups which seal against the pipe wall. These cups have been designed to give PIG velocities between 1 and 4 metres per second, to operate in the pressure range 7 - 70 bar, and to "blow over" if the differential pressure exceeds 3.5 bar. The latter feature

enables satisfactory gas flow to be maintained in the unlikely event of vehicle stoppage.

The remaining requirements have been achieved by extensive research into the structural significance of defects and the modelling and measurement of the response of the inspection equipment when such defects are encountered in the laboratory. The criterion of detection sensitivity required by British Gas for various defect types is shown in Table 1.1. When such defects are encountered during an inspection run the response from the PIG sensors, which describe the defect, are recorded on magnetic tape together with positional information which is accurate to within 1.5m. The on-board intelligence required to provide the necessary signal processing before data storage is one of the more significant achievements in the PIG design. Spurious indications are removed during the interpretation of inspection data which takes place once the tape has been returned to OLIC.

1.4(iii) Principles of defect detection

The principle whereby the PIG locates and detects all pipe-wall defects is that of magnetic flux leakage (Forster (1982)). Figure 1.16 illustrates how metal loss at any point in the pipe-wall results in the rejection of flux from the pipe material into the surrounding media which can be detected by a field measuring device placed on the inner pipe surface. The maximum effect is obtained when the pipe material is magnetically saturated as the flux rejection from metal loss cannot be sustained by

FEATURE	DETECTION SENSITIVITY	SIZING ACCURACY
Pitting corrosion	0.4t	± 0.1t
General corrosion	0.2t	± 0.1t
Circumferential gouging	0.4t	± 0.1t
Axial gouging	0.2t	± 0.1t
Repaired damage	0.2t	± 0.1t
Depth of cracking	0.2t	± 0.1t
Length of cracking	0.2D	± 0.02D

t = Nominal pipe wall thickness

D = Nominal pipe diameter

TABLE 1.1

Minimum inspection requirements for seam welded pipelines operating at stress levels up to 0.72 MSYS

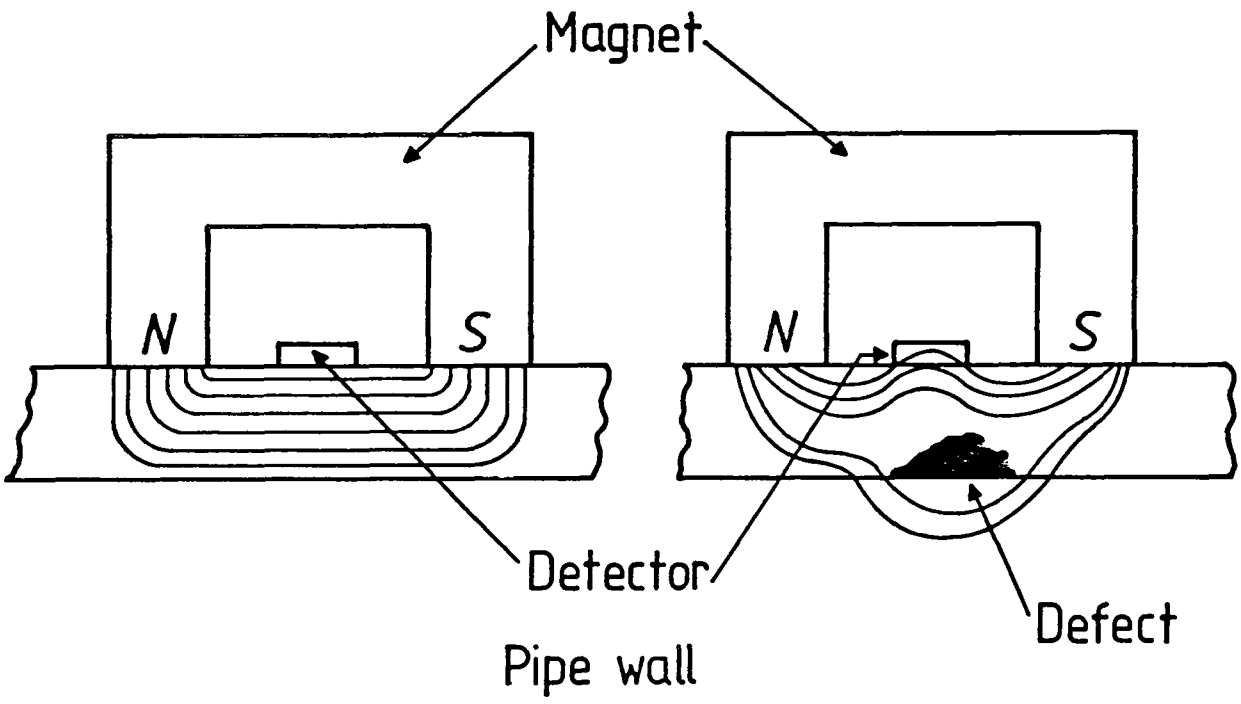

Figure 1.16

Illustration of the use of magnetic flux leakage to detect pipe wall thickness defects.

the remaining material.

The magnetizing field on the PIG is provided by axial arrays of permanent magnets which are held in contact with the inner surface of the pipe-wall. Figure 1.17 shows a schematic representation of the PIG and indicates the position of one set of field measuring devices (e.g. search coils) between the north and south poles of the magnetic circuit. The static flux diagram shown in Figure 1.16 is not valid once the PIG is in motion as the production of eddy currents around the circumference of the pipe causes significant distortions to the field profile, and the positioning of these sensors towards the rearward magnetic poles is advantageous for the detection of defects on both inner and outer surfaces of the pipe-wall. Small defects on the inner pipe surface are not considered as harmful as corresponding defects on the outer surface because the environment inside the pipe is relatively free from moisture and the rapid growth of a pit due to corrosion is unlikely. This is not the case for outer surface defects which are potentially hazardous in comparison. The differentiation between these types of defects is, therefore, essential.

The second array of sensors, remote from the primary magnetic circuit, provides this information by detecting inner defects only. Incorporated into these detectors are small pieces of permanent magnet material that provide a very localized flux concentration in the pipe material. Consequently only defects/metal loss close to the sensor

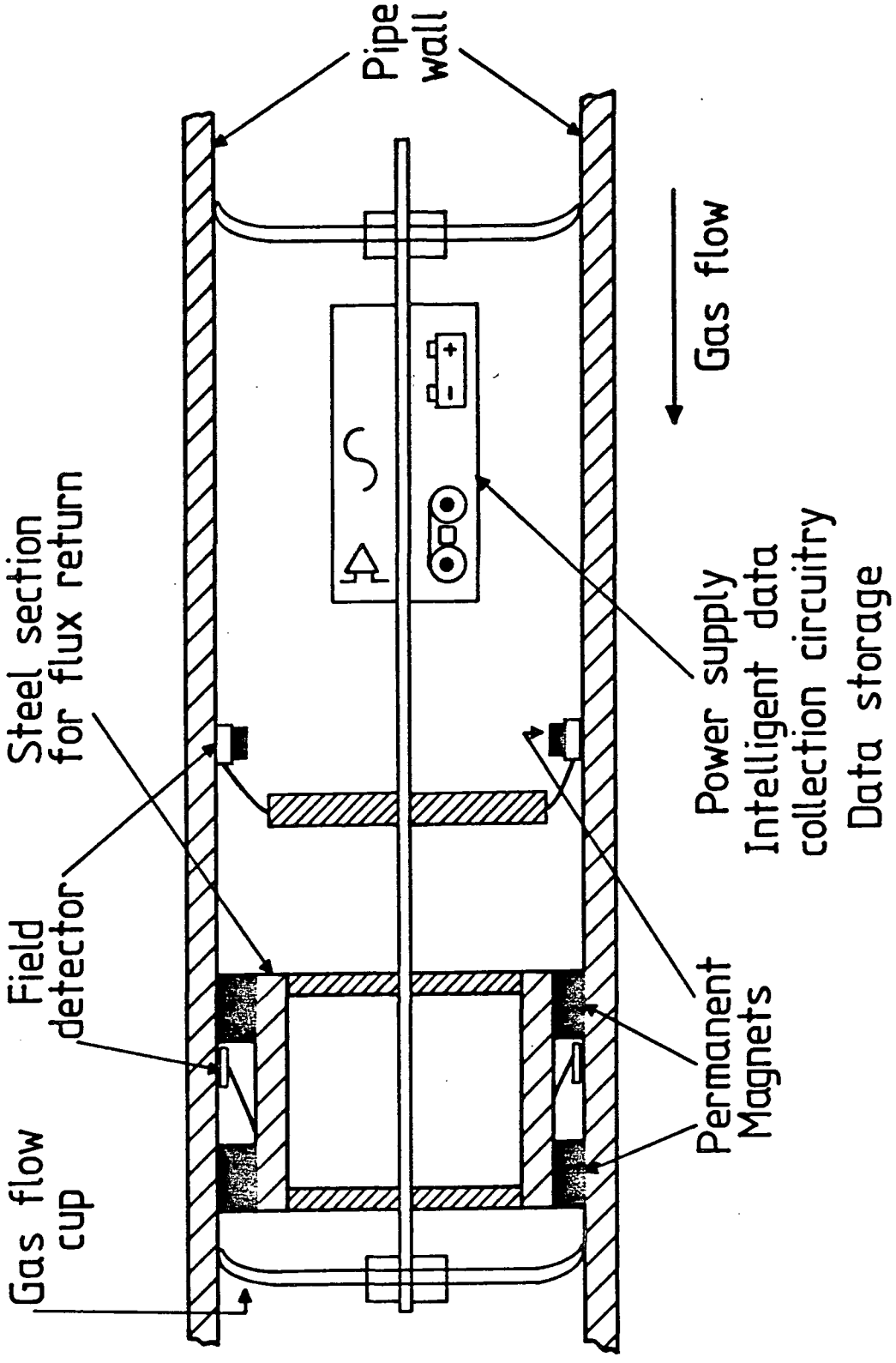

Figure 1.17

Schematic representation of the PIG vehicle.

cause sufficient flux distortion to result in detection of the same.

1.4(iv) The Magnetic Categorization of Pipe Steels

In order to predict accurately the behaviour of the PIG in the various pipe steels encountered in the British Gas network, the Physics group at OLIC model the magnetic circuit using finite element packages (PE2D and TOSCA) which require detailed knowledge of the initial magnetization characteristics of the individual steels. Until recently such information was not available and a collaborative project was devised between the Physics group at OLIC and a research team in the Solid State Group, Department of Physics, University of Durham, to investigate the magnetic properties of these materials in detail.

The project involved the categorization of the magnetic properties, chemistry, metallography, mechanical properties, texture and domain structure of the many pipe-steels known to exist in the network. Some of these areas were studied in greater detail in order to gain an understanding of the physical processes giving rise to the behavioural properties. These will be referred to, where relevant, later in this thesis. The work presented later deals specifically with the magnetic categorization of both bulk and small steel samples, and the development and use of models to achieve the accurate parameterization and prediction of the magnetization curves. The results obtained are of direct relevance to the modelling of

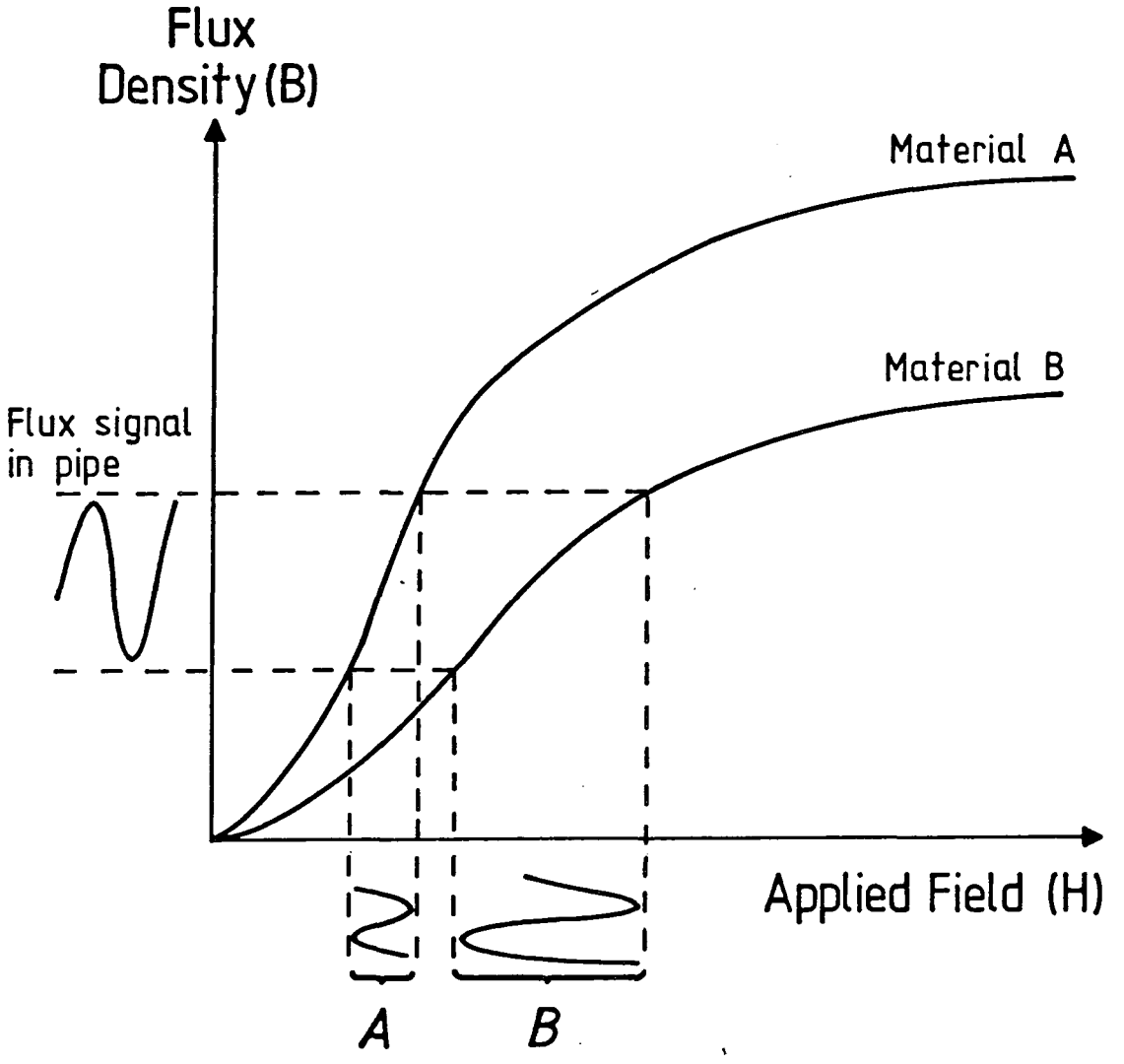

Measured field signals
from defect in pipes of
materials A and B

Figure 1.18

Variation of signal detected by PIG for same defect in different pipe materials.

the PIG's behaviour in the various pipe-steels.

The manner by which variations in the magnetic properties of steels affect the output from the PIG's sensors is most readily understood by referring to Figure 1.18. The distortion of the flux by identical defects in different steels is the same, but the signals measured at the surface of the pipe steel are proportional to the effective changes in the field and depend, therefore, on the shape of the steel's magnetization curve. By referring to this figure it is easy to see that the largest signals are recorded for steels approaching saturation. A knowledge of the magnetic properties of the various pipe-steels, therefore, enables OLIC to predict the range of signals generated by the PIG. With this information it is possible to minimize this variability by careful PIG design, and so enhance the accuracy and reliability of the on-line inspection service.

CHAPTER 2

HARMONIC ANALYSIS OF B-H LOOPS - THEORY

2.1 Introduction

For many years now attempts have been made to fit equations to the magnetization curve of a ferromagnetic material with a view to using the equation in mathematical models of transformer calculations, the solution of eddy current generation problems and the theory of magneto-modulation probes (Trutt et al. (1968), Widger (1969), Wurm (1949), and Mikhailovskii and Spektor (1957)). Non-linear magnetizing characteristics, neglecting hysteresis, have been represented by a series of exponentials (MacFadyen et al. (1973)), polynomials (Widger (1969)) or analytic functions (Lim and Hammond (1970)). The inclusion of hysteresis in such characteristics has been described by complex permeability (O'Kelly (1972), (1975a,b), (1977)), trapezoidal loops (Atkinson and Thomas (1975)) and analytic functions (Shturkin and Stoinskaya (1969)). Each particular form for the magnetization curve can have advantages and disadvantages over other forms depending on the shape of the material's characteristic and the ease of computation, but with the fast computing facilities now available increasing use is being made of multipoint representations of a measured family of B-H loops, which permits extra-polation for any intermediate values (Zahrewski and Pietras (1971)). A disadvantage of all these models is the inability directly to determine the required

parameters experimentally without recourse to computational curve fitting techniques on pre-recorded data. An exception to this, however, is the use of a Fourier series to represent the B-H loop (Davis (1971)).

The representation of the distortion to the applied field waveform, caused by the non-linear magnetization curve of the core material, by a Fourier series is a natural consequence of studies into the behaviour of transformer cores and magneto-modulation probes. It is well known that flux harmonics are always present in individual transformer laminations, for example, even though the total flux waveform in the core is maintained as a pure sinusoidal function by feedback techniques (Wilkins and Drake (1965), McFarlane and Harris (1958)). Such effects are found to be greatest in the corner regions (Brailsford and Mazza (1962), Moses and Thomas (1973)) where the 3rd and higher odd order harmonics form streamlines of flow in closed circular paths. The increased eddy-current loss in these areas (classically proportional to $\Sigma\ f^2 B^2_{max}$) due to the increased harmonic presence has, therefore, been suggested as a mechanism for the anomalous loss in transformer cores (Basak and Moses (1978)).

Extensive use of the presence of flux harmonics has also been made in the operation of magneto-modulation probes or ferroprobes (Shturkin and Stoinskaya (1969), Fridman et al. (1971), Mikhailovskii and Spektor (1957)). The existence of a d.c. magnetic field in the vicinity of such devices produces even order harmonics in the

output voltage whose amplitude has been shown to be a measure of this steady state field for various drive field conditions and material characteristics (Rogachevskii and Shtamberger (1967), Ponomarev (1970)). These probes, therefore, have applications in the non-destructive testing of magnetized ferromagnetic parts and are used, for example, to detect and measure the stray fields arising from defects in the structure.

The use of a Fourier series to represent the induction (flux) waveform of a ferromagnetic test material under alternating applied field conditions during non-destructive testing was first suggested and demonstrated by Davis (1971). He stated that a study of the harmonic coefficients permitted the extraction of more information from the B-H loop than is contained simply in the "crossing-point" parameters. The coercivity (H_c) and the remanence (B_r) do not, for example, hold any representation of the curvature of the "knee" of the magnetization curve which, for some materials, can alter significantly while the crossing-point parameters are relatively unaffected. The waveform analyser built to record the harmonic amplitudes and phases essentially consisted of narrow band-pass filters and Davis described the use of this instrument to monitor the heat treatment of steel plate more effectively than the conventional methods. Since then there have been several reports in the literature of the use of harmonic analysis in non-destructive testing (Sandovskii and Syrochkin (1971), Soulant and Brisker (1972), Davis (1973), Frankfurt et al. (1981), Mapps and White (1982)).

While these and other applications of the technique will involve the repetitive examination of nominally identical materials under equivalent magnetizing fields, it is important to establish the sensitivity of the various parameters to changes in the experimental conditions. In particular, changes in the degree of saturation of the magnetization will produce a significant difference in the harmonic content of the B-H loop. Until the recent independent papers of Willcock and Tanner (1983) and Ponomarev (1983b,c,d) no detailed analysis of the contributions of the various harmonics to the loop shape had been presented, nor had there been any consideration of saturation effects. The results of both analytical and numerical calculations on the sensitivity of various harmonics to loop shape are presented here and the most reliable harmonics to use in such analyses are identified.

2.2 The Effect of Saturation on Harmonic Content

The onset of saturation in a material will have a marked effect on the harmonic content of the induction waveform. Once the maximum amplitude of the applied field (H_o) is large enough to achieve saturation, any further increase in the amplitude of this driving field will only affect the form of the induction wave. As H_o increases, longer periods of time will be spent at saturation and, in the limit H_o tends to infinity, the induction waveform will be a square wave. In order to predict and study the effect on the harmonic amplitudes

of such saturation effects, therefore, it was necessary to derive analytical expressions for the harmonic content of model magnetization curves.

Previous harmonic analysis work, in the various fields described above, has been done using sinusoidally varying applied fields. In such cases the harmonic content of the induction waveform is due entirely to the magnetic behaviour of the test material and the magnitude and phase of the various harmonics are, therefore, a direct measure of the magnetic properties of the material.

The use of a ramped applied field (triangular waveform) is less common and it implies that not all the harmonic content of the induction waveform is caused by the material properties. Indeed, in the limit of a constant susceptibility the harmonic content would be that of a triangular wave. It has been suggested (Ponomarev (1983c)) that if the function H(t) is well defined the harmonic content from this function can be subtracted from the total harmonic content of the induction wave B(t) to reveal the material related harmonic content arising from the magnetization waveform M(t) (see equation (2.1)).

$$B(t) = \mu_o [H(t) + M(t)] \qquad (2.1)$$

Although such a correction is often useful, it must be pointed out here that it is only correct to first order as each component frequency present in the applied field waveform will generate its own harmonic series based on that frequency. Without such a correction the direct comparison of analysis results obtained under linearly

ramped field conditions is, however, still meaningful and, as the triangular wavefunction permits analytical solutions for the harmonic content with separable variables, this approach has been adopted here.

2.2(i) Analytical model for zero coercivity

While it is impossible accurately to express a B-H loop for a real material as a simple function (see section 2.1), a somewhat idealized magnetization curve has been adopted here in order to derive analytical expressions for the harmonic content. The curve consists of three parts and is sometimes referred to as the piecewise linear approximation (Ponomarev (1983b,c,d)). As seen in Figure 2.1(a) the magnetization M varies linearly with H for $-H_s \leq H \leq H_s$, and is constant for $H_s \leq H \leq H_o$ and $-H_o \leq H \leq -H_s$. The magnetization curve has no hysteresis (i.e. the coercivity is taken as zero) and the permeability is assumed to be very high and therefore that $B \simeq \mu_o M$. Alternatively the correction proposed by Ponomarev can be applied, in which case the subsequent analysis still applies but the induction wave B(t) is replaced throughout by the magnetization wave M(t).

Under these approximations and a linearly ramped H field (Figure 2.1(b)), the induction wave varies as shown in Figure 2.1(c). It has the form of a truncated triangular wave described by

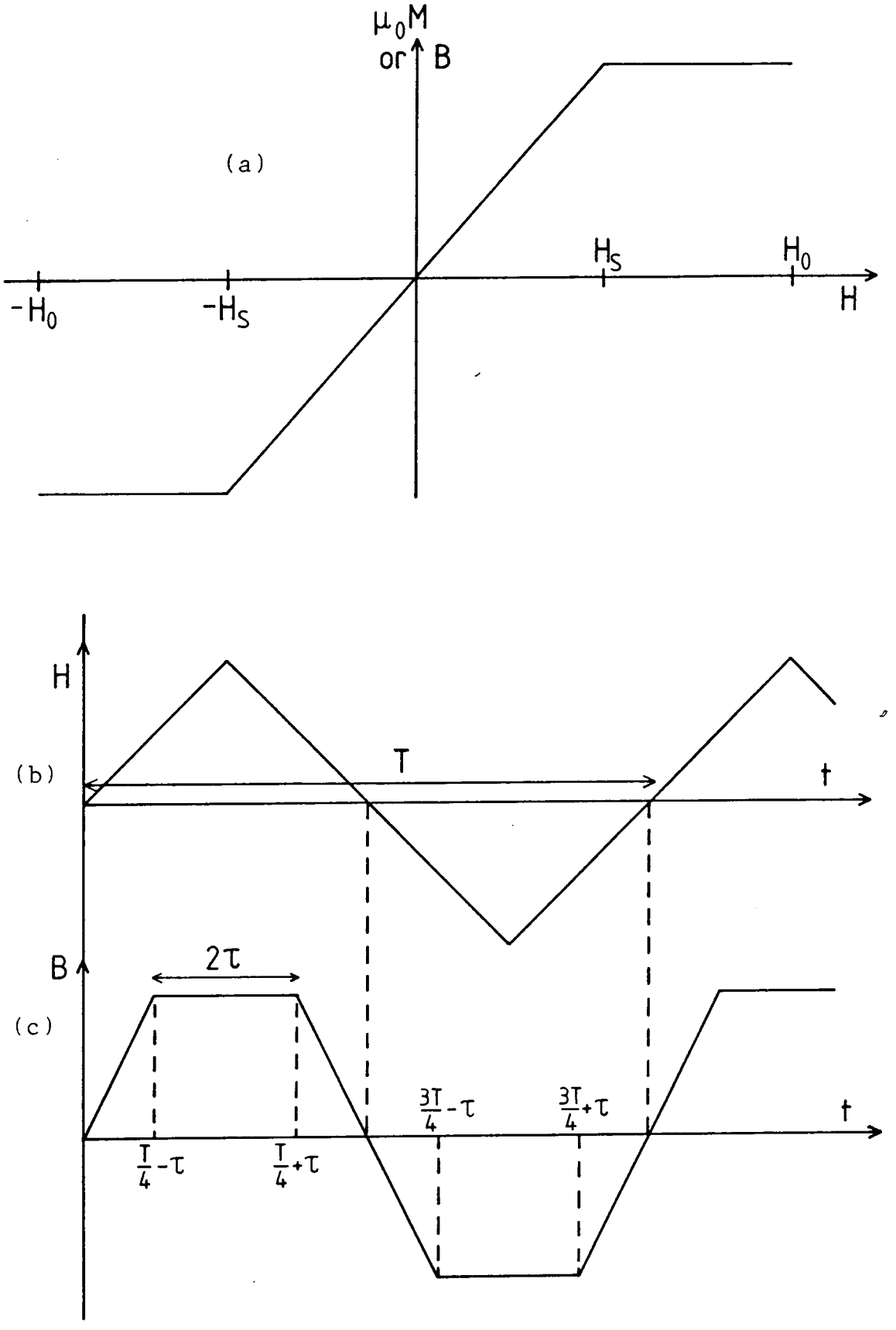

Figure 2.1 (a) Magnetization curve for zero coercivity model. (b) Triangular waveform of linearly ramped applied field. (c) Flux wave for zero coercivity model.

$$
\begin{aligned}
B(t) &= at && (0 \leq t \leq \frac{T}{4} - \tau) \\
&= a(\frac{T}{4} - \tau) && (\frac{T}{4} - \tau \leq t \leq \frac{T}{4} + \tau) \\
&= a(\frac{T}{2} - t) && (\frac{T}{4} + \tau \leq t \leq \frac{3T}{4} - \tau) \\
&= -a(\frac{T}{4} - \tau) && (\frac{3T}{4} - \tau \leq t \leq \frac{3T}{4} + \tau) \\
&= -a(T - t) && (\frac{3T}{4} + \tau \leq t \leq T)
\end{aligned} \qquad (2.2)
$$

where T is the time period of the flux wave, 2τ is the time spent at saturation each half cycle, and "a" is the gradient of the curve away from saturation.

Variation of the parameter τ reproduces the effect on the induction wave caused by changing the maximum amplitude of the driving field, and as τ is altered the parameter "a" must also change in order to ensure the same value of saturation induction B_s (or magnetization M_s).

Following Davis, the induction wave is expanded as a Fourier series

$$B(t) = B_{max} \sum_{n=1}^{\infty} A_n \sin(n\omega t + \phi_n) \qquad (2.3)$$

where A_n are the harmonic amplitudes and ϕ_n are the phase angles with respect to the applied field. This expansion is identical to

$$B(t) = B_{max} \sum_{n=1}^{\infty} (a_n \cos n\omega t + b_n \sin n\omega t) \qquad (2.4)$$

where $A_n^2 = a_n^2 + b_n^2$ and $\tan\phi_n = a_n/b_n$.

Standard Fourier analysis theory (Pain (1976)) gives

$$a_n = \frac{2}{T} \int_0^T B(t) \cos (2\pi nt/T)dt \qquad (2.5)$$

$$b_n = \frac{2}{T} \int_0^T B(t)\sin(2\pi nt/T)dt$$

where $T = \frac{2\pi}{\omega}$, the period of the waveform.

Substitution of equations (2.2) into (2.5) yields, after much manipulation, the following expressions for a_n and b_n:

$$a_n = 0 \text{ for all } n \qquad (2.6)$$

$$b_n = 0 \text{ for even } n \qquad (2.7)$$

$$b_n = \frac{8a}{T}\left(\frac{T}{2\pi n}\right)^2 (-1)^{\frac{n-1}{2}} \cos\left(\frac{2\pi n\tau}{T}\right) \text{ for odd } n \qquad (2.8)$$

Thus for the waveform of Figure 2.1(c) all cosine terms and all even powered harmonics of the sine terms are absent, as is the case for any symmetrical repetitive waveform. It must be noted that this absence of even powered harmonics was found experimentally in the harmonic analysis of sheet steels reported by Davis (1971). Also of note is that in the limit $\tau = 0$ and $a = \frac{2\pi}{T}$, (2.8) reduces to

$$b_n = \frac{4}{n^2\pi} (-1)^{(n-1)/2} \qquad (2.9)$$

the well-known Fourier coefficients for a triangular wave of unit amplitude and 45^o slope.

The changes in the odd harmonic amplitudes b_n as a function of τ, but constant B_s, are shown in Figure 2.2. Increasing τ corresponds to increasing H_{max} and hence driving the material further and further into saturation. Figure 2.2 demonstrates that the third harmonic amplitude shows very little change when the sample is driven into saturation for up to 10 percent of the cycle. The higher harmonics are much more sensitive and care must be taken to ensure identical driving field conditions if they are to be used for B-H loop characterization. The 5th, 7th and 9th harmonics are insensitive to saturation effects only up to 7 percent, 5 percent, and 2 percent of the cycle respectively. Thus for monitoring changes in the material introduced by external treatment, the 3rd harmonic is the most reliable parameter to monitor.

The existence of oscillations about zero in the higher order harmonic amplitudes has been observed experimentally and also considered analytically by Ponomarev (1983a,b). The oscillations shown here (Figure 2.2) to be a consequence of increasing the parameter τ are equivalently explained by Ponomarev as the result of a "Latitudinal Mechanism". This term relates to the change in width, as a function of drive field, of the e.m.f. pulse induced in the search coil(s) used to measure the material's flux. Ponomarev also considers a "Time Mechanism" as the reason for the appearance of oscillations, particularly in the even order harmonics, as a function of increasing d.c. field (not considered here). Here it is the relative time shifts of the e.m.f. pulses

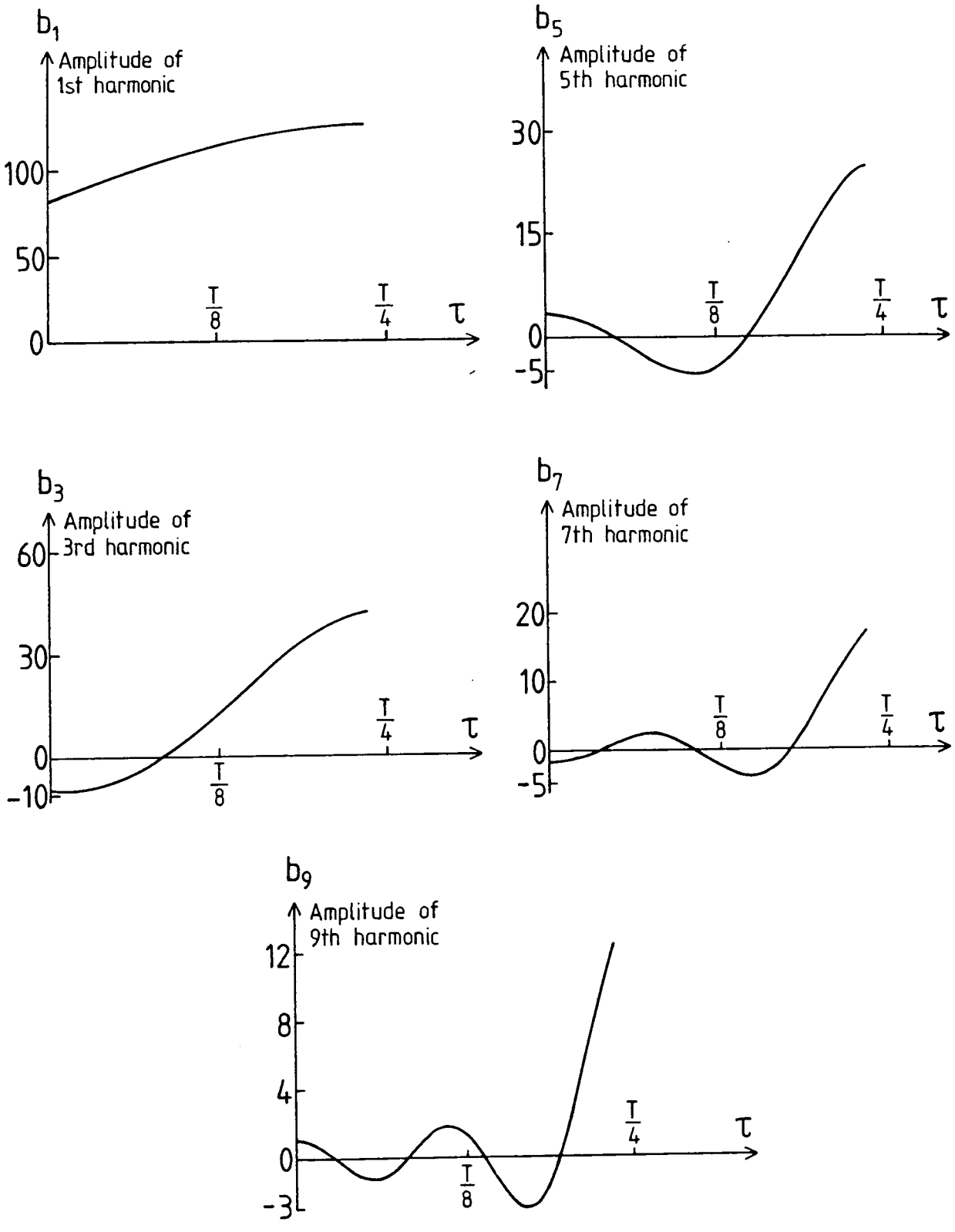

Figure 2.2 Predicted behaviour of odd powered harmonic amplitudes as amplitude of the applied field is increased.

resulting from the now asymmetric flux waveform which cause the oscillations to be present.

2.2(ii) Analytical model for non zero coercivity

The use of an idealized B-H loop such as shown in Figure 2.1(a) implies that the B(t) waveform is necessarily an odd function (if time zero is defined by H = 0 at t = 0). The step to a non-zero width loop, such as shown in Figure 2.3(a), results in a similar B(t) waveform, but displaced with respect to the time origin. This introduces cosine terms into the expressions for the Fourier components.

Under conditions of a linearly ramped field, the flux wave B(t) is as shown in Figure 2.3(c). Explicitly this is described as:

$$
\begin{aligned}
B(t) &= a(t - \delta) && (0 \leq t \leq \frac{T}{4} - \tau') \\
B(t) &= a(\frac{T}{4} - \tau' - \delta) && (\frac{T}{4} - \tau' \leq t \leq \frac{T}{4} + \tau' + 2\delta) \\
B(t) &= a(\frac{T}{2} + \delta - t) && (\frac{T}{4} + \tau' + 2\delta \leq t \leq \frac{3T}{4} - \tau') \\
B(t) &= -a(\frac{T}{4} - \tau' - \delta) && (\frac{3T}{4} - \tau' \leq t \leq \frac{3T}{4} + \tau' + 2\delta) \\
B(t) &= -a(T - t + \delta) && (\frac{3T}{4} + \tau' + 2\delta \leq t \leq T)
\end{aligned}
\qquad (2.10)
$$

where T is the time period of the flux wave, 2τ is the time spent at saturation each half-cycle, δ is a direct measure of the coercivity, "a" is the gradient of the curve away from saturation, and $\tau' = \tau - \delta$.

Substitution into (2.5) yields

$$a_n = 0 \qquad (2.11)$$

$$b_n = 0 \qquad (2.12)$$

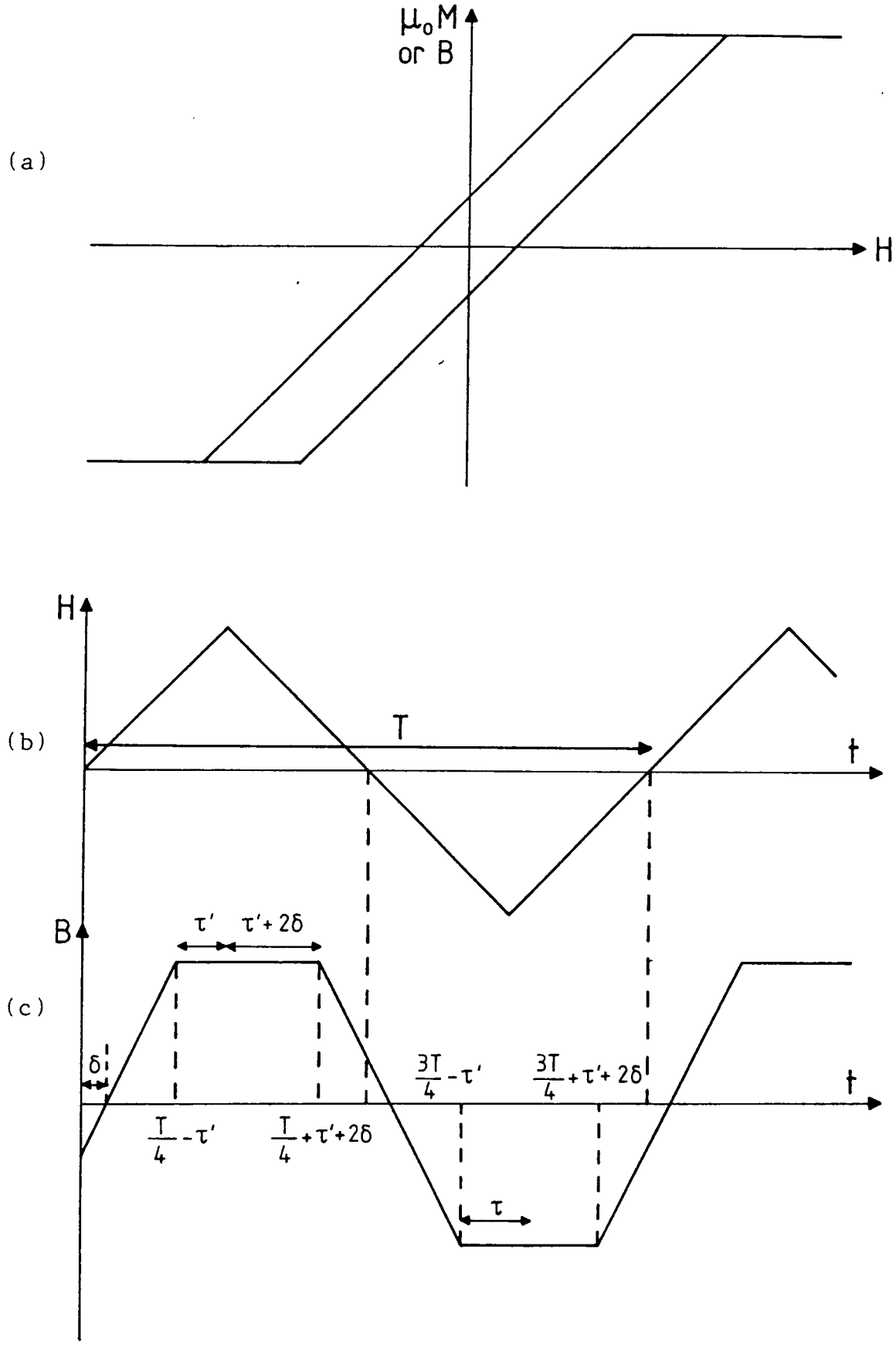

Figure 2.3 (a) Magnetization curve for nonzero coercivity model. (b) Triangular waveform of linearly ramped applied field. (c) Flux wave for nonzero coercivity model.

for all even n and

$$a_n = -\frac{8a}{T}\left(\frac{T}{2\pi n}\right)^2 (-1)^{\left(\frac{n-1}{2}\right)} \cos\left(\frac{2\pi n\tau}{T}\right) \sin\left(\frac{2\pi n\delta}{T}\right) \quad (2.13)$$

$$b_n = \frac{8a}{T}\left(\frac{T}{2\pi n}\right)^2 (-1)^{\left(\frac{n-1}{2}\right)} \cos\left(\frac{2\pi n\tau}{T}\right)\cos\left(\frac{2\pi n\delta}{T}\right) \quad (2.14)$$

for all odd n.

Inspection of equations (2.13) and (2.14) immediately reveals that for $\delta = 0$ equation (2.13) reduces to (2.6) and (2.14) reduces to (2.8). There is, therefore, consistency between the two models. For small values of $n\delta$, it is seen in particular that a_n is proportional to δ, that is the coercivity, and b_n is independent of δ to first order.

In Figure 2.4 the variation in both even (cosine) and odd (sine) terms for the odd ordered harmonics is shown as a function of coercivity for various values of drive field, but keeping B_s constant. Figure 2.4 demonstrates the relative insensitivity of the 1st and 3rd odd harmonic amplitudes to changes in coercivity of up to 10% of H_{max}. It also shows the near linear relationship between the 1st and 3rd even harmonic amplitudes and the coercivity (H_c) in this region. These observations are particularly true for the smaller drive fields (smaller values of τ) which are a more realistic representation of the drive fields used in many experimental situations. Note, for example, that with a value of τ equal to 0.25 x T/4 the test material will spend one quarter of the cycle time period at saturation, a fraction rarely exceeded

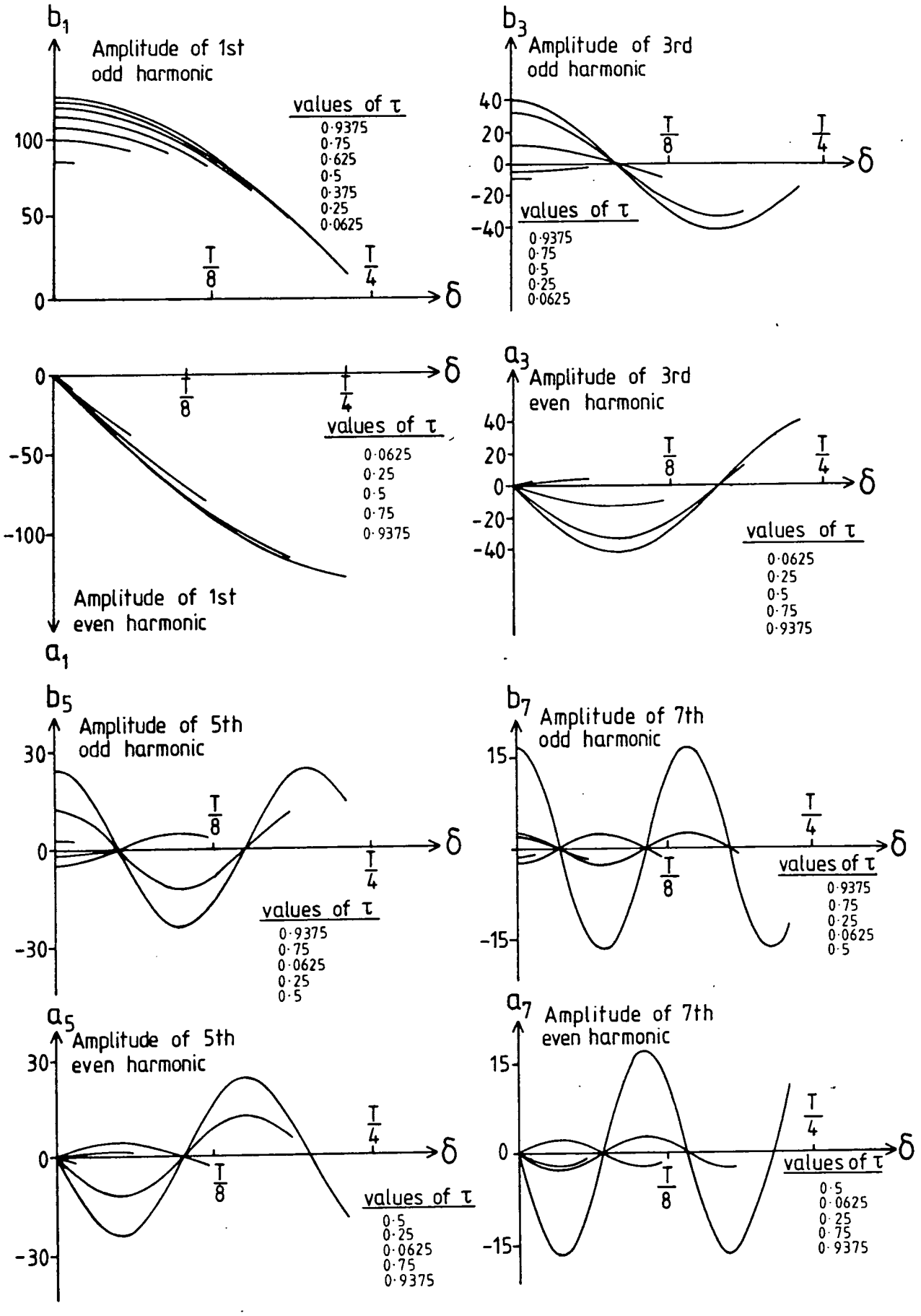

Figure 2.4 Predicted behaviour of even and odd terms for odd powered harmonics as coercivity is increased. Series of curves shown on each graph correspond to various values of the driving field which are listed in the order in which the curves cut the y axis.

in practical non-destructive testing applications.

In addition, it is noted that the behaviour of the 1st even harmonic amplitude with coercivity is largely unaffected by changes in the driving field, all the curves having approximately the same gradient. This harmonic amplitude is, therefore, the most reliable parameter to study when monitoring changes in the coercivity of a material.

In order to ascertain the affects on the harmonic amplitudes of changes in the remanence induction B_r, the same information needs to be presented in a different form. Figure 2.5 shows that for a fixed value of coercive field an increase in the driving field results in corresponding increases in both the gradient of the inclined region of the piecewise linear approximation and the value of B_r. By plotting the various harmonic amplitudes as a function of τ for various values of δ , therefore, the affects of a changing remanence induction can be assessed (see Figure 2.6). It can be seen that for small values of τ (and δ), the conditions normally prevalent for very soft magnetic materials (e.g. Mumetal* and high purity iron), there is a near linear relationship between the 1st odd harmonic and τ in this region. The even harmonics and higher order odd harmonics are seen to be largely independent of τ but, as noted in section 2.2(i), the limit to which such invariance extends decreases with increasing order. Under these conditions, therefore, the results suggest that changes in the main loop shape,

---

* Telcon Metals, Crawley.

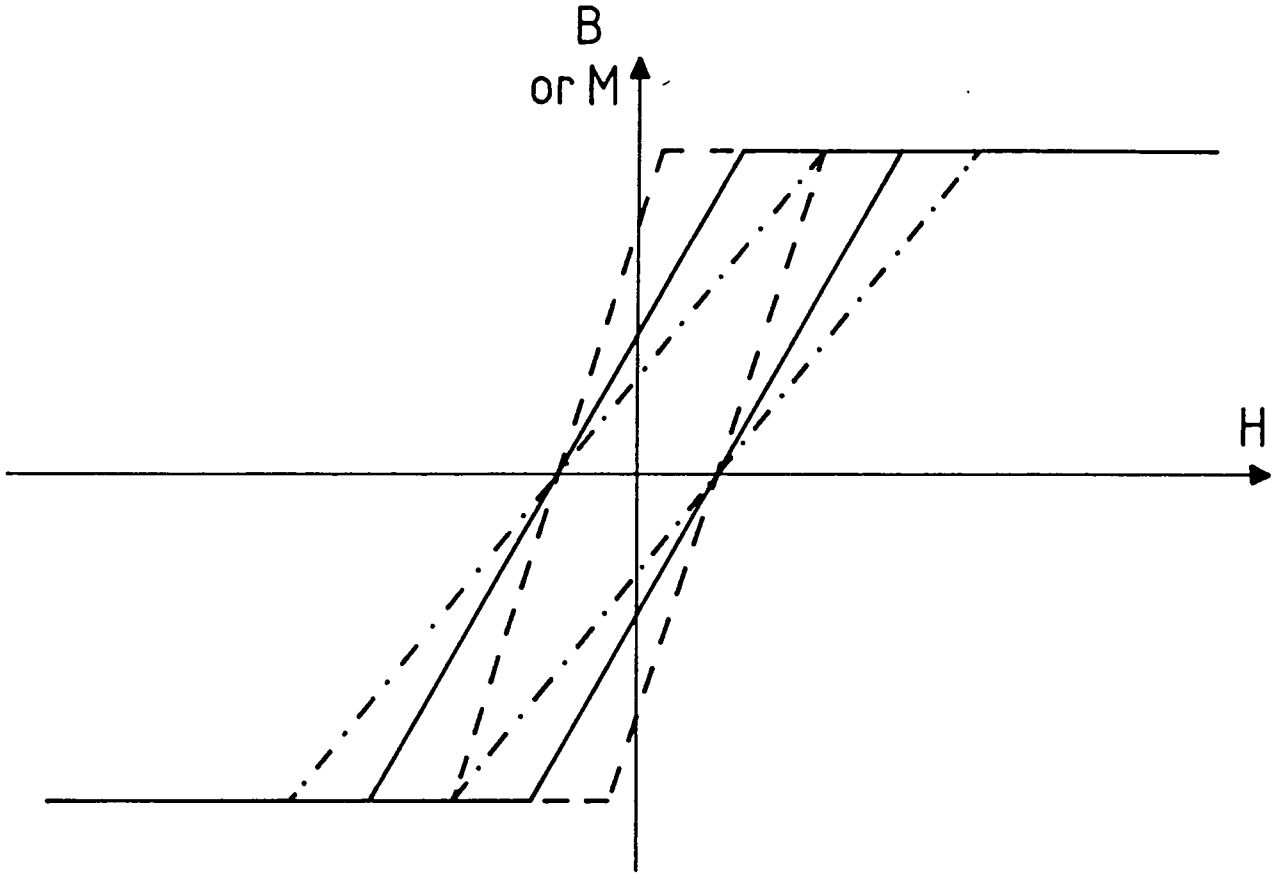

Figure 2.5 Illustration of direct relation between B_r and maximum differential permeability for a fixed value of coercive field.

that is in the gradient of the inclined region in the piecewise linear approximation, are reflected by proportional changes in the amplitude of the 1st odd harmonic, and any variations in the value of remanence induction B_r are then best studied using this parameter.

For the study of harder magnetic materials (e.g. pipe-steels and, in the limit, permanent magnet and magnetic tape materials) the values of τ and δ are increased in order to best represent the magnetization curves. For these conditions of large τ it can be seen that both 1st odd and 1st even harmonics are largely independent of τ while the higher order harmonics show regions of linear behaviour with τ depending on the value of τ prevalent for the particular material. The interpretation of the behaviour of the harmonic amplitudes from such materials, while more complex, is, therefore, still possible.

A particular example of this is the form of a major magnetization curve of pipe-steels as determined by a conventional yoke permeameter. Figure 2.7 shows such a B-H loop for a typical pipe-steel and reveals that, while it can be approximated by a small value of δ (≈ 0.15) the value of τ which produces the best fit is in the region of 0.8. By referring to the plots of Figure 2.6 it can be seen that the harmonic amplitudes which show the greatest change for such values of τ are the 5th and 7th power harmonics. Indeed, when the value of the parameter δ is also considered it is clear that the even order harmonic terms have a greater amplitude than the odd order harmonics for these particular powers

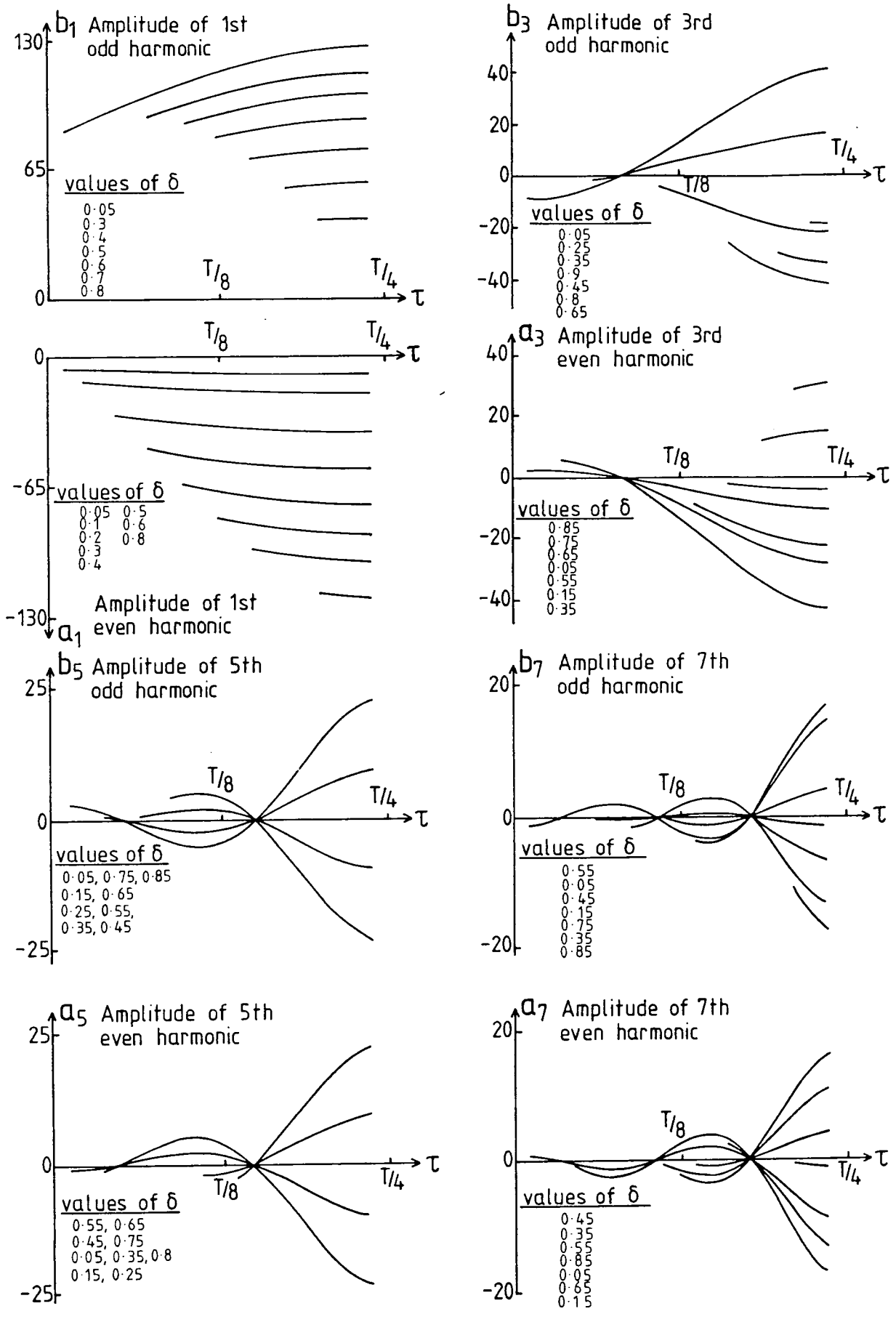

Figure 2.6 Predicted behaviour of even and odd terms for odd powered harmonics as driving field is increased. Series of curves shown on each graph correspond to the various values of coercivity which are listed in the order in which the curves cut line $x = T/4$.

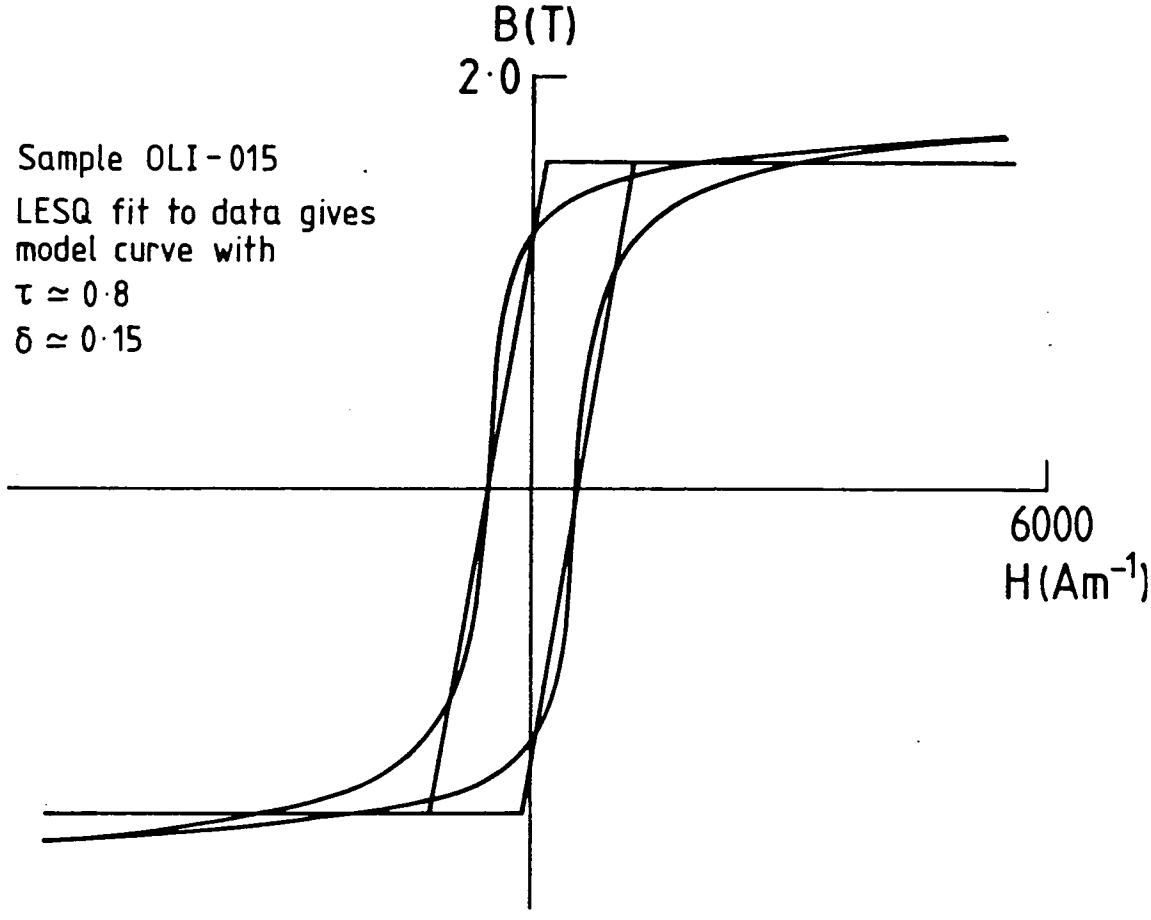

Figure 2.7 Full magnetization loop for a typical pipe steel (OLI-015) and the least squares best fit to this curve using the non-zero coercivity model.

This suggests, therefore, that small variations in the remanence induction, B_r, for these materials will be reflected by proportional changes in the 5th and 7th harmonic amplitudes, with the 7th even harmonic amplitude showing the greatest absolute sensitivity to such change.

2.3 Other models for the Magnetization Loop

Over the years many other models for a hysteresis loop function have been presented within the context of harmonic analysis mainly in the fields of magneto-modulation probes and electrical circuit analysis (see, for example, Mikhailovskii and Spektor (1957) and Rogachevskii and Shtamberger (1967)). These have been excellently presented in the recent review of the fundamental analytical calculations by Ponomarev (1983d).

In this article, analytical expressions for the piecewise linear model under triangular waveform field conditions are given which are equivalent to those presented here. Ponomarev presents the results in terms of amplitudes and relative phases for each component frequency rather than considering both even and odd terms as is the case here. As a result, some vital information such as the linear relationship between coercivity and 1st even harmonic amplitude is lost. He has, however, extended the analysis to include the effects on the harmonic amplitudes caused by the presence of a superimposed d.c. magnetic field (H_o) and shows how the 2nd harmonic amplitude, in particular, may be used to estimate the

d.c. field level. Results are also presented for both piecewise linear and arctangent approximations to the magnetization loop under sinusoidal field conditions. Whilst the latter model is potentially a more accurate representation, the expressions given for both approximations are so complex that the variables related to H_c, H_s and H_o cannot be obtained in separable form. Ponomarev points out that it is, therefore, extremely difficult to understand the physical meaning of his results.

2.4 Reconstruction of B-H loops from Harmonic Information

A study of the harmonic content of a series of B-H loops, obtained from a test material whose magnetic properties are changing, does not give a clear indication as to which harmonics, if any, are responsible for the shape of the various regions of the B-H loop. An alteration in loop shape affects the amplitude of all the harmonics simultaneously and, although the magnitude of the amplitude changes may be different for each harmonic, it is extremely difficult to attribute a shape change in a particular region of the loop to a specific harmonic.

Ponomarev (1983d) considered this problem, but the lack of computational facilities obviously forced him to state that "the transition from discrete spectra of magnetization to the remagnetization curve is difficult to put into practice". The availability of a microcomputer here, however, has allowed this problem to be investigated

by digitally reconstructing B-H loops from harmonic amplitude and phase information. The loops were calculated and plotted using a 4032 Commodore PET microcomputer, a Bede Scientific Instruments MINICAM interface and an X-Y recorder. The amplitude of a particular harmonic was altered independently of the others and the effect on the loop shape was observed.

The initial harmonic amplitude and phase values used were obtained from the analysis of a typical B-H loop using a technique described in Chapter 3. No amplitude or phase information above the 9th order was included in the calculation. The amplitude of the 3rd harmonic was then reduced from its initial value to zero in ten equal steps giving a series of eleven B-H loops (Figure 2.8). This procedure was repeated for the 5th and 7th harmonics (Figures 2.9 and 2.10). The phase angles (ϕ_n) were kept unaltered thus explaining the constant separation between the forward and return paths on all the B-H loops.

Figure 2.8 demonstrates that variation of the 3rd harmonic amplitude causes a shortening of the high gradient region of the loop, but most distortion occurs in the region just above the "knee". Alterations of the 5th and 7th harmonic amplitudes increase the length of the high gradient region slightly, but significant distortion also occurs far into saturation. For all the loops the general form of the loop is seen to be largely unaffected by the enforced changes in harmonic content, although changes in the gradient of the high gradient region are observed.

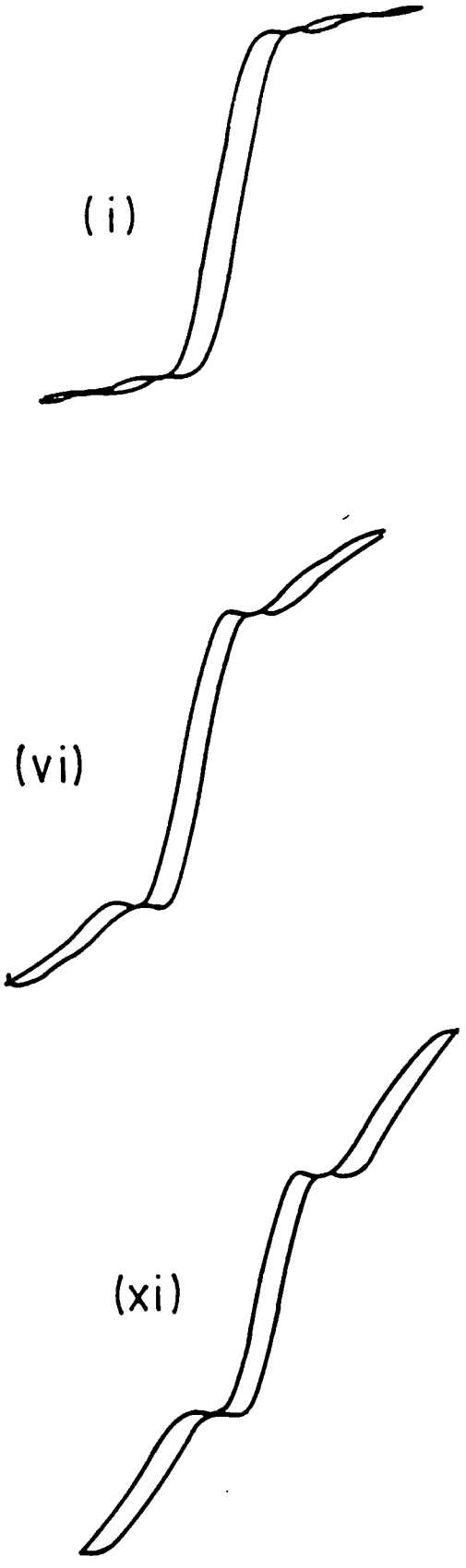

Figure 2.8 Three of the eleven hysteresis loops showing effect on loop shape caused by decreasing third harmonic amplitude. (i) Original curve, (vi), (xi) 50 percent and 100 percent of this amplitude removed, respectively.

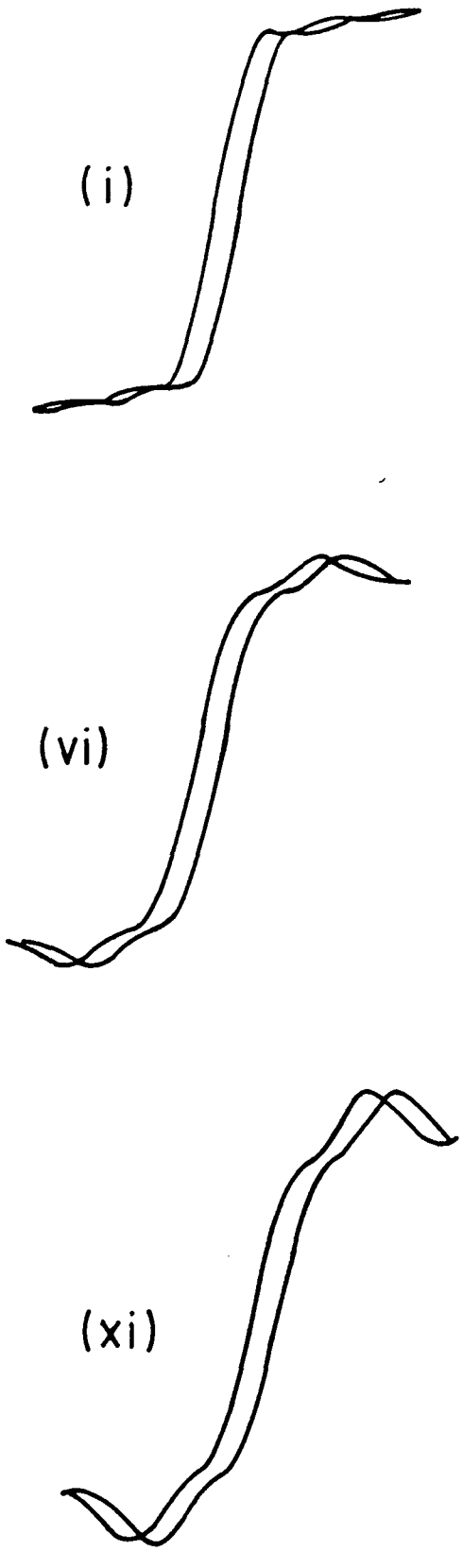

Figure 2.9 Effect on loop shape caused by decreasing fifth harmonic amplitude.

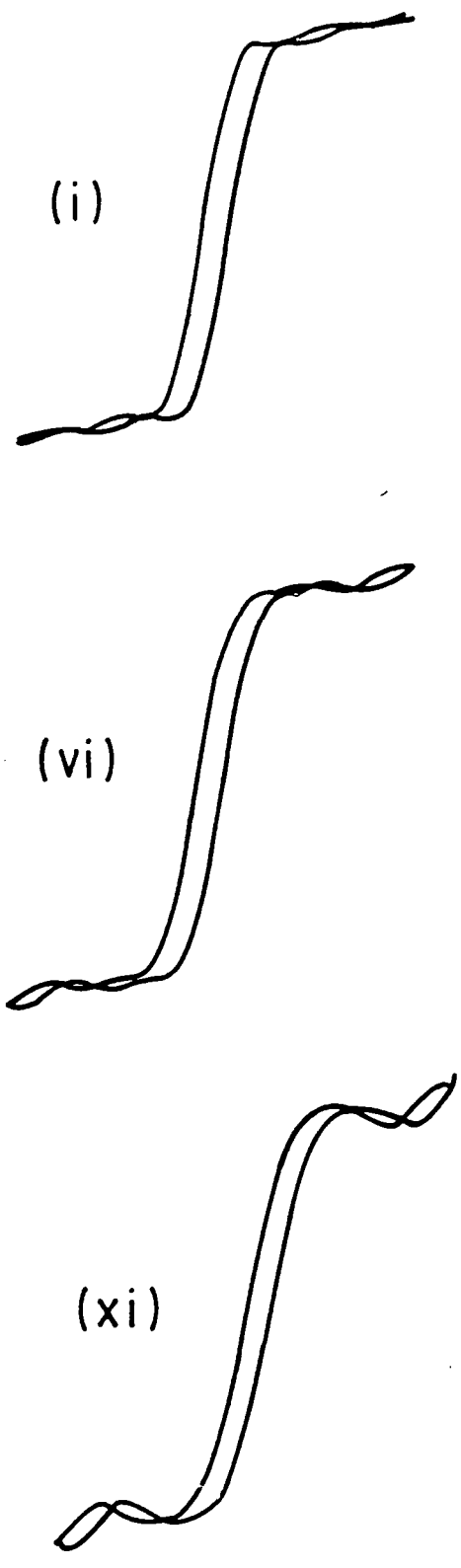

Figure 2.10 Effect on loop shape caused by decreasing seventh harmonic amplitude.

It is well known that the shape of the region around the "knee" of the B-H loop is determined by the irreversible domain wall movement in the material, and the above results suggest that the amplitude of the 3rd harmonic should be the parameter most sensitive to changes in these mechanisms. In a similar way the 5th, 7th and higher harmonics should be sensitive to changes in the magnetization rotation processes in the material.

It is noted that the 3rd harmonic amplitude has much less influence on the saturation region than the 5th, 7th and higher harmonics. This observation agrees with the findings of section 2.2(i) where it was deduced that the 3rd harmonic amplitude is the least sensitive to changes in the degree of saturation in the induction waveform. The increase in the length of the high gradient region, observed when the 5th and 7th harmonic amplitudes were altered, also confirms the findings of section 2.2(ii) where it was suggested that "small variations in the remanence induction, B_r, for these materials will be reflected by proportional changes in the 5th and 7th harmonic amplitudes". The relative invariance of the general loop form is explained by the use throughout of a constant value for the 1st odd harmonic amplitude. Earlier findings also show that any reduction in this parameter would significantly reduce the value of the parameter τ and hence the maximum differential permeability.

2.5 Conclusion

From the analytical models the experimental conditions necessary to obtain reliable harmonic parameterization of B-H loops from ferromagnetic material have been established. Considerable care must be taken concerning the degree of drive into saturation as this can seriously distort the values obtained particularly for the higher order harmonics. For a material exhibiting saturation for up to 10% of the magnetization cycle, however, the 3rd harmonic amplitude remains almost independent of the time spent in saturation. For non-destructive testing applications, therefore, it suggests that the 3rd order odd harmonic and the 1st order even and odd harmonics (proportional to coercivity and maximum differential permeability) are the most reliable parameters to study. Of all the harmonic components these are the most sensitive to material characteristics and least sensitive to experimental conditions.

CHAPTER 3

PRACTICAL APPLICATIONS OF HARMONIC ANALYSIS TECHNIQUES

3.1 Analysis of B-H loops taken from an X-Y plot

3.1(i) Introduction and experimental technique

While the introduction of a linearly ramped applied field, as considered in the previous chapter, involves some nonmaterial related harmonic content, the results presented therein may be applied directly to plotted B-H loops. If such a loop (Figure 3.1(a)) is "unfolded" at its extremes and the reverse magnetization path is mapped forward, the resulting waveform is the induction waveform of the material that would have been observed under ramped field conditions (Figure 3.1(b)), since the equivalence of the field and time axis implies a triangular field-time waveform.

In order to assess rapidly the value of harmonic analysis as an analytical technique without recourse to experiment, therefore, this approach was adopted for a series of B-H loops recorded from a single steel specimen undergoing significant physical change. The flux waveform B(t) was recovered from the pen-recorded loops by using a light pen on the carriage of an X-Y plotter, both being interfaced to a 4032 Commodore PET microcomputer (after Blackburn and Smith (1981)). The interface used was the modular MINICAM system (Bede Scientific Instruments, Durham) exploiting one ADC and two DAC channels of the many modules available. The B-H loops, placed on the

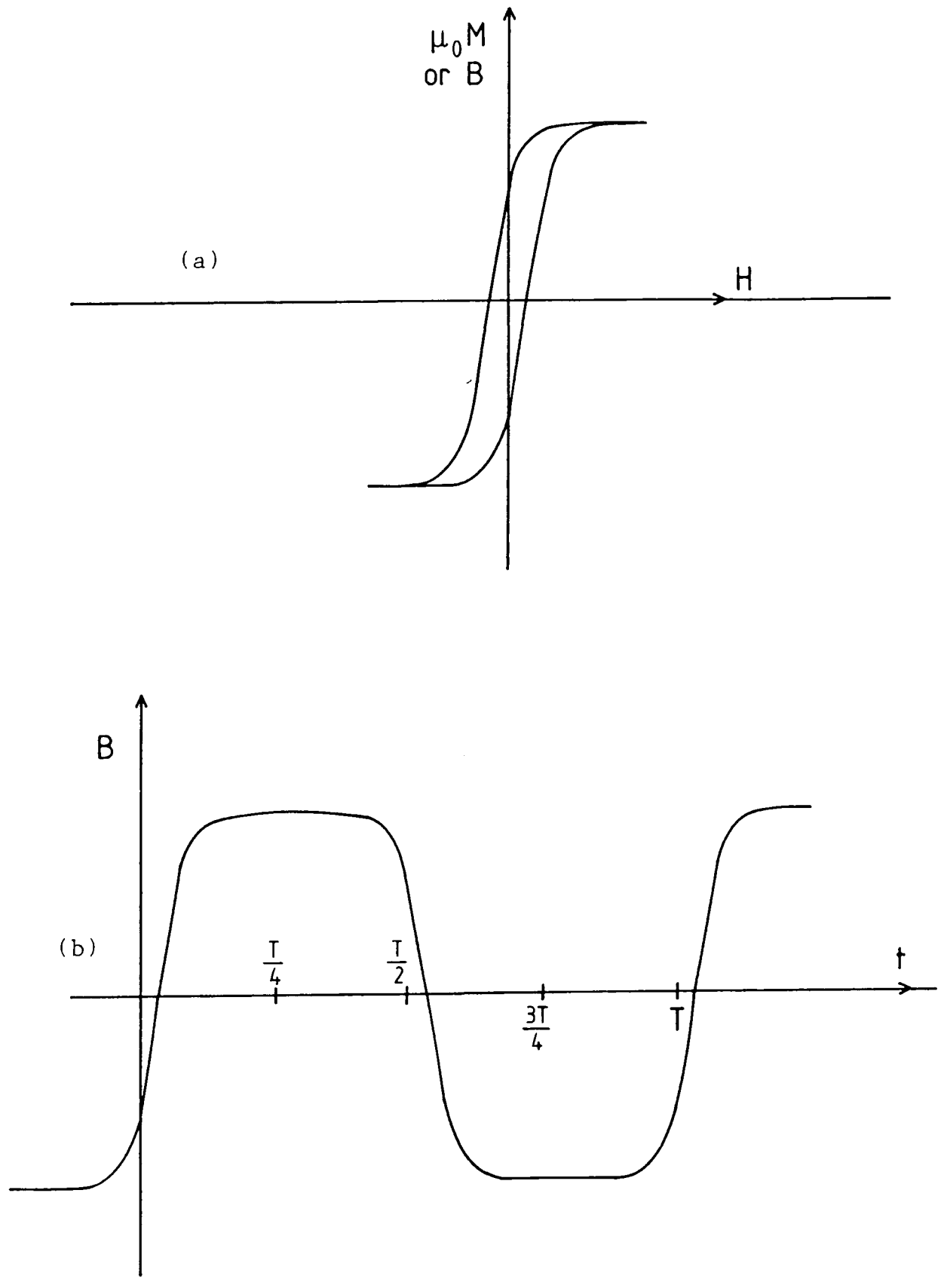

Figure 3.1 (a) Typical hysteresis loop for high permeability material. (b) Induction waveform obtained from the hysteresis loop assuming linearly ramped applied field.

bed of the X-Y plotter, were scanned by the light pen (which incorporated its own light source and detector) under computer control via the DAC channels. The pen detector output was constantly monitored via the ADC channel until, on crossing the B-H line, the output changed abruptly due to the scattering of light by the ink line.

Starting above the extreme right hand limit of the B-H loop, the pen was Y scanned until the ADC signal went low (Figure 3.2(a)). The computer recorded the X-Y coordinates of the light pen, backed it off from the line and incremented the X position. This pattern was repeated until the end of the curve was detected by interpolation (Figure 3.2(b)), at which point the pen's movements were reversed and the lower section of the loop digitized. Once digitized, the determination of the induction wave and the Fourier analysis of the same was then trivial. All software was written in BASIC (see Appendix A).

The internal consistency of the digitization and Fourier analysis of the resulting waveform was tested using a model B-H loop of the form considered in Chapter 2. Digitization of the loop (Figure 3.3(a)) yielded harmonics in very good agreement with those obtained analytically (see Table 3.1). By way of a further check, use was made of these coefficients (up to 10th order) to regenerate the B-H loop and a very satisfactory reproduction of the original was obtained (Figure 3.3(b)).

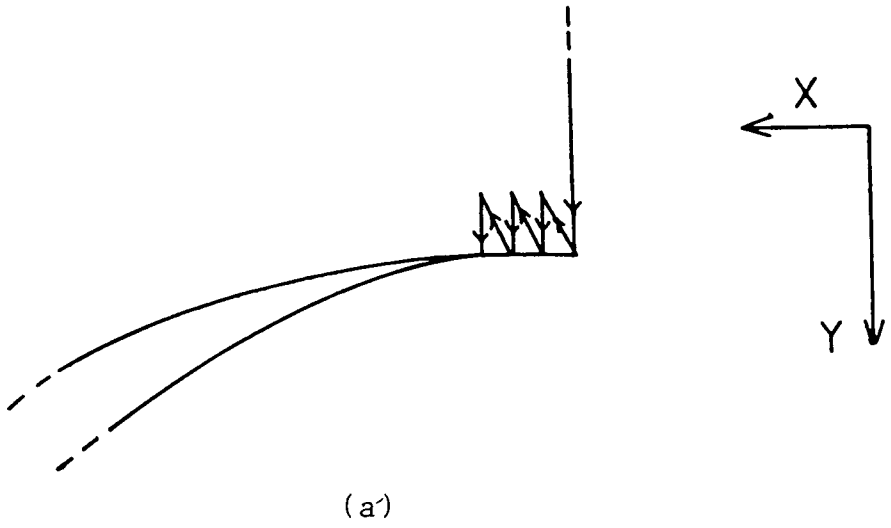

(a)

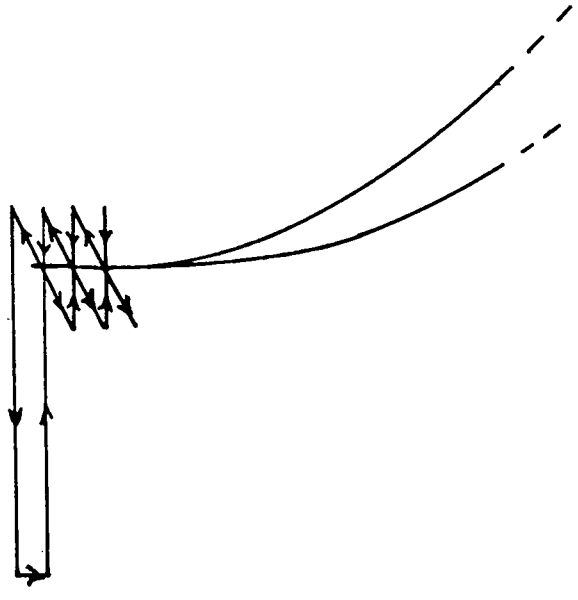

(b)

Figure 3.2 Illustration of path traced by light pen when digitizing hysteresis loop. (a) at start of digitization run, (b) half way through run.

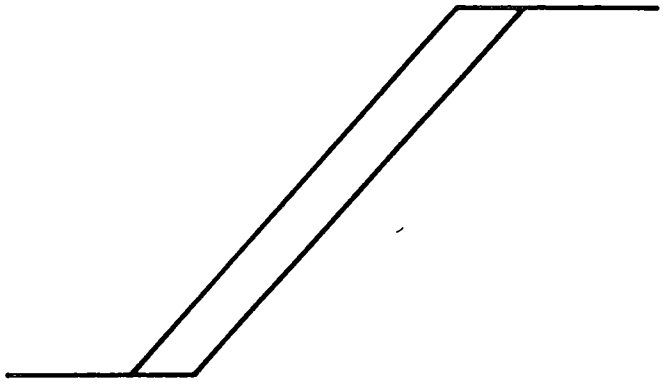

(a)

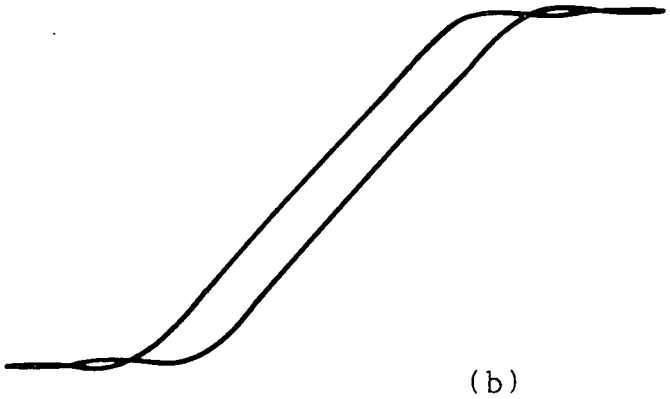

(b)

Figure 3.3 (a) Model B-H loop which permits analytical solution, (b) B-H loop reconstructed using Fourier components obtained from analysis of light pen digitization of (a).

Harmonic	Theory		Experiment	
	Odd	Even	Odd	Even
1st	99.33	-15.73	98.83	-15.25
3rd	9.95	- 5.07	10.16	- 5.33
5th	-2.84	2.84	-2.79	2.86
7th	-0.932	1.83	-0.937	1.86
9th	0.194	-1.23	0.164	-1.10

Table 3.1

Comparison of theoretical and experimentally determined harmonic amplitudes for a model B-H loop

3.1(ii) Experimental results

Once satisfied by the effectiveness of the technique, the series of B-H loops chosen to be studied in this way were of renormalized BS4360 (1979) 50D constructional steel undergoing plastic deformation. These B-H loops, which have been reported elsewhere (Anderson (1980)), revealed significant changes in loop shape during plastic deformation, together with a monotonic decrease in the remanence induction B_r and an increase in the coercive field H_c (see, for example, Figures 3.4(a) and (b)). They were, therefore, considered an ideal test to assess the value of harmonic analysis as an analytical technique.

The B-H loops, taken up to a uniform plastic strain of 8.5%, were analysed for harmonic components up to the 10th power. The variation of the odd order odd power harmonics with plastic deformation is shown in Figure 3.5 (see also Willcock and Tanner (1983(b)). Both first (Figure 3.5(a)) and third (Figure 3.5(b)) odd order harmonics decrease monotonically with strain. The higher order harmonics (Figure 3.5(c)) decrease initially and change sign at a value of strain which decreases with increasing harmonic power. The seventh and ninth harmonics subsequently increase again at higher strain levels. All even power odd order harmonics were found to be absent, in agreement with the predictions of the analytical models presented in Chapter 2. From these model calculations the decrease in first and third odd harmonic amplitudes can be ascribed to a decrease in B_{max} and B_r respectively. Both trends indicate that the time spent in saturation

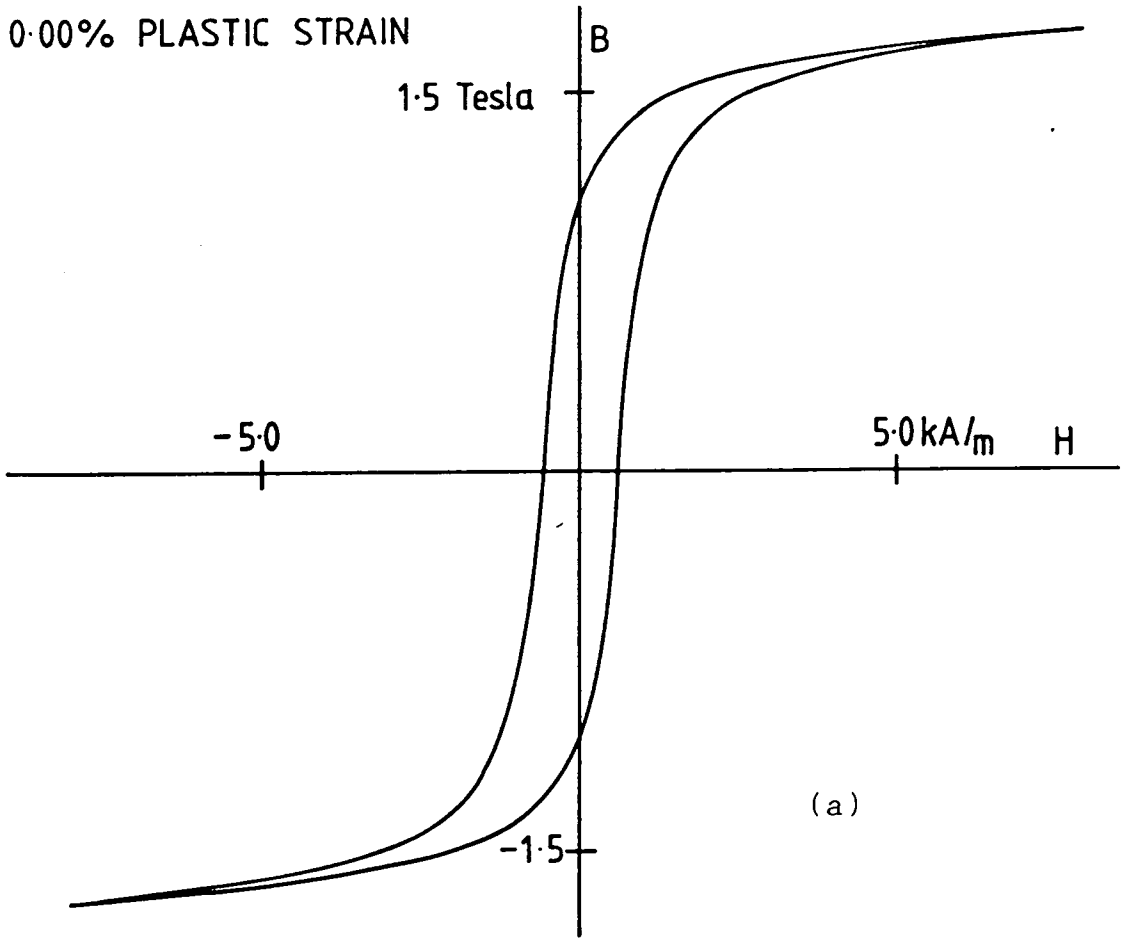

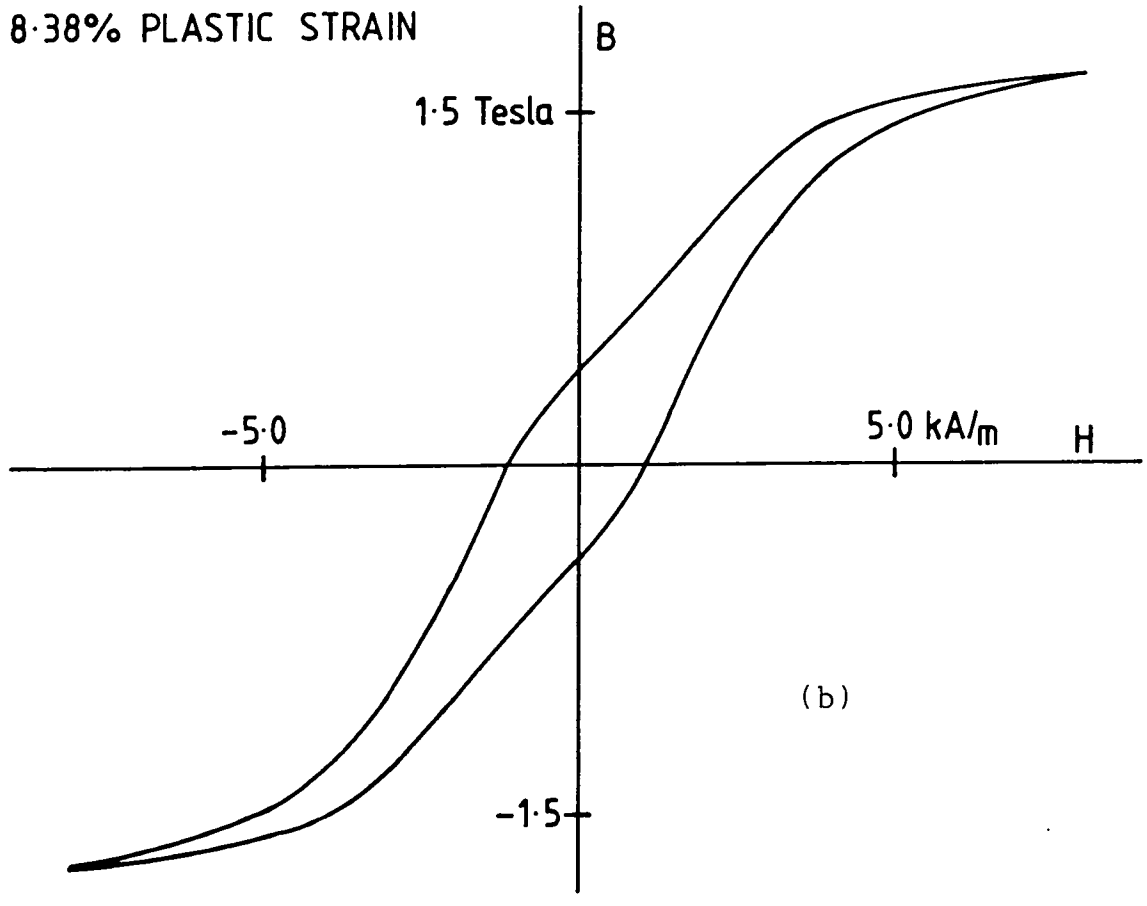

Figure 3.4 B-H loop of sample of 50D steel, (a) before, and (b) after plastic deformation.

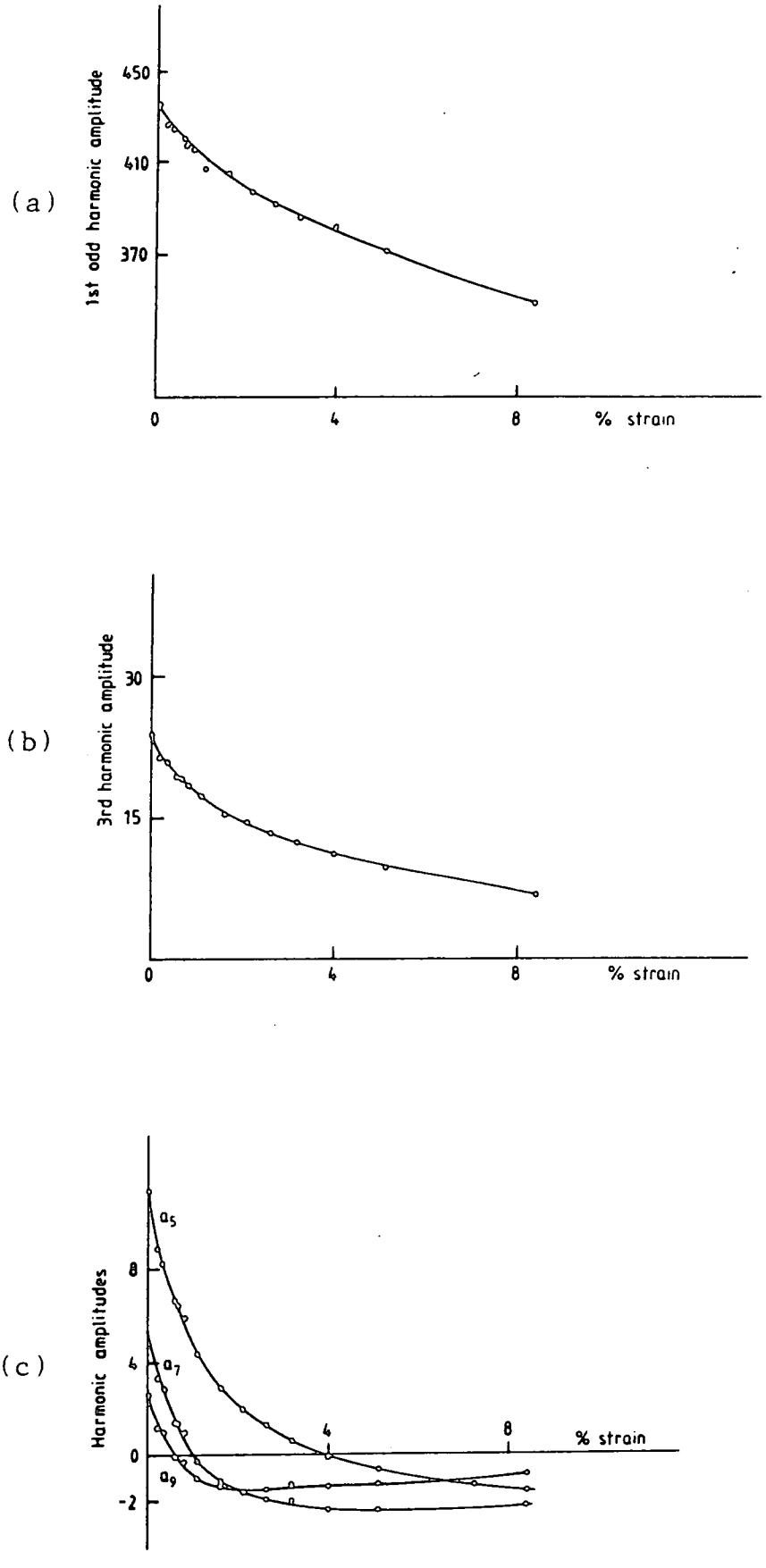

Figure 3.5 Variation of odd order harmonic amplitudes with strain. (a) 1st, (b) 3rd, (c) 5th, 7th and 9th.

is becoming less, thus leading to the rounding of the B-H loop which is observed qualitatively (Anderson (1980)). Although the higher power terms have been shown to predominantly govern the approach to saturation, by referring to the results presented in Chapter 2 of this thesis it can be seen that the observed change in sign of these harmonics can only arise from a significant increase in the coercive field H_c because there is no observed change in the sign of the even order harmonics.

A significant rise in H_c is indeed observed (Figure 3.6) and this is reflected in an equivalent increase in the magnitude of the first power even harmonic. The analytical model predicts that, for constant differential permeability, the first even harmonic amplitude is proportional to the coercivity and, although the absolute magnitude of the change in harmonic amplitude is lower than predicted due to the shearing of the loop, the overall trend is as expected. Figure 3.7 shows, for completeness, the behaviour of the higher even order harmonics, all of which show a monotonic decrease with strain. By recombining the data presented here (Figures 3.5 - 3.7) it is possible to reconstruct the B-H loops at any point in the deformation process, as demonstrated above.

By way of a contrast, Tables 3.2 and 3.3 show the behaviour of the harmonic amplitudes of samples of the same steel before and after annealing and fatigue testing. Annealing of the 50D steel led to a visible squaring of the B-H loop with little change in H_c. This was revealed by significant increases in the 3rd, 5th, 7th

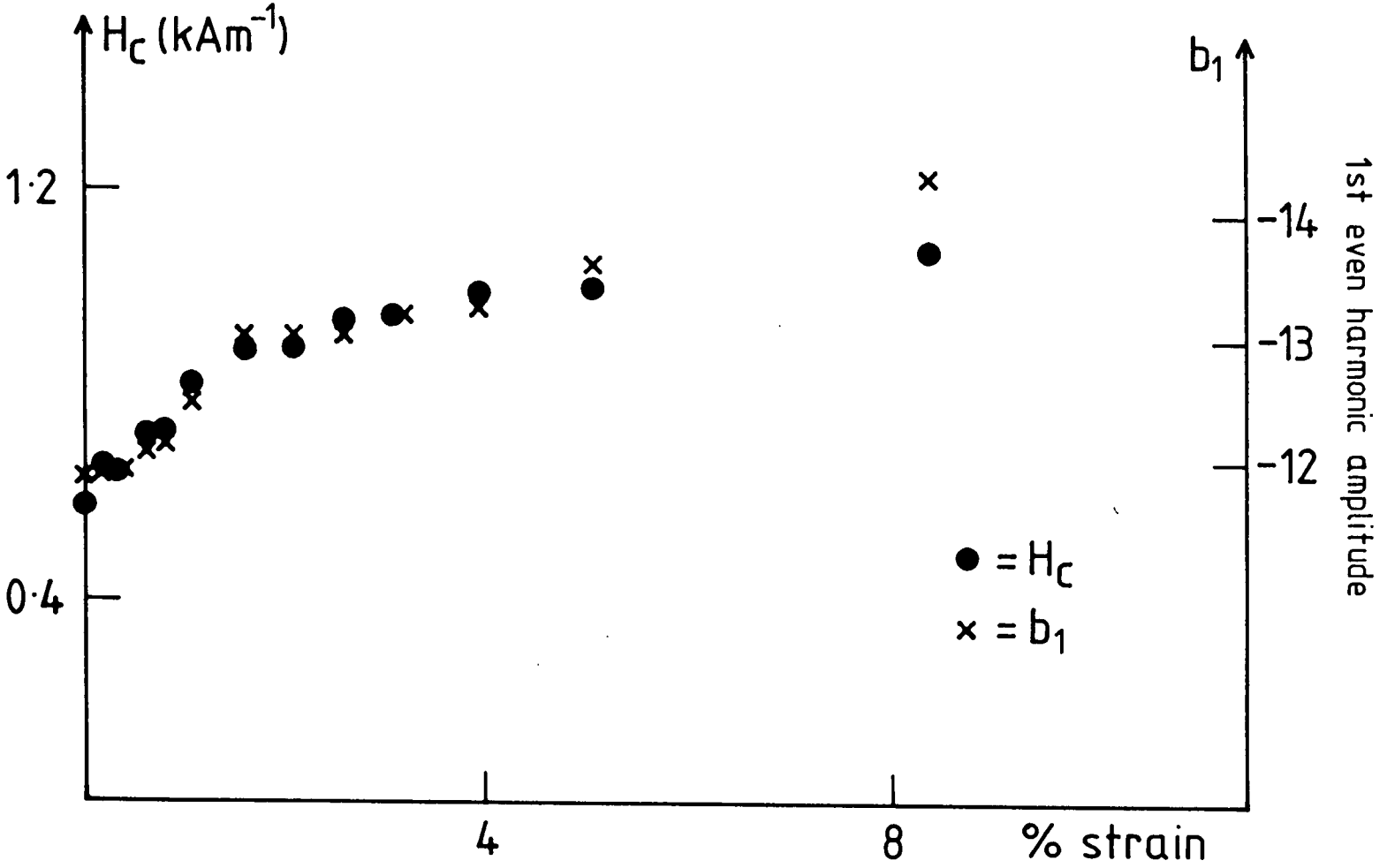

Figure 3.6 Variation of coercivity (solid circles) and 1st even order harmonic amplitude (crosses) with strain.

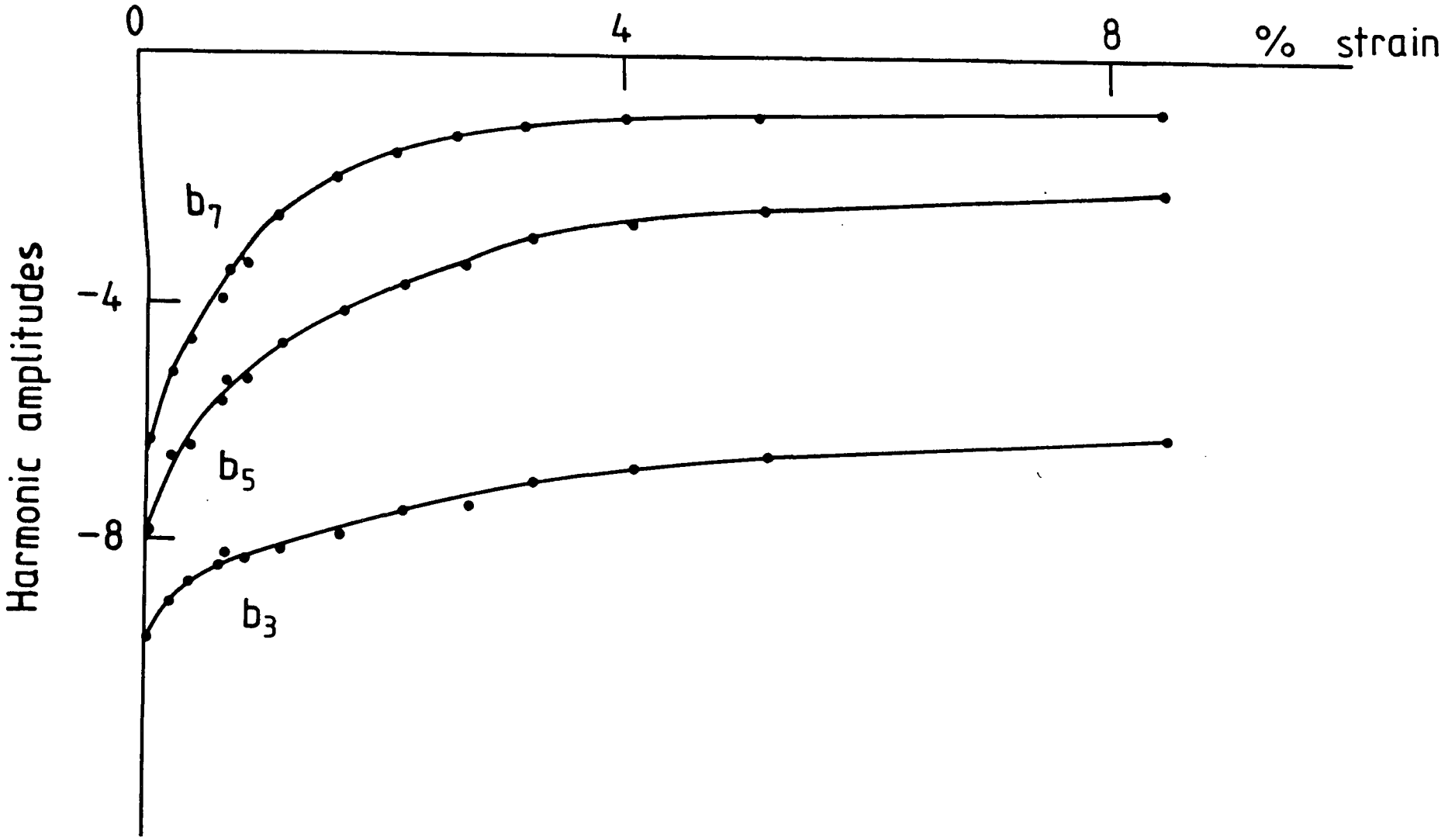

Figure 3.7 Variation of 3rd, 5th and 7th even order harmonics with strain.

Harmonic	As received		After annealing		% change	
	Odd	Even	Odd	Even	Odd	Even
1st	99.3	-12.2	99.3	-11.7	0.0	- 4.0
3rd	24.2	- 9.6	26.6	-10.3	10.0	6.8
5th	11.4	- 7.9	13.4	- 8.8	17.2	10.9
7th	5.3	- 6.3	7.1	- 7.6	32.4	19.4
9th	2.6	- 5.0	3.9	- 6.1	47.5	22.8

Table 3.2

Changes in harmonic amplitudes as a consequence of sample annealing

Harmonic	0 cycles		3.85×10^5 cycles		% change	
	Odd	Even	Odd	Even	Odd	Even
1st	99.3	-12.2	99.1	-13.7	- 0.2	12.4
3rd	22.7	- 9.7	20.0	- 9.9	-11.6	2.9
5th	10.0	- 7.1	7.8	- 6.9	-22.3	- 3.2
7th	4.2	- 5.4	2.5	- 4.9	-40.8	- 9.9
9th	1.9	- 3.8	0.7	- 3.3	-61.8	-13.7

Table 3.3

Changes in harmonic amplitudes as a result of sample fatiguing

and 9th harmonics (Table 3.2).

The fatigue test samples were taken from the body of the steel and also from the heat affected zone (HAZ) of a weld region. For the plain fatigue sample from the bulk steel, no change in harmonic amplitudes or crossing-point parameters was found up to failure just above 7.65 x 10^5 cycles. In the weld fatigue sample, however, visible rounding of the B-H loop occurred just prior to failure at 3.8 x 10^5 cycles, with a significant decrease in B_r and increase in H_c. Similarly significant reductions in the odd power odd ordered harmonics and a large increase in the first even harmonic were found (Table 3.3). All even power harmonics were again absent.

3.1(iii) Conclusions

The harmonic analysis of B-H loops taken during the plastic deformation of 50D constructional steel has verified that associations identified using an idealized analytical model occur in a practical experimental situation. The variation in crossing-point parameters and qualitative changes in loop shape observed (Anderson (1980)) have been related to quantitative changes in harmonic amplitude. The shearing of the B-H loop during plastic deformation is accompanied by a monotonic decrease in first, third and fifth odd order harmonics, while an increase in coercive field with strain is detected by an increasing first even order harmonic amplitude and a change of sign in the higher power odd order harmonics. Similar trends were observed for both annealed and fatigued samples.

It is concluded, therefore, that harmonic analysis provides a valuable and meaningful method for the paramaterization of B-H loops that is particularly well suited to a real time inspection environment. It is readily adapted to automated data collection and permits the reconstruction of the conventional B-H loop at any point.

3.2 B-H loop studies of pipe steels

3.2(i) Description of apparatus

Encouraged by the results obtained from 50D steel, it was decided to collect B-H loop and initial magnetization curve data from samples of all pipe steels relevant to the gas industry. As part of the collaboration between the OLIC, Cramlington and the Physics group at Durham, therefore, a project was devised such that the data would be collected from a magnetic permeameter at OLIC and subsequently transferred to Durham for analysis.

The permeameter used for these studies was a conventional yoke permeameter with a closed magnetic circuit designed to reduce demagnetizing factors to zero by eliminating air gaps (Figure 3.8). The technique used to measure the B-H loop or initial magnetization curve is essentially that given in BS5884 (Determination of Magnetic Properties of Magnetic Materials). The applied field in the bar shaped sample is estimated by a Hall-effect probe placed adjacent to the sample surface, and the magnetic induction in the bar is measured by integrating the emf from a tight fitting multi-turn coil wrapped around it. The

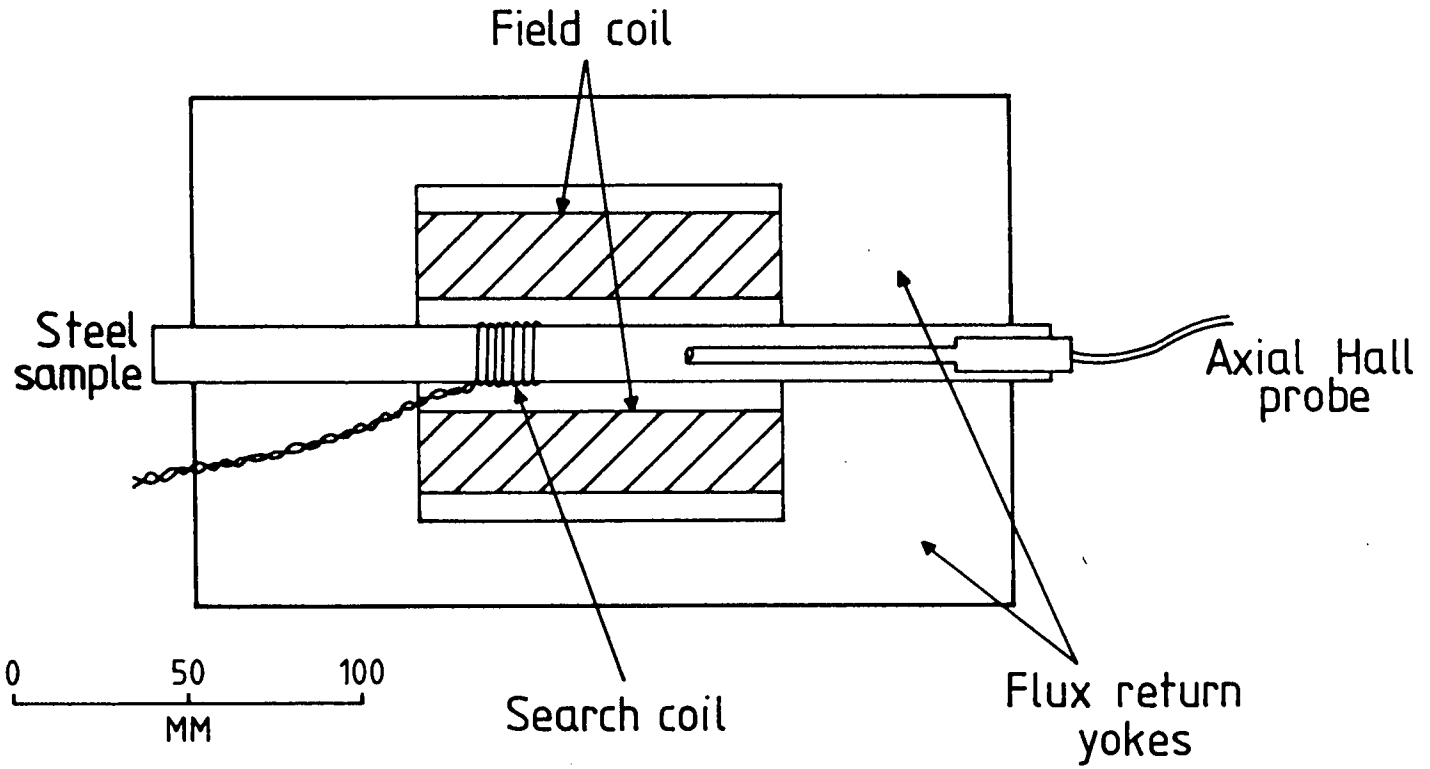

Figure 3.8 Illustration of magnetic yoke permeameter design as used for the determination of the magnetic characteristics of bar shaped steel samples.

applied field, which can be varied from 0 to 40,000 Am^{-1}, is provided by a long solenoid, the axis of which is coincident with the central line of the bar sample. The current supplied to this coil is derived from a voltage programmable power supply operated in constant current mode. The entire apparatus is controlled remotely by a M.I.N.C. mini-computer which uses analogue to digital and digital to analogue converters (ADC's and DAC's) to monitor the output of both gaussmeter and integrating voltmeter as well as providing the necessary input to the power supply (Figure 3.9). The software required to control the current ramping cycle, and hence the experiment, is written in BASIC (see Appendix B), and all data thus obtained is stored directly on floppy disc.

A typical B-H loop study of an initially demagnetized steel sample consisted of 200 pairs of magnetic induction and field values up to a fixed maximum field of 5650 ± 50 Am^{-1} (see, for example, Figure 3.10). This point density was considered necessary if subsequent harmonic analysis of the data up to and including 10th order was to be meaningful. Consequently a lengthy run time of approximately 45 minutes was required which resulted in problems caused by the irregular drift in the signal recorded by the integrating amplifier over such time scales. For short time intervals, however, the drift could be well represented by a linear function and, by taking three readings of the magnetic induction at consecutive half cycles of the loop in quick succession (e.g. B_1 B_1' and B_1'' as shown in Figure 3.11), the effects

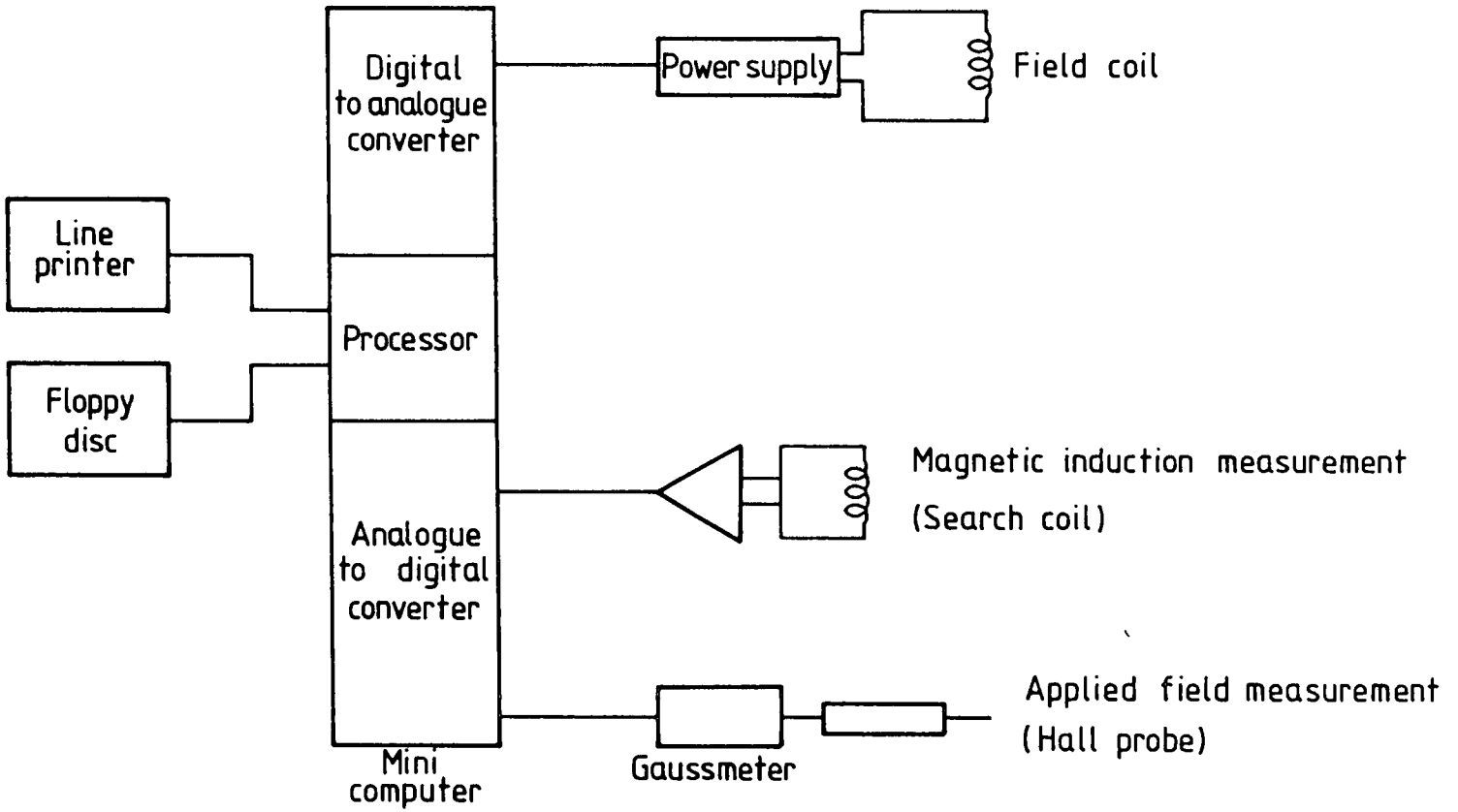

Figure 3.9 Representation of entire apparatus required for the automatic determination of magnetic characteristics using the yoke permeameter.

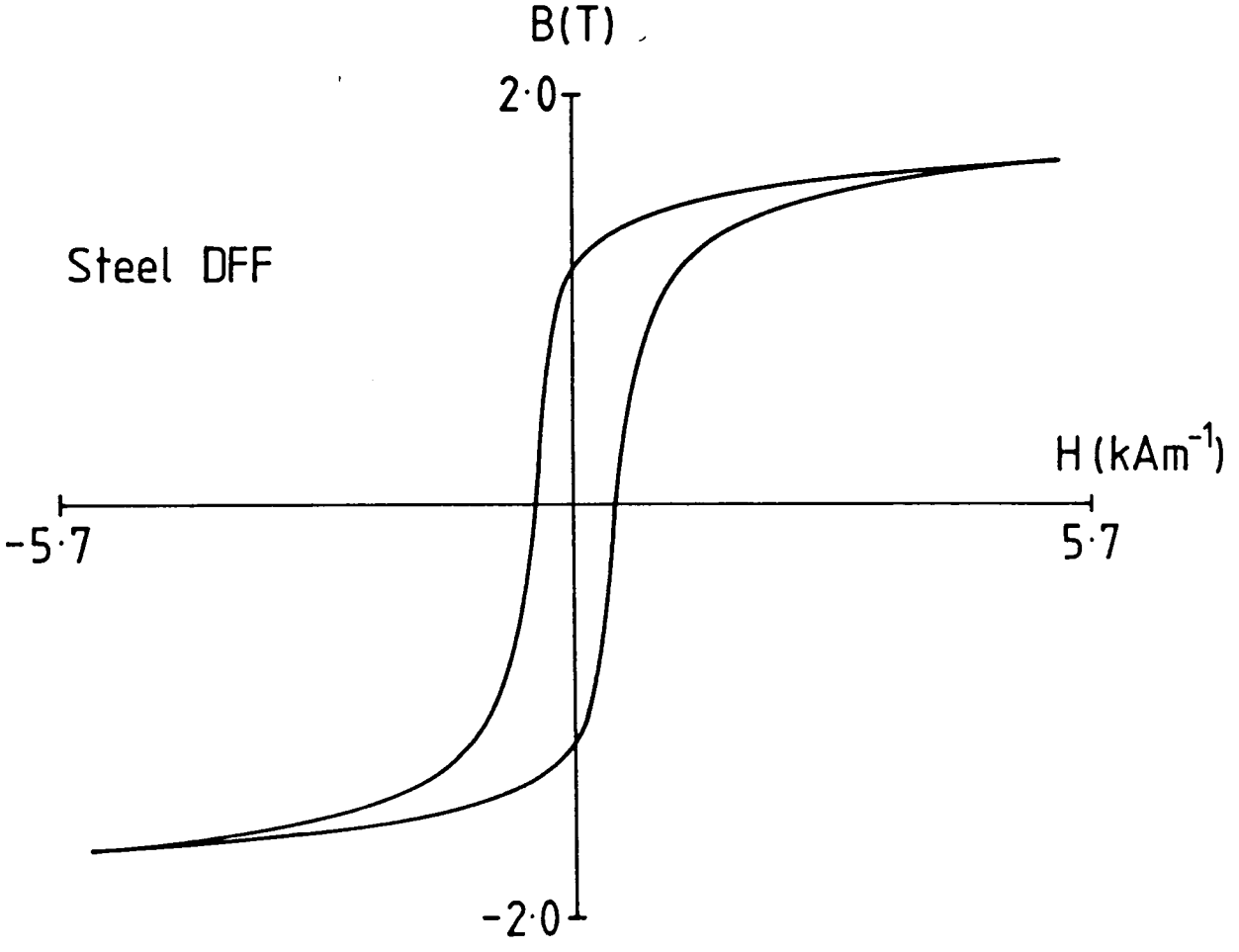

Figure 3.10 Typical magnetization loop recorded by automated yoke permeameter apparatus. The plot was produced by linear interpolation between data points.

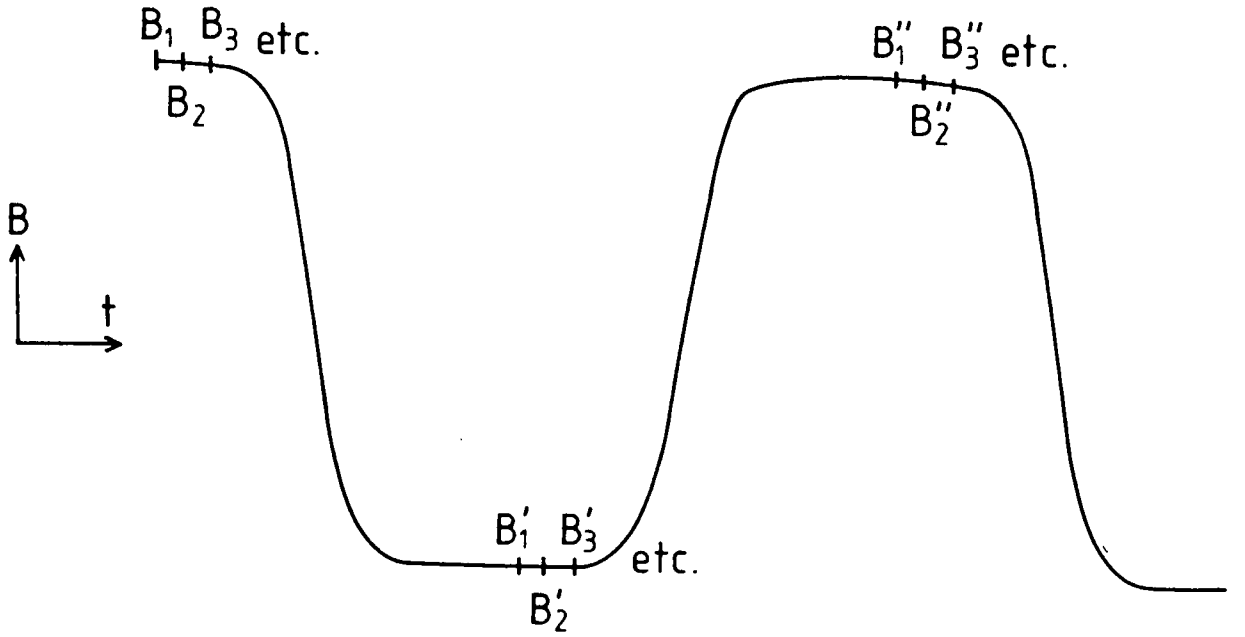

Figure 3.11 Illustration of procedure required to eliminate linear drift (x). $B_1' = -B_1 + x$ and $B_1'' = B_1 + 2x$. Calculation of $B_1 + B_1'' - 2B_1'$ produces result $4B_1$ and eliminates drift.

of such drift were eliminated. This procedure was followed for each required field value, therefore, before the corresponding readings for subsequent field values (e.g. B_2, B_3 etc.) were recorded. Once the complete B-H loop had been recorded in this manner and the results stored on disc, the operator was then prompted to provide another demagnetized steel sample for investigation.

3.2(ii) Transfer of data from OLIC to Durham

The automation of the data taking process allowed several B-H loop or initial magnetization curve studies to be completed each working day with minimum commitment of manpower. As a result, a large body of data rapidly accumulated corresponding to investigations into twenty seven steel types of particular relevance to the gas pipeline industry. Magnetization measurements (both B-H loops and initial curves) were recorded for at least two samples of each individual steel type making the total number of data files recorded exceed one hundred and fifty.

In order to analyse this data conveniently using harmonic analysis and other more conventional techniques, the data had to be transferred from its position on floppy disc at OLIC to an equally accessable form at Durham. The incompatability of the disc drives of the MINC mini-computer at OLIC and the CBM "PET" microcomputers used at Durham made this task non-trivial but, by writing a PET emulation program on the MINC, the data was transferred direct to CBM disc. The emulation program (Appendix

C) reproduced the protocol used by the PET to communicate with its CBM disc drive via the IEEE-488 data bus and, by physically linking the MINC to the CBM disc drive via this port, the transfer of data and program files to and from the separate disc systems was achieved.

3.2(iii) Harmonic analysis of 12 inch pipe-steel data

Software was written for the CBM microcomputer, similar to that given in Appendix A, which routinely performed a Fourier analysis of all pipe-steel data files and plotted the results, where required, on an X-Y recorder. The most interesting individual system studied in some detail by this method was the data recorded from 41 samples of 12 inch diameter pipe-steel. It had been indicated that this steel type was of particular interest to British Gas because of small periodic irregularities in the pipe wall thickness imparted to the steel during manufacture. These regions are detected by the PIG during pipeline inspection and the recorded signals are large enough to obscure the information from genuine wall thickness defects. Considerable interest was expressed, therefore, in the harmonic analysis results obtained from the many samples taken from this pipe-steel to see if the magnetic behaviour fluctuations were related to material differences in these regions.

Twelve inch pipe-steel is manufactured as a seamless pipe. The process involves piercing a hole into a rod of steel as it is extracted from the furnace and then hammering it to the required size and shape with four

symmetrically positioned hammers as it passes around an inner mandrel . The pipe is advanced and rotated slightly between consecutive blows with the result that the four-fold circumferential thickness variation (Figure 3.12(a)) caused by the hammer impact spirals along the length of the pipe (Figure 3.12(b)). Figure 3.12(c) shows diagramatically how this manifests itself in the signals recorded by the PIG during inspection.

The 41 samples, whose magnetization characteristics were studied, had been taken at equal intervals from around the circumference of the pipe. It was expected, therefore, that the magnetic behaviour of these samples, and hence the harmonic amplitudes, should show a similar four-cycle variation to the thickness variation when plotted out as a function of circumferential position. All the harmonic amplitudes, however, showed a significant and similar single-cycle variation.

Figures 3.13(a), (b) and (c) show, for example, the variation of the 3rd odd order and 7th odd and even order harmonics as a function of circumferential position. It can be seen that these harmonic amplitudes show a gradual reduction with position until approximately sample 33, at which point there is a more rapid increase back to the original values. The only harmonic amplitude to show the opposite trend with position was the 1st even order harmonic (Figure 3.14(a)). The behaviour of this harmonic reflects that of the coercive field, H_c, and there is a good correlation between the two as predicted by the findings of Chapter 2 (Figure 3.14(b)).

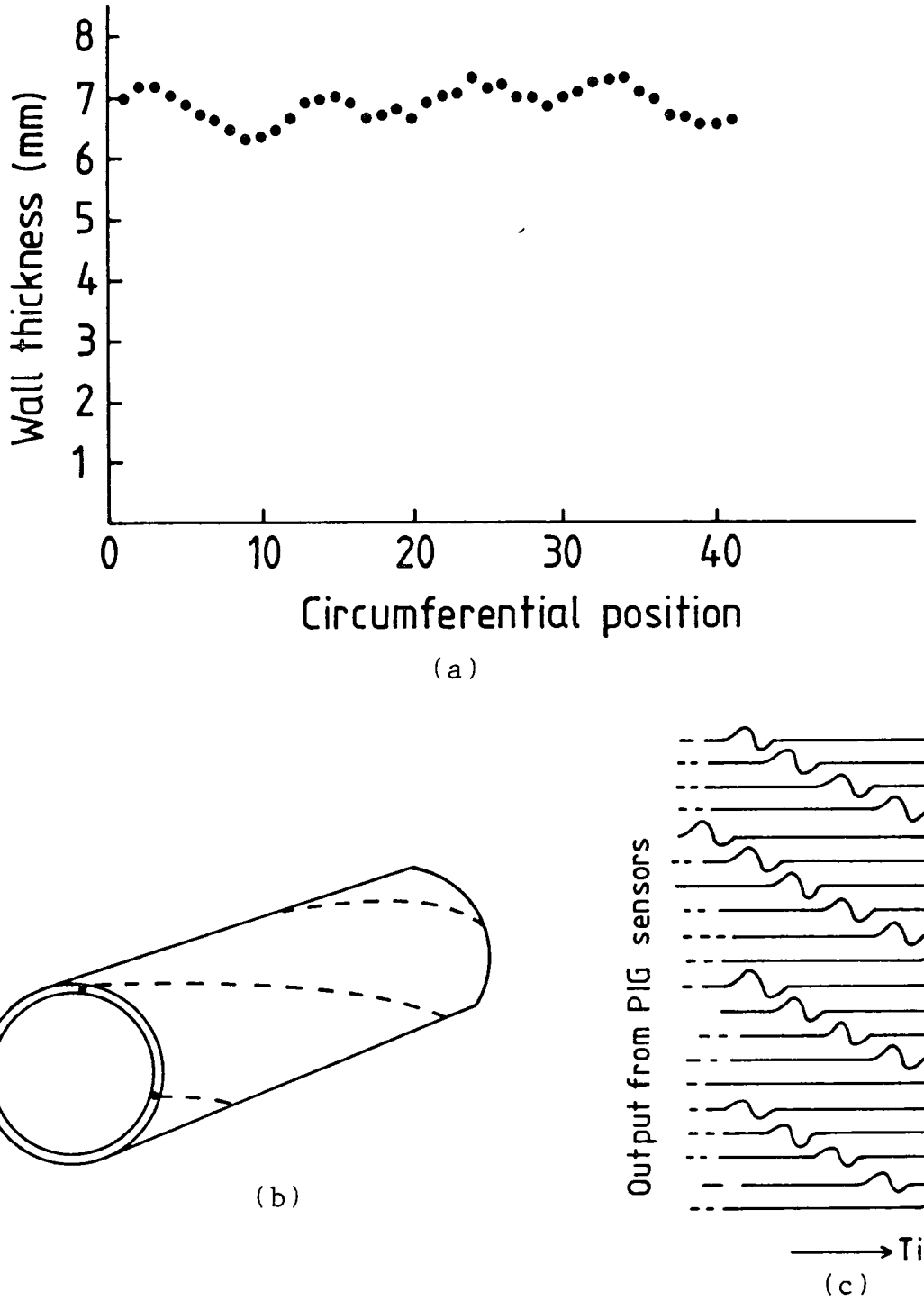

Figure 3.12 (a) Wall thickness data for 12 inch pipe showing four-fold circumferential variation. (b), (c) Illustration of spiralling effect of thickness peaks caused by manufacturing process and how it is manifest in PIG sensors output.

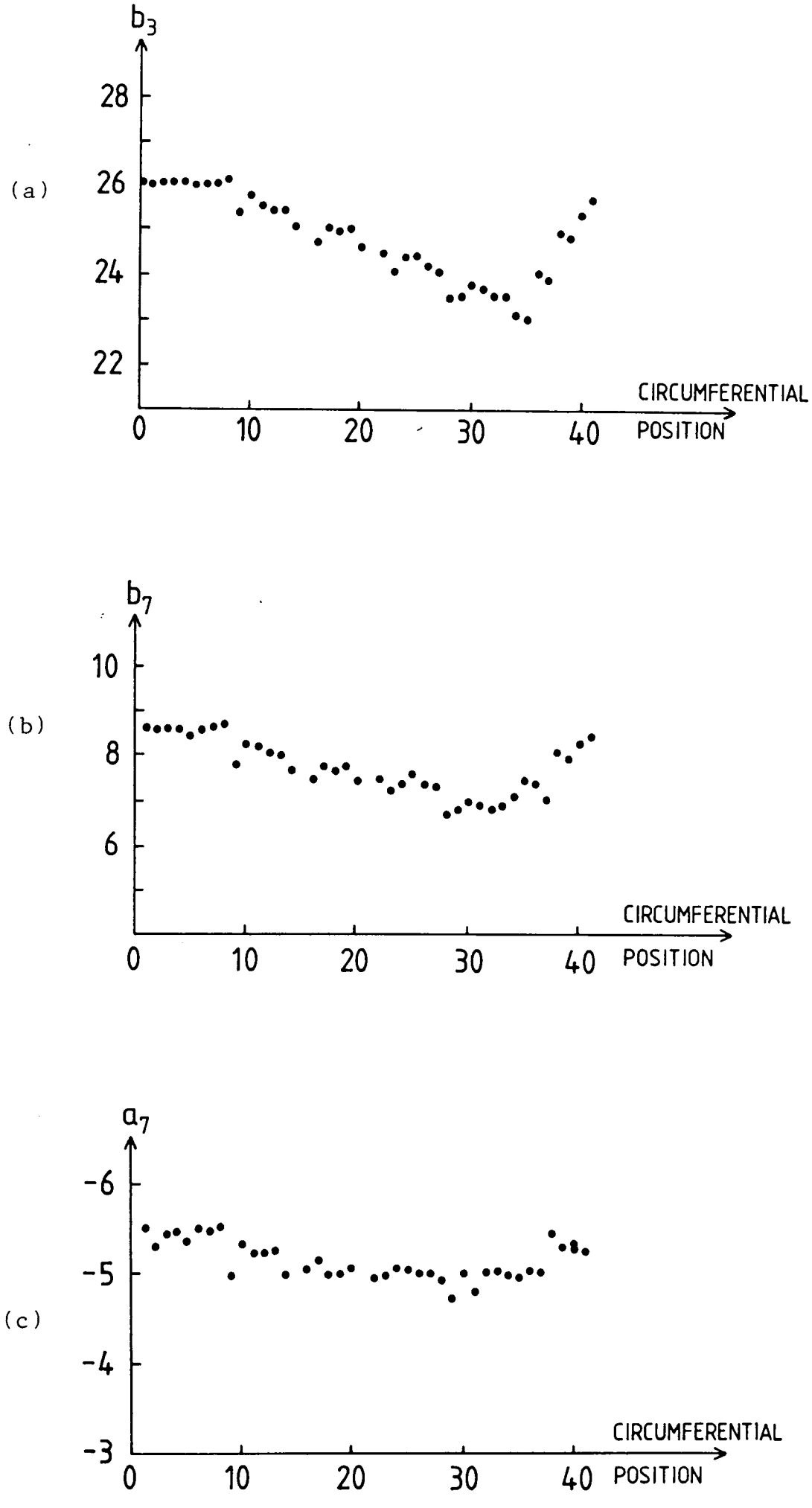

Figure 3.13 Variation of (a) 3rd odd order, (b) 7th odd order and (c) 7th even order harmonics with circumferential position for 12 inch pipe.

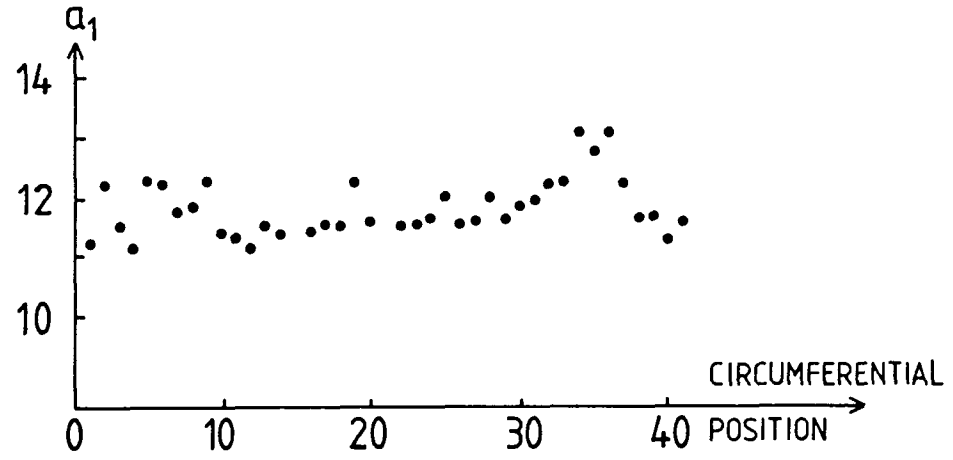

(a) Variation of 1st even order harmonic with circumferential position.

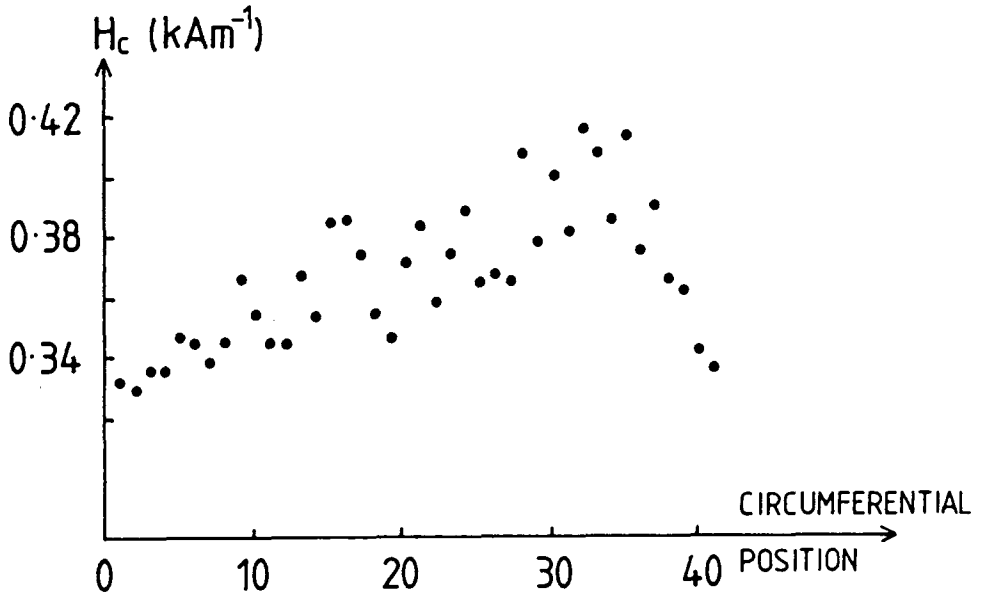

(b) Variation of coercive field (H_c) with circumferential position.

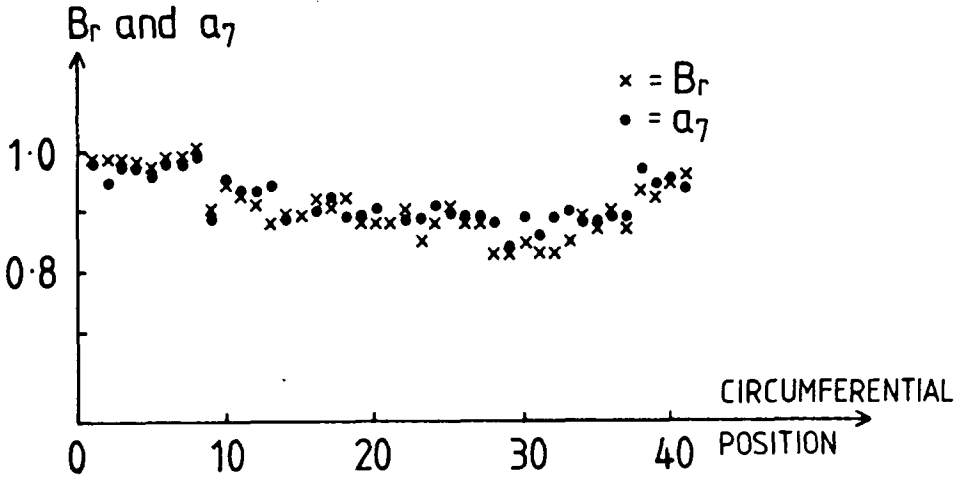

(c) Variation of remanence and 7th even order harmonic with circumferential position.

Figure 3.14

There is also an excellent correlation between the behaviour of the remanence induction, B_r, and the 7th even order harmonic, again predicted in Chapter 2. This is shown in Figure 3.14(c) where values of B_r (crosses) and 7th even harmonic amplitude (points), normalized to their respective maxima, have both been plotted on the same axes.

The above results clearly demonstrate that the magnetic properties of 12 inch pipe-steel show a single-cycle variation with circumferential position, first revealed by harmonic analysis results, that is not detected by the PIG during pipe-line inspection. It was concluded, therefore, that the signals generated by the PIG can be attributed directly to the known four-cycle variation in pipe-wall thickness and are not related to real physical differences in the steel at these positions. This knowledge, combined with the regularity and similarity of such signals, then allowed British Gas to overcome the problem by using a signal analysis technique to deconvolve any signal from a genuine pipe-wall defect from that of the background signal.

The origin of the single-cycle variation of magnetic behaviour with position was unclear until a closer examination of the pipe-wall thickness measurements revealed that the predominant four-cycle variation was overlaid on a smaller single-cycle thickness variation. The latter is revealed clearly by averaging out the higher frequency term (Figure 3.15(a)) and, when inverted, an excellent correlation exists between this and the magnetic behaviour

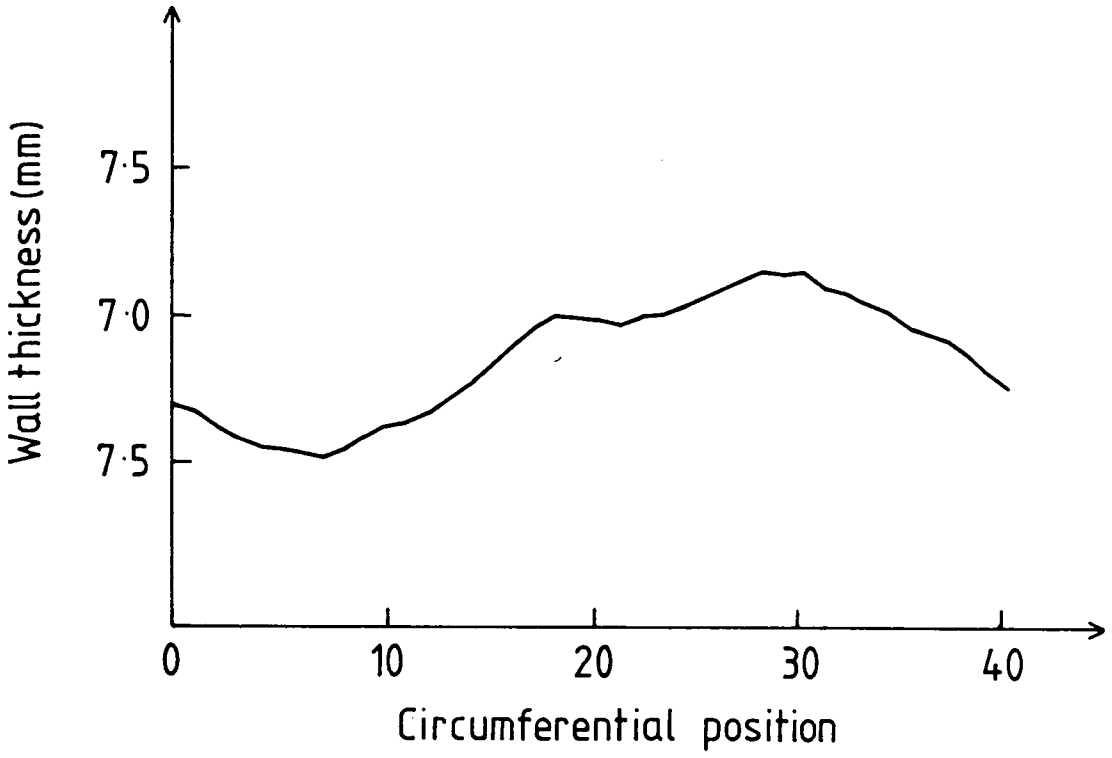

(a) Single cycle wall thickness variation for 12 inch pipe.

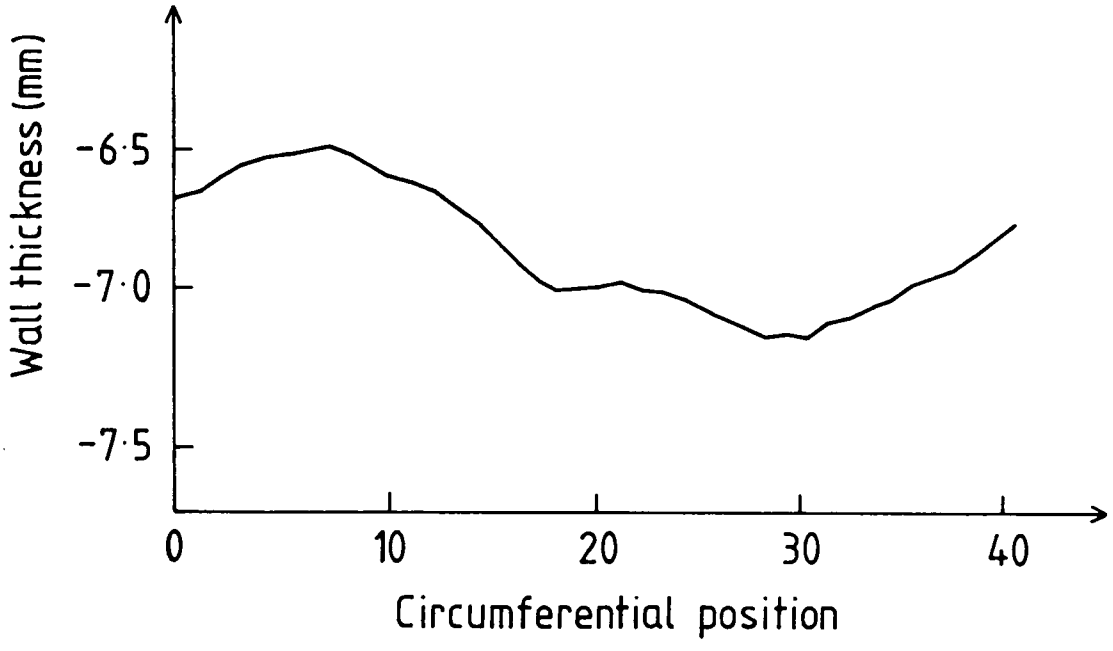

(b) Inverted single cycle wall thickness variation for 12 inch pipe.

Figure 3.15

(Figure 3.15(b)). This suggests, therefore, that the pipe-wall thickness variations have two origins, of which only one affects the magnetic properties.

The single-cycle thickness variation can only occur at the piercing stage of manufacture by means of a slight misalignment between the centre of the steel rod and the piercing jig. The steel is hottest at this point and it has been suggested (Durham Contract Progress Report 28.7.82) that during the rapid cooling, which takes place before the hammering stage, the ferrite grains present in the steel's microstructure grow preferentially in the regions with the increased wall thickness, as the rate of cooling in these areas will not be as great. This variation in grain size, which has yet to be verified experimentally, was then postulated as being the source of the differences in magnetic behaviour. The behaviour of the coercive field, H_c, as a function of circumferential position, however, does not give credence to this argument. Figures 3.14(b) and 3.15(a) show that the behaviour of the coercive field and pipe-wall thickness correlate well and, as it is well known (Ruder (1934), Yensen and Ziegler (1935), Doring (1938), Mager (1952), Goodenough (1954) and Gutnov et al. (1973)) that there is an inverse relation between the coercive field and the grain size (d_g) (viz. $H_c = \frac{A}{d_g} + B$, where A and B are constants) for materials which exhibit grain structure, this suggests that the grain size should be a minimum when the pipe-wall thickness is greatest.

It is postulated here that, while there may be a

slight increase in ferrite grain size in these regions, there could also be an increased pearlite fraction here caused by the migration of the cementite present in the pearlite phase to the thicker pipe-wall areas as the solidification process sweeps through the material. Results presented later in this thesis, and those obtained independently elsewhere (private communication Tanner (1984)), suggest that the pinning of domain walls responsible for the coercive field is approximately 8 times stronger in the pearlite phase than the ferrite phase. Consequently an increase in the pearlite fraction will have a more profound effect on the coercive field than small changes in the ferrite grain size and the observed increase of H_c would then be explained.

3.2(iv) Harmonic analysis of all other pipe-steel data

The B-H loop data of the remaining twenty six steel types were analysed in an identical manner to the 12 inch data. The harmonic amplitudes thus obtained were transferred to the site VAX-11 computer at Cramlington, via the laboratory based MINC minicomputer, and were added to a data file containing other parameters relevant to all steel types, which had been amassed by colleagues working on the same project. These included ferrite and pearlite grain sizes, pearlite fractions, Vickers hardness measurements, coercive field values, Ultimate Tensile Stress results etc. (see Appendix D). A statistical software package called BMDP (Biomedical Data Programs Statistical Software (1981)) was then used to

plot the harmonic amplitudes against all the other variables (including inverse values) in the hope that unexpected correlations between the various sets of values would be found.

The results, however, were disappointing because, apart from the expected correlations between the first and third even order harmonics and the coercive field (Figure 3.16(a),(b)) and between the seventh even order harmonic and the remanence induction (Figure 3.16(c)), the only plots of note were non-linear curves relating certain odd power odd order harmonics to maximum permeability values (Figure 3.17(a), (b) and (c)). It had been hoped that correlations might have been found between the harmonic amplitudes and other variable(s) (e.g. chemical composition, Vickers Hardness etc.) which are not obviously related to the magnetization curve. Had this been observed, it would have allowed an estimation of the magnetic properties of hitherto unknown steel types from simple physical measurements which only required small sample sizes.

In a further attempt to find such correlations the initial magnetization curve data files of all the steel types were Fourier analysed to give odd power odd order harmonic amplitudes only. These values were transferred to the VAX and plotted as above but no correlations of any significance were found.

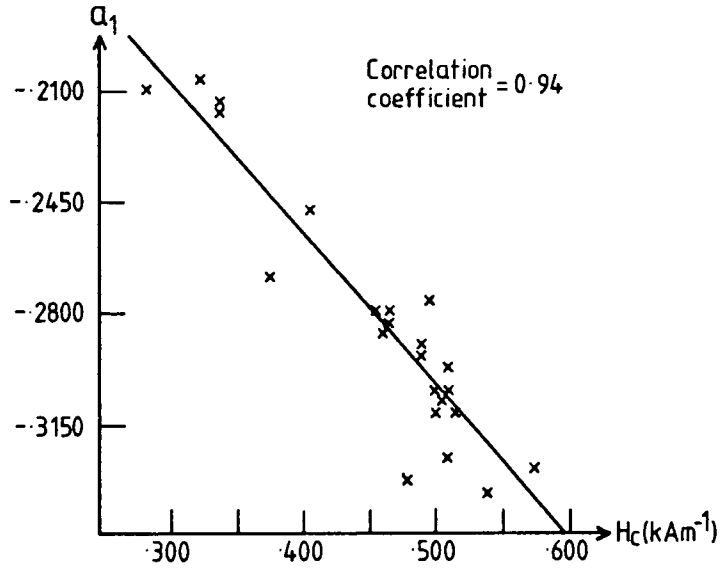

(a) Correlation between 1st even order harmonic and coercive field for all pipe steels.

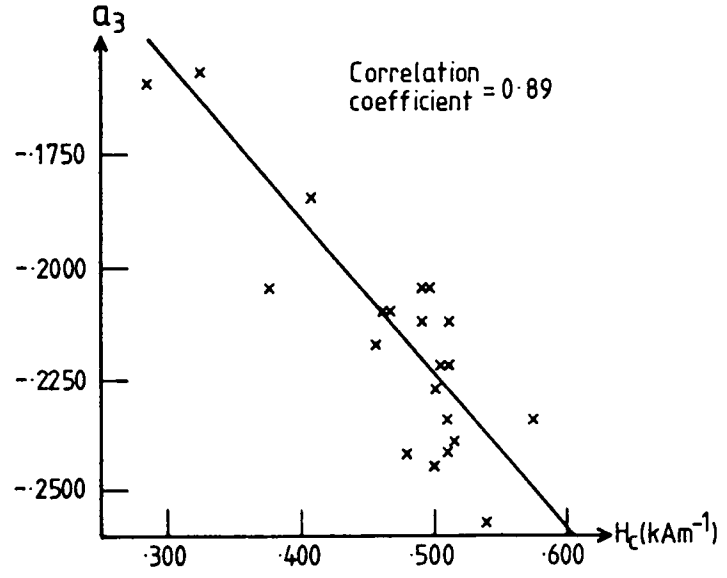

(b) Correlation between 3rd even order harmonic and coercive field for all pipe steels.

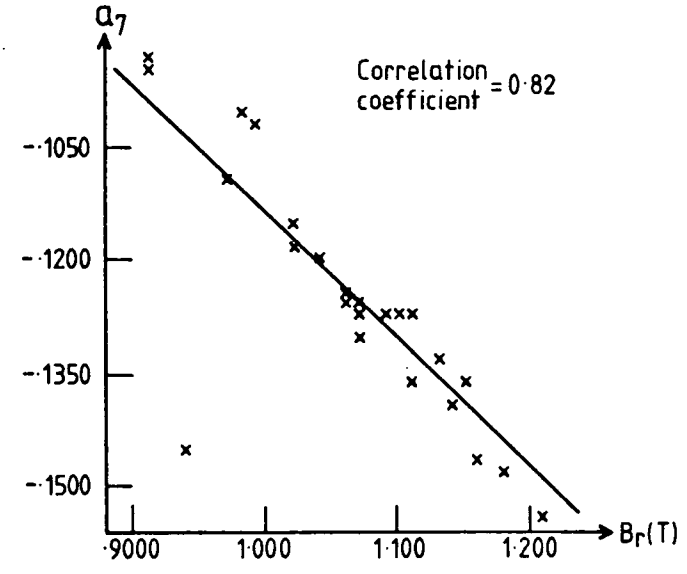

(c) Correlation between 7th even order harmonic and remanence induction for all pipe steels.

Figure 3.16

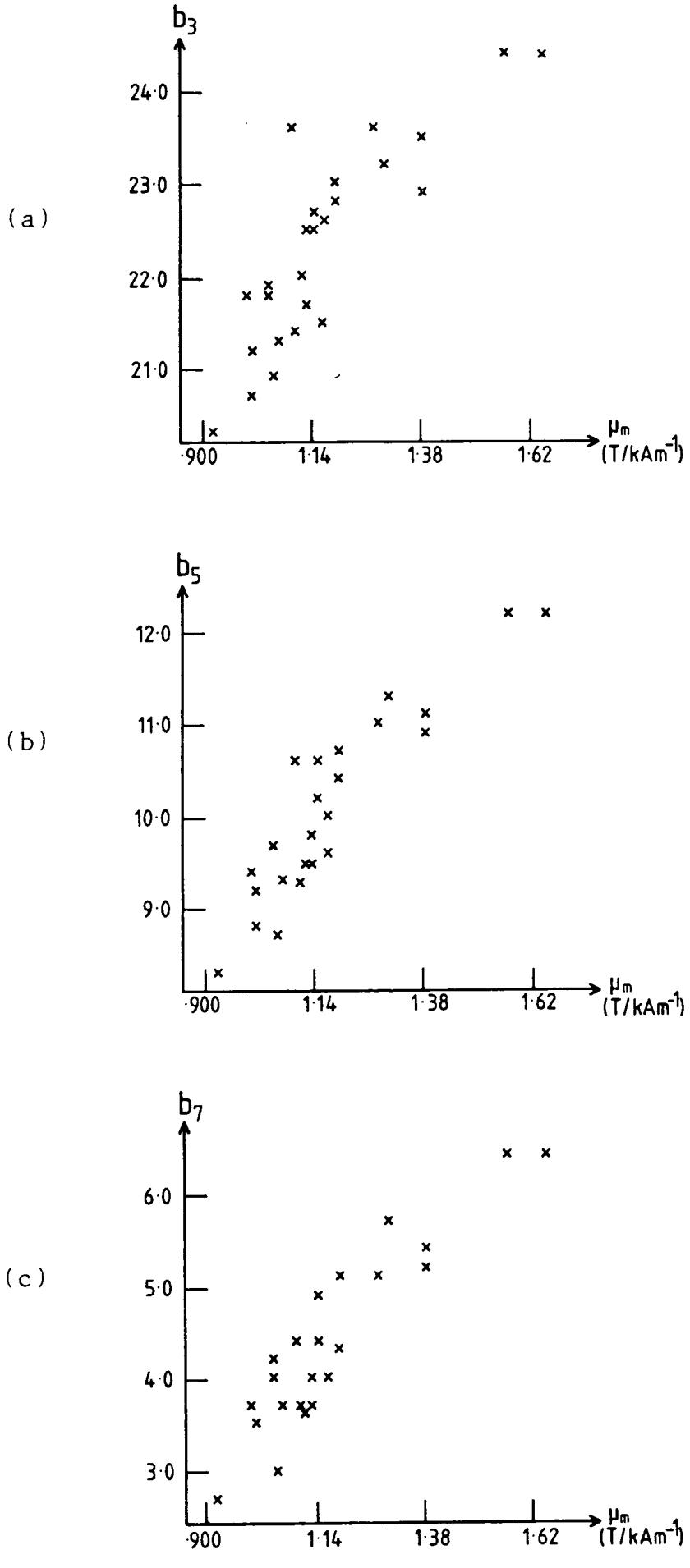

Figure 3.17 Variation of (a) 3rd odd, (b) 5th odd and (c) 7th odd harmonics with maximum permeability for all pipe steels.

3.2(v) Reconstruction of B-H loops from harmonic information

In order to ascertain exactly how many harmonic amplitudes would be required in order to obtain a reasonable reproduction of a B-H loop, a detailed study was made on six steel types (015, DFE, DFD, DHP, 030 and 2401) which represented the complete range of magnetic behaviour observed in pipe-line steels. Harmonic coefficients up to 20th power were calculated from the original B-H loop for each steel type and stored on disc. The B-H loops were then reconstructed using various degrees of harmonic information with the aid of a PET microcomputer and the results plotted out on an X-Y recorder. Loops were calculated and plotted for harmonic content up to and including the 3rd, 5th, 7th, 11th, 15th and 19th power respectively. An example of a typical series of curves thus obtained is shown in Figure 3.18.

A detailed investigation of parameters associated with the B-H loop was performed on all curves and the results compared to the values obtained from the original loop. The parameters chosen for this study were the coercive field (H_c), the remanence induction(B_r), the maximum value of induction (B_m), the maximum value of permeability (μ_m) and the value of the maximum differential permeability (μ_{diff}) taken at H_c. Table 3.4 shows a summary of the results obtained from all loops expressed in terms of a percentage error from the values recorded from the original loops. It can be seen that the para-

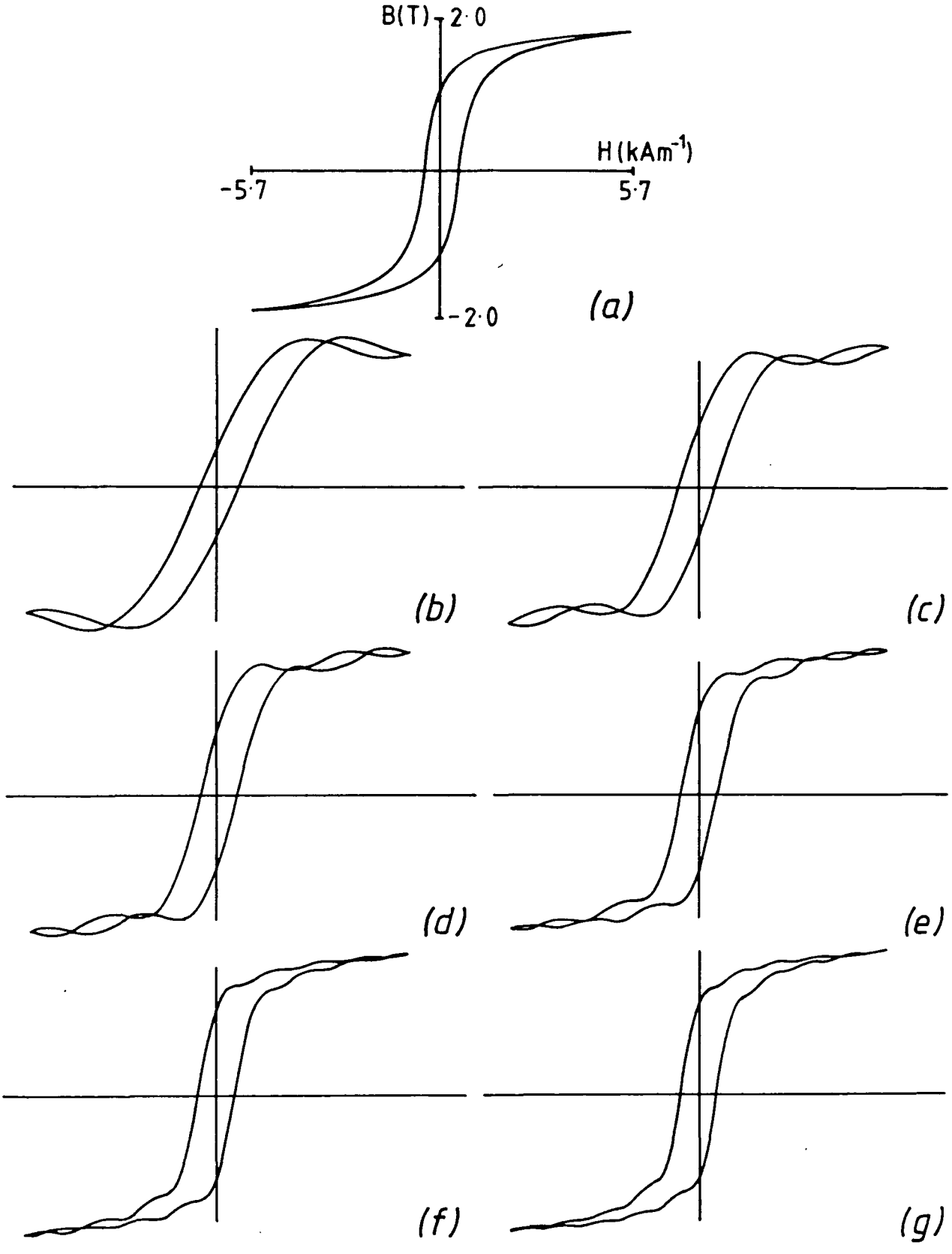

Figure 3.18 Example of typical series of B-H loops (for steel 030) reconstructed using harmonic content up to (b) 3rd, (c) 5th, (d) 7th, (e) 11th, (f) 15th, (g) 19th powers. (a) is the original curve.

Loop Parameter	Order of limit of harmonic information included	Average % error
H_c	3	10.8
	5	8.9
	7	8.2
	11	6.8
	15	5.5
	19	4.3
μ_{max}	3	- 39.9
	5	- 24.8
	7	- 15.5
	11	- 4.6
	15	+ 1.7
	19	+ 3.2
μ_{diff} at H_c	3	- 75.1
	5	- 67.9
	7	- 55.9
	11	- 48.0
	15	- 38.2
	19	- 30.9
B_{max}	3	+ 1.1
	5	0
	7	+ 1.1
	11	+ 1.1
	15	+ 1.8
	19	+ 1.6
B_r	3	- 56.3
	5	- 42.2
	7	- 31.2
	11	- 16.5
	15	- 6.2
	19	- 2.0

Table 3.4

Average percentage errors for various loop parameters determined from B-H loops reconstructed from varying degrees of harmonic information

meters B_r and μ_{diff} are reproduced least reliably indicating the extent to which sharp changes in gradient are represented by harmonic terms of higher power than those considered here. The other parameters are reproduced more precisely and errors are brought below the 7% level once harmonic information up to the 11th power is supplied.

The results presented here suggest, therefore, that, in order to obtain a satisfactory reproduction of the B-H loop, harmonic amplitudes up to the 11th power must be known to within a reasonable tolerance. Use must then be made of the results in Table 3.4 to correct those loop parameters which are known to be in error.

3.2(vi) Conclusion

The B-H loop and initial magnetization curve data files for twenty seven steel types have been recorded using an automated yoke permeameter and the results stored on floppy disc. Subsequent harmonic analysis of the 12 inch pipe-steel data revealed for the first time a single-cycle variation of magnetic behaviour with circumferential position which correlated well with a hitherto unrecognized single-cycle pipe-wall thickness variation. As a result, it has been concluded that the spurious signals recorded by the intelligent PIG during pipe-line inspection of 12 inch pipe are due entirely to the dominant four-cycle thickness variation and do not, therefore, reflect material changes. The origins of both four-cycle and single-cycle thickness variations have been

identified to stages in the manufacturing process and a difference in pearlite fraction with circumferential position, caused by a non-uniform cooling rate, has been postulated as the source of the single-cycle magnetic variation.

The first even harmonic shows an excellent correlation with coercive field (H_c) for all steel types as does the seventh even harmonic amplitude with remanence induction (B_r). These results confirm the findings of Chapter 2. Further correlations, which would have permitted a reconstruction of the magnetization curves from parameters not obviously related to the steel's magnetization characteristics, were sought but not found. A detailed study in the regeneration of B-H loops from harmonic information revealed that any such correlations should predict all harmonic amplitudes up to the 11th power to a reasonable tolerance. The correction of loop parameters B_r and μ_{diff} as indicated in Table 3.4 would, however, be essential.

CHAPTER 4

THE DURHAM VIBRATING SAMPLE MAGNETOMETER

4.1 Introduction

The desire for information about the variability of magnetic properties of small pipe-steel sections, as a function of orientation and position in the pipe wall, required the development of a magnetometer capable of measuring the full magnetization curve. A wide variety of methods for the measurement of magnetic moments occur in the literature (see, for example, the reviews of Foner (1967), Dwight (1967), Humphrey (1967), Bates (1970) and Foner (1981)), but the usual methods employed can be divided into three major classes: measurement of a force on a material in a non-uniform magnetic field, measurement of magnetic induction in the vicinity of the sample, and indirect measurements of phenomena which involve the magnetic properties.

The force method (e.g. Faraday balance) is a sensitive technique which has been employed for many years. It is, however, difficult to measure the magnetization in a truly uniform magnetic field using this method since the presence of a field gradient is essential to the production of the force, and a field value averaged over the sample volume must, therefore, be used. For similar reasons the force method is not easily adaptable to routine measurements of magnetization versus applied field or crystallographic direction, and anomalous results have been observed in highly anisotropic samples (Wolf (1957))

caused by forces due to unconsidered components of field gradients. Furthermore, significant problems are caused by sample position instability and some care is required in order to obtain reliable results.

Numerous indirect techniques for measuring magnetic moments include measurement of the Faraday effect, the ferromagnetic Hall effect and microwave ferromagnetic resonance measurements. These techniques are capable of extremely high sensitivity but cannot be considered as a general method because they are limited to particular phenomena observed in a limited class of materials, about which considerable prior knowledge is required.

The measurement of magnetic induction, on the other hand, can be applied to all materials and is basic to a wide variety of magnetic measurement techniques. These include conventional flux integration magnetometers and both vibrating coil and vibrating sample magnetometers (Bates (1963)). Flux integration techniques are limited by the accuracy and reproducibility of sample positioning, the noise produced by background field variations and coil vibrations and, most critically the inevitable drift of the integrator circuitry. When used in conjunction with the usual laboratory electromagnet, extensive modifications to the magnet are invariably required to permit sample motion along the field direction. This usually involves passing a drive rod through one of the magnet pole faces, with the result that the magnet ceases to be a general laboratory facility (Pauthenet (1950)).

The vibrating coil magnetometer (V.C.M.) and the

vibrating sample magnetometer (V.S.M.) both depend on small amplitude harmonic oscillations of the pick-up coil (search coil) and sample respectively to provide an a.c. signal of stable frequency, whose amplitude is proportional to the magnetic moment of the sample. In both cases a sensitivity equalling that of the force method (Foner (1974) and (1975)) is possible using appropriate signal amplification techniques. The major sources of error (sample positioning, background field noise and vibration amplitude) can all be eliminated to first order (or higher) and, unlike the force measurement technique, the applied field can be swept through the complete magnet range. Problems caused by the sensitivity of the VCM to field inhomogeneity usually result in a preference for the VSM except at very low temperatures and fields, where the use of a VCM avoids introducing vibrational energy in the specimen (Kaeser et al. (1965)).

A consideration of the above, therefore, resulted in the selection of a vibrating sample magnetometer to measure the variations in magnetic behaviour of small pipe-steel sections. This chapter contains a detailed description of the development and performance of the Durham VSM, together with a review of the relevant literature (see also Hoon and Willcock (1985)).

4.2 Historical development of the VSM and principles of its operation

The inception of the VSM arose directly from the use of flux integration magnetometry techniques. Research

workers at the time (Plotkin (1951), Blackett (1956), and Van Oosterhout (1956)) realized the desirability of vibrating the sample near the search coils. This not only allowed rapidly repeated readings to be made but permitted easy amplification of the signal induced in the search coils due to the a.c. nature of this signal. High sensitivity could also be achieved by increasing the number of turns on the search coils. The search coil impedance had been a limitation with the ballistic galvanometer due to the low impedance of this instrument, no longer a problem with the high impedance "electronic" voltmeter used to measure the a.c. signal.

The principle of VSM operation is, therefore, based on the fact that, as long as the nominally dipolar non-uniform external field ($h(\underline{r})$) arising from the magnetic moment of the sample threads the detection coils, an e.m.f. is induced within the coils. In principle this e.m.f. is proportional to the magnetic moment of the sample and, thus, also its magnetization. This can be expressed more formally by considering, for convenience, a "one-dimensional" system in which a moment m_z is vibrated with amplitude a_o and frequency w_o along z, the axis of a thin coil. The instantaneous position of the moment relative to the coil plane is written

$$z = z_o + a_o \exp(iw_o t) \qquad (4.1)$$

and the induced e.m.f. Σ is given by

$$\Sigma = \frac{-\delta\phi}{\delta t} \qquad (4.2)$$

where ϕ is the flux in the coil system. The Principle of Reciprocity (Guy (1976)) allows us to write

$$\phi = \mu_o \underline{m} \cdot h(\underline{r}) \tag{4.3}$$

which becomes $\phi = \mu_o m_z h(z)$ (4.4)

in the one dimensional system considered here.

Thus equation (4.2) becomes

$$\Sigma = - \mu_o m_z \left(\frac{\delta h(z)}{\delta t}\right)_{z = z_o} \tag{4.5}$$

and by substituting equation (4.1) for z and expanding h(z) as a Taylor series we have

$$\Sigma = -\mu_o m_z \left[a_o W_o i \left(\frac{\delta h(z)}{\delta z}\right)_{z_o} \exp(i w_o t) + a_o^2 w_o \left(\frac{\delta^2 h}{\delta z^2}\right)_{z_o} \exp(2 i w_o t) + \cdots \right] \tag{4.6}$$

The component of the induced signal of frequency equal to the frequency of vibration may, therefore, be written as

$$\Sigma_{w_o} = k \mu_o m_z a_o W_o \exp(i w_o t) \tag{4.7}$$

where k is a constant whose value is specific to the sample-coil geometry (see section 4.4).

Thus the e.m.f. produced by the search coils is shown to be proportional to the amplitude (a_o) and frequency (w_o) of vibration as well as the magnetic moment (m_z) of the sample.

The early VSM's described by Blackett (1956) and Van Oosterhout (1956) were relatively crude instruments

in which the sample moment, coil axis and vibration direction were all colinear (as considered above). Van Oosterhout achieved calibration of his instrument by direct comparison with the output obtained from the saturation moment of a nickle sample of dimensions equal to that of the test sample, while Blackett preferred recording the current, in a small coil surrounding the sample, required to achieve zero net signal. Both techniques are valid, although the former does not allow for possible fluctuations in the vibration amplitude or frequency, while the latter "Domenicali coil" technique (Domenicali (1950)) requires the field from both sample and coil to be well described by the dipole field. Blackett also describes the use of a narrow band-pass filter/amplifier tuned to the vibration frequency (30 Hz) to reject unwanted mains pick-up.

A much more rigorous approach to the design and operation of the VSM, however, was described by Foner (1956, 1959). Figures 4.1 and 4.2 show the apparatus used by Foner in which the sample motion is shown, for the first time to be perpendicular to the applied field. Measurements of magnetic moment were recorded by adding a portion of the reference signal (appropriately phased) to balance the sample signal. At balance the magnetic moment of the sample is proportional to the reference voltage divider setting, and is independent of any changes of vibration amplitude, frequency or amplifier gain/linearity. The reference signal was usually derived from a permanent magnet reference sample, but provision was also made to replace this by a small d.c. coil (indicated by the

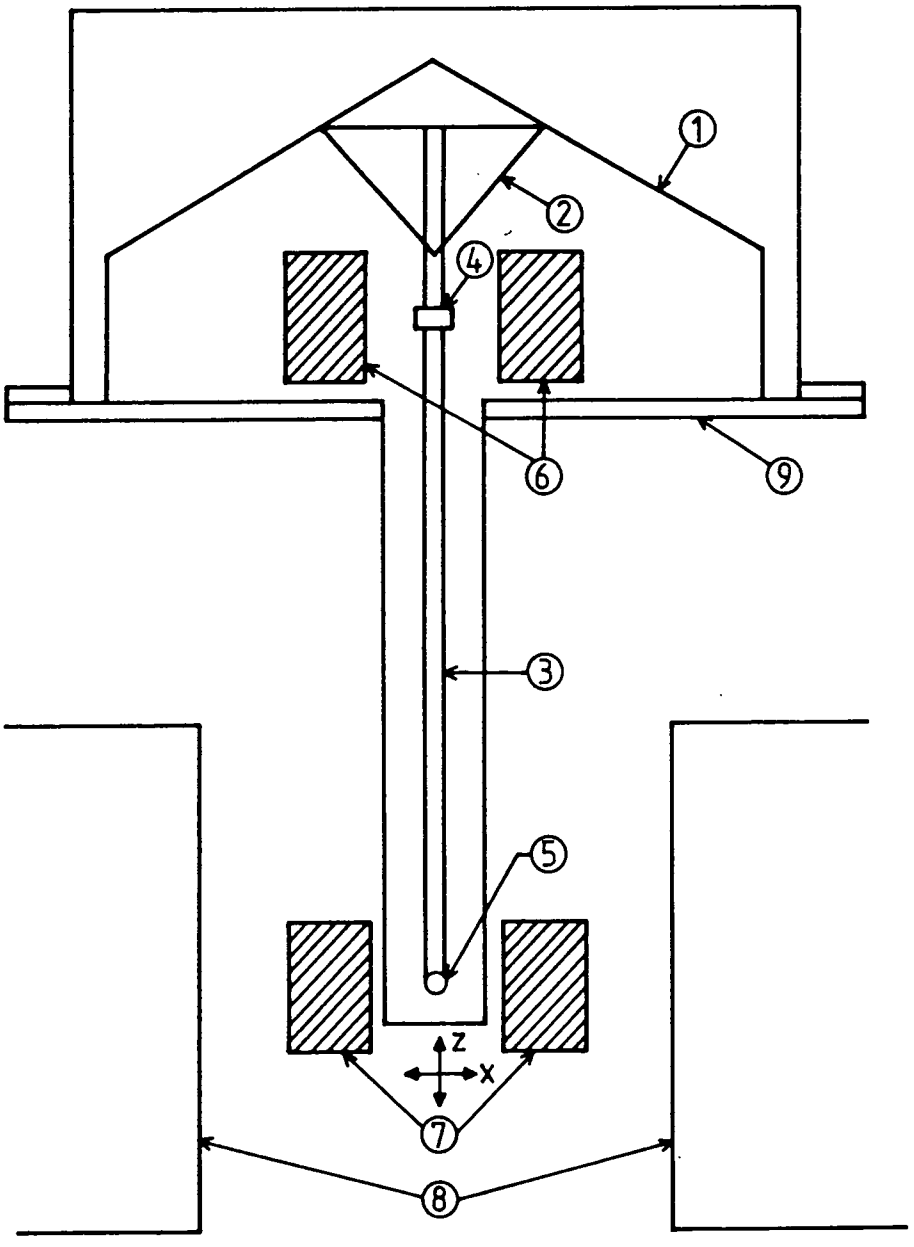

Figure 4.1 The Foner magnetometer (Foner (1959)). (1) loudspeaker transducer, (2) conical paper cup support, (3) drinking straw, (4) reference sample, (5) sample, (6) reference coils, (7) sample coils, (8) magnet poles, (9) metal container.

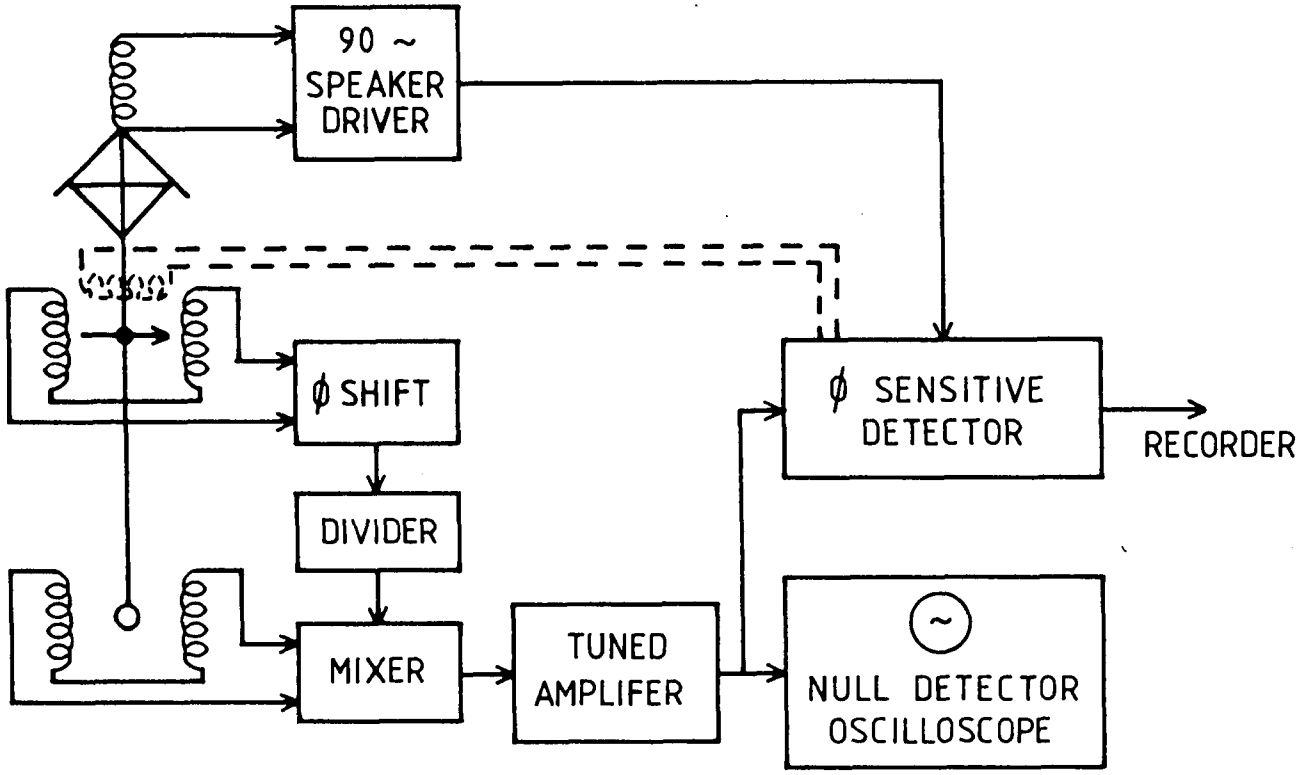

Figure 4.2 Block diagram of electronic system for Foner magnetometer.

dashed lines in Figure 4.2). The current to the coil was regulated by a servo-loop monitoring the null output signal, and a voltage proportional to this balancing current was recorded. Calibration of the complete system was again achieved either by use of a constant current sample coil or the saturation moment of a small sphere of pure nickel.

Figure 4.2 also shows the first reported use of a phase sensitive detector to achieve signal to noise ratio enhancement. The phase sensitive detector (p.s.d.), sometimes referred to as a lock-in amplifier/analyser, can be regarded as a narrow band pass filter/amplifier which "locks in" to a frequency determined by an external reference source. By providing the p.s.d. with a reference signal derived from the source of sample vibration, therefore, the instrument will only measure the amplitude of the pertinent part of the search coil signal. Considerable enhancement of the signal to noise ratio (> 80dB) is possible with respect to a white noise background and, by operating the VSM at frequencies well removed from mains frequency (or its harmonics), noise from such sources can also be rejected. The use of the p.s.d. with VSM systems has, therefore, become routine.

The behaviour of the search coil systems as a function of sample displacement was also considered for the first time by Foner. He presented results showing the sensitivity function (coil output versus sample displacement) for his coil systems and emphasized the importance of positioning the sample at a "saddle-point", where the output signal

is independent of small sample displacements in any direction (see Section 4.4). By connecting the pair of coils he used in series opposition and rigidly clamping them to the magnet pole faces, Foner also achieved insensitivity to magnetic field instabilities and avoided mechanical coupling between the vibration source and the coils. The latter effect, if present, results in the generation of signals of the same frequency as that of the vibrating sample that are difficult to reject even when using phase sensitive detection techniques.

The Foner magnetometer was highly successful and his design and principle of operation have, therefore, become generic to many subsequent VSM's. We note, for example, that the measurement techniques used by Springford et al. (1971) when describing the use of a VSM with a superconducting solenoid magnet were first suggested by Foner (1959). Apart from further descriptions of VSM's for use at low temperatures (Redfield and Moleski (1971) and Gerber et al. (1982)), the majority of subsequent VSM literature has, therefore, been concerned with the two main features common to all VSM's; the transducer mechanism responsible for providing the stable, periodic sample vibration and the stationary assembly of detection coils.

Specific analyses of various detection coil systems have been presented by Smith (1956), Mallinson (1966), Springford et al. (1971), Bowden (1972) and Guy (1976 a , b), while, more recently, comprehensive studies of the relative merits of more general coil geometries have

been described by Pacyna (1982), Zieba and Foner (1982a) and Pacyna and Ruebenbauer (1984). In practice, however, the detection coil geometry is often dictated by physical constraints, such as magnetic field orientation, its uniformity and access, rather than simply the theoretical efficiency and signal to noise ratio (Hoon and Willcock (1985)).

A variety of transducers for providing stable sample vibration has also been described. Flanders and Doyle (1962), Noakes et al. (1968), and Redfield and Moleski (1971) have, for example, described various motor and crank arrangements. Foner (1956, 1959), Springford et al. (1971), Hoon (1983) and most commercial designs have used electro-mechanical "loudspeaker" transducers, whilst Mangum and Thornton (1970) have employed a piezoelectric "bimorph" suitable for the vibration of small sample masses in confined volumes.

The "loudspeaker" type of transducers, whilst inherently simple and mechanically quiet, must, in general, be carefully stabilized with suitable electronic feedback networks if they are to exhibit long term amplitude and frequency stability. Further, the transducer must be capable of dissipating quite large amounts of power in apparatus incorporating either large sample masses (e.g. weakly magnetic paleomagnetic rock samples) or long sample rods (such as are necessary in deep superconducting magnet cryostats). On the other hand, motor and crank mechanical transducers, whilst more mechanically complex, are simpler electronically, having excellent stability, although

they are often criticized as being mechanically noisy. Mechanical noise, however, is usually the result of inadequate balancing and mechanical isolation and a mechanical double crank design, used on the Durham VSM, has recently been reported (Hoon and Willcock (1985)) from which such problems are almost totally absent.

4.3 The Durham VSM Hardware

4.3(i) The double crank VSM and motor drive

A detail of the double throw crank used on the Durham VSM is shown in Figure 4.3. This precision component comprises of 3 sections, driving, driven and 180^{o} crank-pin central web assemblies, which are turned from brass and joined together by demountable split tube pins. The 180^{o} double crank-pin design provides the successful solution to the problem of mechanical noise minimization in motor driven V.S.M's. It achieves this by careful static balancing of the masses attached to each crank-pin (sample rod, drive rods, aluminium con rods etc.) and by virtue of the 180^{o} disposition of the crank-pins on the central web. Out of balance dynamic forces are minimized, therefore, and no net work is done against gravity, resulting in very smooth running. The bob weights on the upper balancing shaft may easily be trimmed to permit balancing of widely differing sample and sample rod masses.

The double crank design is clearly rather more sophisticated than the simple designs of Flanders and Doyle (1962), Noakes et al. (1968), and Redfeld and Moleski (1971) which either employed no con rod or contained

Figure 4.3 (a) and (b) (overleaf). Detail of double throw crank/con rod/bearing assembly which clearly reveals the three sections of the crank and both big and little end bearings.

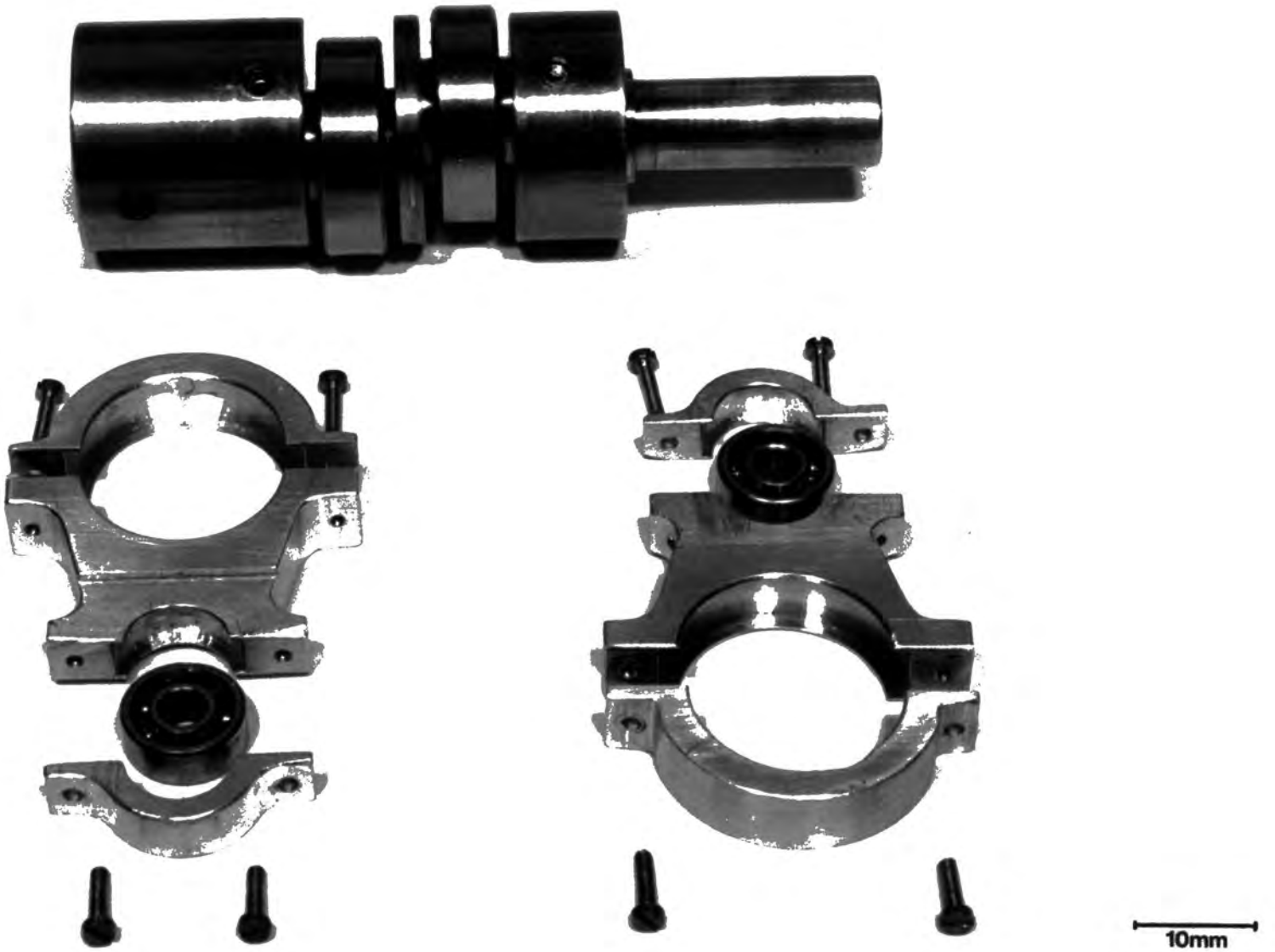
10mm

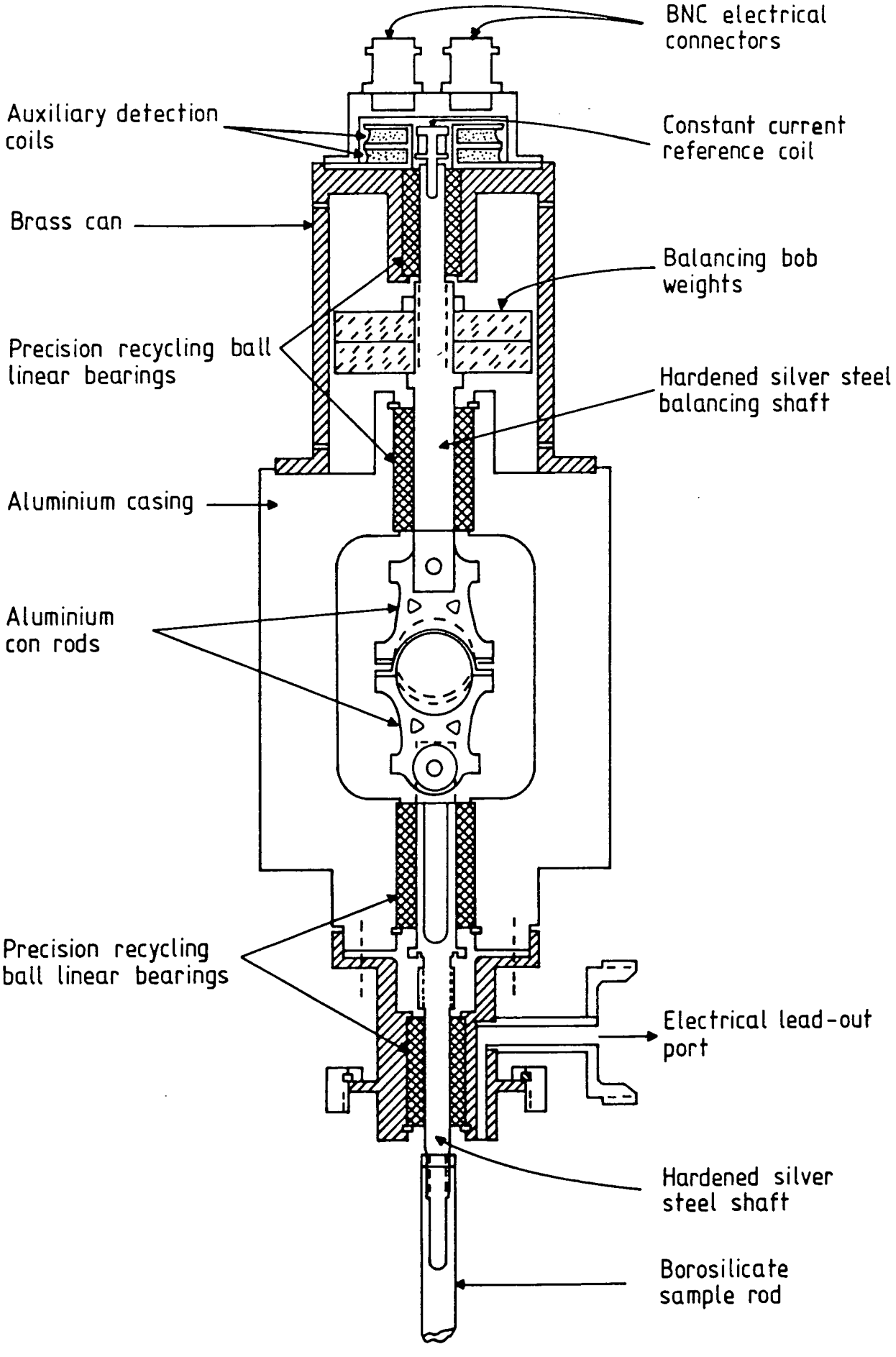

Figure 4.4 (a) and (b) (overleaf). Detail of design and construction of VSM vibrating head assembly.

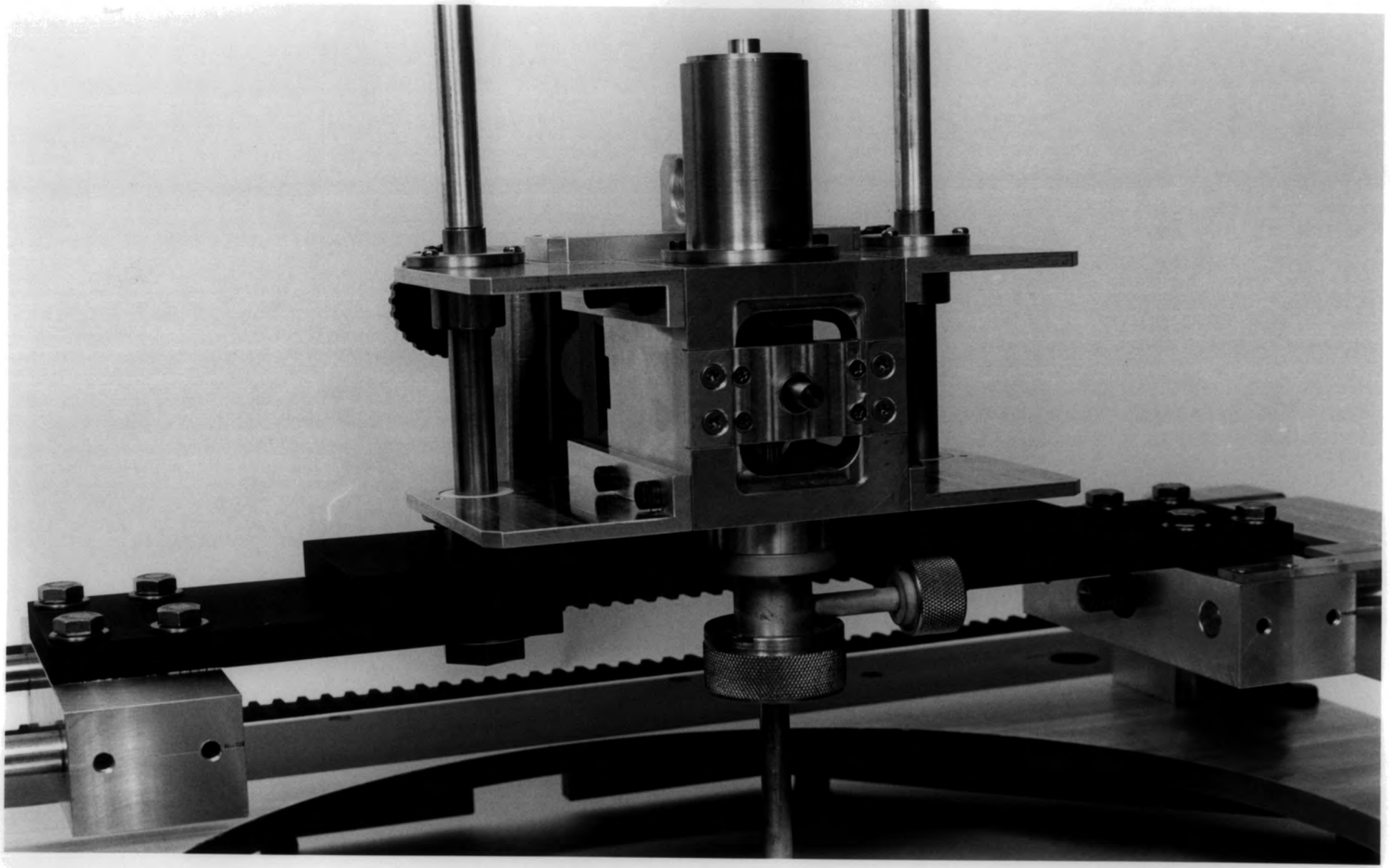

The means of rotation of the V.S.M. crank is provided by a low noise synchronous 3 phase star wound hysteresis induction motor (240V, 50W) which runs at half supply frequency, thus minimizing the possibility of cross talk with the signal channel. A 2 μF phase shifting capacitor connected between two of the stator windings enables the motor to be run from a single phase supply and determines its rotation direction. A variable frequency sine wave generator, Quad 50E commercial audio amplifier and matching transformer provide the variable frequency 240 V a.c. motor supply. The motor frequency is continuously variable in the range 15 to 70 Hz although to avoid mains supply harmonics, mechanical resonances and noise, oscillator frequencies in the range 62 to 76 Hz (motor rotation 31 to 38 Hz) have been found preferable. If phasing or anti-phasing of the motor drive with respect to an external reference or noise source is necessary this is simply achieved by phase shifting the oscillator signal prior to amplification. The absolute frequency stability of the vibrating sample is clearly twice that of the drive frequency as the maximum rated torque is well in excess of the dynamic load and is, therefore, typically stable to parts in 10^5. Amplitude stability is dictated by mechanical tolerances alone and variations of 10 μm compared to the crank throw of 3.00 mm are also typical.

4.3(ii) The Magnet, Power Supply and VSM head mounting assembly

Static magnetic fields up to 1.3T (at 30A) are provided

by an 8 inch air-cooled Newport Instruments Type D electromagnet employing double taper pole tips with a face diameter of 100 mm and a 59.1 mm air gap. The design of the pole tips (Figure 4.5) features a compromize between removing all ferromagnetic material which subtends an angle of greater than $\sim 55^{o}$ from the pole axis, thus maximizing the air gap field (Zijlstra (1967 a)), and ensuring that the correctly designed search coils (see Section 4.4) are mounted in a uniform field region. The field uniformity in the gap has been determined experimentally by carefully mapping out the spatial field intensity with the aid of a Hall-effect probe gaussmeter. For fields between 0 and 1 tesla the homogeneity was found to be better than 0.2% within a sphere of radius 10 mm centred on the sample position. The field volume, thus described, more than adequately contains the entire range of sample volumes used on the VSM. The field homogeneity data, some of which is illustrated in Figure 4.6, thus allows the local external field acting on the sample to be predicted accurately from a field measurement at a position significantly removed from the central region of the magnet air gap.

The magnet current is supplied by a Newport Instruments C224 350 volt-30 amp. supply which consists of a control unit and three phase motor generator. Whilst the current stability of this supply is good (1 part in 10^4 per hour) there is the inevitable presence of some ripple which yields ripple field amplitudes of 2 μT at zero d.c. field and 6 μT at 1T. The ripple field is predominantly 50 Hz

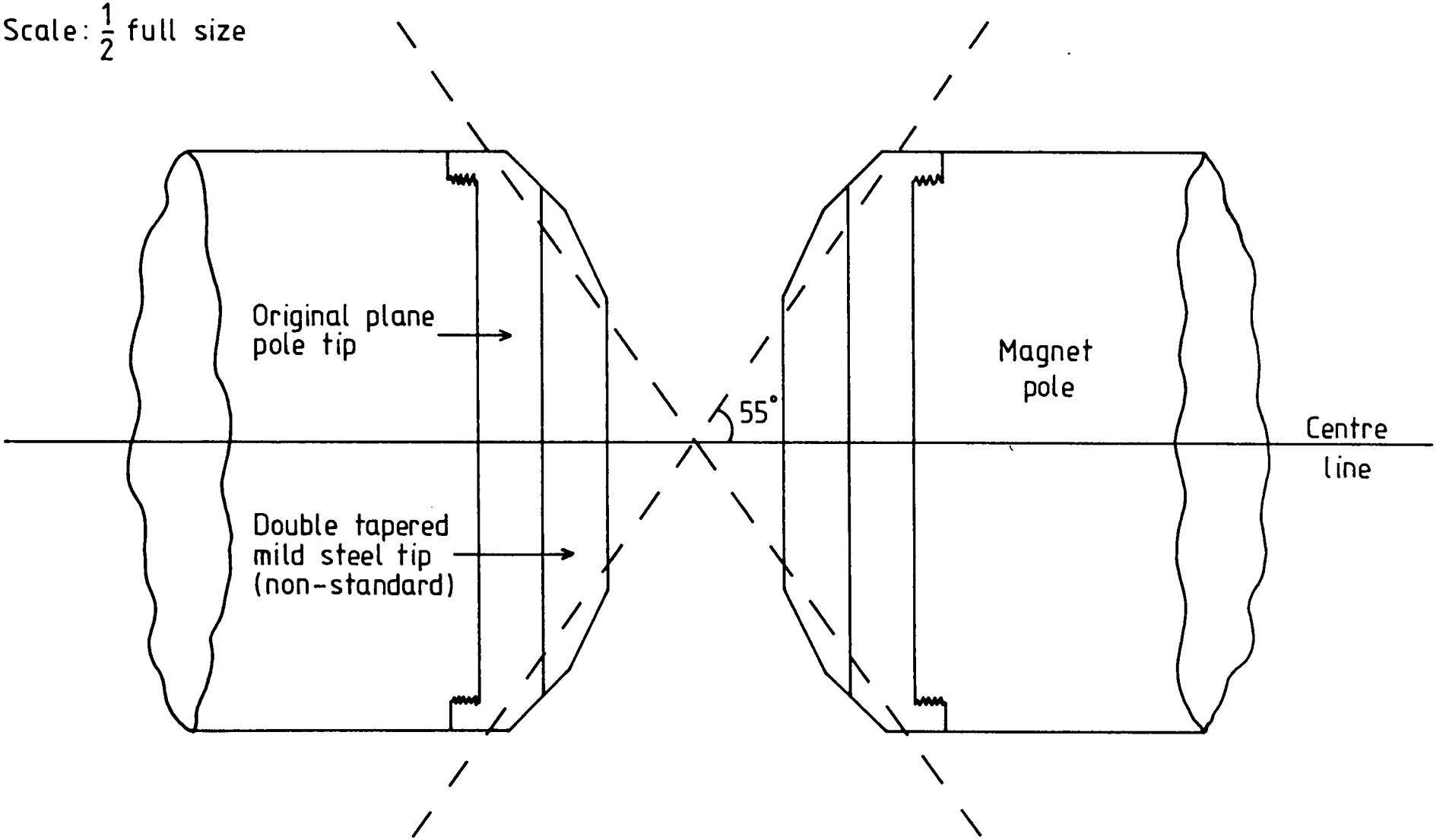

Figure 4.5 Detail of pole tip design featuring non-standard double tapered mild steel addition to original plane pole tip.

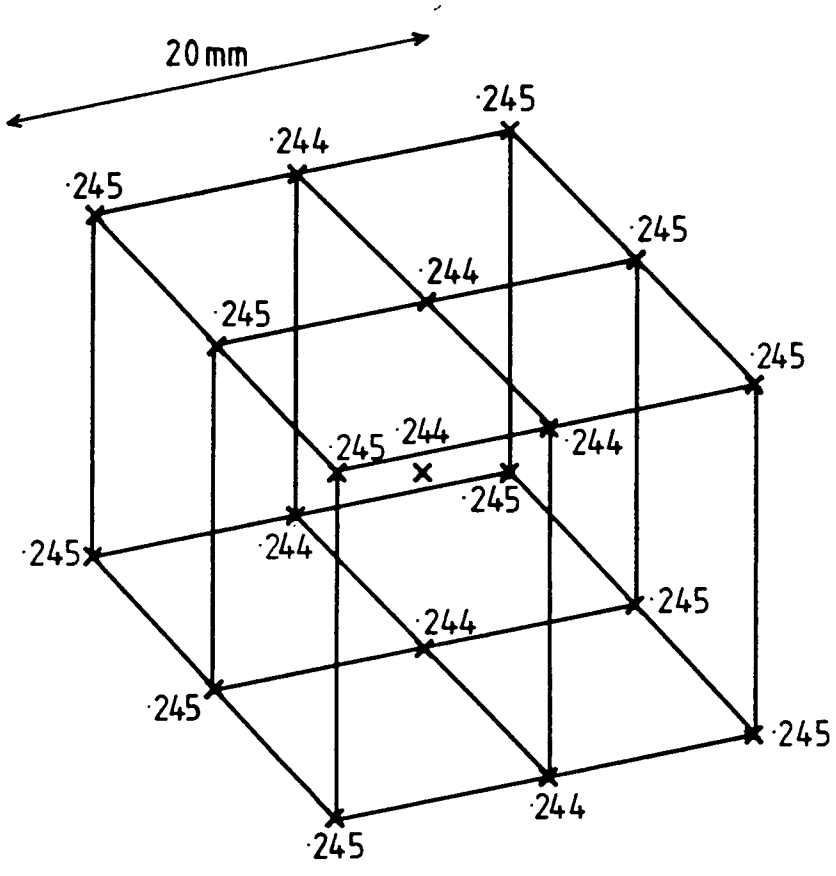

Figure 4.6 Field values (in tesla) measured on surface of cube of side 20mm centred on sample position.

but some 24 Hz also appears as the coil current is increased. The 24 Hz component has its origin in the generator, this being the three phase generator commutator slip field frequency. Although the perpendicular detection coil geometry preferred by the author is sensitive to the ripple field variations when individual coils are considered, a ripple field rejection ratio of 10^{-4} has been achieved compared to the single coil case by carefully balancing the composite detection coil system (see section 4.4(iii)).

The electromagnet yoke/coil/pole-piece assembly is secured to its fixed base via a rotating table which allows the independent rotation of the magnet through a full 360^{o} angle. The VSM vibrator head (described earlier) forms part of a head plate assembly which is placed on a table that is rigidly attached to the same magnet base in such a way that it does not hinder the rotation of the magnet. This facilitates the study of the angular dependence of magnetization once great care has been taken to accurately centre both the sample and magnet air gap on the rotation axis.

The transmission of vibration from the VSM head plate assembly to the support table is prevented by a pneumatic isolation collar placed between the two (Figure 4.7). The support table also has four tapered protrusions and clamps which allow the head plate and table to be rigidly clamped to each other when loading or unloading samples, thus preventing lateral movement of the plate on the isolation collar. Movement of this kind is undesirable

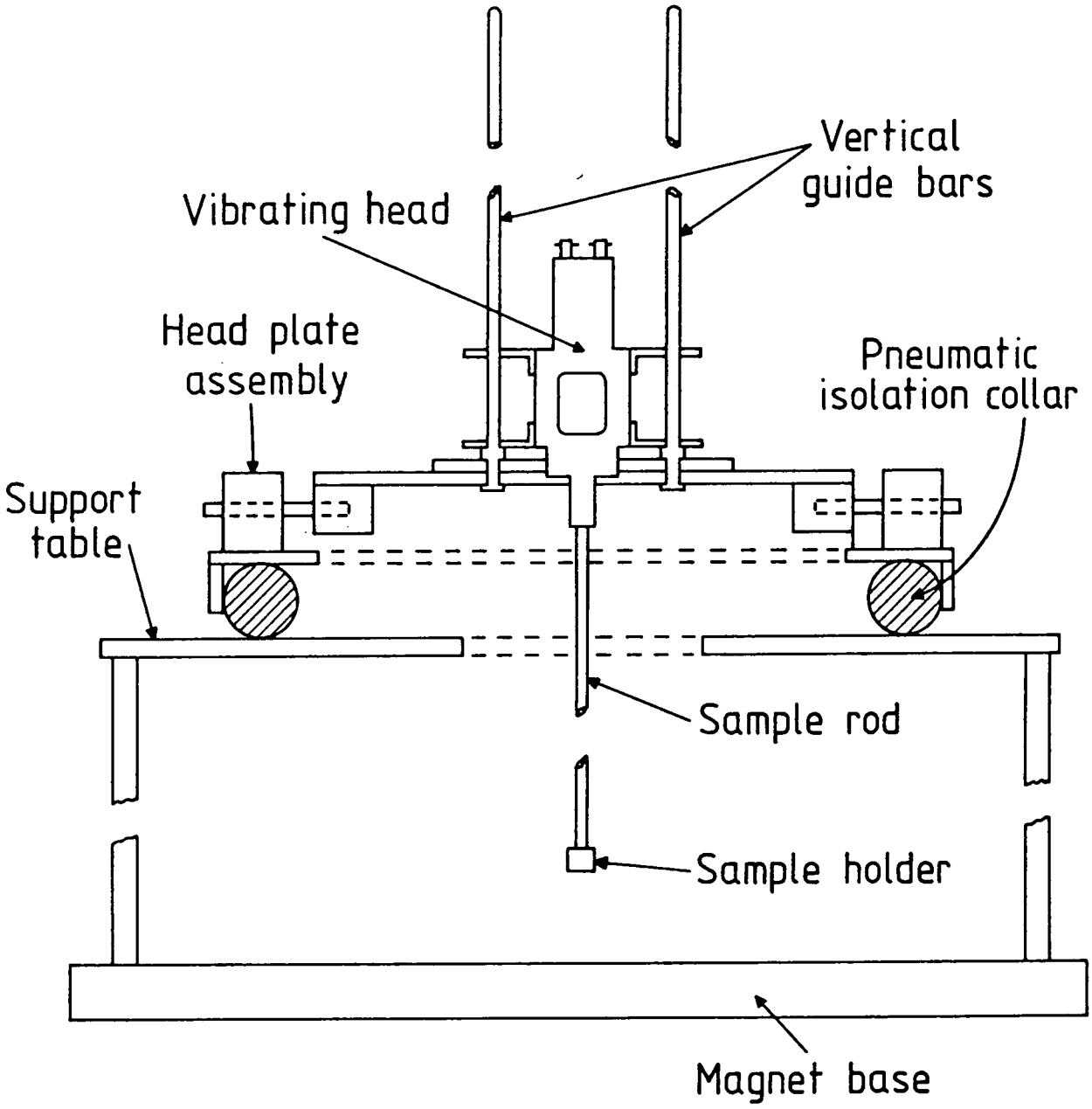

Figure 4.7 (a) and (b) (overleaf). Detail of design and construction of VSM head plate assembly, isolation collar, support table and vertical guide bars.

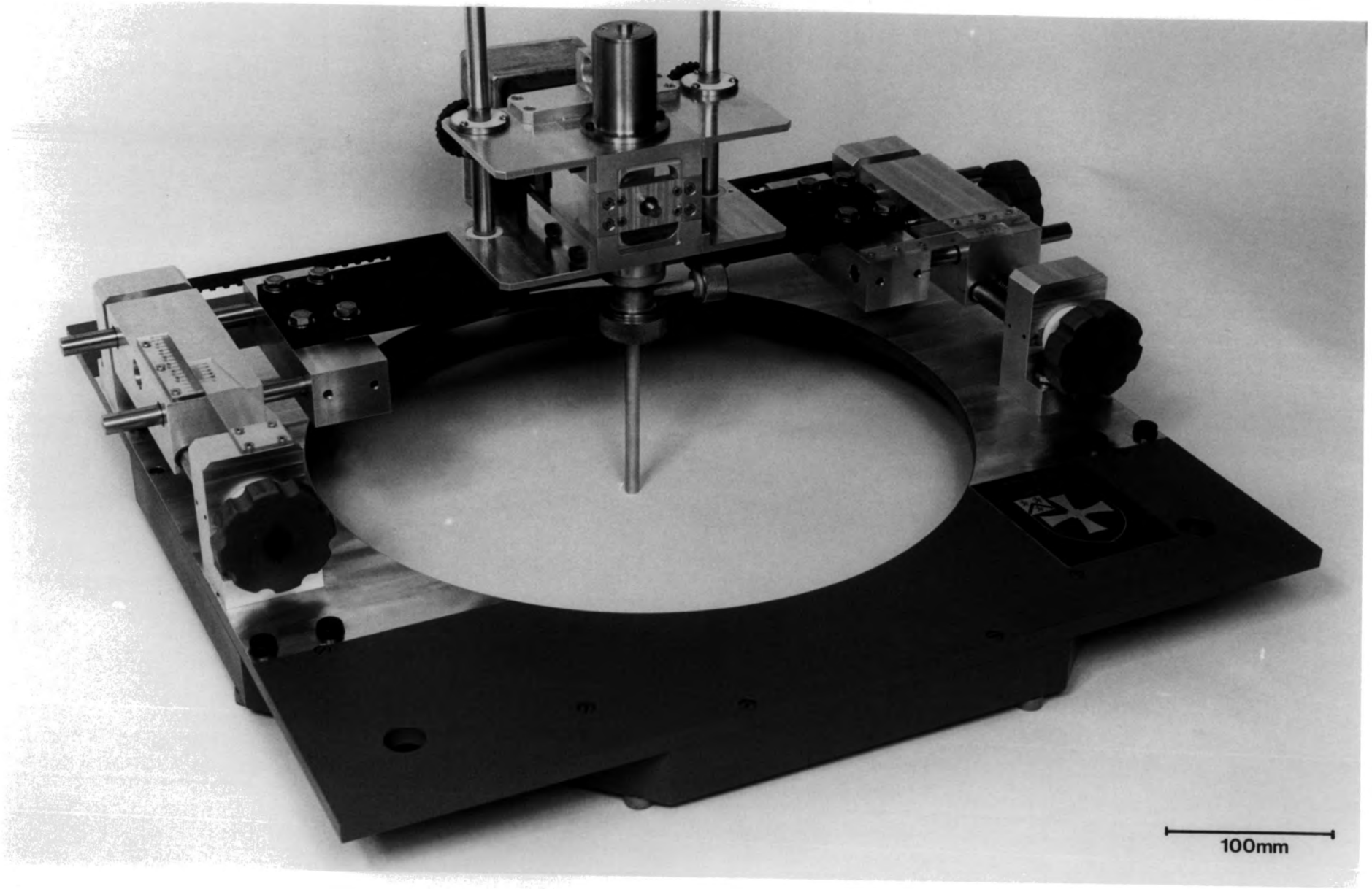
100mm

as it could result in the displacement of the VSM away from the saddle point of the search coils sensitivity function.

4.3(iii) The Variable Temperature Cryostat

A conventional Oxford Instruments CF 1200 helium gas flow cryostat operating in the range 4.2 to 500^{o}K has been incorporated into the VSM design as a demountable fitting. Special attention has been paid to mounting the cryostat positively with two quick-release clamps which permit the rotation of the magnet independent of the cryostat, helium transfer system and dewar. One, axially mounted, supports the tail of the cryostat from the magnet base, while the other, which supports the upper section of the cryostat, is fitted into a radiused cut-out in the upper yoke of the magnet. Both clamps have been made and fitted to a high tolerance in order that the axis of the cryostat's sample space and the rotation axis of the magnet are coincident. This arrangement prevents sympathetic vibration of the cryostat, thus avoiding noise generation at high fields, does not restrict magnetization measurements as a function of angle and ensures accurate and repeatable sample location.

The centring of the sample with respect to the cryostat is assured by a PTFE (polytetrafluoroethylene) slide bearing on the bottom of the sample rod which locates on the cryostat sample space wall. The loading and removal of samples in and from the cryostat is facilitated by mounting the vibrator head on detachable vertical guide bars within the head plate assembly (see Figure 4.7).

Also incorporated in this assembly is a precision x-y movement mechanism, constructed of 12.7mm non-magnetic stainless steel bars and phosphor bronze bearings, which permits accurate positioning of the sample support rod with respect to the neck of the cryostat (Figure 4.8). This increases the repeatability and accuracy of sample positioning further by minimizing pivoting of the sample rod about the lower PTFE bearing which may otherwise occur.

A gold-0.07 iron-chromel thermocouple , attached to the heater block at the base of the sample space, measures the sample space temperature. Whilst this method of temperature measurement is not entirely field independent, the fluctuation in the thermocouple e.m.f. observed by the author, less than $0.1^{o}KT^{-1}$ between 0 and 1 tesla, was comparable with the absolute precision of such thermocouples. Failure to check the magnitude of the field dependence of the temperature sensors, which is highly specific to both sensor type and system geometry, can cause significant errors in thermometry (Sample and Rubin (1977)).

For a more precise determination of the sample temperature an additional sensor (carbon glass resistor or thermocouple) may be passed down the sample support rod and placed adjacent to the sample. The disadvantage incurred by this practice is to increase the residual noise signal, although this inconvenience is largely offset in automated apparatus where subtraction of the field dependent residual signal from the raw data set

Figure 4.8 Illustration of design and construction of precision x-y movement mechanism which forms part of VSM head plate assembly.

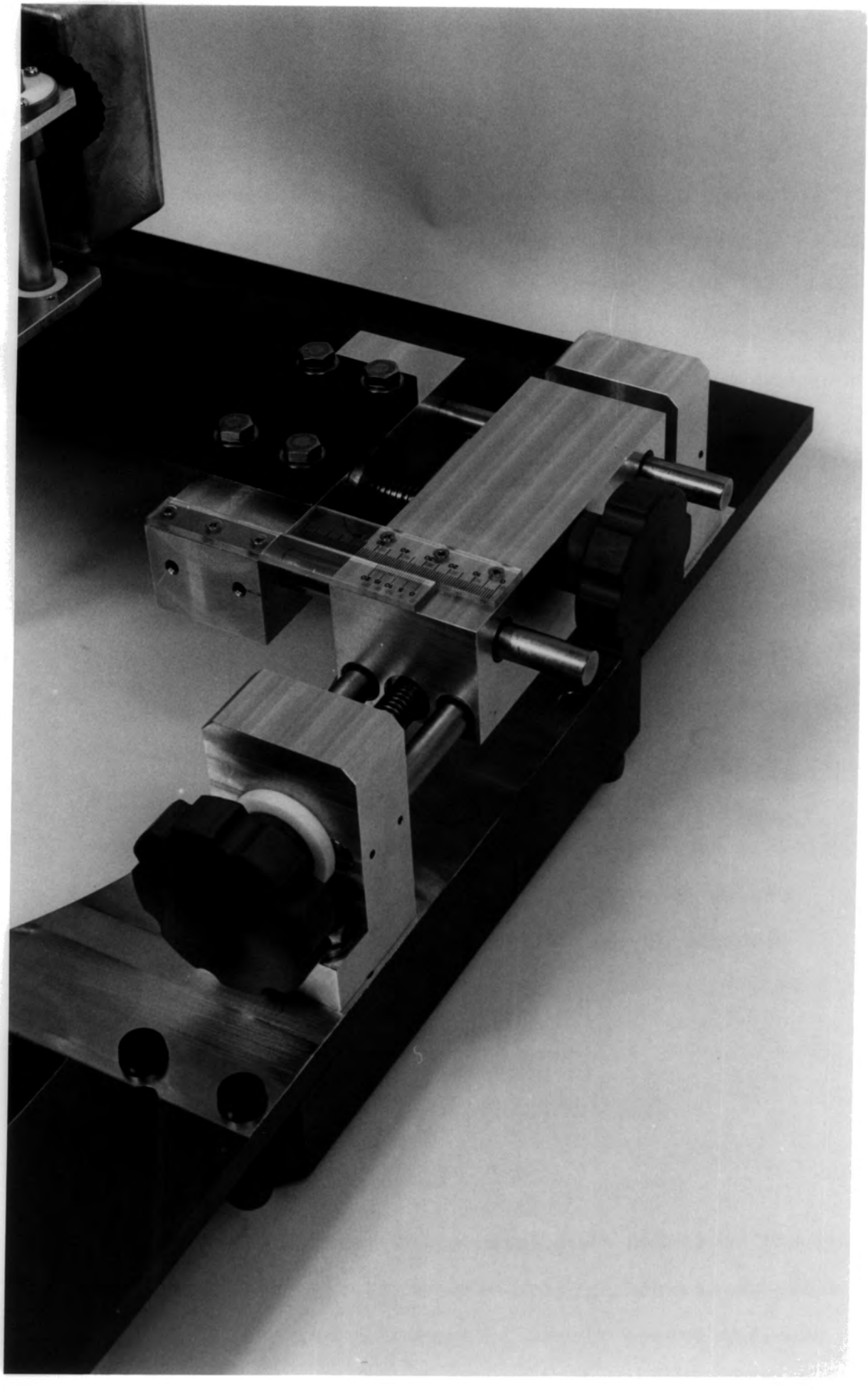

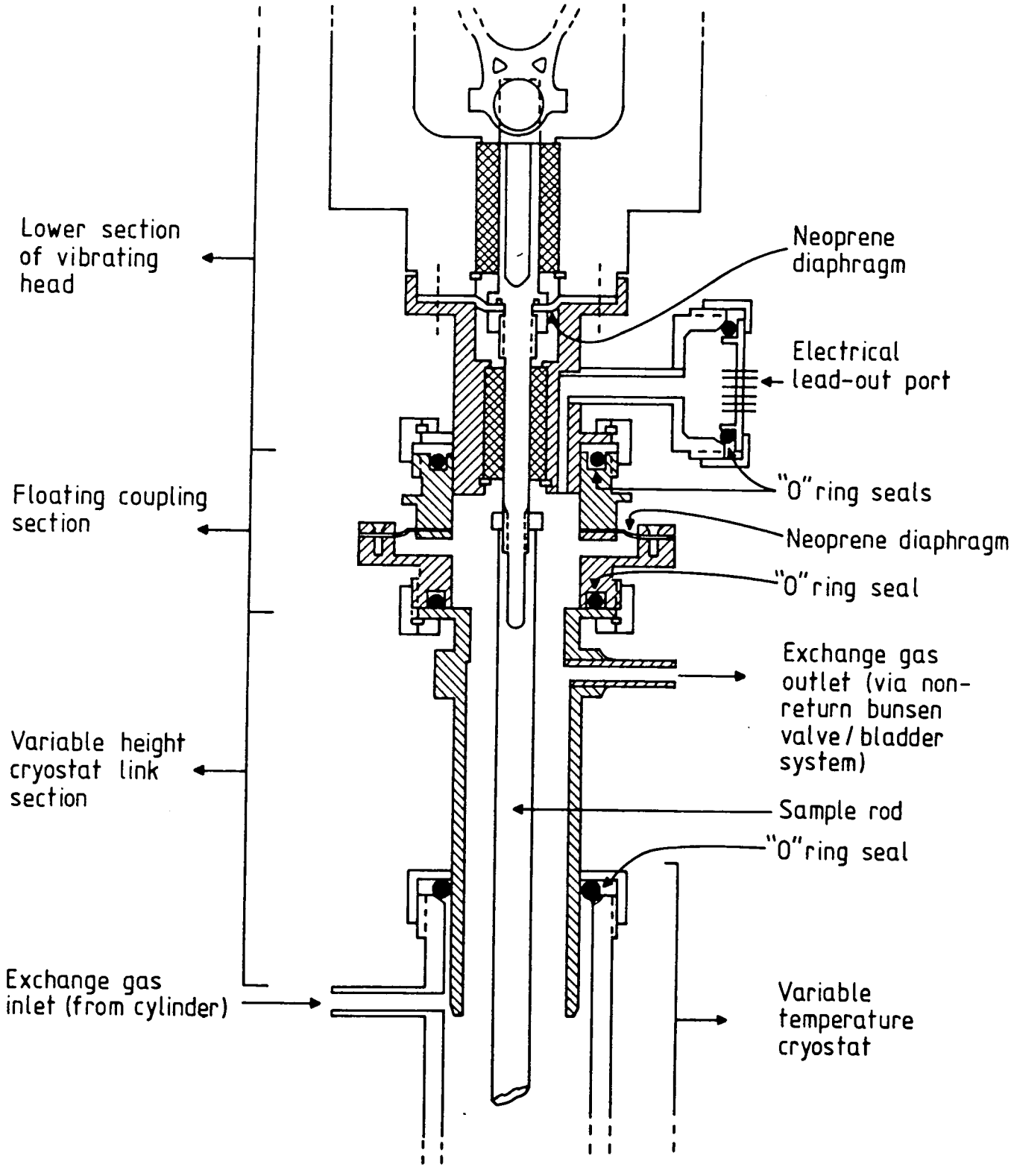

Figure 4.9 Detail of design and construction of coupling between gas flow cryostat and VSM vibrating head section.

the axis of sample vibration (Foner (1959), (1974) and (1975) , Mallinson (1966), Bowden (1972), Bragg and Seehra (1976), Guy (1976a,b), Pacyna (1982), Zieba and Foner (1982a) and Pacyna and Ruebenbauer (1984)). Attempts have been made to quantify the detection sensitivity and efficiency of such systems both experimentally (Foner (1959), Case and Harrington (1966), and Bowden (1972)) and theoretically (Mallinson (1966), Bragg and Seehra (1976), Guy (1976b), Pacyna (1982), Zieba and Foner (1982a) and Pacyna and Ruebenbauer (1984)), and the existence in the literature of apparently conflicting claims for the superiority of specific coil systems is principally due to differing definitions of detection efficiency. To this end, Willcock and Hoon have tried, in a recent paper (Hoon and Willcock (1985)), to allay further confusion by presenting general comments pertinent to a practical discussion of the relative merits of the various detection coil systems based on a consistent definition.

All theoretical considerations of detection coil system response involves the calculation of a sensitivity function $G(\underline{r})$ which characterizes the dependence of the induced signal upon the position and orientation of the magnetic moment and pick-up coil geometry. The explicit form of $G(\underline{r})$ depends on the adopted approach to calculation, whether by consideration of the field from a point dipole (Pacyna and Ruebenbauer (1984)) or by use of the Principle of Reciprocity (Zieba and Foner (1982a)), but the general equivalence of either method is apparent. The design of a suitable coil system corresponds to maximizing the

sensitivity function of the detection coil array, whilst positioning the coils such that $G(\underline{r})$ is constant in the region of the vibrating sample ($\underline{r} = \underline{r}_o$). Ideally a broad saddle point region (for which $\frac{d}{dr}G(\underline{r}_o) \rightarrow 0$) occurs about $\underline{r}_o$ in all displacement directions. This ensures minimizing calibration errors due to sample positioning errors and it also minimizes the sensitivity of the detection coil array to sample shape effects (Foiles and McDaniel (1974)).

In practice it is extremely difficult to achieve a broad three dimensional saddle point without producing either an unacceptable reduction in the absolute value of $G(\underline{r})$ or resorting to complex multiple coil arrays (Bowden (1972)). It is also difficult, in practice, to predict coil dimensions from "ideal" values of $G(\underline{r})$ chosen a priori, and it has been pointed out (Hoon and Willcock (1985)) that much qualitative information about the behaviour of detection coil systems can be extracted from a careful consideration of the components of the dipole field appropriate to the coil configuration used.

4.4(ii) The selection of a detection coil system

A consideration of the detection coil systems capable of detecting the component of sample moment colinear with the external field ($\underline{B}$) and perpendicular to the axis of sample vibration ($\hat{\underline{a}}$) must include the geometries of Foner, Mallinson and Bowden. The difference between these specific coil geometries is indicated by Figure 4.10. It can be seen that:-

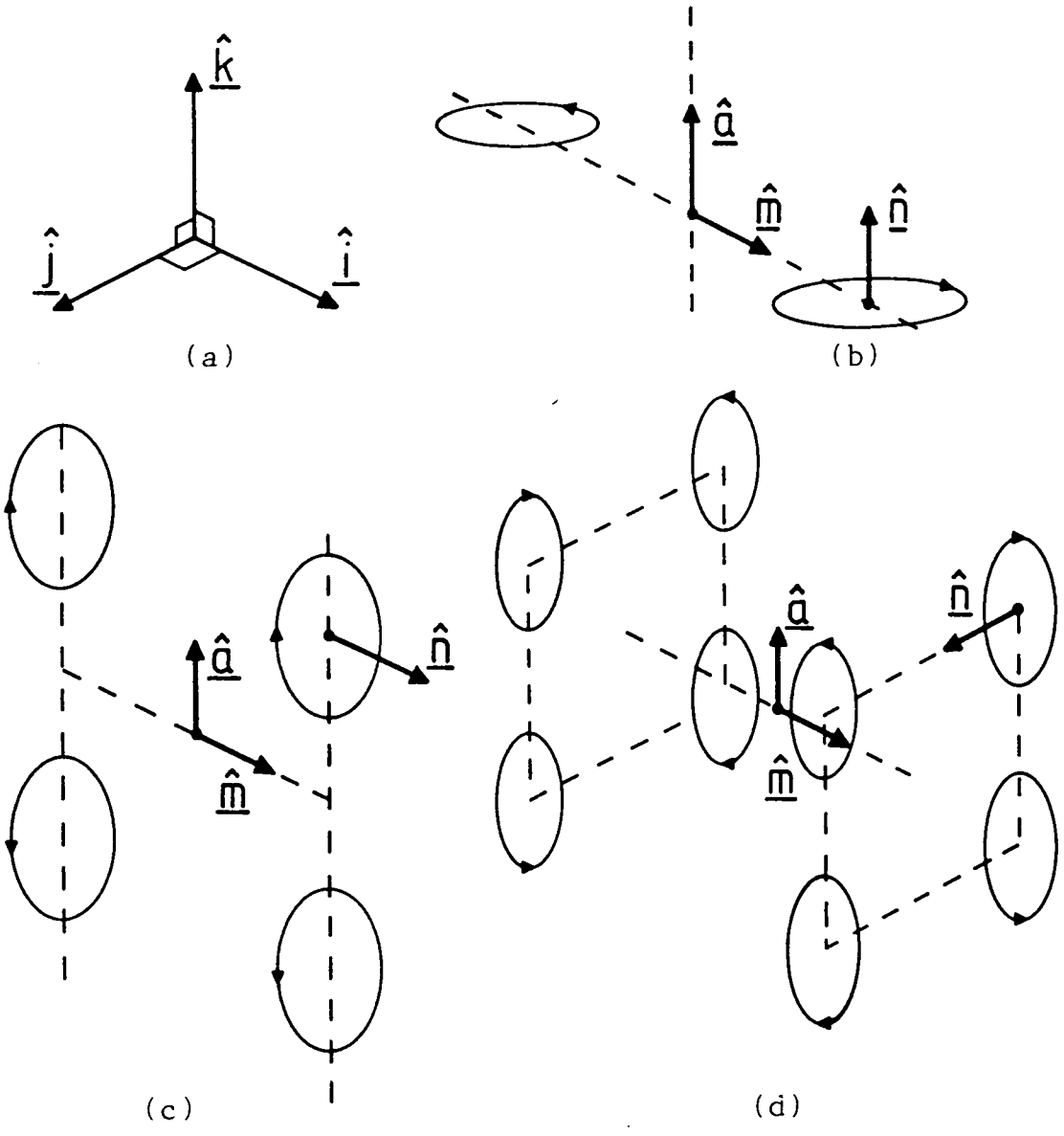

Figure 4.10 Comparison of the detection coil geometries of (b) Foner, (c) Mallinson and (d) Bowden. (a) defines the coordinate system, and the electrical sense in which the individual coils are interconnected is indicated by the arrows.

(i) the coil axis ($\hat{\underline{n}}$) is parallel to the vibration axis for Foner's two or four coil geometry (i.e. $\hat{\underline{a}}.\hat{\underline{n}} = 1$ and $\hat{\underline{m}}.\hat{\underline{n}} = 0$).

(ii) the coil axis is parallel to the moment direction for Mallinson's four coil geometry (i.e. $\hat{\underline{a}}.\hat{\underline{n}} = 0$ and $\hat{\underline{m}}.\hat{\underline{n}} = 1$), while

(iii) the coil axis is orthogonal to both $\hat{\underline{a}}$ and $\hat{\underline{m}}$ for Bowden's eight coil geometry (i.e. $\hat{\underline{a}}.\hat{\underline{n}} = 0$ and $\hat{\underline{m}}.\hat{\underline{n}} = 0$)

and, after much consideration of and deliberation over the relative merits of these specific systems as described in the literature, Mallinson's geometry was selected as being the most suitable for the Durham VSM. The main reasons for this choice are summarized below, but the reader is also referred to Hoon and Willcock (1985).

Bowden's geometry requires the use of eight identical detection coils symmetrically positioned with respect to the sample and the magnet air-gap field. The main advantage of this system is that it is capable of achieving very broad saddle point regions. Indeed, Bowden has shown (Bowden (1972)) that signal changes of less than 1% are observed for sample displacements of $\pm$ 2.6 mm, $\pm$ 6.4 mm and $\pm$ 4.8 mm in the $\hat{\underline{m}}$, $\hat{\underline{n}}$ and $\hat{\underline{a}}$ directions respectively using such a system. These figures are at least an order of magnitude better than any others previously reported (Foner (1959) and Case and Harrington (1966)) and, as such, represent a significant improvement in coil system design. The disadvantages of the design, however, are numerous and include the complexities of manufacturing, balancing and positioning the whole system

within the magnet field gap. The existence of these difficulties, therefore, were considered to outweigh the advantage of an excellent saddle point region, thus resulting in the rejection of this coil geometry.

The comparison of Foner's and Mallinson's geometry was less straightforward, being complicated by conflicting claims of system superiority in the literature. Detailed considerations of the nature of the dipole field and the available magnet air-gap volume for positioning detection coils, however, indicate quite clearly which system is capable of the greater signal output.

Using the coordinate system defined by figure 4.11 (where the unit vectors $\hat{\underline{x}}$ and $\hat{\underline{z}}$ are identical to the vectors $\hat{\underline{m}}$ and $\hat{\underline{a}}$ of Figure 4.10) it is obvious that the set of detection coils in both Foner's and Mallinson's geometry are only sensitive to changes in the field component B_x arising from the vibrating moment. Assuming the field external to the moment to be well described by the dipole field (Foiles and McDaniel (1974)) we have:

$$\underline{B} = \frac{-\mu_0}{4\pi}\left(\frac{\underline{m}}{r^3} - \frac{3(\underline{m}.\underline{r})\,\underline{r}}{r^5}\right) \qquad (4.8)$$

and hence $$B_x = \frac{\mu_0 m}{4\pi r^3}\left(3\cos^2\phi\cos^2\theta - 1\right) \qquad (4.9)$$

for all θ, ϕ and r.

Constant B_x contours, calculated from equation (4.9), are shown in Figure 4.12, plotted as a function of r and θ within the x-z plane. It is noted that B_x is axially symmetric about the x axis and Figure 4.12, therefore, represents sufficient information to allow a meaningful

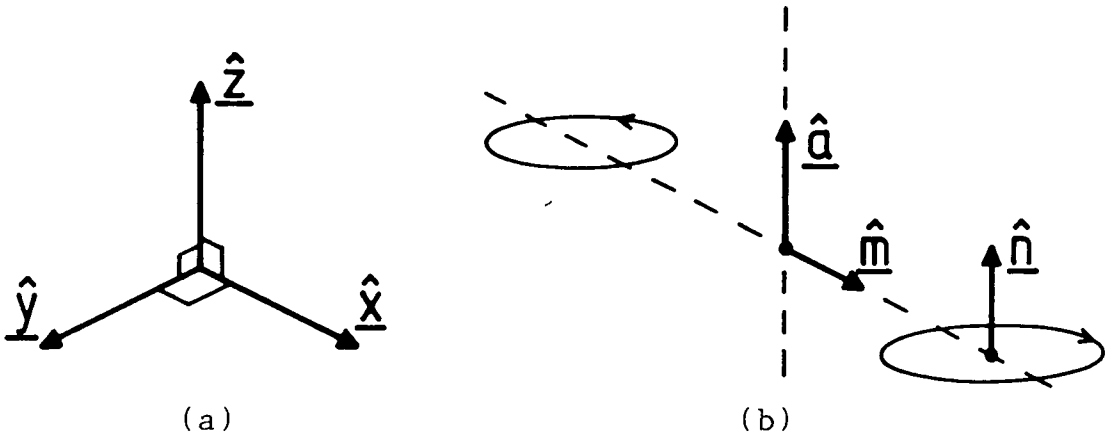

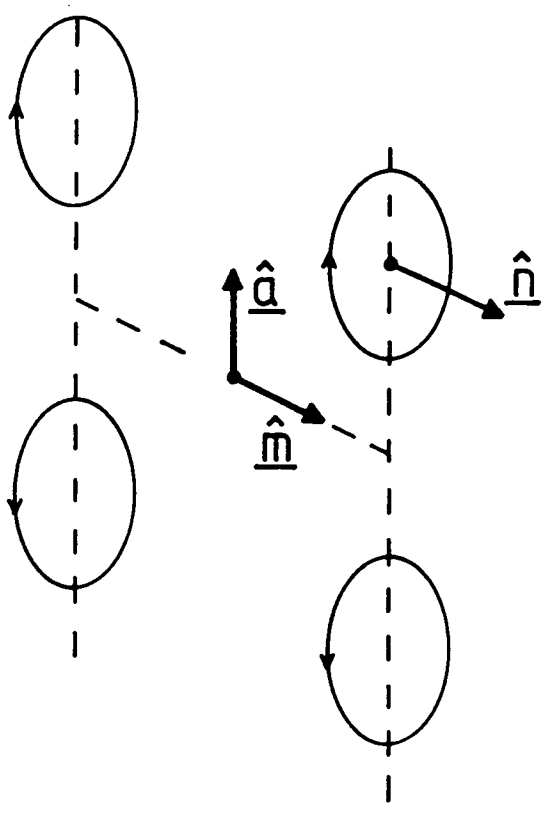

Figure 4.11 (a) Definition of $\hat{x}$, $\hat{y}$, $\hat{z}$ coordinate system as used to describe (b) Foner's and (c) Mallinson's coil geometries (see text).

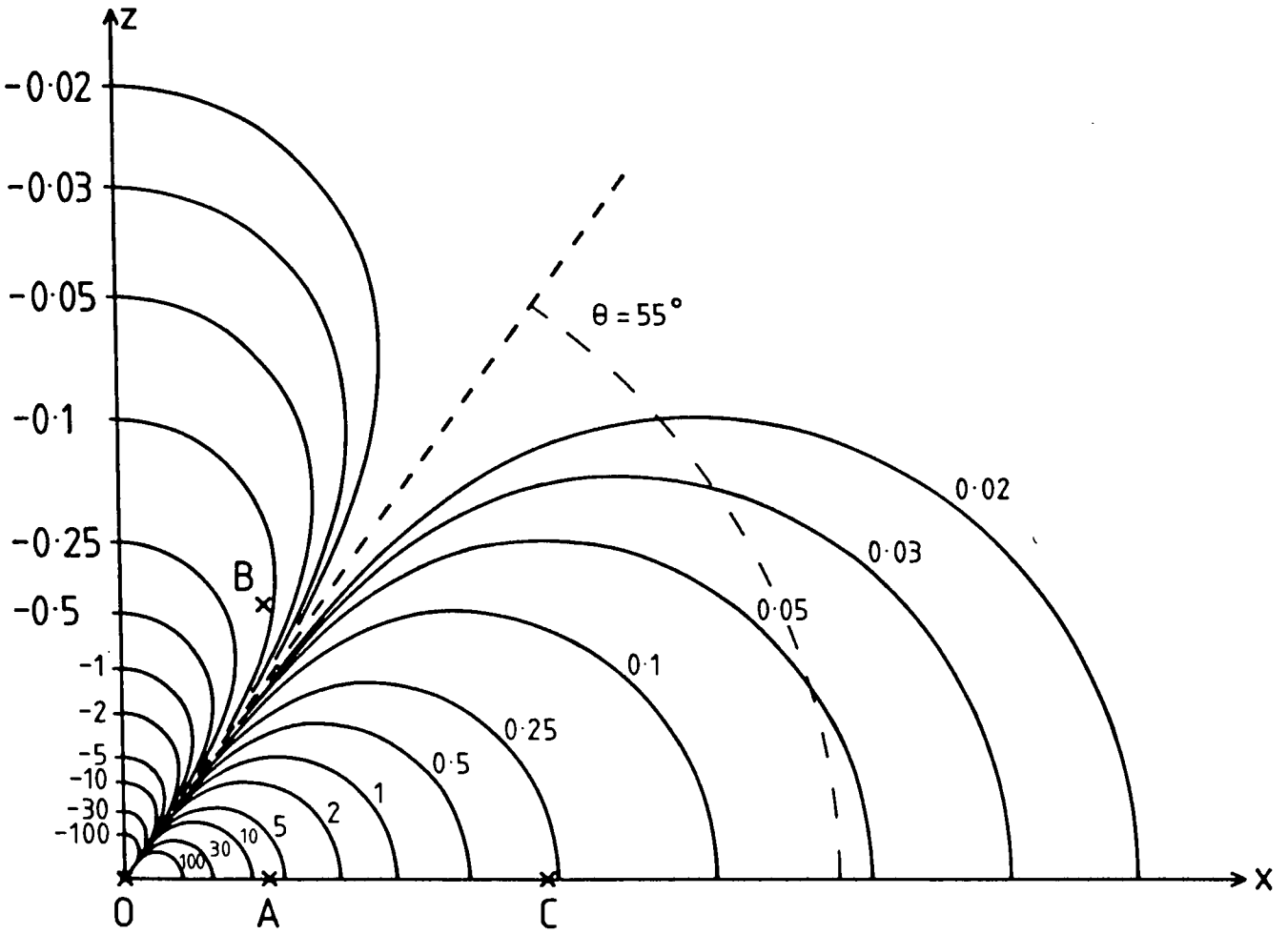

Figure 4.12 Constant B_x contours (arbitrary units) plotted as a function of radial distance (r) and theta in the x-z plane. The B_x contours have rotational symmetry about the x axis and reflectional symmetry in the y-z plane.

discussion of detection coil response.

An exact calculation of the response of Foner's or Mallinson's coil system requires the calculation of the integral of $\frac{dB_x}{dz}$ taken over the complete area of the coil system. Unfortunately, it is not possible to obtain such expressions in closed form, thus necessitating the use of a harmonic series of Legendre polynomials (Zieba and Foner (1982a)) or linear combination of complete elliptic integrals (Pacyna and Ruebenbauer (1984)) when making these calculations. The use of the two dimensional approach to coil design, however, allows the detection coils to be modelled by forward and return conducting sections and permits qualitative comparisons of the two coil systems to be made.

The two dimensional approximation, first suggested and used by Mallinson (Mallinson (1966)), considers the difference in the e.m.f. induced in the forward and return conductors to be a reasonable representation of the coil output. An inspection of Figure 4.12 reveals that, for values of $\theta > 55^{o}$, there is a reversal in the sign of B_x first pointed out by Mallinson. With the forward conductor positioned at A, placing the return conductor in this negative region (for example at B), therefore, serves to enhance the coil output because the e.m.f. induced in both conductors is in the opposite direction (i.e. in the same coil sense). The exact position of the point B above the 55^{o} line is not critical, but considerations of thermal noise in the coil or the extent of the uniform air-gap field may, in practice, limit

the diameter of the coil. The positioning of the forward and return conductors for a Foner coil of identical diameter is indicated by positions A and C respectively. Here, the e.m.f. in both conductors is induced in the same direction (opposite coil sense) and the net coil output is dependent on the r^{-3} fall off of B_x with r. The distance OA is normally determined by a physical constraint, such as the presence of a variable temperature cryostat, and the comparison of the output of identical Foner and Mallinson coils, subject to this constraint, favours the latter.

Once further physical constraints on coil size are considered, for example the air-gap volume available for siting detection coils, the comparison between Foner and Mallinson coils can, no longer, consider identical diameter coils. The available air-gap, usually defined by the difference between magnet pole separation and cryostat diameter, must contain forward and return conductor windings as well as coil former material in the Foner system, whereas the whole of this region may be occupied by the forward conductor windings alone in the Mallinson system. A greater number of windings is possible, therefore, with the Mallinson geometry and this, combined with the now reduced diameter Foner coils, serves to increase further the output of the Mallinson system with respect to that of Foner. Another less obvious advantage of Mallinson's coil system arises from a consideration of magnet images. This effect will be discussed in greater detail later (see Section 4.7) and it is sufficient to

state here that the inevitable presence of images in conventional electromagnets serves to enhance the signal induced in Mallinson coils whilst detracting from that induced in Foner coils.

The main criticism of Mallinson's detection coil geometry which has been pointed out many times in the literature (see, for example, Bowden (1972) and Zieba and Foner (1982a)) is that the individual coils are directly sensitive to field fluctuations and the ripple of the d.c. field in particular. This, however, need not be a problem if care is taken during coil construction to produce a set of identical, balanced coils which are then mounted in a uniform field region. Substantial rejection of the ripple field signal is then possible which permits the use of phase sensitive detection techniques without the risk of incurring saturation effects in the initial amplifier stages.

4.4(iii) The design, construction and properties of the coil system

The difference between the diameter of the tail of the CF1200 cryostat (38 mm) and the magnet pole separation (59 mm) allowed a thickness of approximately 10 mm for each pair of Mallinson type detection coils, their mounting plates (cheek plates) and screening/protection covers. The chosen design is illustrated in Figure 4.13 and shows the system to consist of accurately turned tufnol coil formers mounted on 1 mm thick brass shim cheek plates which, in turn, are rigidly clamped to the

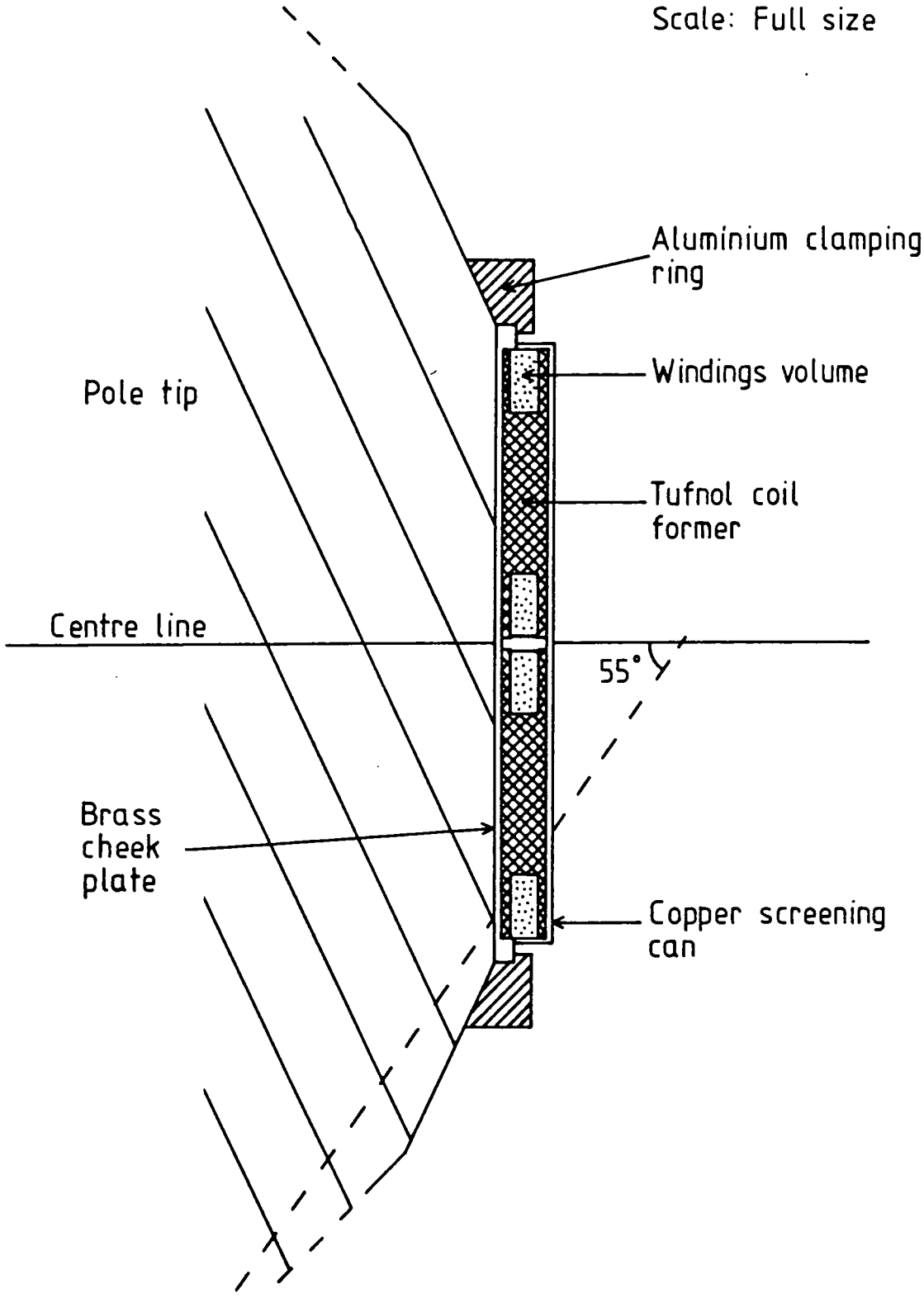

Figure 4.13 Illustration of design of detection coil, cheek plate and screening can assembly. Adjustable expanding brass bars bear on the aluminium rings to clamp whole assembly rigidly to pole tips.

pole faces of the magnet pole tips by adjustable brass bars. A copper screening cover/can covers each pair of coils and serves both to protect the coils from mechanical damage and to provide electrical screening from undesirable external sources. The volume of the detection coil windings is described by inner and outer diameters of 25 mm and 45 mm respectively and a width of 5 mm. The complete coil is seen to be positioned within the uniform field region provided by the plane pole tip surface in such a way that the upper return windings are almost completely contained above the $\theta = 55^{o}$ boundary. The separation of each pair of coils about the plane of symmetry by 2 mm was deliberately chosen to flatten the coil system's sensitivity function for mean sample position displacements in the vertical direction.

The detection coils were wound evenly, using 44 s.w.g. enamel-coated copper wire, to a total of 4600 turns for each coil. The balancing of the set of four coils was achieved by removing turns to firstly equate the inductances of the individual coils in isolation from the other three, and then finely balancing all four coils in situ on the cheek plates in a similar manner. The measurements were all recorded using a Wayne-Kerr LCR bridge using a frequency (100 Hz) as close as possible to the intended VSM drive frequency, and great care was taken to ensure thermal stability (after handling the coils) before results were recorded. At the end of the balancing process the inductances of each of the four coils in situ were 830 $\pm$ 3 mH, 830 $\pm$ 4 mH,832 $\pm$ 4 mH

and 833 $\pm$ 4 mH respectively.

The complete search coil/cheek plate assemblies were mounted on the magnet pole faces and experiments were performed in order to assess the ripple field signal rejection capabilities of the balanced coil system. A small amplitude a.c. magnetic field was provided in the magnet air gap by a pair of Helmholtz trim coils, provided as a magnet accessory, and the e.m.f. induced in a single detection coil was compared to that induced in the complete coil assembly. The frequency of the a.c. field was chosen to be 24 Hz, this being the three phase generator commutator slip field frequency, because it represents the known ripple field noise signal whose frequency is closest to the frequency of sample vibration (see section 4.3(ii)). The results obtained from this study are as follows:-

Single coil signal = 1.004 $\pm$ 0.001 V (r.m.s.)

Combined signal from all four coils = 0.88 $\pm$ 0.01 mV (r.m.s.)

The effective signal from a single coil in the complete coil system, therefore, is 0.22 mV and this represents a ripple field signal rejection ratio of approximately 2×10^{-4} compared to the isolated single coil. This result clearly indicates that the degree of ripple field rejection is limited by the accuracy to which the detection coils have been balanced, and even greater care taken during the balancing procedure could reduce this value further.

Further experiments were conducted on the coil system to determine the sensitivity function of the system as

a function of sample displacement in the x, y and z directions (see Figure 4.11). A small single layer constant current coil, mounted on the sample rod (see Figure 4.14), was used to provide a constant magnetic moment and the movement of this moment with respect to the detection coil system was achieved, in the absence of the cryostat, using the x-y movement mechanism and the vertical guide bars of the head plate assembly (see Section 4.3(iii)). The voltage output from the detection coil system as a function of sample displacement in the three directions is shown in Figure 4.15. It can be seen that a 1% signal stability is achieved for displacements of $\pm$ 1.5 mm, $\pm$ 2.1 mm and $\pm$ 2.5 mm in the x, y and z directions respectively. Whilst these figures are not as good as the corresponding displacements of $\pm$ 2.6 mm, $\pm$ 6.4 mm and $\pm$ 4.8 mm reported by Bowden for his eight coil system (Bowden (1972)), they compare very favourably with the only other previously reported figures of Foner (Foner (1959)) and Case and Harrington (Case and Harrington (1966)) for which values of $\pm$ 0.5 mm are typical.

In conclusion, therefore, the results of the investigations into both the ripple field rejection properties of the Durham VSM coil system and the extent of the saddle point region of the system's sensitivity function have justified the selection of Mallinson's coil geometry for the Durham VSM.

4.5 Signal detection and Residual Noise

The signal from the sample moment detection coil system and the external field applied to the sample are

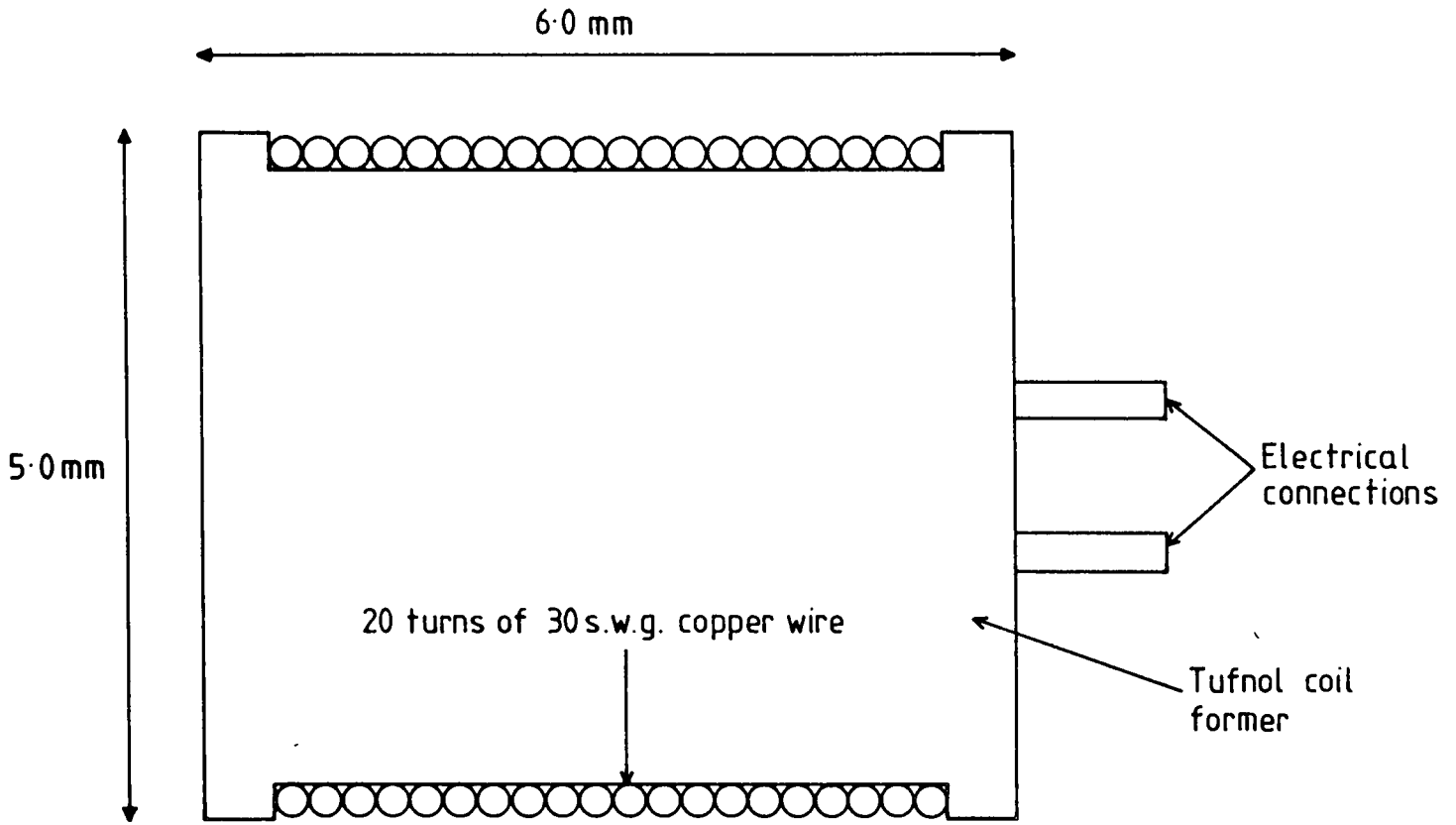

Figure 4.14 Design of small single layer constant current coil used to provide a constant magnetic moment for coil sensitivity function, linearity and magnetic image experiments (see text).

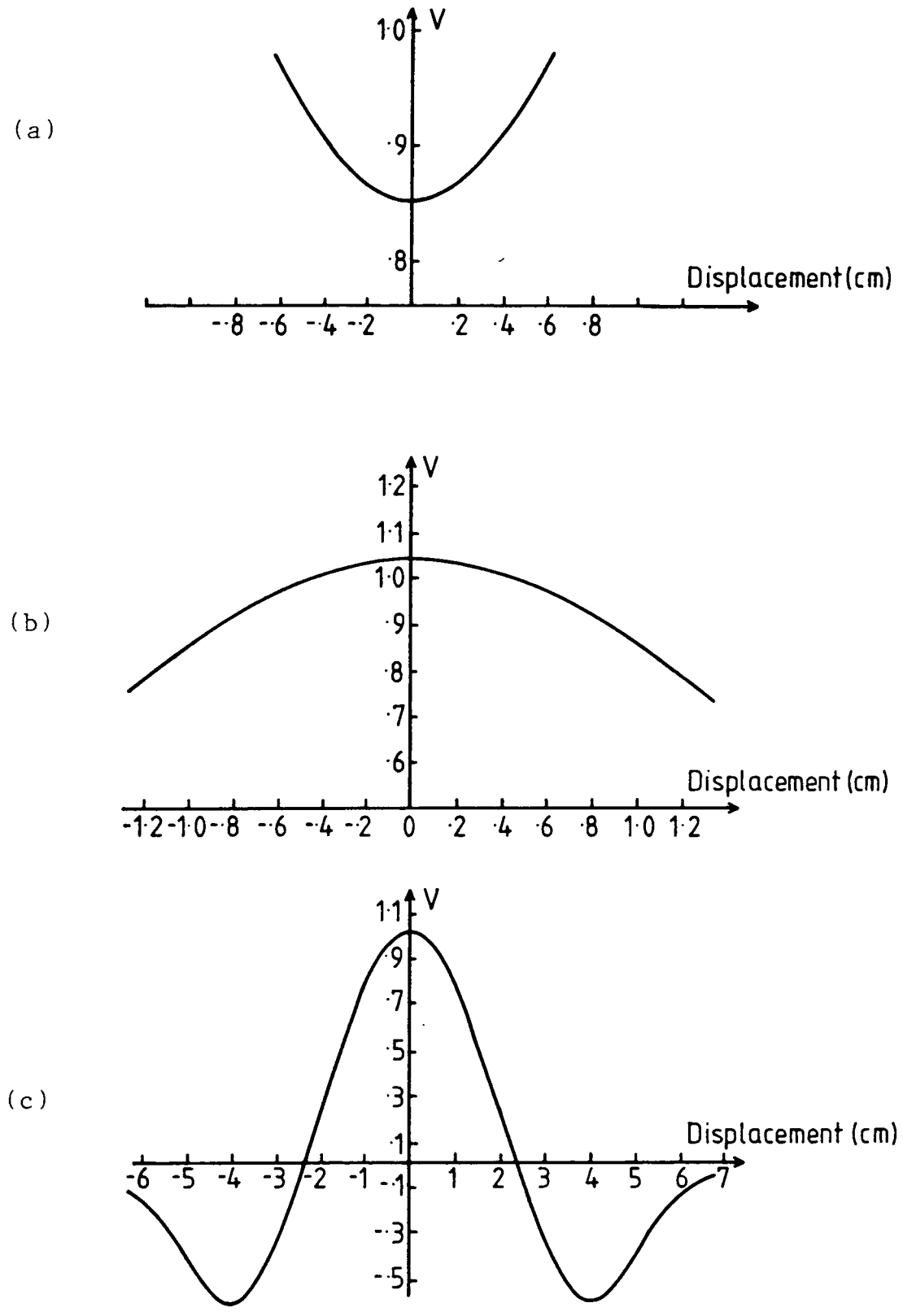

Figure 4.15 Sensitivity functions of the Durham Mallinson coil geometry. The plots indicate the voltage output from the detection coil system as a function of sample displacement in the (a) x, (b) y and (c) z directions.

measured conventionally with a Brookdeal 5206 phase sensitive detector (PSD) and a Bell 640 Hall-effect probe gaussmeter respectively. The four moment detection coils are arranged in pairs, each pair being connected in opposition so that the signals from the separate pairs are of equal amplitude but are in anti-phase. These two anti-phase signals, A and B, are then combined by the PSD using its (A-B) input mode. This method of coil connection is advantageous as working in common mode rejection not only cancels noise pick-up in the coils and their leads, but also yields good earth loop immunity. Further noise reduction has been obtained by paying careful attention to earthing, using the branch structure system and, in particular, earthing the magnet frame, cheek plates and signal lead screens to a single point.

The combined effect of clamping the detection coils and placing the pneumatic isolation collar between the VSM head and support table has eliminated the residual noise signal due to the sympathetic vibration of the apparatus at the drive frequency. Indeed, the residual signal, which is observed when no sample is present, comprises a pure diamagnetic contribution alone, arising from the PTFE sample holder and boro-silicate down rod. A typical residual signal plot is shown in Figure 4.16 and reveals a small d.c. offset to this diamagnetic trend By removing the VSM head completely from the table it has been shown that this effect is not due to vibration effects and it has been suggested that it is due to the noise power spectrum intrinsic to the motor generator

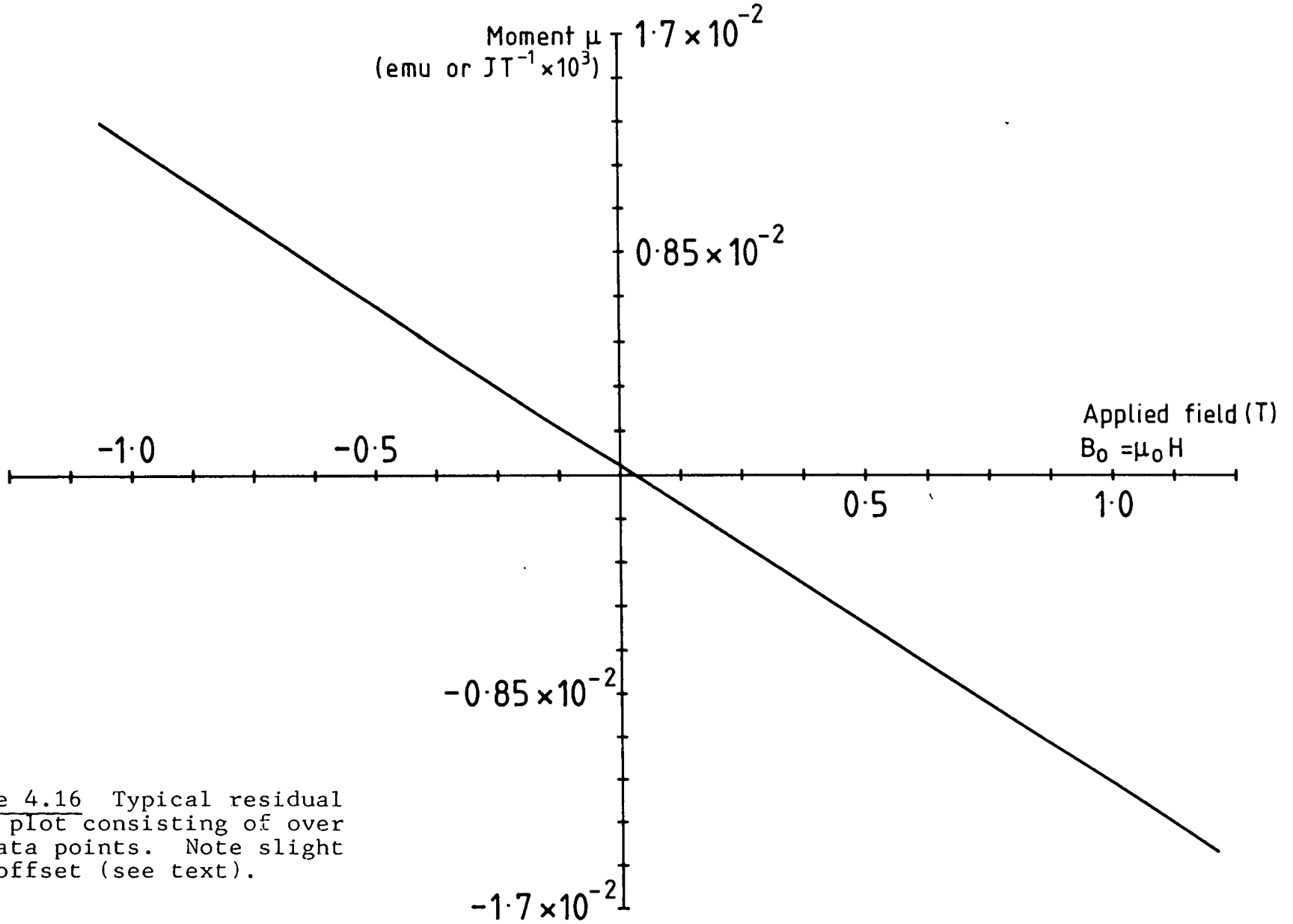

Figure 4.16 Typical residual noise plot consisting of over 200 data points. Note slight d.c. offset (see text).

supply (private communication Mr. D.B. Lambrick).

PTFE has been chosen as the sample holder material because it is both weakly diamagnetic (comparable to glass and quartz) and chemically inert, enabling the removal of magnetic contaminants with nitric acid. Further, PTFE exhibits low coefficients of friction and thermal expansion and possesses good machining properties.

The signal contribution from the sample holder can be comparable or greater than that of the sample for very low moment samples. In such cases either the difference between two plots, one with and one without the sample, can be determined, or use can be made of signal inversion in the detection coils sample displacement sensitivity function to cancel the sample holder's signal contribution. The latter approach simply requires that a further PTFE section be added to the sample support rod, appropriately displaced along the rod until its contribution to the signal exactly cancels that of the sample holder. It should be noted here that such action is not possible with Foner's detection coil geometry, thus adding further support to the author's preference for Mallinson's geometry.

4.6 Calibration and linearity

4.6(i) Linearity

The linearity of the complete V.S.M. moment detection system was determined using the same single layer current carrying coil described in Section 4.4. With the sample coil situated centrally on the saddle-point of the detection coil system, the output from the P.S.D. was determined

as a function of sample coil current. The current was varied by three orders of magnitude and a least squares fit to the data (see Figure 4.17) indicates the linearity over this wide signal range to be better than 1 part in 5500 ($\sim$ 0.02%) at constant air-gap field.

4.6(ii) Calibration

If the current carrying coil dimensions are accurately known, the moment produced by passing unit current may be calculated and an absolute coupling constant between sample and detection coil system may be determined (Foner (1959), Springford et al. (1971)). It must be stressed, however, that this constant is particular to the external field geometry of the current carrying coil (or a magnetized sample of identical geometry) (Foner (1959), Foiles and McDaniel (1974), Zieba and Foner (1982a)) and cannot, therefore, be applied to a general sample geometry.

In order to avoid approximations to this sample geometry dependent coupling constant, the author prefers to establish the instrument calibration constant using high purity (99.99% or better) samples of annealled polycrystalline or single crystal nickel, whose dimensions are identical to those of the material under investigation. This approach requires that the magnetization of nickel be independently determined and, whilst it is known to be a continuously increasing function of applied field up to 20T, its behaviour has been sufficiently well documented (Pauthenet (1982a,b)) to permit the extrapolation of the magnetization at an internal field of 1T for the

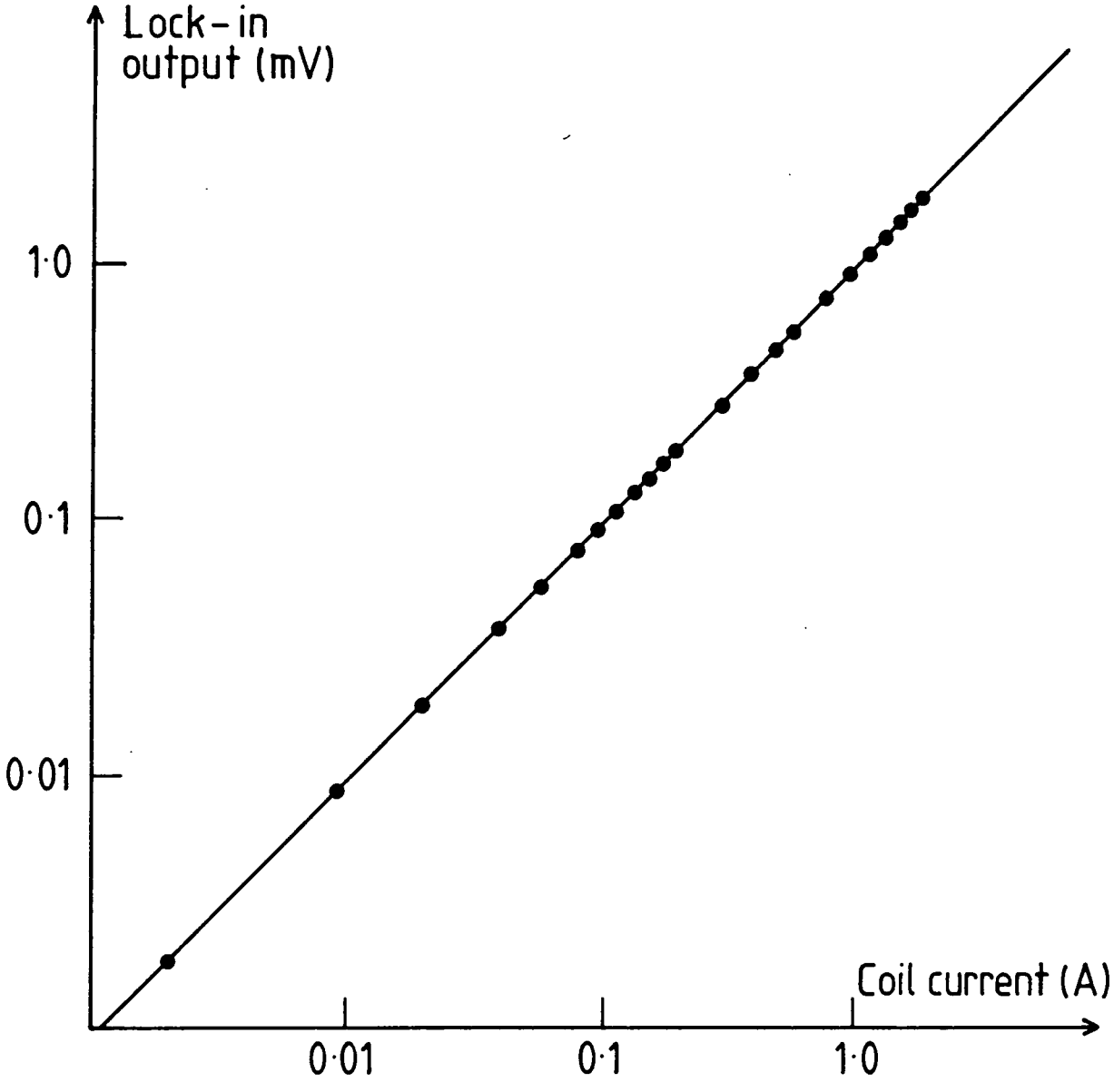

Figure 4.17 A log-log plot of detection coil output versus sample coil current for Durham VSM which indicates linearity to better than 0.02% over three orders of magnitude of signal strength.

temperature range 4.2 - 300 K (Graham (1982)).

The limit on precision using this calibration technique, apart from that inherent in the original absolute measurement of the magnetization of nickel, is the determination of the internal field in the calibration sample. This requires the designation of a demagnetizing factor for both calibration and test samples which, strictly speaking, should be field dependent (Bozorth and Chapin (1942)) as the appropriate calculations of demagnetizing factors (Osborn (1945) and Stoner (1945)) are only valid for uniformly magnetized bodies. Uncertainty in the calibration sample demagnetizing factor is not too critical, however, as the magnetization of nickel varies particularly slowly with internal field in the region of 1T and small errors in the determination of the internal field within the calibration sample can be tolerated. The variation in the saturation magnetization with temperature (θ), by comparison, is more critical and, after a careful study of the literature (Pauthenet (1982a,b) and Graham (1982)), the following values were selected as a local laboratory standard:

$$M_s = 4.917 \times 10^5 \ JT^{-1}m^{-3} \quad \left.\begin{array}{l}\\ \\ \\ \\ \\ \end{array}\right) \text{at } 288^{\circ}K \text{ and 1T internal field} \qquad (4.10)$$

$$\frac{dM_s}{d\theta} = -214 \ JT^{-1}m^{-3}K^{-1} \qquad (4.11)$$

It is conceded, however, that the above approach to calibration is not universally ideal and that instances occur when appropriate theoretical corrections to computed coupling constants, as discussed by Zieba and Foner (Zieba and Foner (1982a)), should be made.

4.6(iii) Temperature effects on calibration

Whilst conducting an intensive study on a Nickel single crystal a 5% signal increase over a period of seven hours was observed. Careful investigation revealed that this effect was not sample dependent but was caused by an increase in magnet pole-piece temperature of 2.5°K. Two mechanisms are thought to be responsible; the differential expansion of the pole-piece/yoke system and the expansion of the detection coils and thus their effective cross-sectional area.

Differential expansion of the pole-piece/yoke system was caused by local heating of the poles due to the proximity of the field coils. This results in a small decrease in the magnet air gap and, hence, in the working separation of the two sets of detection coil pairs. It can be seen that this will cause an increase in the sensitivity of the detection coil system, as will the direct expansion of the individual coils.

In order to maintain the pole-pieces at a constant temperature, co-axial cooling tubes have been inserted into previously existant blind holes within the core of the poles (see Figure 4.18). Careful adjustment of the rate of water flow through the system, to maintain constant pole-piece temperature with respect to room temperature, permits the VSM sensitivity to be kept stable to better than 1% of the total signal over several hours. Measurements taking less than 30 minutes, therefore, can be made with a precision which approaches 0.1% of the signal size.

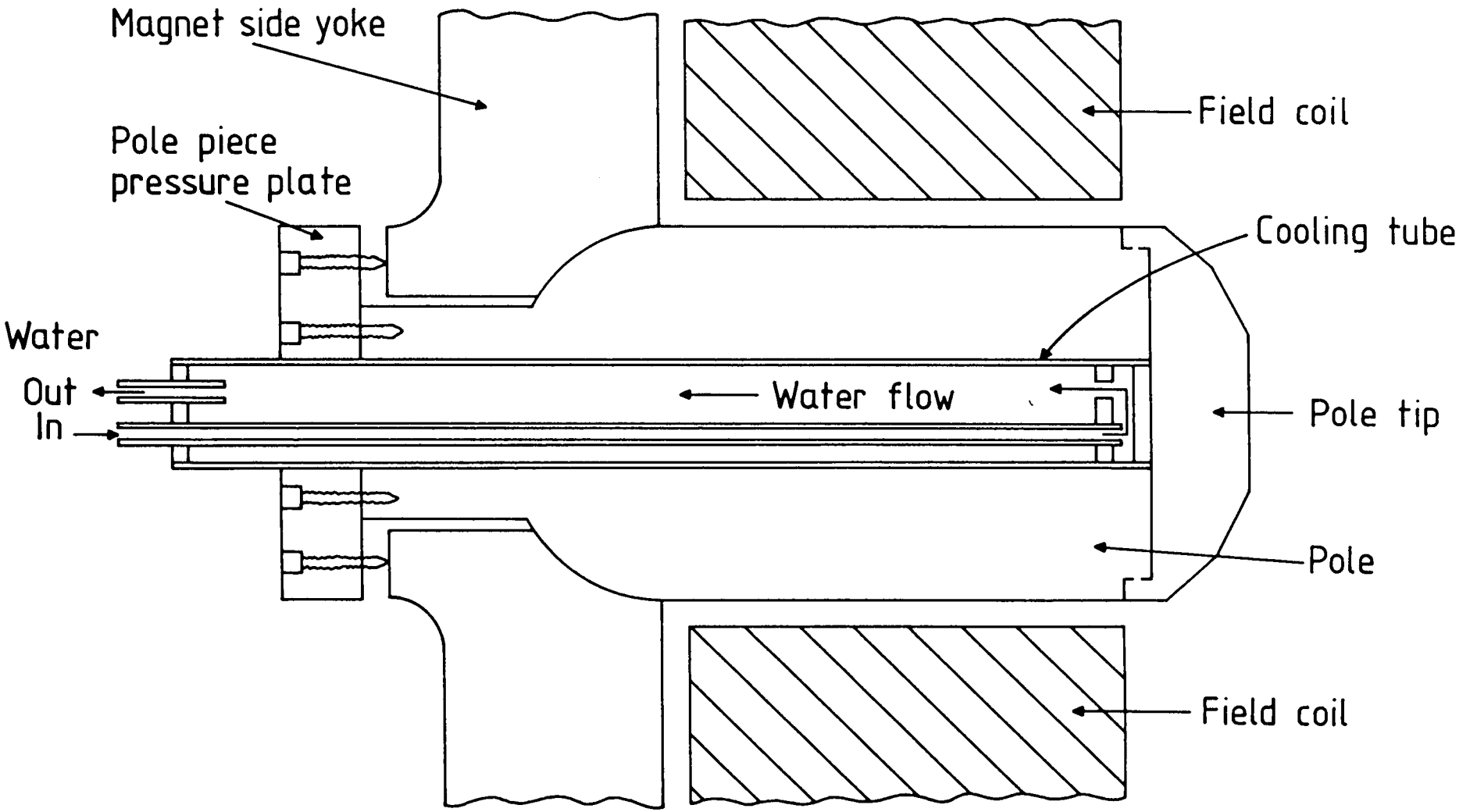

Figure 4.18 Detail of design and operation of magnet pole cooling tubes.

It is apparent from Figure 4.18 that the smaller the detection coil separation the more stringent the requirement for thermal stability of the magnet, and the implications of the above observations are obviously of importance to other VSM systems employing air-cooled electromagnets.

4.7 Magnetic Images

4.7(i) Introduction

The concept of magnetic images, so called because of their similarity to the concept of electrostatic images, was first discussed by Weiss (Weiss and Forrer (1926). By analogy to the electrostatic case, one replaces the induced magnetization in the varying permeability pole-piece material due to the vibrating sample's magnetic moment with magnetic images of varying magnitude. The time-varying flux threading the VSM detection coils then arise not only from the magnetized sample, but also from the magnetic images of the sample. It is clear, however, that, as long as the detection coil geometry, the relative positions of sample, detection coils and pole-pieces, and the permeability of the pole-pieces remain unchanged, the image field will produce a constant proportional change in the input signal. Although the effect of the magnetic images might be significant, it will, under such circumstances, remain unobservable. Changes in the permeability of the pole-pieces with air-gap field, however, will cause the signal contribution from the images to alter and a difference in total signal may

then be detected. Stoner et al. recognized this and correctly stated (Stoner et al. (1970)) that these "field-dependent" images would only be manifest if the pole-piece permeability changed rapidly with field. Their thesis was vindicated by their investigation of the field-dependent sensitivity of their magnetometer using a saturated nickel sample, obtaining a maximum sensitivity change of 3.8%.

Previous workers (Smith (1956), Foner (1959) and Case and Harrington (1966)) had conducted similar experiments using constant moment samples, either saturated nickel or small constant current coils, but none had found field dependent signal changes significantly greater than the noise fluctuations in their measurements (typically 0.1 - 1.0%). Foner (Foner (1959)), aware that images must exist, suggested a mechanism of eddy-current shielding to explain the apparent lack of detectable image change.

Exhaustive image experiments have also been conducted on the Durham VSM and, while no field-dependent images were observed (within the tolerance of the experiments), the results indicate, it is believed for the first time, direct evidence of the existence and magnitude of the image signal in a VSM electromagnet system. (Similar observations have been made recently in a superconducting solenoid (Zieba and Foner (1982b))).

4.7(ii) Image experiments

The experiment to determine the presence of field-dependent images was straightforward. It involved the use of the same single layer constant current coil described in section 4.4(iii) to provide a constant magnetic moment while the air-gap field was varied between 0 and 1.2 tesla (the field maximum for the electromagnet). The values of PSD output versus field thus obtained are shown in Table 4.1 and are corrected for the inevitable diamagnetic signal contribution from the sample coil material. By referring to this table it is clear that the detected signal is constant to within 3 parts in 1558 (i.e. 0.19%) which is consistent with the precision of the experiment. This null result, in itself, is extremely important as it allows the valid use of the calibration factor obtained with a nickel sample at an internal field of 1T at all fields accessible in the electromagnet.

A second experiment was then conducted using the constant moment coil to provide direct evidence of the existence and magnitude of the image signal. One pair of detection coils was mounted rigidly in position but independent of the pole-piece (to which it is normally clamped) using non-ferrous clamps and supports. With the air-gap field at zero tesla, having previously demagnetized the magnet pole-pieces, the signal from the pair of coils was observed as the electromagnet was removed from the vicinity of the sample/coil system. That this was possible was due to the magnet frame being mounted on a track which permitted the lateral displacement

Current in constant moment sample coil (A)	Magnet air gap field (T)	Phase Sensitive Detector Output (mV)
1.4573	0	1.5585 ± 0.003
1.4579	0.244	1.5595 ± 0.003
1.4585	0.401	1.5600 ± 0.003
1.4585	0.605	1.5595 ± 0.003
1.4585	0.805	1.5590 ± 0.003
1.4583	1.006	1.5585 ± 0.003
1.4583	1.205	1.5575 ± 0.003

TABLE 4.1

Values of detection coil system output, when measuring a constant moment sample, for various magnet air gap fields

of the magnet independent of the VSM support table. The signal observed before and after removal of the magnet was 147.2 $\pm$ .2 μV and 109.5 $\pm$ .2 μV respectively, indicating an image signal contribution of 37.7 μV which represents 25.6% of the total signal normally observed.

A consideration of the formation of the magnetic images from the magnetic poles of the sample moment reveals that an infinite series of equally spaced images, all having moments which are parallel to the sample moment, "exist" within the magnet poles (see Figure 4.19). The signal from each successive image dipole, however, falls off with dipole/coil separation r as the dipole field and only the nearest images will contribute significantly to the total signal. This effect was also studied by observing the coils output in the absence of the magnet at sample coil/detection coil separations determined by the expected image positions, so mimicking the presence of perfect magnetic images. The signal observed at each of the three most proximate image dipole positions (A,B,C as indicated in Figure 4.19) was summed and found to be 36.2 $\pm$ 3 μV. The relatively poor precision of this result is due to difficulty experienced in estimating the sample coil /detection coil separation without disturbing the detection coil orientation. It does, however, indicate that the images observed within the demagnetized magnet pole-pieces can be considered as "perfect" images.

To the author's knowledge, this is the first direct evidence for the existence and magnitude of magnetic images within VSM electromagnet systems, and thus confirms

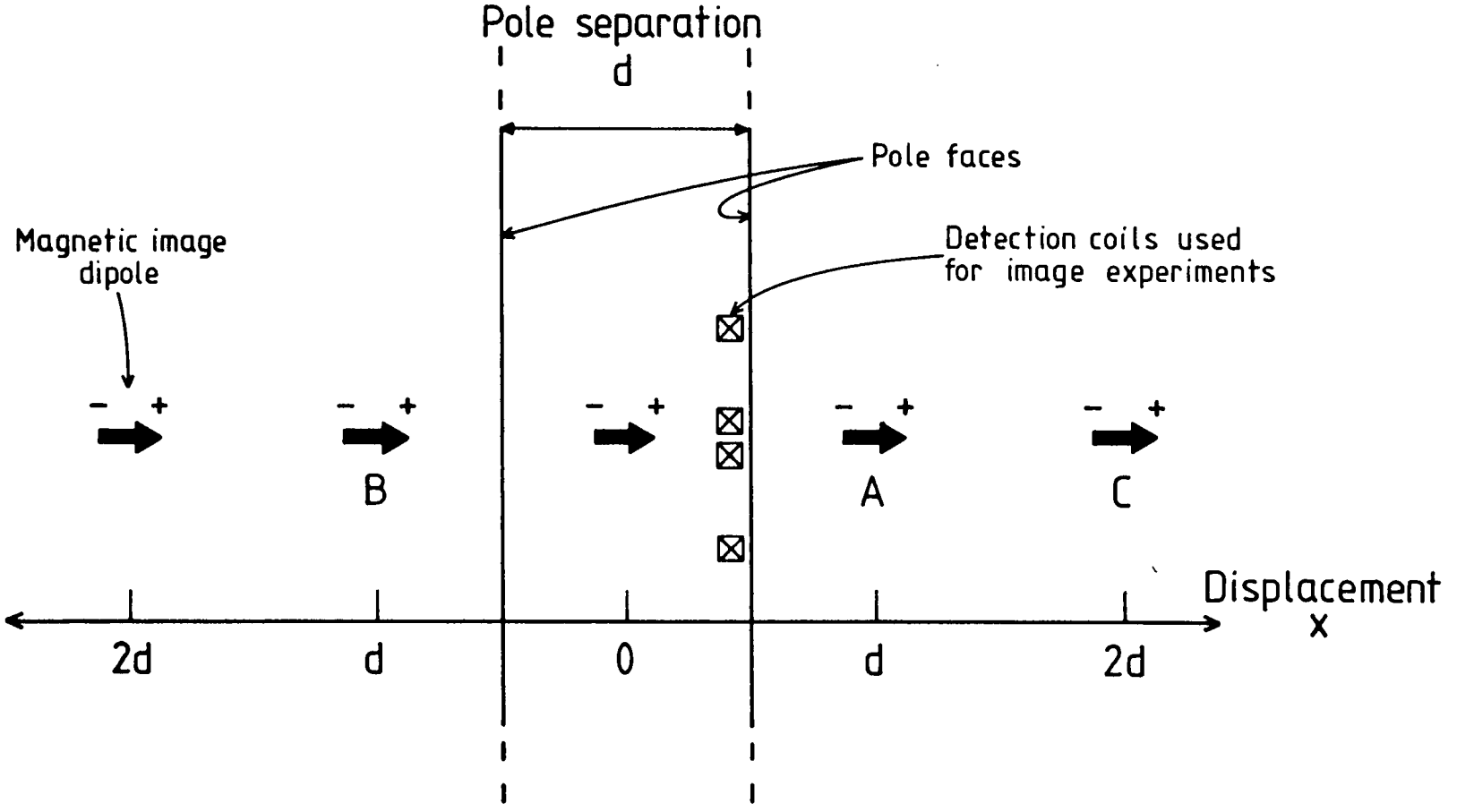

Figure 4.19 Illustration of location of the magnetic images for a magnetic dipole located at the centre between parallel pole pieces of separation d.

the thoughts of various authors (e.g. Foner (1959), and Zijlstra (1967b)) that images must be present even though they cannot be detected by conventional experiments. The results also show that the signal contribution from the image dipoles has the same polarity as that from the sample dipole when using Mallinson's detection coil geometry thus serving to enhance the detection sensitivity of this coil system (by approximately 25% in the Durham VSM). This, however, is not the case with Foner's geometry, and a consideration of Figure 4.19 and the arguments presented in Section 4.4(ii) indicates clearly that the presence of perfect magnetic images will be detrimental to the total signal detection sensitivity of this coil system. Not only does the presence of perfect images further vindicate, therefore, the selection of Mallinson's geometry for the Durham VSM, it also shows that exact calculations of the sensitivity functions of coil systems (Pacyna (1982), Zieba and Foner (1982a) and Pacyna and Ruebenbauer (1984)) are fundamentally incorrect because they do not consider the coil systems in the presence of permeable material.

4.7(iii) Calculation of field-dependent images

Having shown experimentally both the presence of perfect magnetic images at low field and the absence of field-dependent images (within experimental tolerance), it now remains to resolve these two apparently conflicting results. It is well known that the magnitude of successive images decreases by a factor α (Zijlstra (1967b) and

Stoner et al. (1970)) where

$$\alpha = \frac{\mu_{eff} - 1}{\mu_{eff} + 1} \qquad (4.12)$$

and $\mu_{eff} = \frac{dB}{dB_o}$, the differential permeability (where $B_o = \mu_o H$). A calculation of the magnitude of the field-dependent image signal, therefore, should consider how α varies with magnet air-gap field. This involves an estimation of the differential permeability of the pole-tip material, the formation of images being a surface effect, which, in turn, requires the calculation of the induction (B) in the magnet poles at a specific air-gap field.

The VSM magnet's pole-tips, poles and field coils have dimensions as shown in Figure 4.20. Each coil has 2,500 turns of copper strip and, together with the magnet poles/pole-tips, they produce an air-gap field of 1.2T for a coil current of 22A. The current density, τ, in the windings at this field value, therefore, has been calculated to be $1.75 \times 10^6 Am^{-2}$.

The air-gap "field" (B_{air}), has two sources, the "field" due to the current in the coils (B_i) and the "field" due to the presence of the magnetized pole-piece material (B_m), such that

$$B_{air} = B_i + B_m \qquad (4.13)$$

B_m is determined both by the magnetization of the pole-piece material (M) and the geometry of the air-gap/pole-tips. Zijlstra has presented results in graphical

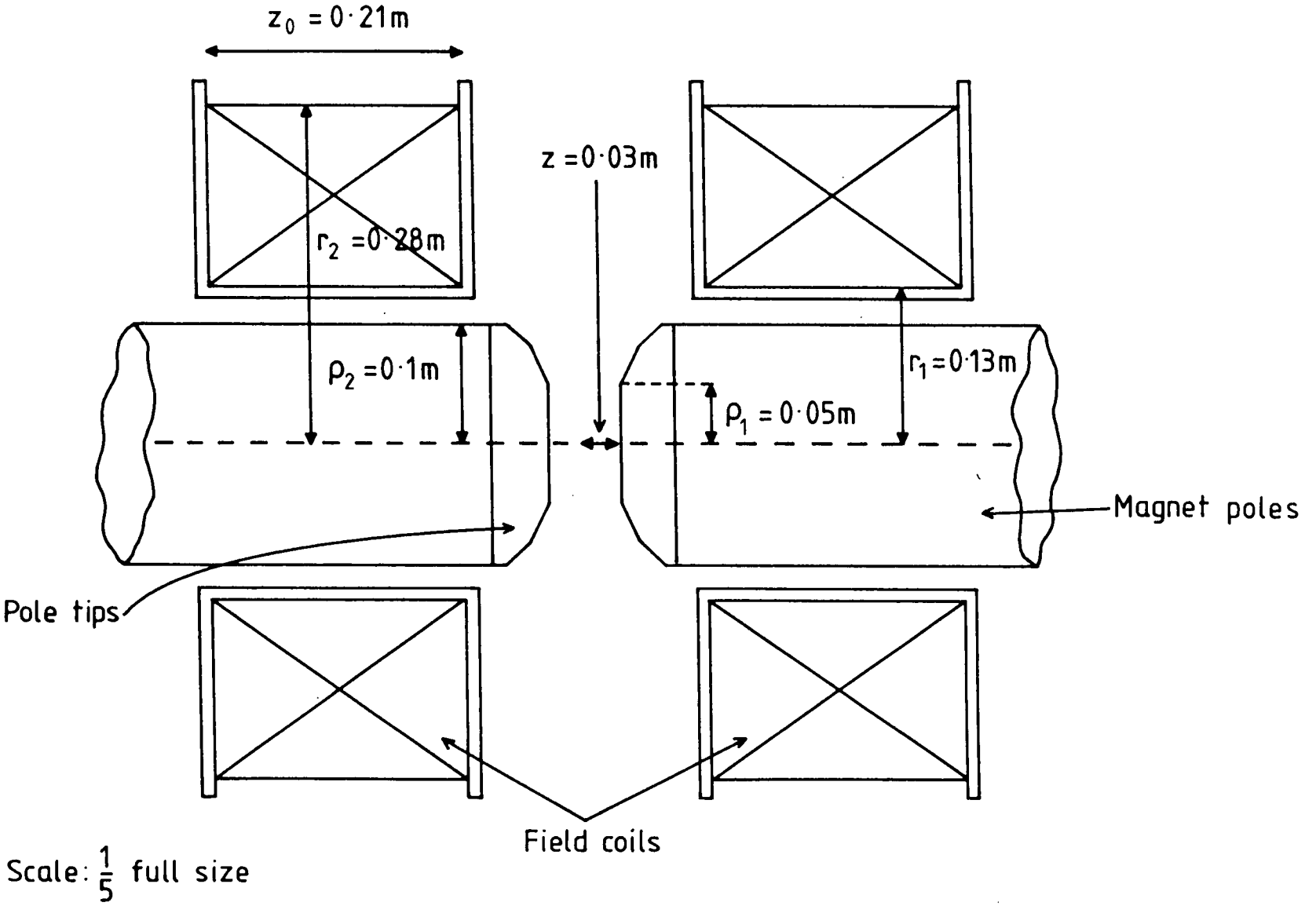

Figure 4.20 Illustration of design and construction of Newport Instrument Type D electromagnet's coils and poles/pole tips.

and algebraic form which permit the calculation of B_m from the geometry (Zijlstra (1967a)), and, with the plane-faced conical tips described here, contributions to B_m arise from both planar and conical regions. Using the results of Zijlstra we have:

$$B_m = 2\mu_o M \left(L_o + \frac{\ln\left(\frac{\rho_2}{\rho_1}\right)}{3\sqrt{3}} \right) \qquad (4.14)$$

where L_o is a function of $\beta \left(= {}^{z}/_{\rho_1} \right)$ given by:

$$L_o = \frac{1}{2}\left[1 - \frac{\beta}{(\beta^2+1)^{0.5}} \right] \qquad (4.15)$$

Substituting for the values of z, ρ_1 and ρ_2 gives

$$B_m \sim \mu_o M\ (0.767) \qquad (4.16)$$

Expressions to calculate the value of B_i from thick solenoids are also given by Zijlstra (Zijlstra (1967a)). Here we have:

$$B_i = \mu_o \tau r_1 F_1 \qquad (4.17)$$

where F_1 is a function of $\gamma \left(= \frac{r_2}{r_1} \right)$ and $\delta \left(= \frac{z_o}{r_1} \right)$ given by:

$$F_1 = \frac{1}{2} \ln \left[\frac{\gamma + (\gamma^2+\delta^2)^{0.5}}{1 + (1+\delta^2)^{0.5}} \right] \qquad (4.18)$$

It should be noted that equation (4.17) calculates the value of B_i on the coil axis at one end of the coil. The calculation of the value of B_i on the coil axis but removed from the coil, therefore, requires the evaluation of B_i for an extended coil followed by the subtraction of the contribution for that part of the coil absent in reality.

By following this approach, a value of $B_i \approx 0.13$ T has been calculated for the VSM coils at a coil current of 22A. The total air-gap field (B_{air}) at this current value is equal to 1.2 T and, by using the results of equations (4.13) and (4.14), the values of B_m and $\mu_o M$ are found to be approximately 1.07 T and 1.4 T respectively. This means, therefore, that, at a coil current of 22A and an air-gap field of 1.2 T, the induction (B) of the pole-tip and pole-piece material is approximately given by B = 1.4 tesla.

In order to assess the effect on image signal caused by increasing the induction in the pole-tips from zero to this value, the differential permeability (dB/dB_o) of the pole-tip material needs to be calculated at 1.4 T and compared with its maximum value (prevalent at low fields). Although magnetization data for the mild steel pole-tip material used on the VSM is unavailable, a reasonable estimate of the size of this effect may be made by considering the initial magnetization curve of a typical mild steel. Such a plot is shown in Figure 4.21, and measurements taken from this plot yield approximate values of 1735 and 200 for the maximum differential permeability and the value of this parameter at B = 1.4 T respectively. Whilst this represents an 88.5% reduction from the initial value of μ_{eff}, the corresponding change in the value of α, as given by equation (4.12), is only 1.0%.

In order to confirm that this change in differential permeability is observed in the VSM magnet, a B-I plot

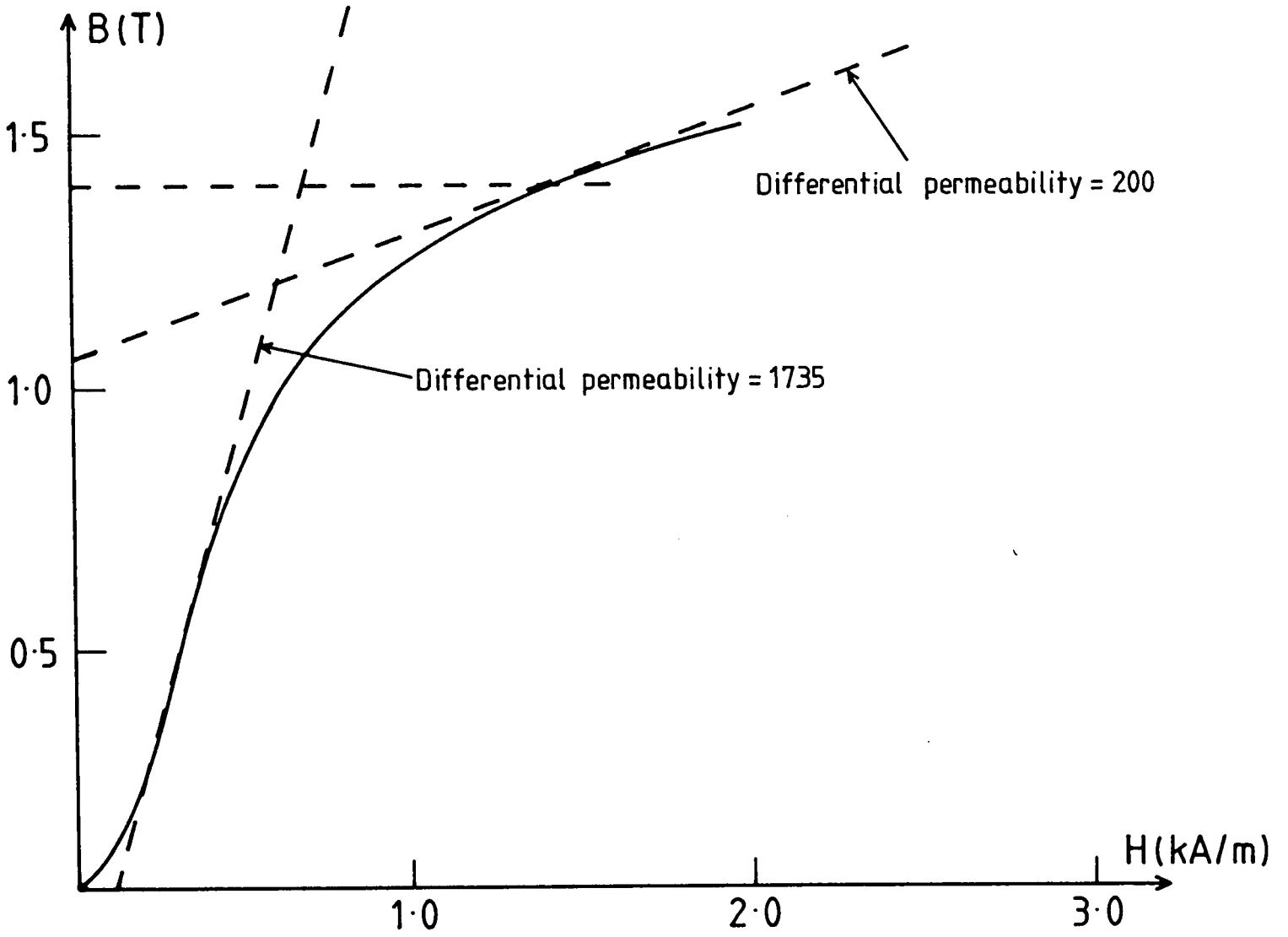

Figure 4.21 Initial magnetization curve of a typical mild steel as measured by the yoke permeameter described in Chapter 3.

for the magnet was obtained. Figure 4.22 shows this data, which has been corrected for the contribution to the field from the coil current (B_i), and measurements of the curve gradient at 0 and 1.4 T reveal an 89.0% change from the original value of μ_{eff}. The typical mild steel data can, therefore, be considered to be a good approximation to the characteristic of the magnet pole / pole-tip material.

A change of 1% in the value of α produces a corresponding image signal change of 1% but, as the contribution of the image signal to the total signal is 25%, this would only cause a 0.25% change in the total signal. As the tolerance on the results of the experiment to detect field-dependent images was 0.19% (see Section 4.7(ii)), it is suggested that the noise on this data obscured the signal change resulting from the field-dependent image contribution.

In conclusion, therefore, the results of these considerations of images have confirmed both the presence of perfect images at low air-gap fields and the absence of detectable field-dependent images. the former is explained by a value of $\mu_{eff} = 1735$ at low field which yields a value for α of 0.999. The absence of a large field-dependent signal is due a relatively large value of μ_{eff} at the limiting magnet air-gap field. This suggests that the field limitation in the magnet air-gap is lack of field coil windings rather than a low volume of pole material, a finding that is confirmed by the absence of a plateau region in Figure 4.22.

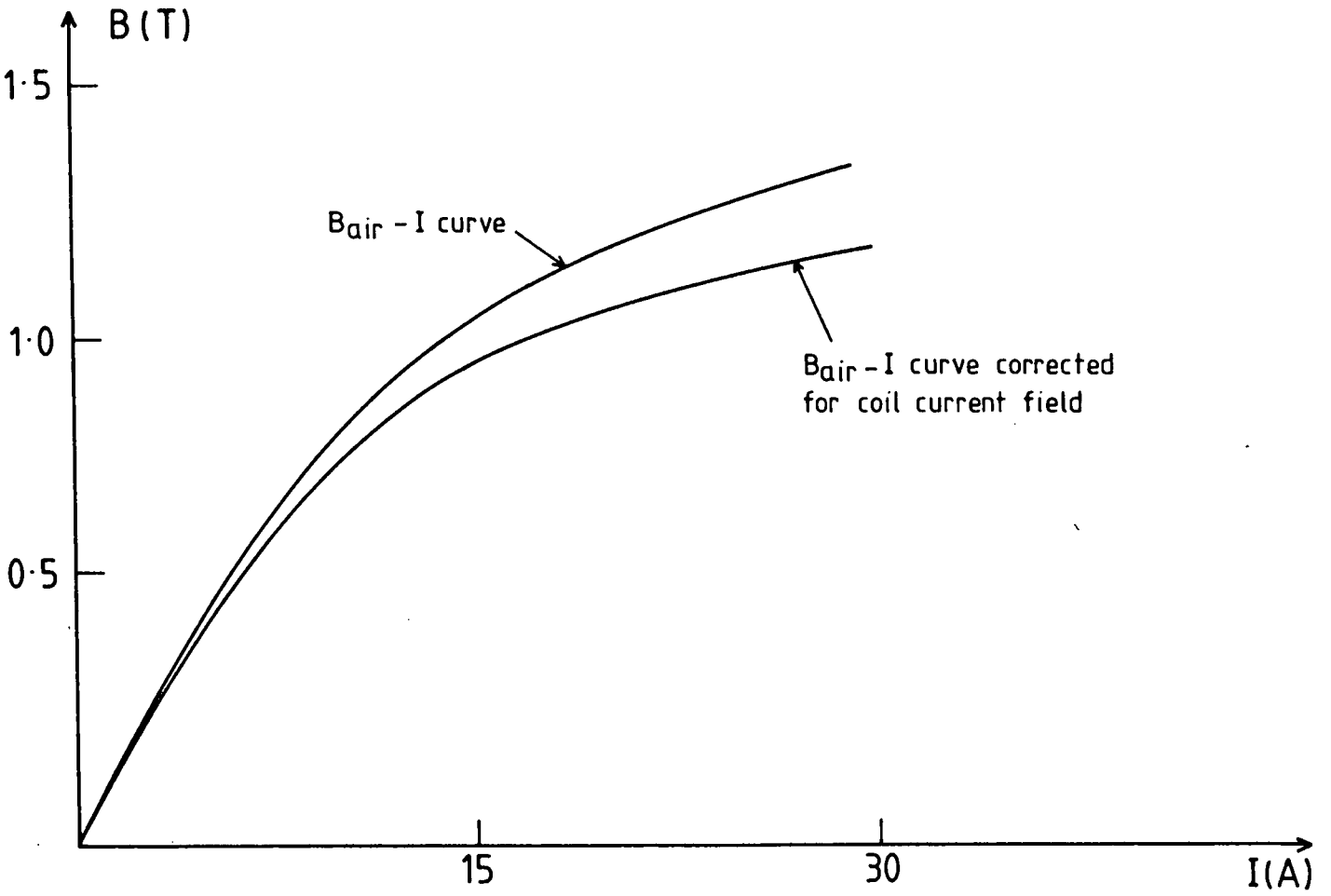

Figure 4.22 Plot of magnet air gap field versus magnet coil current for Newport Instruments Type D electromagnet with the modified pole-pieces.

CHAPTER 5

AUTOMATION OF THE VSM

5.1 Introduction

Not long after the commissioning of the VSM as an item of research apparatus, it became apparent that the instrument would be heavily over-subscribed, as several research group members expressed an interest in using it. The majority of experiments conducted on the VSM require the investigation of a standard magnetization curve (e.g. full magnetization loop or initial magnetization curve) which would be repeated for many different sample materials. Some of these studies involve the task of substantial data acquisition in order that a meaningful analysis may be performed (Chantrell et al. (1978), Hoon et al. (1983), Hoon et al. (1985)). It is not uncommon, therefore, for a full magnetization loop study to contain nearly two hundred pairs of magnetization and field values. This would occupy the VSM operator for several hours if the instrument is operated manually and, apart from being tedious, the length of the experiment increases the susceptibility of the results to the drift of the recording apparatus. It was considered desirable, therefore, to automate the VSM completely, replacing the operator by a microcomputer-interface system complete with a comprehensive user-friendly software package. Not only would this reduce experimentation time, thereby increasing the work capacity of the instrument,

it would also allow the operator to spend the time analysing previously recorded data.

The recent advances in microcomputer technology, and the availability of relatively inexpensive microcomputer/ interface systems, have brought this task well within the scope of any research laboratory. By using such systems the costly replacement of existing manually operated magnet power supply units by their modern programmable counterparts is avoided. In this chapter we describe and refer to the equipment used to automate the VSM, but the reader should note that the choice of instrumentation was primarily determined by the existing laboratory equipment. Indeed, the approach to the automation is quite general and could have been achieved using a variety of equivalent products. The total extra cost incurred by automating the VSM, therefore, has been kept below £1,500.

5.2 Additional hardware requirements

Apart from the phase sensitive detector (PSD), gaussmeter and signal generator/ amplifier described in the previous chapter, the only additional items required for complete automation are a microcomputer, an interface system and a digital voltmeter (DVM). The single restriction on these items is that the microcomputer must support some inter-device communication standard (e.g. IEEE-488 or RS 232) which is also supported by the PSD and DVM. The addition of a disc drive and printer to the microcomputer, though not essential, is extremely useful

for convenient, quick data storage/retrieval and data output. The interface system used can be quite general but, in order to fulfil the tasks demanded of it as described here, it must contain analog to digital converters (ADC's), digital to analog converters (DAC's), stepper motor drivers and TTL compatible binary outputs.

The system constructed by the author contains a CBM 4032 microcomputer (plus a standard CBM floppy-disc drive and printer), a Bede Scientific Instruments MINICAM interface and a Fluke 8860A DVM, all of which support the IEEE-488 (GPIB) parallel data bus standard. The microcomputer itself does not have a full IEEE-488 specification, as described by the IEEE-488 (1978) GPIB standard, from within BASIC, but machine-code routines are available (Fischer and Jensen (1980), West (1982)) which provide this. The combination of microcomputer and interface, therefore, forms the core of the control system from which all peripherals are controlled. The software required to do this is written in BASIC and is stored permanently on floppy disc.

The MINICAM interface (Bede Scientific Instruments, Durham) is an inexpensive modular system for which a range of plug-in boards is available. These include the required ADC's, DAC's, stepper motor drivers and General Purpose Output Boards (GPOB's). The GPOB provides 16-bit binary representations of the decimal numbers input to them and the individual output bits, which are TTL and 5V CMOS compatible, can be used to trigger external equipment. The simple construction of the

interface rack also permits the "in-house" fabrication of non-standard boards to perform tasks peculiar to a single item of apparatus. We describe later how this adaptability has been used to facilitate the automation of the VSM.

5.3 Remote magnetic moment and field measurement

The remote measurement of the external field applied to the sample and its resulting magnetic moment is reasonably straightforward. As mentioned in an earlier chapter, the field is measured using a Bell 640 Gaussmeter plus transverse Hall probe) which has sensitivity settings ranging from 0.1 to 30,000 gauss. The Fluke DVM, which has a full IEEE interface, records the analog output from the gaussmeter at the request of the microcomputer, and the data is then transmitted back to the microcomputer via the GPIB. The Fluke is operated in its auto-ranging mode throughout the experiment and it is externally triggered into taking a reading by a signal from MINICAM's GPOB. The microcomputer converts the voltage level to a field value from a knowledge of the range on which the gaussmeter is operating. This parameter is keyed in by the operator during the program's initialization procedure.

The main disadvantage incurred using the Bell gaussmeter is that it must remain on one sensitivity setting throughout the experiment because the instrument has no intelligent interface. The full scale range that is selected, therefore, must reflect the maximum external

field required during the experiment and this results in a loss of precision in low field measurements. This can be overcome if a remote ranging gaussmeter, such as the LDJ 511RR, is used. The microcomputer is then able to select the most suitable sensitivity setting throughout the experiment by sending the appropriate combinations of TTL voltage levels from MINICAM's GPOB. It is also apparent that the remotely controlled DVM is only required to monitor the analog output of the gaussmeter. The provision of a gaussmeter with an IEEE-488 interface would remove this requirement but, to the author's knowledge, no manufacturer currently produces such an instrument.

The measurement of the magnetic moment of the sample is made by a phase sensitive detector which offers a considerable enhancement of the signal to noise ratio (see Chapter 4). The instrument used here, a Brookdeal (EGeG) 5206 Lock-In Analyser, has a full IEEE interface which permits measurements to be recorded remotely via the GPIB. The magnetic moment, and hence the magnetization, is calculated from the amplitude of the induced voltage in the detection coils. This requires a knowledge of the induced voltage from the Nickel calibration sample and the mass of both calibration and test samples. These values are also provided by the operator at the beginning of the experiment.

The microcomputer is able to exercise absolute control over the PSD. It can alter the sensitivity, time constant and phase of the analyser, for example,

as well as requesting data from it. Use has been made of this ability by writing software that eliminates any direct interaction between the operator and the PSD. The instrument can, therefore, be set up exactly as required by typing simple commands to the microcomputer. The configuration of the analyser can be displayed on the VDU and seen at a glance. Any accidental disturbance of the instrument is prevented by using the remote operating mode to disable the front panel switches.

5.4 Communication problems via the GPIB

The communication between the CBM 4032 microcomputer and both the Fluke Multimeter and Brookdeal Lock-in analyser via the IEEE bus (GPIB) is not quite trivial. Both the Fluke and the Brookdeal have full IEEE interface specifications and they expect the controller to be equally capable. In particular, both devices expect to be polled by the controller to determine their status when data is expected from them. The 4032 is not capable of conducting either a serial or parallel poll directly from BASIC but, by using machine code routines, such polls are possible. Texts dealing specifically with CBM microcomputers (Fischer and Jensen (1980), West (1982)) contain outlines of such routines and, by referring to these, a general machine code routine was written to conduct a serial poll of any IEEE device. This code was blown into an EPROM which was then placed in a spare socket inside the microcomputer. A complete description of the location and listing of this machine code routine

is to be found in Appendix E.

Although communication between the controller and the Fluke and Brookdeal was possible without conducting a serial poll, the unreliability of the data transfer often produced data corruption and sometimes a system crash, neither of which could be tolerated. The addition of the serial poll has, therefore, ensured complete reliability of the remote data taking process.

5.5 Automatic field control

The electromagnet's field coil current is supplied by an elderly motor generator which provides a unipolar 350 volt - 30 amp constant current supply (see Chapter 4). The only modifications that have been made to this supply are the provision of an internal precision voltage source and the screening of various internal leads. The precision voltage supply has been used to replace the reference battery in the error amplifier circuitry, thus eliminating the regular and costly replacement of such a battery. The screening of all internal leads, in particular those leading to and from the error amplifier circuit, has substantially reduced the 50 Hz noise present in the supply's output.

Full magnetization loops requiring both forward and reverse fields, cannot be obtained with this supply unless the connections from the supply to the magnet are reversed. This was achieved manually by a standard reversing switch, and normal working practice involved switching the motor generator off, and allowing it to come to rest, before the connections were reversed.

Two potential hazards were avoided by this practice. Firstly, it removed the possibility of reversing the connections to the magnet with significant current flowing through it. Such an action would result in the generation of a large back e.m.f., due to the flux collapse in the magnet, that could damage both magnet and supply unit. It also prevented the motor generator supply seeing an infinite impedance load (open circuit) for large fractions of a second. This would cause the potential generated by the supply to rise dramatically until the load was reconnected, at which point large field transients would occur in the magnet as the supply regained its stability. As a result, the field applied to the sample would no longer be progressing in smooth increments, thus forcing a departure from the sample's major magnetization curve. The biggest obstacle to complete automation of the VSM was, therefore, the provision of a safe and reliable method of current reversal that avoids the above hazards.

The remote control of the supply current was achieved by simply using a stepper motor to drive the main current control potentiometer. The drive is transmitted from the stepper motor to the ten-turn potentiometer by a 15:1 Muffet gearbox which is connected to the rear end of the potentiometer shaft (see Figure 5.1). In this way, the whole gearbox/motor assembly is contained inside the supply unit, and the manual operation of the current control potentiometer (when desired) is unimpeded. The motion of the stepper motor is controlled by the

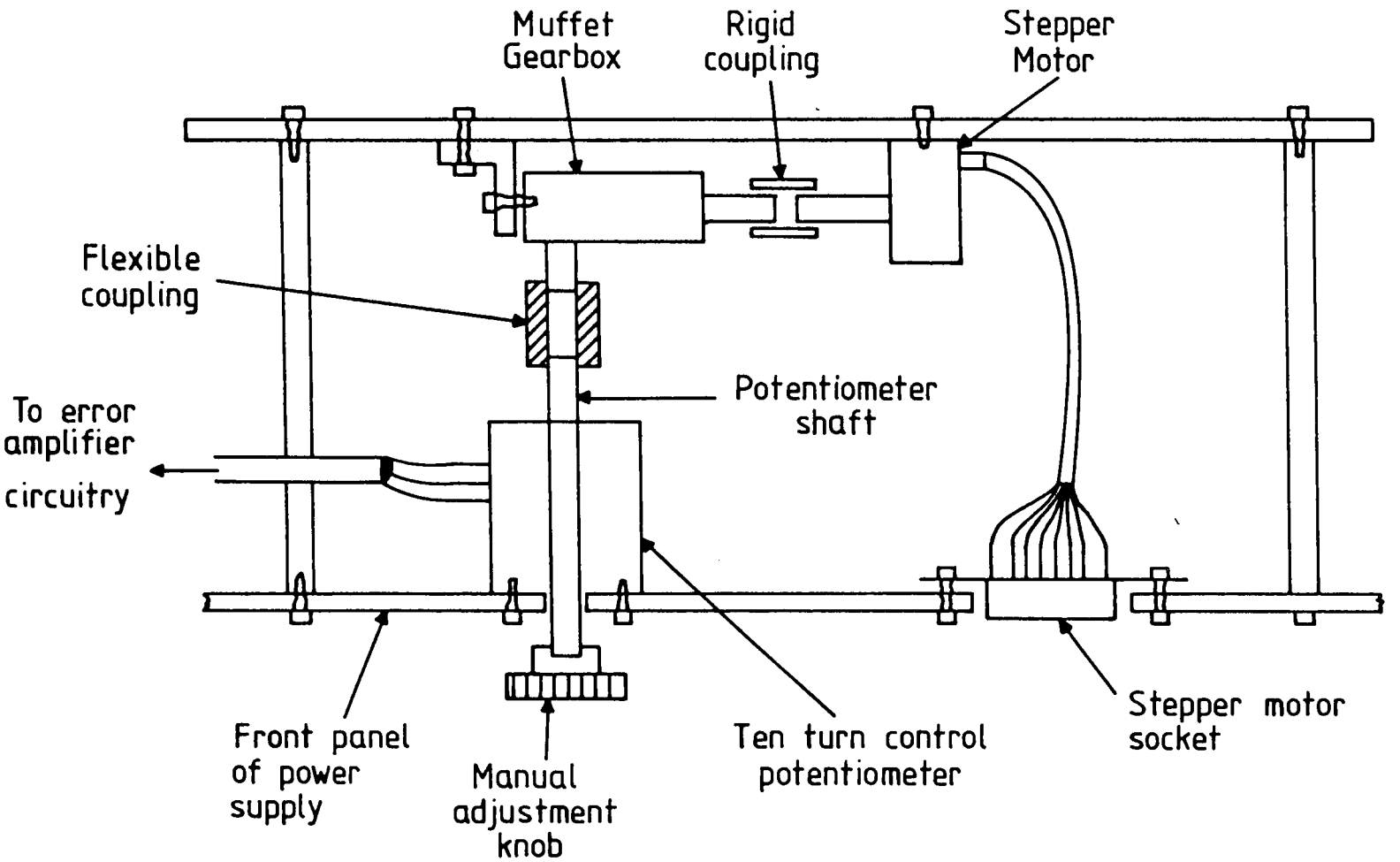

Figure 5.1 Illustration of stepper motor/gearbox assembly which permits the remote control of the supply current.

microcomputer, via a driver board in MINICAM, which is able to select the direction of rotation, the total step movement and the time interval between each step. Measurements have shown that a single step results in a field change of approximately 3 gauss when the magnet is operated in its linear current-field region (see Figure 4.22). The field stability at any value has been found to be $\pm$ 0.3 gauss over a period of several hours.

The remote reversal of the magnet supply is achieved using a power-latching relay operated by logic circuitry that is either manually or computer controlled. The safe operation of this reversal relay is ensured by determining the magnet current before changeover takes place. A low resistance (2.5 mΩ) has been added in series with the magnet and, by monitoring the voltage potential across the resistor, the controller/microcomputer is able to make sure that minimal current is flowing before attempting reversal. The potential is measured by the Fluke Multimeter which now has two voltage signals to monitor, the other being the analog output from the gaussmeter. A Time Electronics 9812 programmable switch, which is controlled via the GPIB, performs the necessary switching of inputs to the Fluke at the request of the microcomputer. In this way the remote reversal of magnet current is prevented until the current falls below a set limit of 1×10^{-2} amps. Exactly the same criterion is applied by the human operator, who is able to monitor the potential across the 2.5 mΩ resistor by using the

programmable switch in its manual mode. (It should be noted here that the provision of a commercial programmable switch is not essential and the switching of inputs to the Fluke can be achieved by a "home-made" relay board for the MINICAM system (see, for example, section 5.9).

The procedure adopted by the microcomputer when controlling the current, therefore, is to monitor the field value, whilst ramping the current up and down, until it approaches the remanence value of the pole pieces (150 gauss (or 12 kAm^{-1})). At this point both field values and magnet current are studied until the current falls below 1×10^{-2} amps and the microcomputer initiates the current reversal.

The problem of voltage transients occurring at changeover is avoided by the very short duration of the "open circuit" condition. The maximum operating time for the relay (25 milliseconds) is much smaller than the response time of the supply's control circuitry and the output remains stable as a result.

The logic circuitry which controls the reversing relay is contained on a printed circuit board which, together with the latching relay and the 2.5 mΩ resistor, is also mounted inside the supply unit. The mode of operation of the circuitry, whether manual or remote, is selected by a panel mounted switch. Indicator lights and analog voltage signals provide visual or remotely sensed indications of the state of the logic at all times. The circuitry also contains a voltage comparator

network which automatically prevents any current reversal for magnet currents greater than 0.15 Amps. While this current value is not as low as the criterion of 1×10^{-2} amps that is required for a smooth reversal, it is still low enough to avoid permanent damage if the supply is reversed accidentally. The occurrence of such damage has been made less likely still by the addition of a high power diode in reverse bias across the supply. Any back e.m.f. from the magnet coils will be sunk by the diode and will not, therefore, reach the supply. (A detailed description of the logic circuitry and how is it controlled and monitored under both manual and remote control is given at the end of this chapter (see Section 5.9)).

5.6 Safety protection of the current reversal apparatus

In order to ensure the completely safe operation of the power latching relay throughout an experiment, certain precautions must be taken to prevent the slightest possibility of current reversal at high fields. Such possibilities include the corruption of the logic circuitry by electrical noise from other laboratory apparatus, and the accidental operation of the circuitry caused by electrical failure or human error. The latter case is prevented by the voltage comparator over-ride system already described, but even spurious reversals at currents less than 0.15 amps are unwanted because the experimental data will be corrupt and a repeat experiment is necessary.

The logic circuitry is designed to be as resistant as possible to external noise, but even the remotest possibility of corruption, and hence current reversal, cannot be tolerated. Whilst it is extremely difficult to remove these possibilities completely; it is possible to prevent the consequences of such effects. This approach has been followed here. Two switches have been added, in parallel to each other, which normally interrupt the power supplied to the set and reset coils of the latching relay (see Figure 5.2). One is a manual toggle switch which resets when released. The other is a dual-in-line (d.i.l.) relay which is operated remotely via MINICAM (see section 5.9). The addition of the switches means that the logic state can be monitored and altered either remotely or manually before the latching relay is energized briefly by either switch. Any corruption of the logic circuitry will not, therefore, cause a reversal of the magnet supply until either of these switches is deliberately activated. The microcomputer is able to detect and correct these unprompted reversals by monitoring the analog voltage indications of the logic state via an ADC in MINICAM. This ability is most useful when reversing the current as the microcomputer is able to check that the operation has been successful. Any failure in the reversal procedure causes a repetition of the command to reverse until it has been done. The reliability of the system to reverse on command approaches 100% and the most common cause of a consistent failure is the fault of the operator

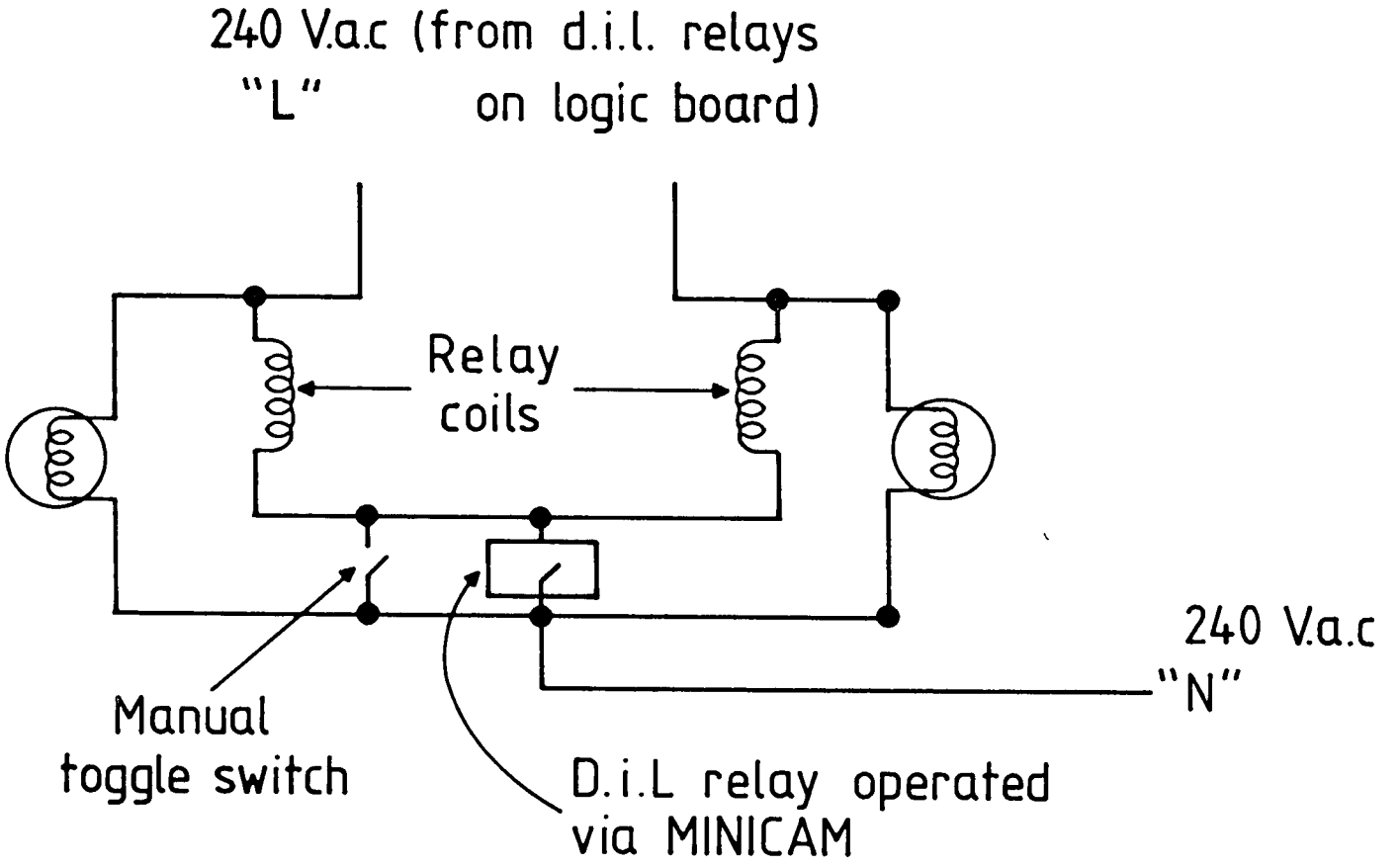

Figure 5.2 Detail of manually and remotely operated switches which interrupt power to set/reset coils of main reversal relay.

in neglecting to switch the logic circuitry to remote control.

Further safety considerations must include the effects of mains power failure and microcomputer "systems crash". Power failures of several minutes duration do not cause problems as the motor generator will be stationary long before power is restored. The generator will not then restart until a starter button is manually operated and there is no possibility, therefore, of a high field current reversal. Short mains failures, of the order of 20 seconds, are more of a problem. Once the generator has been tripped out by the failure it will slow down, and eventually come to rest after approximately one minute despite the return of power. Until it is stationary, however, it is still able to produce a significant output.

The logic control circuitry always powers up in the "forward" state and any mains failure lasting longer than 3 to 4 seconds will result in the logic reverting to this state on power return. If the magnet is being operated in the reverse mode at the moment of failure there could be a disastrous reversal on the return of power. For this to occur a spurious signal would have to be sent to the remotely operated switch which isolates the relays energizing coils, but this is not totally inconceivable.

The protection of the logic circuitry's power supply during such failures is all that is required to avert this potential danger. A 12 volt lead-acid battery

is switched in to supply the circuitry when failures occur and it can sustain the integrity of the board for several minutes. An indicator lamp signals the operation of the battery. On the return of power the battery and lamp are switched out and the battery is continuously trickle charged, thus eliminating the need for its regular maintenance which would otherwise interrupt the constant use of the VSM.

A "systems crash" in the microcomputer will only damage the magnet if it occurs when the current is above the maximum continuous current rating, as it will remain at this setting indefinitely. Overheating and damage to the magnet would normally occur but for the addition of a thermal snap-switch placed in thermal contact with the current windings. The switch contacts are connected in series with the manually operated generator stop switch and, on reaching the critical temperature, the switch breaks, the power to the generator is removed and the current in the magnet coils rapidly reduces to zero.

The addition of the above safety features has, therefore, eliminated the damaging effects to magnet and supply of all the foreseen failures in the apparatus and the method of operation. The current reversal procedure has been made more complex as a result, and there is a fixed sequence of events that the microcomputer must follow in order to control the current ramping for any magnetization study. By way of example, Figure 5.3 shows a flow chart indicating the sequence necessary

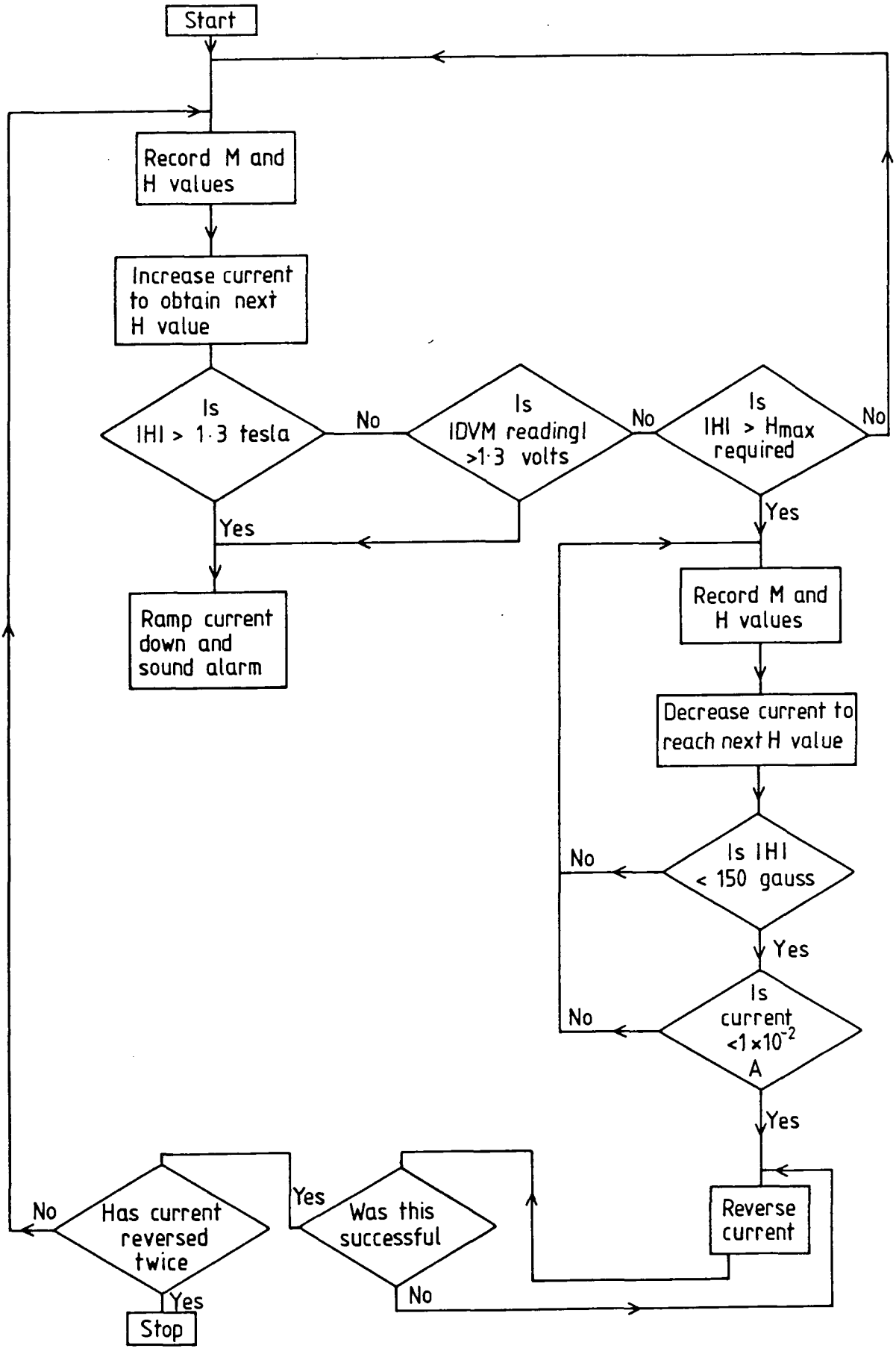

Figure 5.3 Flow chart indicating sequence of operations required to control supply current for a full magnetization loop study.

to control the supply current for a full magnetization loop. With reference to the chart it can be seen that additional conditional statements have been added to prevent the microcomputer trying to reach a field value not possible with the present electromagnet or to detect an over-range condition in the gaussmeter. These clauses have only proved to be necessary because of operator error in selecting an incorrect gaussmeter range or maximum field value. Apart from such human errors the current control system has now been operating successfully for over two years, during which time no failure has occurred.

5.7 Software requirements for automated VSM operation

The complete VSM apparatus, described so far, is shown in diagrammatical block form in Figure 5.4. The remote operation of the entire system requires a software package which has a firm command of the equipment, but still permits flexibility of operation. A user-friendly control program has been written, therefore, which allows the operator to specify the exact nature of the experiment as well as the detailed configuration of the apparatus.

The program has been written as a collection of sub-routines, with each one performing a specific task. For example, there are subroutines for increasing and decreasing the current before and after current reversal, as well as subroutines for recording magnetization and field values, and reversing the current direction etcetera. The advantages of this method of program construction

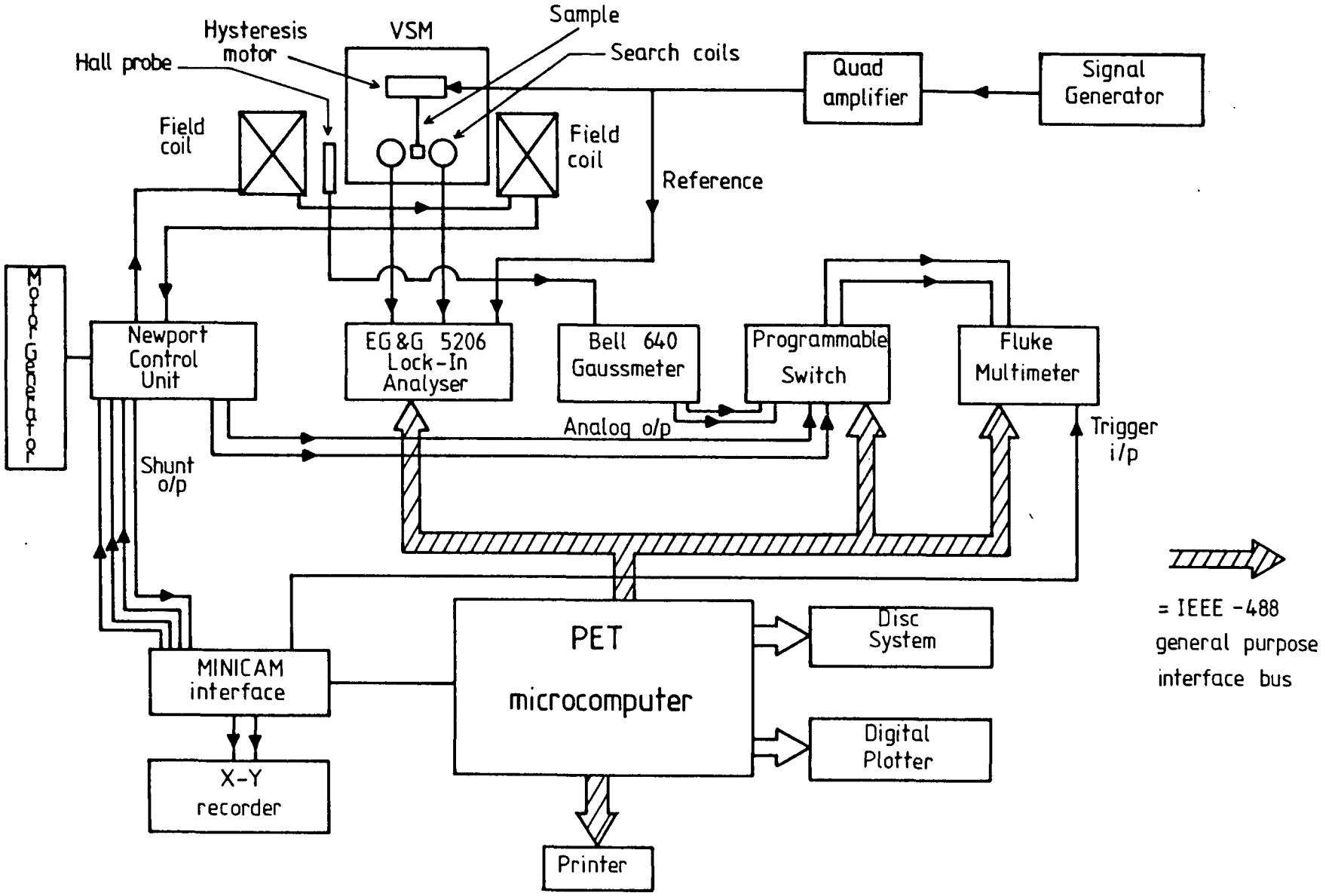

Figure 5.4 Block diagram of VSM and all the peripheral equipment required for automatic operation.

are twofold. Firstly, the instruction set, which determines the form of the experiment by the order in which the subroutines are called, is relatively short and simple. Secondly, it permits the presentation of menus of options to the user, thereby creating greater flexibility in both the form of the experiment and the detailed requirements of the form chosen.

The initial part of the program involves considerable interaction with the user while the peripheral equipment is set up. The contact between the user and the equipment is reduced to a minimum and, where this is unavoidable, full details of any manual settings are requested. The user then decides on the form of the experiment, choosing between a full magnetization loop, an initial magnetization curve or a detailed study of the coercive field. Information must then be provided about the maximum applied field required, the number of data points to be recorded between certain chosen field values, the mass of both test and calibration samples, and the signal amplitude recorded for the calibration sample. At each stage the information given can be checked and corrected if a mistake has been made. When this is complete the microcomputer is left to conduct the experiment.

During the course of the run messages are displayed on the VDU which give the user information about the current state of the experiment. Also displayed are the ten pairs of magnetization and field values, recorded at each selected field setting, from which the average

and standard error results are calculated. These results are then stored on floppy disc from where they can be plotted and/or listed at the end of the experiment. The results are plotted on an X-Y recorder via two DAC's in MINICAM using a separate program. Alternatively the corrected curve can be plotted, after allowance is made for the sample's demagnetizing field, if the user has supplied the relevant demagnetizing factor. Figure 5.5 shows a typical magnetization loop of a Nickel sample, obtained using the control program, for which no demagnetizing correction has been made. The greatest data point density has been chosen to coincide with the region of greatest magnetization change and falls off as saturation is approached. The whole run consists of 200 pairs of magnetization and field values for external fields up to a maximum of 1 tesla and took approximately two hours to complete.

The automation of the VSM, therefore, has not only proved itself far quicker than the equivalent manually operated experiment, it has also allowed the user to spend his time analysing the data instead of collecting it!

Complete listings of and notes about the VSM control program and the plotting program are given in Appendices F and G respectively.

5.8 Future development

It is intended that the next development of the VSM apparatus will involve the automation of the gas-

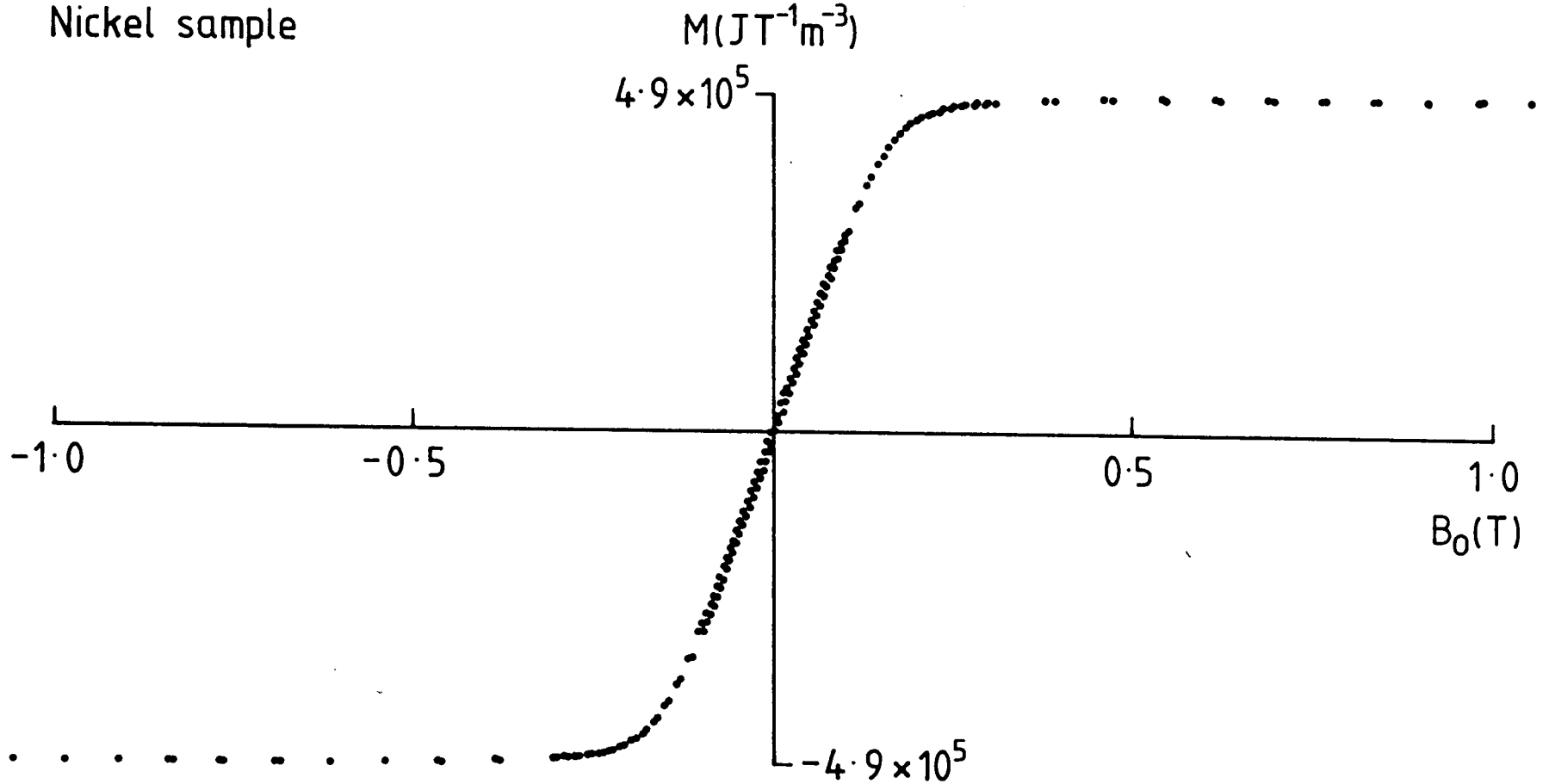

Figure 5.5 Typical full magnetization loop study on a polycrystalline nickel sample. The three field regions having different data point densities are clearly visible.

flow cryostat system (described in Chapter 4), a schematic diagram of which is shown in Figure 5.6.

The operation of the system is straightforward. The flow of helium into the cryostat, and the pressure of helium exchange gas in the sample space, are both controlled by needle valves in the exhaust and cylinder lines. The exchange gas temperature is determined from a thermocouple output by a conventional temperature controller (Oxford Instruments 3120 Temperature Controller), which then regulates the power supplied to the heater in order to maintain the gas temperature at the selected value. The setting of the controller is achieved using either a front panel potentiometer or a 0-5 Volt analog signal. Once the apparatus has been assembled, therefore, the monitoring and adjustment of the exhaust line and sample space pressure, together with the reseting of the temperature controller, is all that is required for its efficient operation.

The automation of this system will be both simple and inexpensive as it is planned to make use of the available DAC, ADC and stepper motor drive boards on MINICAM. The pressure in both exhaust line and sample space will be determined remotely by the output from two pressure transducers. Any adjustment will then be made by a pair of stepper motors which will alter the needle valve settings. The selection of the operating temperature will be made by an analog signal input to the temperature controller from a DAC in MINICAM, although the microcomputer will also monitor the thermocouple

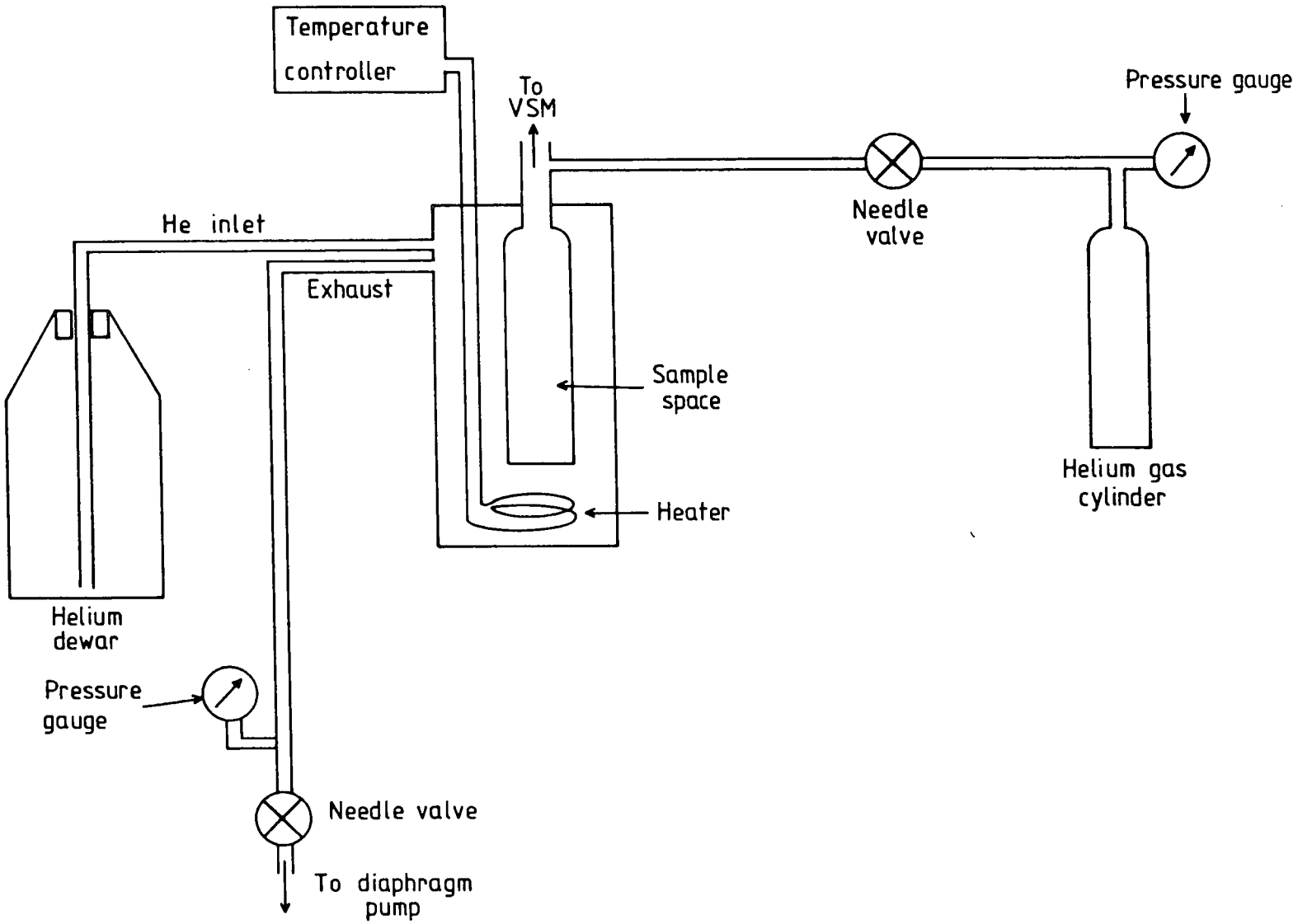

Figure 5.6 Schematic representation of the gas-flow cryostat system for the Durham VSM.

output independently. In this way the microcomputer will be able to ensure the onset of temperature stability before making any magnetic measurements.

Additional software will have to be written to control these extra functions for the duration of the experiment. Once this is complete, however, an automated series of magnetic measurements between 4.2 and 500 K will then be routine.

5.9 Detailed description of logic circuitry and additional circuitry required for normal operation

The integrated circuit that forms the core of the logic circuitry is a 7470 and-gated J-K positive-edge-triggered flip-flop (Figure 5.7(a)). When all the inputs to the 7470 are held high the two outputs toggle on the positive edge of a pulse supplied to the clock input (see Figure 5.7(b)). These TTL outputs are used to drive two dry contact dual-in-line (d.i.l.) reed relays, which have a 240 V a.c. switch rating, via a DS 3686N equivalent relay driver (Figure 5.8(a)). The d.i.l. relays, in turn, control the supply of 240 V a.c. to the mains rated set and reset coils of the power-latching relay (Figure 5.8(b)). Thus the positive edge of each clock pulse supplied to the 7470 causes the relay contacts to reverse state.

The clock pulse is supplied manually by a standard push-button switch, mounted on the supply unit, which has been made "bounceless" by a simple bistable constructed from a pair of NAND logic gates (Figures 5.9(a) and

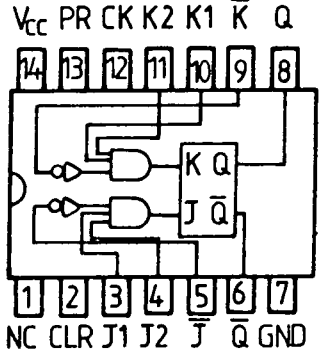

The 7470

$J = J1 \cdot J2 \cdot \overline{J}$

$K = K1 \cdot K2 \cdot \overline{K}$

$V_{CC} = 5V$

(a) Detail of 7470 flip-flop.

INPUTS					OUTPUTS	
PRESET	CLEAR	CLOCK	J	K	Q	$\overline{Q}$
L	H	L	X	X	H	L
H	L	L	X	X	L	H
L	L	X	X	X	L	L
H	H	↑	L	L	Q_0	$\overline{Q}_0$
H	H	↑	H	L	H	L
H	H	↑	L	H	L	H
H	H	↑	H	H	TOGGLE	
H	H	L	X	X	Q_0	$\overline{Q}_0$

(b) Logic table for 7470 flip-flop.

Figure 5.7

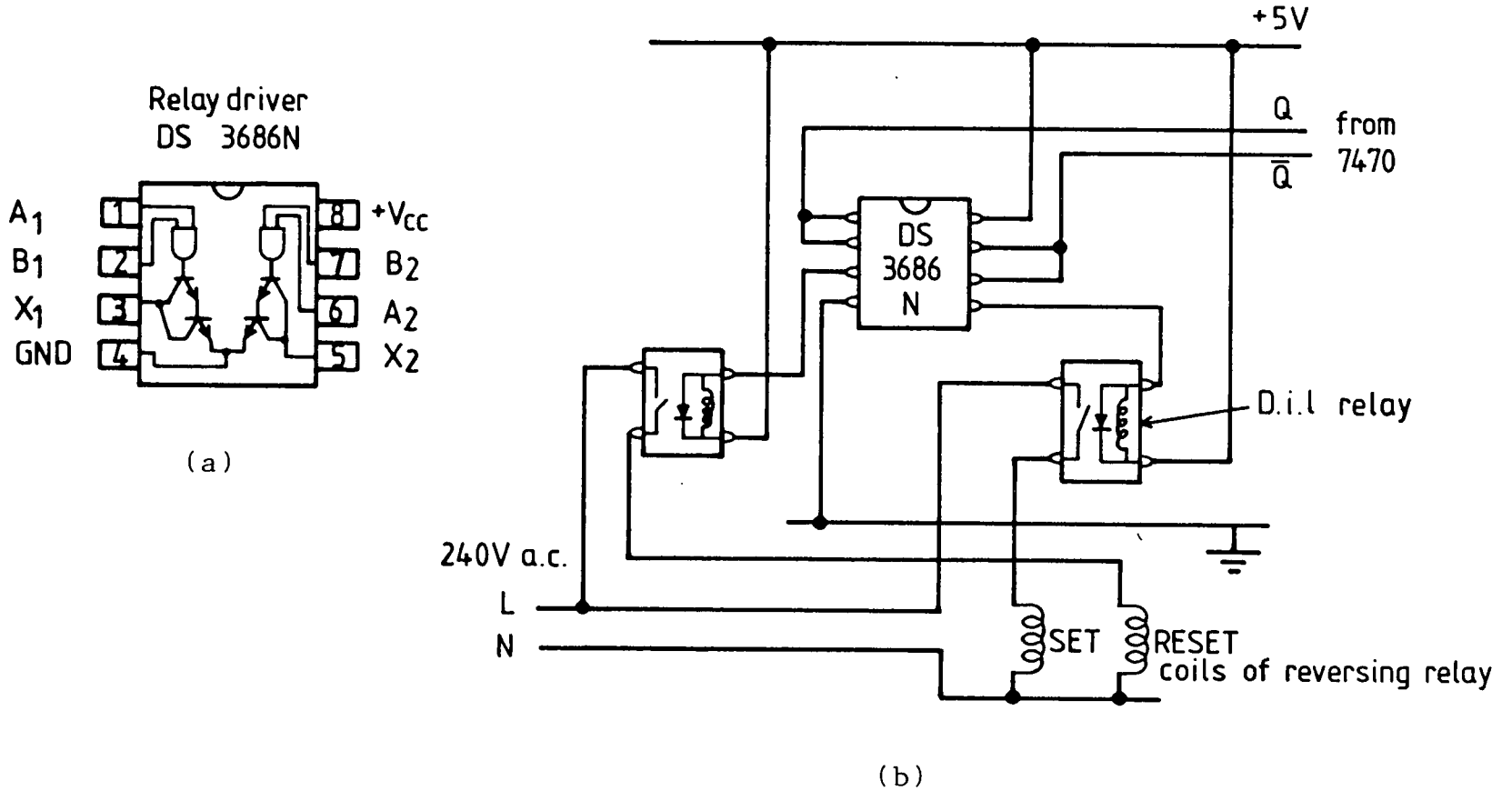

Figure 5.8 (a) Detail of DS 3686N relay driver. (b) Illustration of use of DS 3686N and d.i.l. relays to control the supply of 240V a.c. to the set/reset coils of main reversal relay.

(b)). Bounce on any pair of switch contacts cannot be tolerated as it would cause the logic, and hence the latching relay, to toggle an indeterminable number of times. The logic signal transmitted to the clock input of the 7470 is normally in the low state and it becomes high only when the switch is fully depressed.

The microcomputer uses two relays to mimic the action of the manual switch when remote control is required. These relays are located on an "in-house" fabricated board situated in the MINICAM rack (Figure 5.10). The TTL inputs to the board are provided by MINICAM's GPOB. The relays A and B share a common terminal which is held to earth. By activating A (with relay B off), and vice-versa, the relay board outputs are equivalent to the manual switch in its relaxed or depressed state respectively. When both relays are off the outputs are equivalent to the manual switch being mid-way between both sets of contacts. Thus, by following the correct sequence the microcomputer is able to copy the action of the manual switch exactly and thereby create a logic reversal. This sequence is:

(a) activate relay A,

(b) deactivate relay A, and activate relay B,

(c) deactivate relay B.

As stated earlier, the logic signals required to activate the relays are provided by MINICAM's GPOB. When this board is addressed initially with the parameter N% set equal to zero all the outputs rise to a high state (TTL = "1"). Hereafter, the outputs give a binary representation of the N% value used when addressing

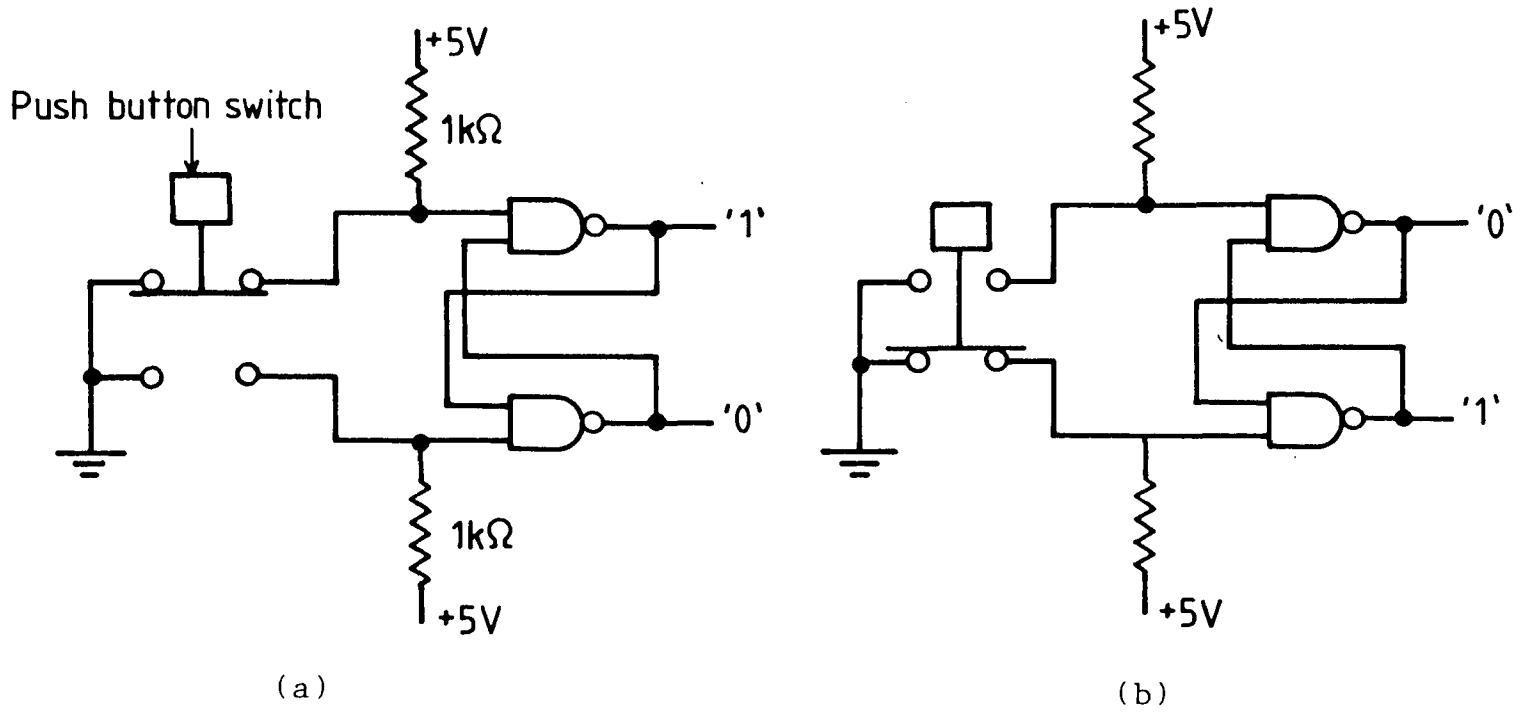

Figure 5.9 Illustration of use of a pair of NAND logic gates to achieve a bounceless switch. (a) Switch released. (b) Switch depressed.

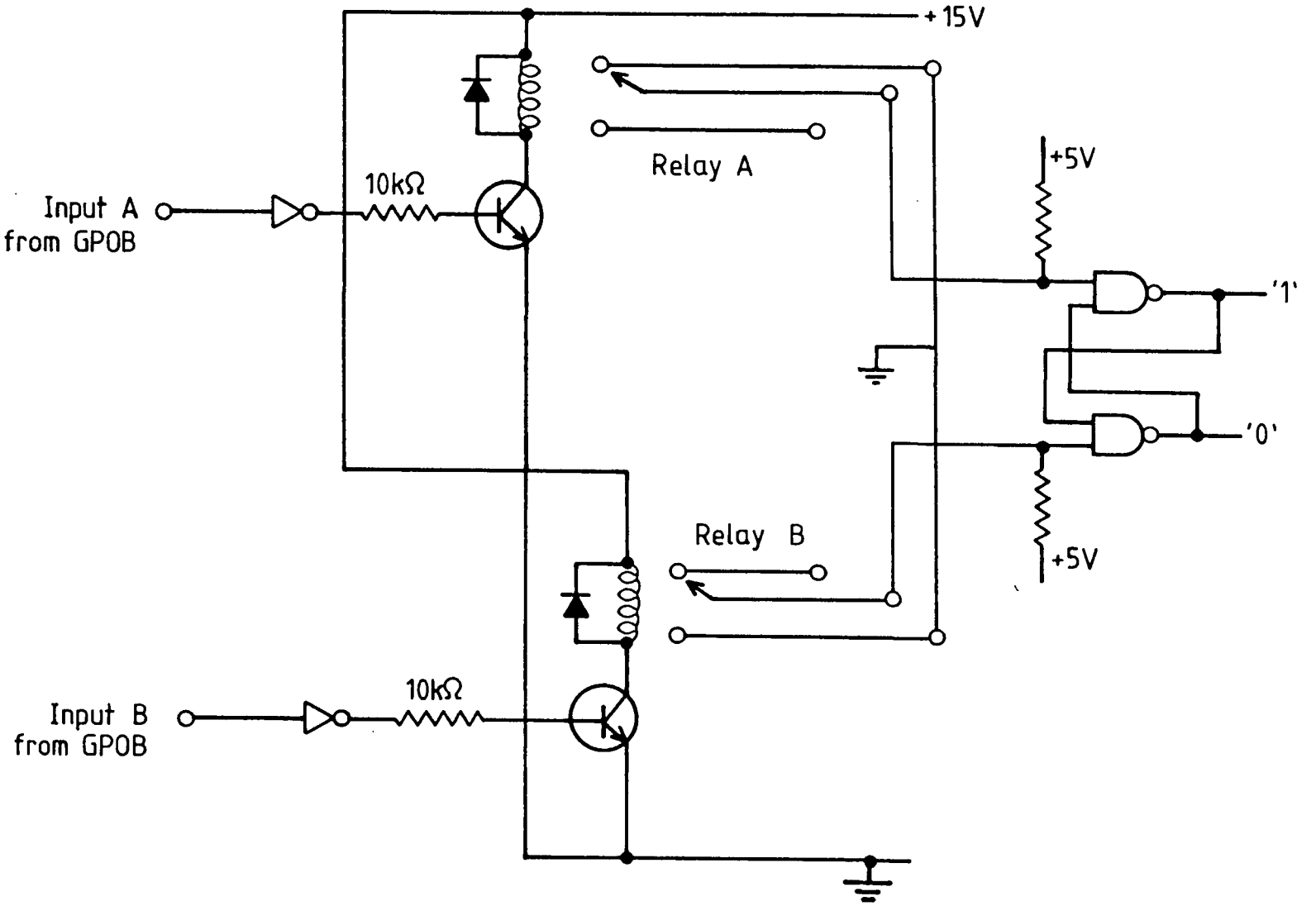

Figure 5.10 Detail of "in-house" fabricated board, for use in MINICAM rack system, which mimics action of manual push-button switch.

the board, with a low state (TTL = "0") being equivalent to a binary 1 and a high state equivalent to a binary 0. The relay board (Figure 5.10) inverts the logic and this inverted signal switches the relay via a transistor. The electrical connections are such that addressing the GPOB with N% = 2 activates relay A only, N% = 0 deactivates both relays and N% = 4 activates relay B only (see Appendix F).

The interchange of the inputs to the NAND gate bistable, from the push-button switch to the relay board, is achieved by a double-pole double-throw switch that is mounted on the supply unit. The addition of this switch eliminates any ambiguity as to the method by which the logic circuitry is being controlled, and so prevents simultaneous "dual control". The operator must select, therefore, the desired mode of operation when beginning an experiment and, in so doing, excludes the unrequired mode.

Visual representation of the state of the logic on the circuit board is provided by two mains-rated neon bulbs (Figure 5.11(a)). They are connected in parallel across the set and reset coils of the latching relay, and indicate whether the logic state/magnet current is in the forward or reverse direction. The further addition of a mains coil relay across either the set or reset coil allows the microcomputer to determine the current direction. It senses the switching action of this relay by using an ADC on MINICAM that has been modified to provide its own source signal voltage V_o

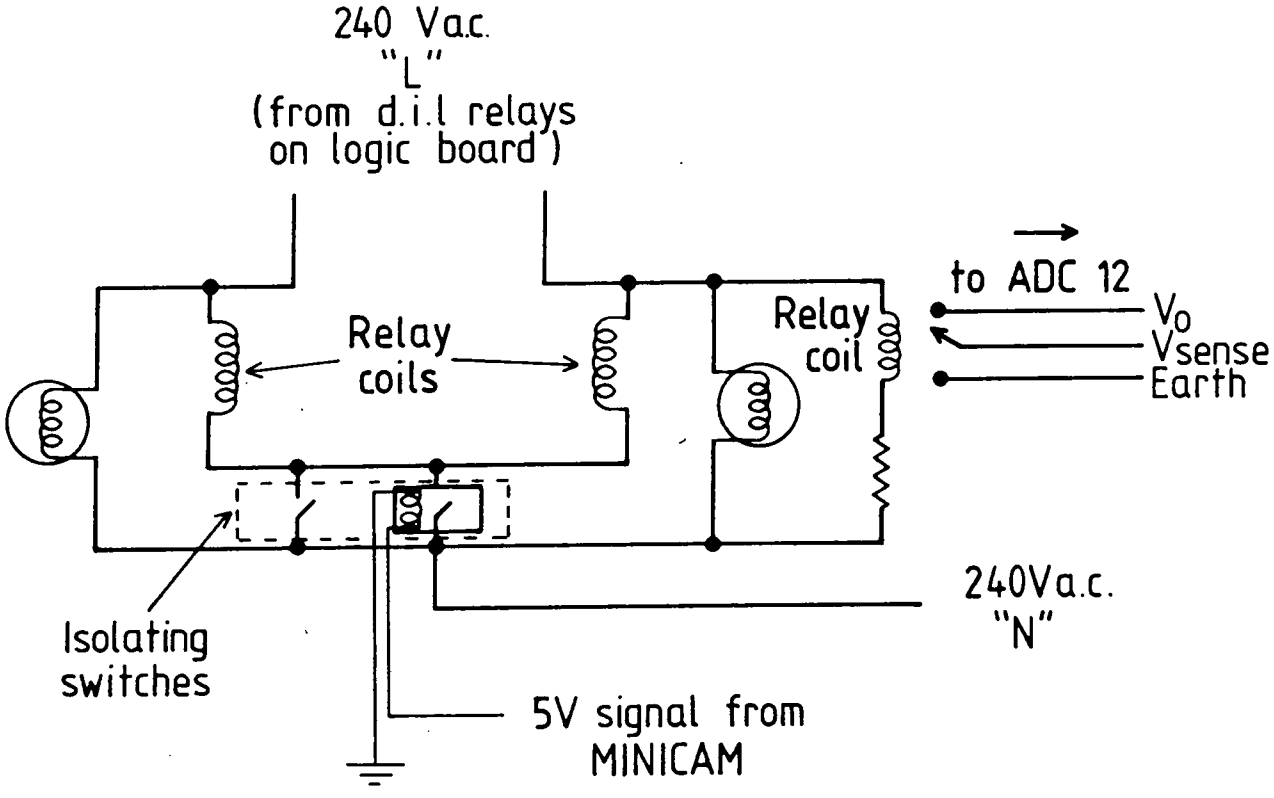

(a) Detail of the mains-rated neon bulbs indicating logic state, the relay used to remotely sense logic state and the remote operation of the isolating switch.

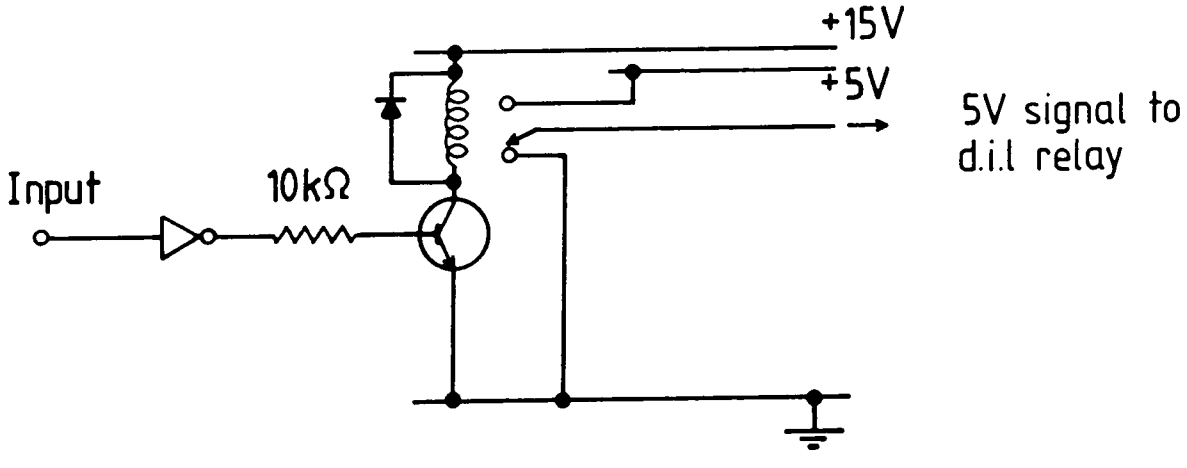

(b) Detail of the "in-house" fabricated board, located in MINICAM, which provides 5 volt signal to remotely operated isolating switch.

Figure 5.11

(Figure 5.11(a)). Any failure of the circuitry to reverse states can, therefore, be noted and corrected both under manual and computer control. Also shown in Figure 5.11(a) are the two isolating switches (in dotted box) which form part of the safety protection of the latching relay system (see section 5.6). The d.i.l. relay is operated by a 5 volt signal supplied by a further relay on the "home-made" MINICAM relay board (Figure 5.11(b)). It also receives its input signal from the GPOB with the parameter N% set to 1.

The voltage comparator, which disables the 7470 when the magnet current is too great, is a high performance 311 voltage comparator requiring low input currents whose output is directly TTL compatible (Figure 5.12(a)). The J and K inputs to the 7470 flip-flop are each the and-gated resultants of three separate inputs, one of which is inverted (i.e. $J = J_1 \cdot J_2 \cdot \bar{J}$, $K = K_1 \cdot K_2 \cdot \bar{K}$). The Q and $\bar{Q}$ outputs will only toggle on the positive edge of the clock pulse if the J and K inputs are in the high state. If both J and K inputs are forced low, the TTL outputs will remain unaltered and are not affected by any subsequent transition or state at the clock input (see Figure 5.7(b)). Thus, by arranging the TTL output of the 311 to undergo a transition to a high state when the magnet supply potential exceeds 1 volt, and by feeding this signal directly to the $\bar{J}$ and $\bar{K}$ inputs of the 7470, the desired disabling of the logic circuitry is achieved. Before the magnet supply potential reaches the 311 it

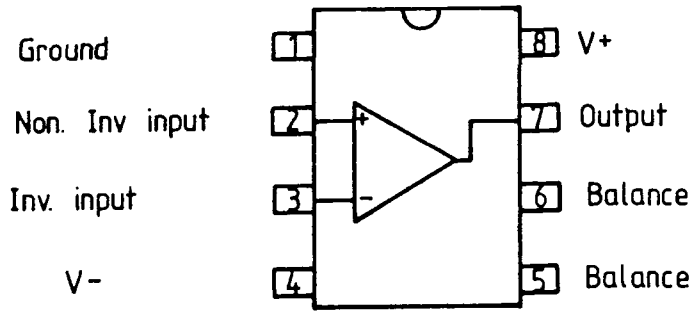

(a) Detail of 311 voltage comparator.

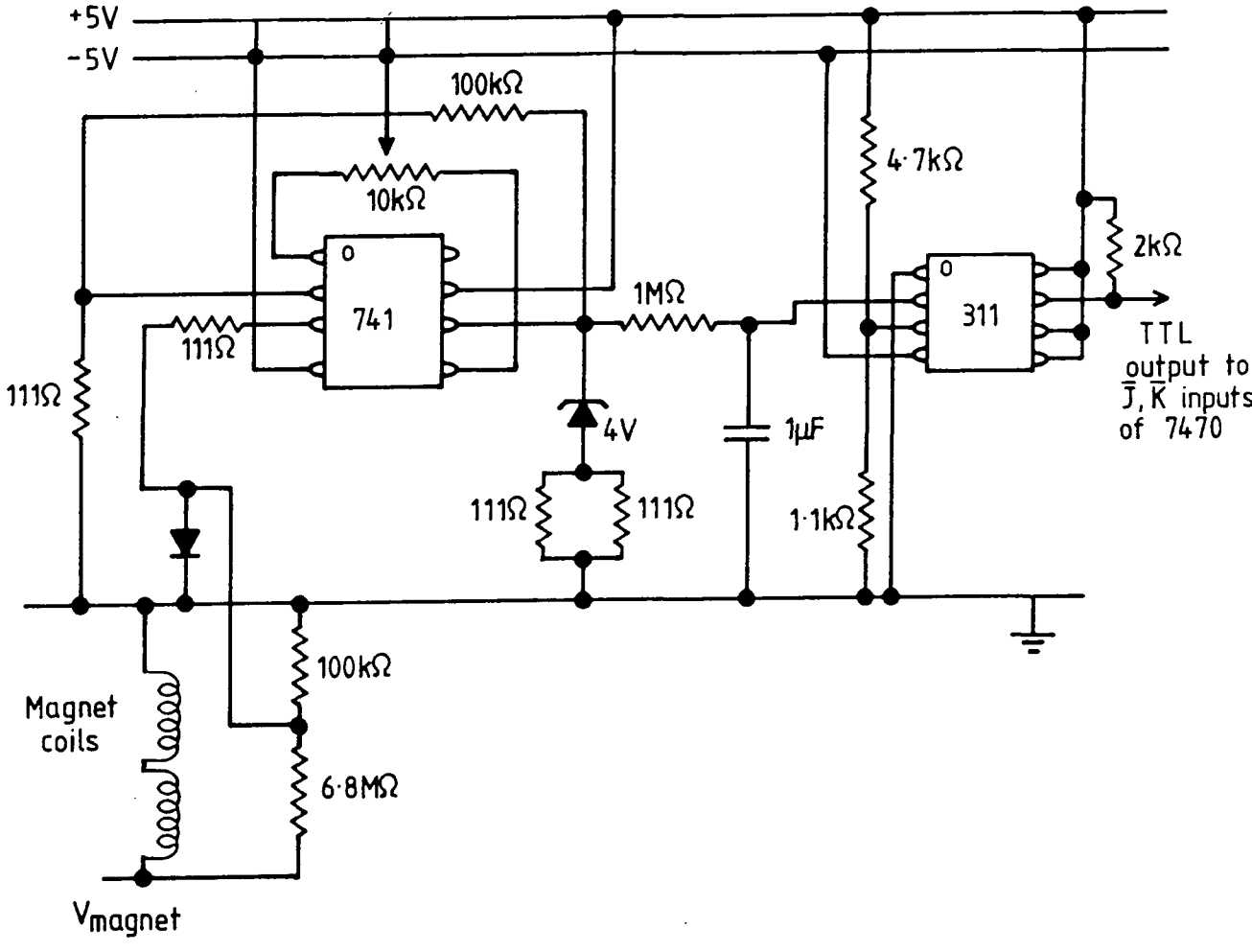

(b) Illustration of the design of the section of circuitry which monitors magnet supply voltage and disables 7470 flip-flop. The signal voltage is potentially divided, amplified and filtered before comparison is made with a fixed voltage level (approximately 1 volt).

Figure 5.12

is potentially divided and amplified by a non-inverting amplifier. Overvoltage protection for the amplifier is provided by diodes at both input and output stages, and its output is filtered to rid it of the 50 Hz noise present in the magnet supply. ($\frac{1}{RC}$ is equal to 10 Hz). The maximum voltage obtainable after this stage, when the 741 is saturating, is 2 volts so the reference voltage for the 311 comparator is set to 1 volt. This part of the circuit is shown in figure 5.12(b).

Both the 741 and the 311 require a bipolar 5 volt supply. The only power rail on the logic board, however, is + 5V and the - 5V rail has to be provided by two ICL 7660 voltage converter i.c's (Figure 5.13(a) and (b)). The total current drain on the - 5V rail has been measured to be approximately 20 mA and this is easily supplied by the pair of 7660's as each is capable of giving 20 mA at - 4V for a supply voltage of + 5V.

The complete circuitry described so far is contained on a printed circuit board inside the power supply unit. Figures 5.14 and 5.15 show the whole circuit both as seen on the p.c.b and diagrammatically. Table 5.1 provides the relevant component list. The only omission from these figures is the inclusion of the 12V lead acid battery which protects the logic circuitry in the event of mains failures (see section 5.6). Figure 5.16 indicates how this has been incorporated into the system and reveals the mains coil relay which performs the necessary switching in/out of the battery.

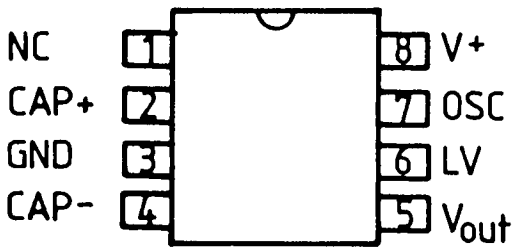

The ICL 7660

(a) Detail of ICL 7660 voltage converter.

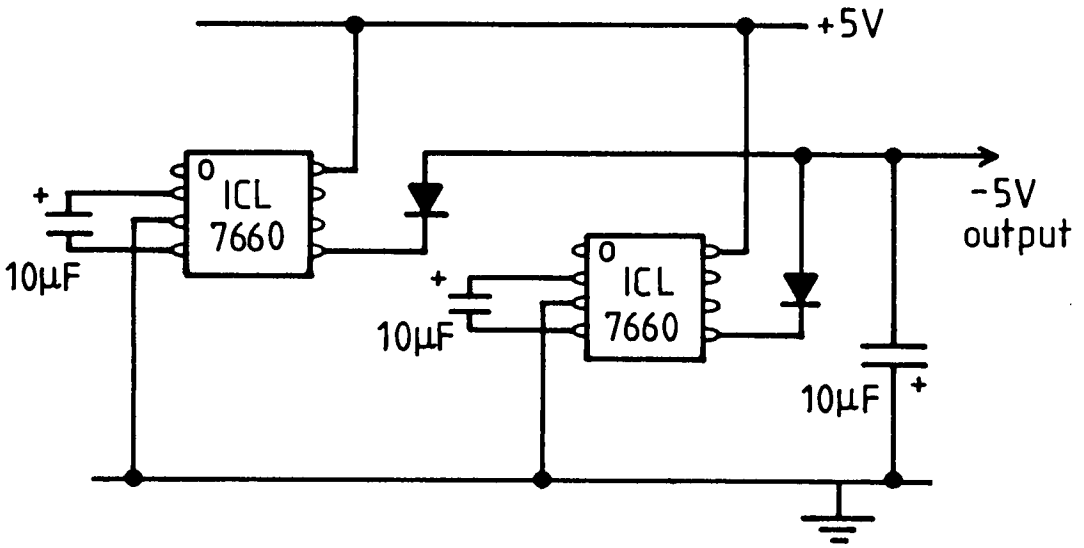

(b) Illustration of use of 7660 to provide - 5V power rail.

Figure 5.13

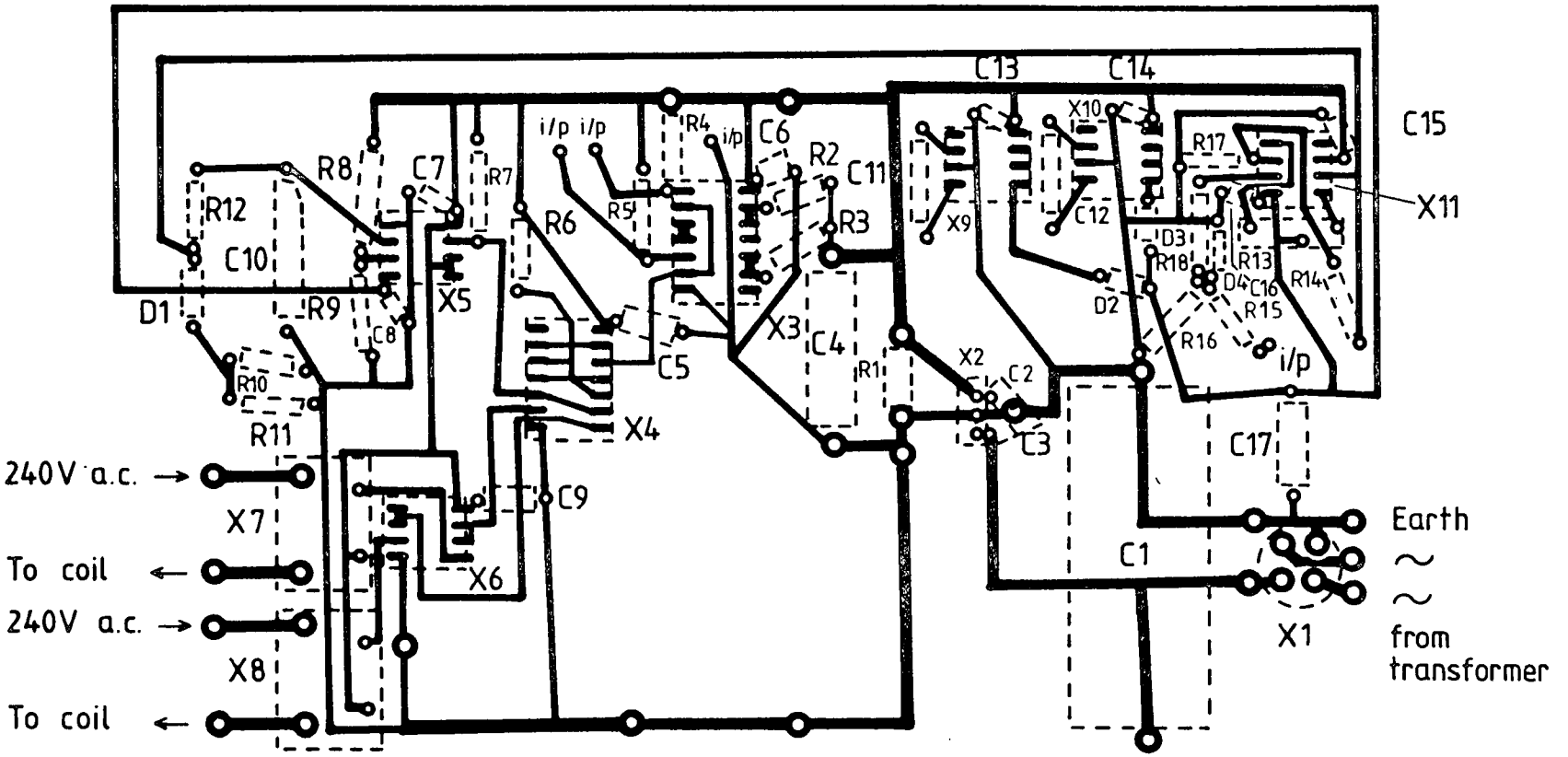

Figure 5.14 The printed circuit board design which contains complete logic circuitry. The components indicated here are listed in Table 5.1.

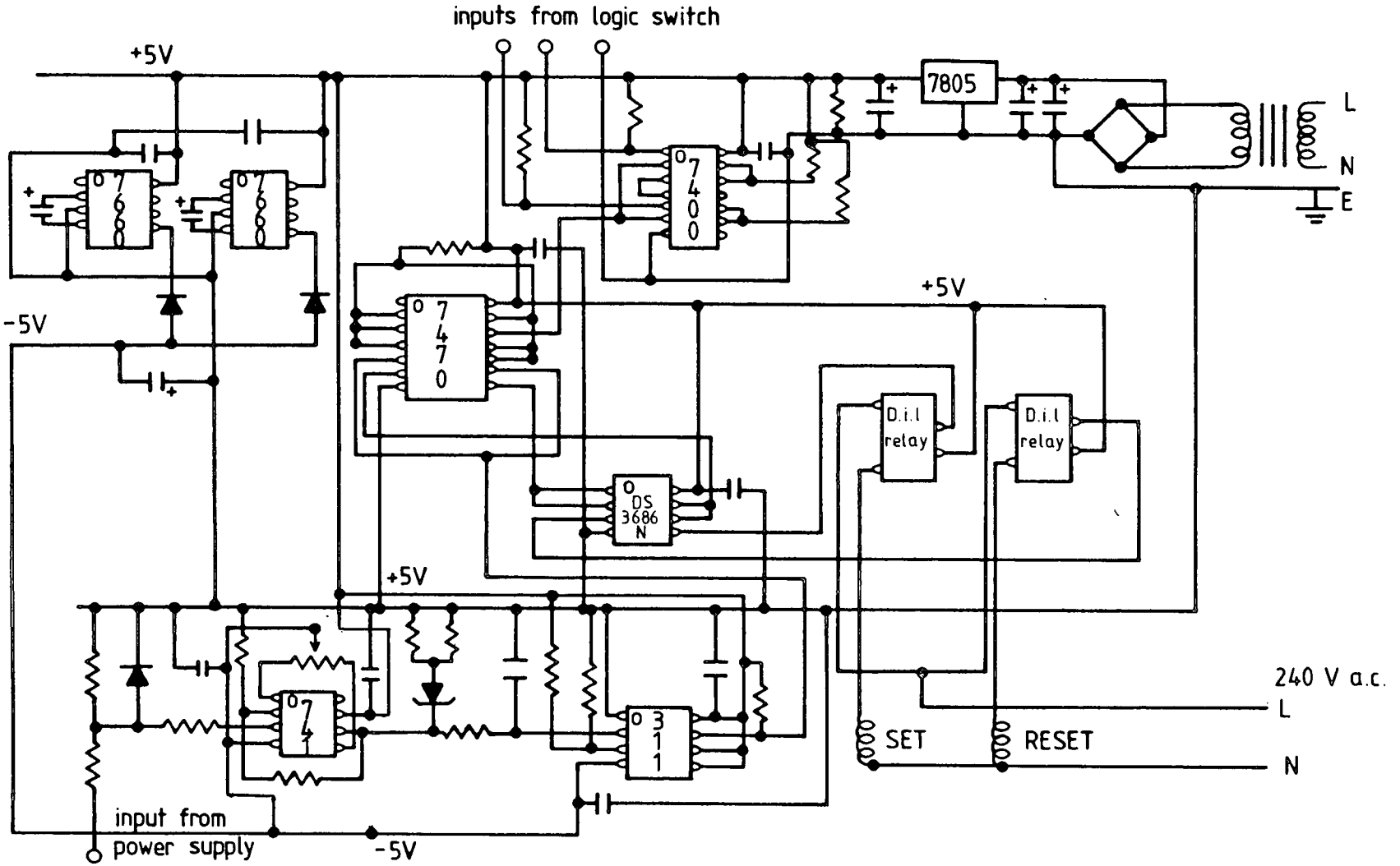

Figure 5.15 Diagrammatical representation of complete logic circuit.

RESISTORS		CAPACITORS		VARIOUS	
R1	4.7K	C1	4700 µF electrolytic	X1	Full wave bridge regulator (R.S. No. 262-157)
R2	1.1K	C2	1 µF electrolytic tantalum	X2	7805 Voltage regular
R3	1.1K	C3	1 µF electrolytic tantalum	X3	7400 NAND gate
R4	1.1K	C4	100 µF electrolytic	X4	7470
R5	1.1K	C5	0.1 µF decoupling	X5	311 comparator
R6	1.1K	C6	0.1 µF decoupling	X6	Relay driver (R.S. No. 306-954)
R7	2K	C7	0.1 µF decoupling	X7	D.i.l. relay (R.S. No. 348-582)
R8	4.7K	C8	0.1 µF decoupling	X8	D.i.l. relay (R.S. No. 348-582)
R9	1.1K	C9	0.1 µF decoupling	X9	ICL 7660 voltage converter
R10	111	C10	1 µF	X10	ICL 7660 voltage converter
R11	111	C11	10 µF electrolytic	X11	741 op-amp
R12	1M	C12	10 µF electrolytic		
R13	10K pot	C13	0.1 µF decoupling	DIODES	
R14	100K	C14	0.1 µF decoupling		
R15	6.8M	C15	0.1 µF decoupling	D1	4V zener
R16	100K	C16	0.1 µF decoupling	D2	General purpose
R17	111	C17	10 µF electrolytic	D3	General purpose
R18	111			D4	General purpose

Table 5.1 List of electrical components on magnet relay printed circuit board

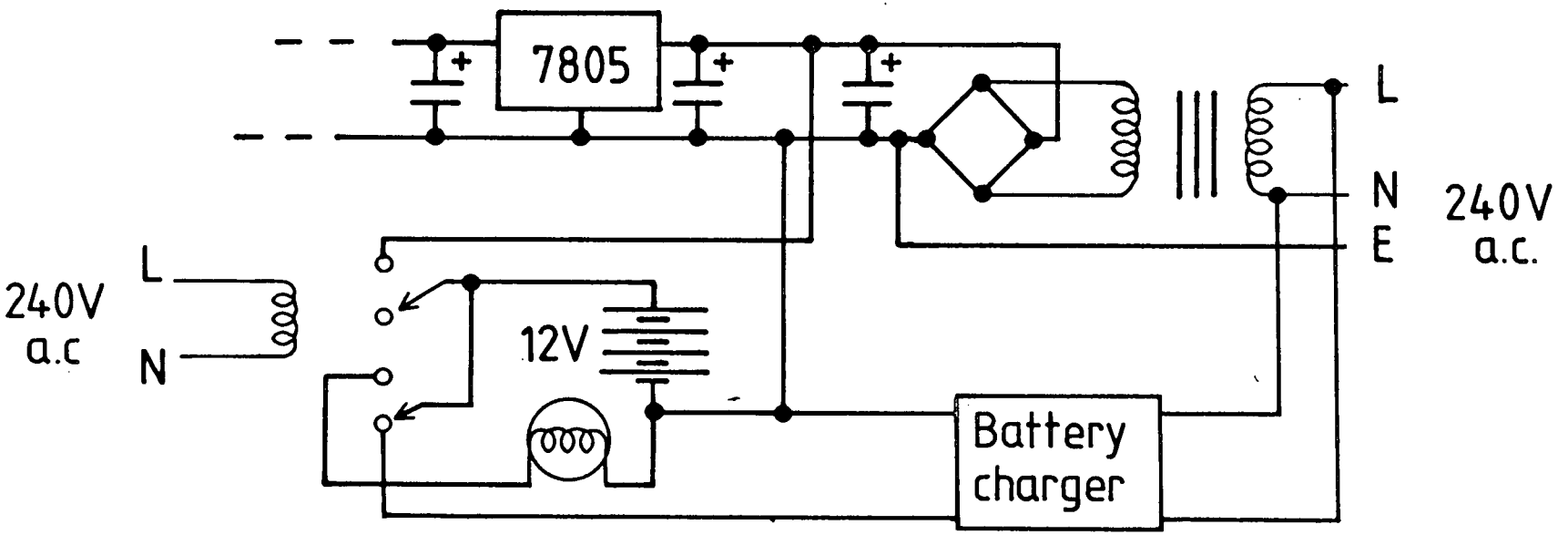

Figure 5.16 Detail of incorporation of 12V lead acid battery and battery charger into logic circuit design.

CHAPTER 6

RELATION BETWEEN PIPE-STEEL METALLURGY, CHEMISTRY, MECHANICAL PROPERTIES AND MAGNETIC PROPERTIES

6.1 INTRODUCTION

Many investigations made during the last 50 years have established definite regular relationships between the structural condition, the chemical and phase composition, and the toughness of materials, on the one hand, and the magnetic properties, on the other (see, for example, Mikheev et al. (1954), Tomilov et al. (1959), Kuznetsov and Mikheev (1964), Morozova et al. (1966) and Konovalov et al. (1982)). Not all the magnetic properties are equally sensitive to changes in the structure and phase composition of a substance. The Curie temperature (T_c) and saturation magnetization (M_s), for example, are not structurally sensitive, being determined by the quantity and type of atoms and their location within the crystallographic lattice (Mikheev & Gorkunov (1981)) while the hysteresis loss, coercive force (H_c) and magnetic permeability (μ) are structurally sensitive. The correlation between the magnetic properties and the structural state of a substance, therefore, requires the detailed study of the many physical parameters describing the material in order to identify those that are relevant. To this end, a team of research workers was formed in the Solid State Physics group at the University of Durham, whose brief was to;

(i) identify the parameters relevant to magnetic flux leakage pipe-line inspection,

(ii) determine the variation in these parameters between pipe specimens,

(iii) develop a model with predictive capability.

Apart from the direct measurement of magnetic properties (see Chapter 3) the areas studied by the team were metallography, compositional chemistry, mechanical properties, texture and magnetic domain observations. A compilation of the data obtained from these investigations, for the twenty seven steel types of interest to British Gas, is shown in Appendix D, and subsequent analysis of this raw data on the site VAX-11 computer at Cramlington was aimed at seeking correlations between the various sets of parameters using the BMDP statistical software package (see Chapter 3) available on this computer.

The present chapter contains a description of the results obtained by the author during the investigation of the magnetic properties of the pipe-steels, which formed part of the more general investigation, as well as correlations between the various parameters revealed using the BMDP package. Together they indicate that the initial magnetization characteristics of any similar pipe-steel can be predicted by a knowledge of the coercive field (H_c) which, in turn, may be derived independently either from direct measurement or a knowledge of the metallography or steel chemistry.

6.2 PARAMETERIZATION AND SUCCESSFUL RECONSTRUCTION/ PREDICTION OF THE INITIAL MAGNETIZATION CURVE.

6.2(i) The Widger polynomial

After the unsuccessful attempt (described in Chapter 3) at obtaining correlations between the harmonic amplitudes, used to parameterize the initial magnetization curve of all steel types, and all the other parameters listed in Appendix D, the parameterization of these curves was repeated using the following polynomials, first suggested by Widger (1969);

$$B = \frac{a_o^{\,1} + a_1^{\,1} H + a_2^{\,1} H^2 + \ldots\ldots + a_n^{\,1} H^n}{1 + b_1^{\,1} H + b_2^{\,1} H^2 + \ldots\ldots + b_n^{\,1} H^n} H \qquad (6.1)$$

$$H = \frac{a_o + a_1 B + a_2 B^2 + \ldots\ldots + a_n B^n}{1 + b_1 B + b_2 B^2 + \ldots\ldots + b_n B^n} B \qquad (6.2)$$

It was found that good fits to the initial magnetization curve were obtained using just the five lowest order parameters (in agreement with Widger (1969)) and, with the aid of the BMDP package, the parameters $a_o^{\,1}$, $a_1^{\,1}$, $a_2^{\,1}$, $b_1^{\,1}$, $b_2^{\,1}$ and a_o, a_1, a_2, b_1, b_2 were individually plotted against all other parameters. The results obtained, however, were disappointing because, apart from reasonable linear relationships between both $a_1^{\,1}$ and $b_1^{\,1}$ versus both Ultimate Tensile Stress (UTS) and Pearlite Fraction, no good correlations were found. The regular relationships that were observed, therefore, only permitted the determination of two of the five parameters required to reproduce the initial curve.

6.2(ii) The Kneppo equation

Following Gonda et al. (1984), a further attempt at parameterization involved fitting the initial magnetization curve data to the single equation.

$$B = A^{(k - \frac{1}{H})} \qquad (6.3)$$

first suggested by Kneppo*. The empirical parameters A and k were obtained by fitting equation (6.3) to the measured curves using the least-squares method of error determination (as was the case for fitting equations (6.1) and (6.2)). It was found that, in order to obtain good fits to the experimental curves, pairs of values of B and H, for which the value of the applied field (H) was less than $0.4 kAm^{-1}$, had to be rejected. A combination of two reasons are thought to be responsible for this; (i) the small field values have comparatively large relative errors and, when these field values are inverted (see equation (6.3)), the least-squares calculation is heavily weighted by them,
(ii) the upward curvature of the low field region of the steel's magnetization curve is not well represented by equation (6.3).

Table 6.1 shows the values of k and A, calculated in this manner, for all steel types. Correlations were sought between these and all other parameters pertinent to the steels and this study revealed good linear relation-

---

* L. Kneppo - Complex Functions in Electrical Engineering (to be published by the Slovak Academy of Sciences, Bratislava, CSSR)

Steel type	LnA	kLnA	k
DFB	0.71438	0.66293	0.928
DFF	0.64954	0.66370	1.022
DFE	0.71248	0.66144	0.928
EEC	0.73886	0.68581	0.928
DME	0.53604	0.66374	1.238
EEB	0.61406	0.65472	1.066
OLI-030	0.74597	0.67447	0.904
OLI-015	0.69677	0.71285	1.023
OLI-010	0.61144	0.69305	1.133
EED	0.72246	0.70961	0.982
DHP	0.52021	0.62896	1.209
OLI-013	0.73365	0.72122	0.983
DWA	0.68966	0.68795	0.998
DHQ	0.82853	0.68796	0.830
2401	0.46211	0.63547	1.375
EEE	0.67671	0.69444	1.026
OLI-017	0.76520	0.71334	0.932
DFD	0.70651	0.67232	0.952
DLR	0.41665	0.63025	1.513
OLI-012	0.67165	0.70631	1.052
EAO	0.84821	0.74686	0.881
DEQ	0.84052	0.78883	0.939
DEZ	0.60791	0.66579	1.095
EER	0.55135	0.64283	1.166
OLI-009	0.70522	0.70505	1.000
OLI-011	0.71759	0.70784	0.986
Sample A	0.309	0.597	1.932
Sample B	2.567	0.664	0.259
Sample C	1.065	0.591	0.555

Table 6.1 The values of LnA($TkAm^{-1}$), kLnA(T) and hence k(mkA^{-1}) for all steel types including heat treated 12 inch steel.

ships between both k^{-1} and LnA (loge A) versus the coercive field (H_c) and reasonable linear relationships between LnA versus % Mn and $\frac{1}{k}$ versus UTS. These relationships may be expressed quantitatively by;

$LnA = 1.313\ H_c + 0.07$	Correlation coefficient** 0.894	(6.4)
$k^{-1} = 1.914\ H_c + 0.10$	Correlation coefficient 0.889	(6.5)
$LnA = 0.308\%\ Mn + 0.32$	Correlation coefficient 0.683	(6.6)
$k^{-1} = 2.35 \times 10^{-3} UTS - 0.27$	Correlation coefficient 0.753	(6.7)

and the plots represented by equations (6.4) and (6.5) are shown in figures 6.1(a) and (b). The exciting discovery indicated by these plots, suggested that the initial magnetization curves of these and similar pipe-steels could be reconstructed/predicted from a knowledge of the coercive field of the material. Only a small sample of a hitherto unstudied steel would then be required to determine its magnetization characteristics as the coercive field can be measured to high precision using the VSM. Before this predictive capability was checked, however, an examination of equation (6.3) revealed several more interesting relationships.

** The correlation coefficient (c) used here is defined as

$$C = \frac{\Sigma (x_i - \bar{x})(y_i - \bar{y})}{\Sigma (x_i - \bar{x})^2 \ \Sigma (y_i - \bar{y})^2}^{\frac{1}{2}}$$

and represents the "goodness of fit". A perfect fit, therefore, will have a correlation coefficient equal to unity.

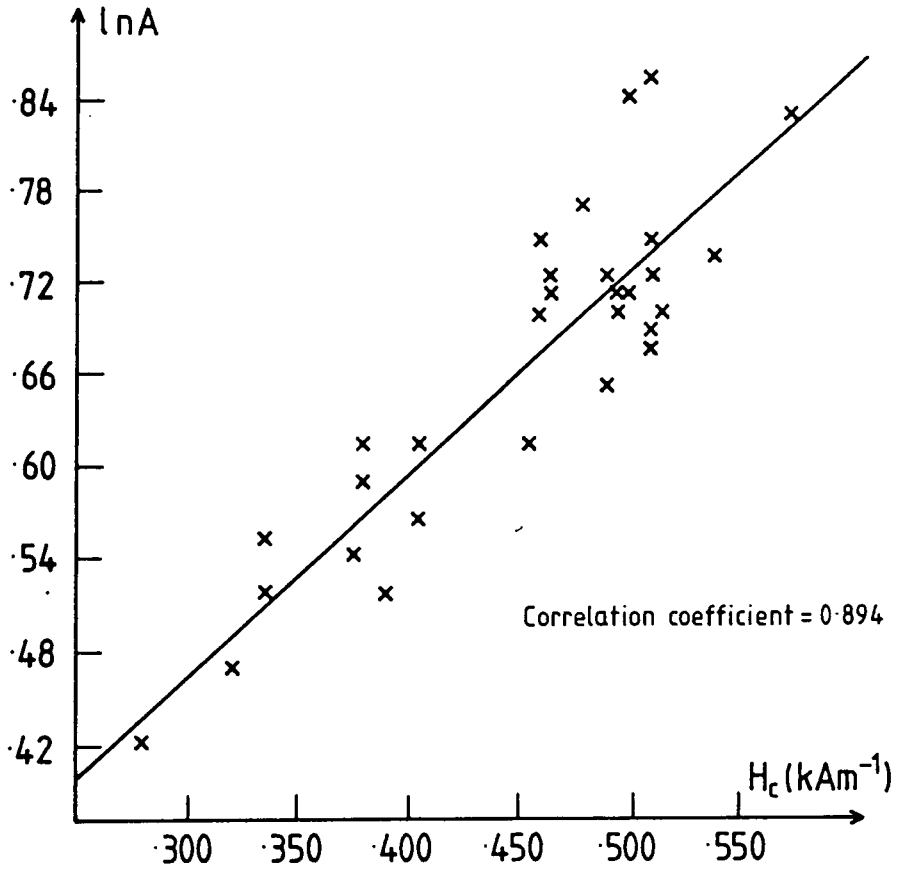

(a) Correlation plot between LnA and the coercive field for all steel types.

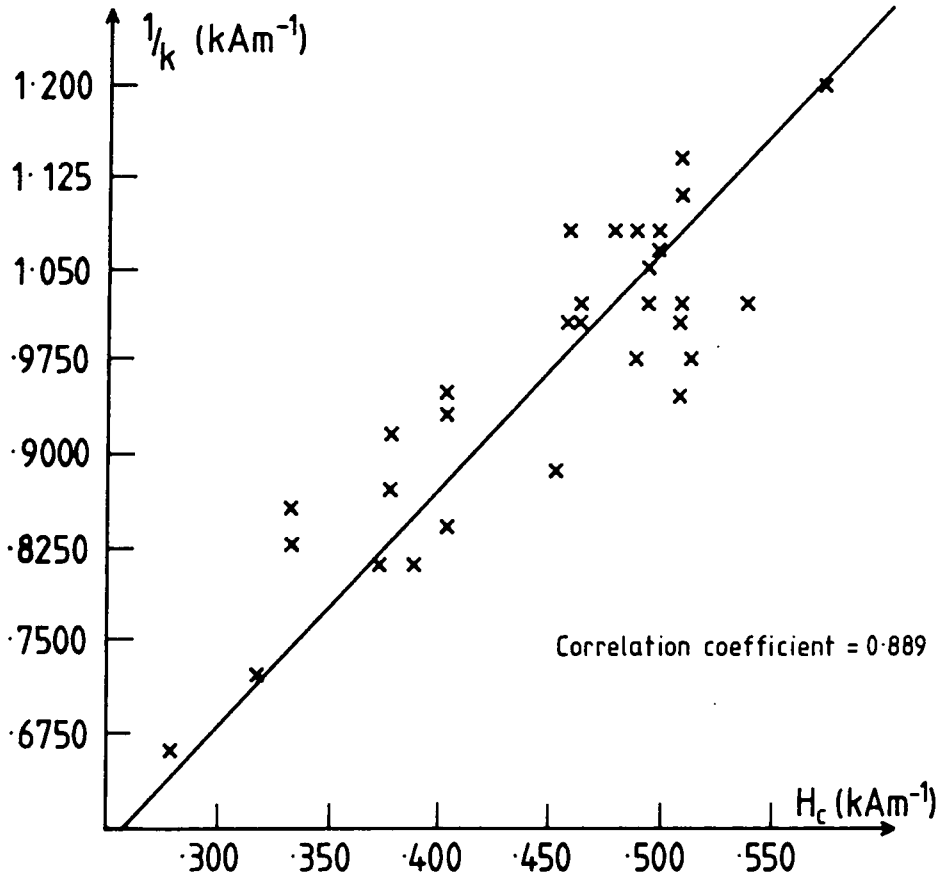

(b) Correlation plot between k^{-1} and the coercive field for all steel types.

Figure 6.1

A consideration of the form of equation (6.3) as H tends to infinity ($B \rightarrow B_s$) reveals

$$B_s = A^k \tag{6.8}$$

and hence

$$\mathrm{Ln}B_s = k\mathrm{Ln}A \tag{6.9}$$

Since the values of B_s have been found to be constant to within 0.6% for all pipe-steels considered here (see also Mikheev and Gorkunov (1981)), equation (6.9) may be rewritten as

$$\mathrm{Ln}A = \frac{C}{k} \tag{6.10}$$

where C is a constant.

Similar manipulations of equation (6.3) (see Appendix H) predicted the following additional relationships:

$$H_{\mu m} = \mathrm{Ln}A \tag{6.11}$$

$$\frac{dB}{dH} = \mathrm{Ln}A \left(\frac{B}{H^2}\right) \tag{6.12}$$

$$k = \frac{(\mathrm{Ln}\ B_s)e\ \mu_m}{B_s} = C_1\ \mu_m \tag{6.13}$$

$$\mu_m = \frac{B_s}{eH_{\mu m}} = \frac{C_2}{H_{\mu m}} \tag{6.14}$$

where μ_m is the maximum value of the permeability, $H_{\mu m}$ is the field value at which the permeability is a maximum and C_1, C_2 are constants.

Values of $H_{\mu m}$ and μ_m were then calculated from the measured curves and the above relationships verified.

The results thus obtained may be summarized by the following;

$$\frac{1}{k} = 1.22\ \mathrm{LnA} + 0.17 \qquad \text{Correlation coefficient } 0.978 \qquad (6.15)$$

$$H_{\mu m} = 1.03\ \mathrm{LnA} - 0.01 \qquad \text{Correlation coefficient } 0.968 \qquad (6.16)$$

$$k = 0.91\ \mu_m - 0.02 \qquad \text{Correlation coefficient } 0.990 \qquad (6.17)$$

$$\mu_m = \frac{0.52}{H_{\mu m}} + 0.38 \qquad \text{Correlation coefficient } 0.917 \qquad (6.18)$$

and, by way of example, Figures 6.2 and 6.3 show the plot represented by equations (6.15) and (6.17) respectively.

By referring to these plots and the above results, it can be seen that the relationships predicted by a consideration of equation (6.3) are found to be very well adhered to in practice, and this confirms, therefore, how well the experimental data is represented by Kneppo's equation.

6.2(iii) Parameterization of magnetization curves of heat-treated steel

A more rigorous test of Kneppo's equation was provided by the extreme behavioural differences of the magnetization curves of three samples of heat-treated 12 inch pipe-steel. The three samples, chosen from the original set of 41 whose magnetic properties were described in Chapter 3, were known to have very similar magnetic characteristics in the as-received state, and they were heat treated in the following manner:

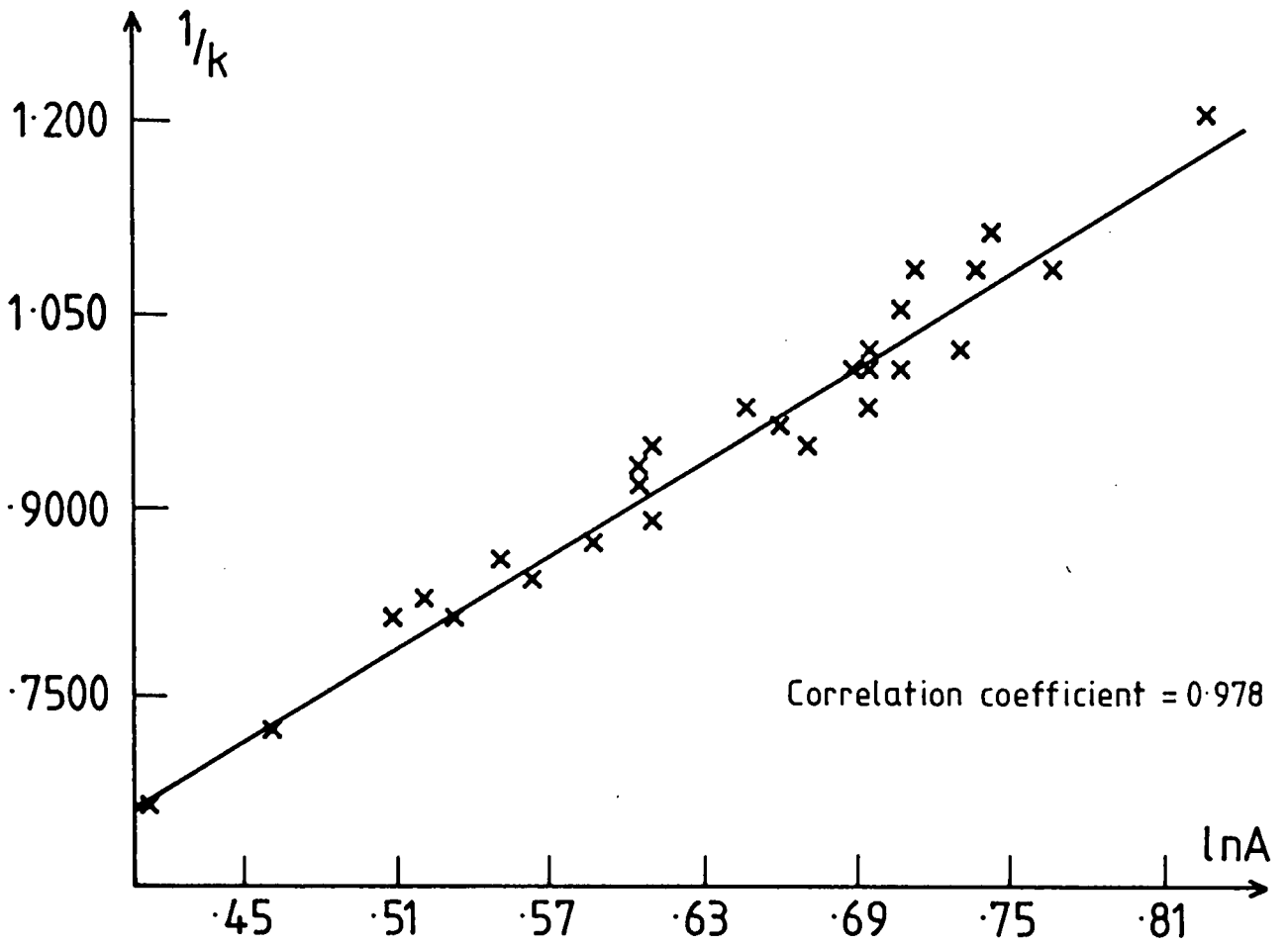

Figure 6.2 Correlation plot between k^{-1} and LnA for all steels.

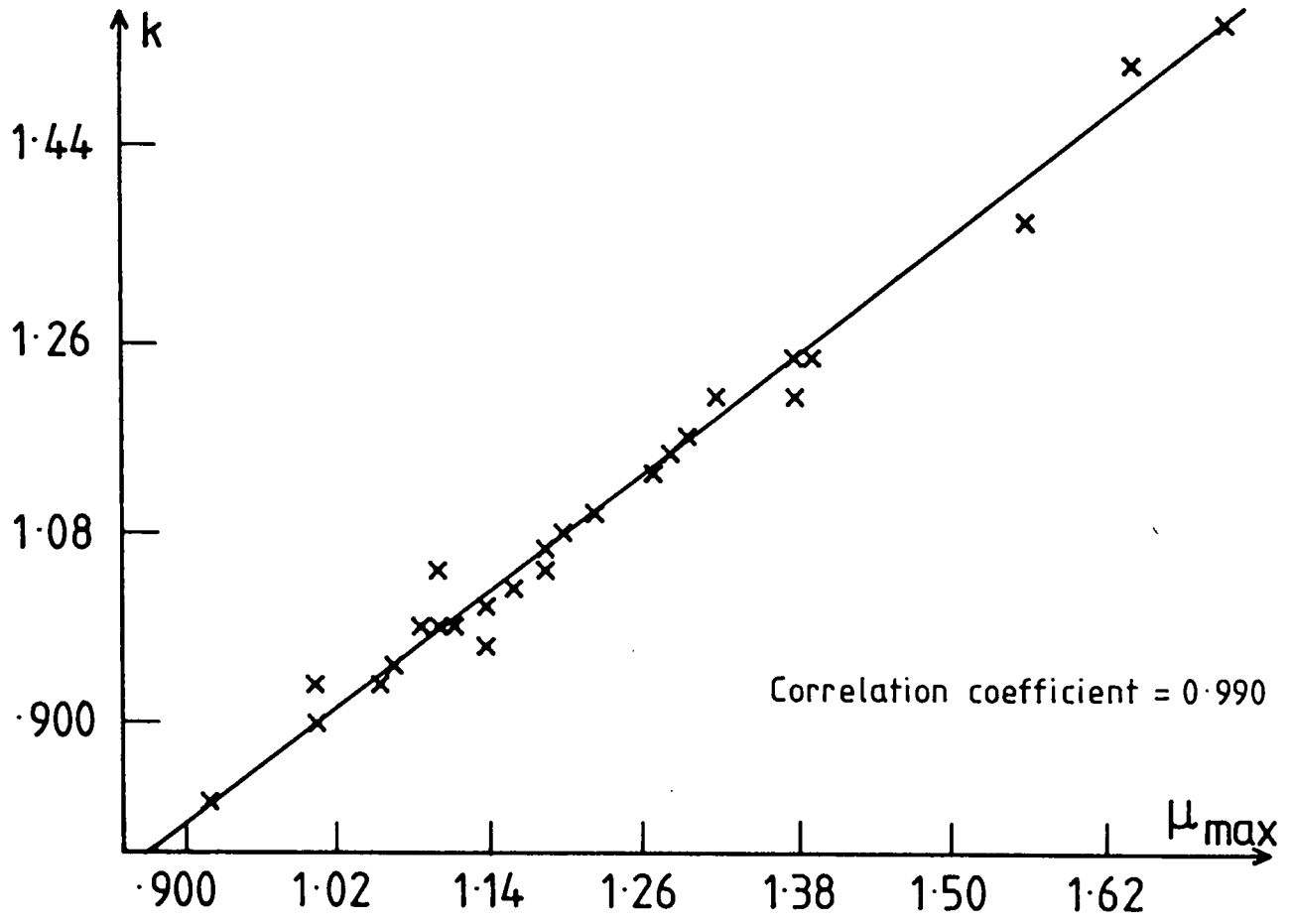

Figure 6.3 Correlation plot between k and the maximum permeability values for all steels.

(i) Sample A - heated to 910°C for one hour and slowly furnace cooled.

(ii) Sample B - heated to 800°C for one hour and water quenched.

(iii) Sample C - heated to 1000°C for one hour and water quenched.

Figure 6.4 shows a comparison between the initial magnetization characteristics of all three heat-treated samples and that pertinent to the as-received state. It can be seen that annealing the material produces a magnetically softer material, due mainly to both the relief of internal strain imparted during the plate manufacture and the growth of the ferrite grains (see Chapter 1 and also section 6.3(iii)). Quenching, on the other hand, produces a much harder magnetic material which has a reduced permeability and hence requires higher magnetic fields to achieve saturation. The degree of hardening, which depends on the severity of the quench and, therefore, the extent of formation of martensite, troostitic pearlite or sorbitic pearlite (see Chapter 1), is readily indicated by the values of coercive field obtained from full magnetization loop studies, viz:

Sample A	244 Am^{-1}
Sample B	769 Am^{-1}
Sample C	2023 Am^{-1}
As-received	344 Am^{-1}

The values of k and LnA were calculated for the magnetization characteristics of these samples by fitting

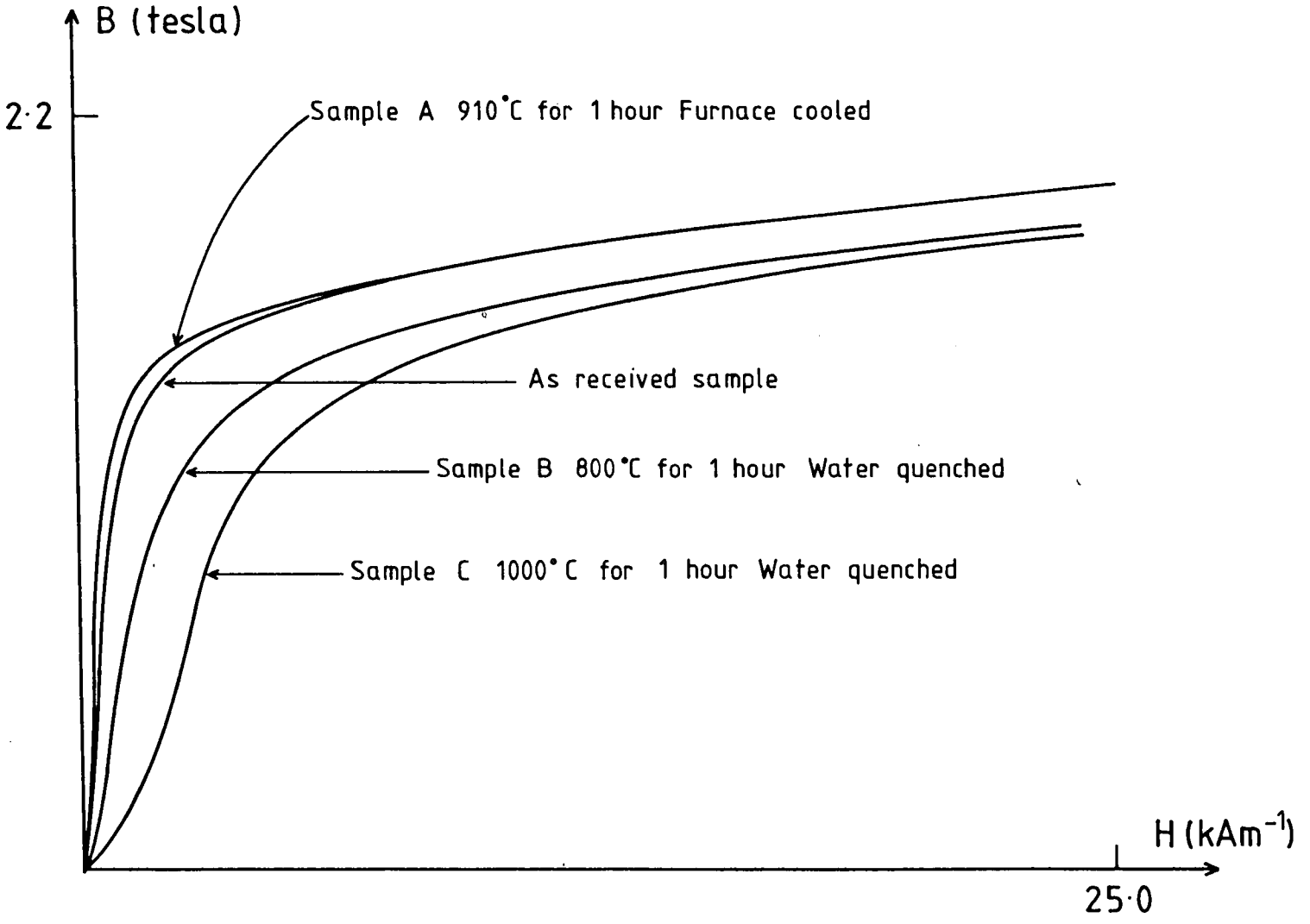

Figure 6.4 Comparison of the differences in magnetic characteristics of samples of 12 inch steel induced by various heat treatments.

a least-squares straight line to a plot of LnB versus H^{-1} (as was the case for the normal pipe-steels). Such a plot yields the values of these parameters directly from the intercept (kLnA) and gradient (- LnA), and an indication of how well the magnetization curve is approximated by Kneppo's equation is obtained from the value of the correlation coefficient of the data to this line. Whereas the correlation coefficient for Sample B (and all normal pipe-steels) was observed to be better than 0.994, thus indicating well fitting functions, the corresponding values obtained for Samples A and C were 0.989 and 0.978 respectively.

It may be concluded, therefore, that, while Kneppo's equation is a good approximation to the form of the magnetization characteristics of the whole range of normal pipe-steels, it is beginning to become less reliable when fitting the curves of heat-treated samples which have undergone extreme physical change.

6.2(iv) Reconstruction of the magnetization characteristics of pipe-steels

A further check on how well the magnetization data is represented by Kneppo's equation may be obtained by plotting B predicted versus B actual, where B predicted is the value of induction calculated at a value of H (using the relevant values of k and LnA) for which a data point B actual exists. A perfect "reconstruction" will give a straight line with a gradient of unity.

This approach was adopted for several normal pipe-steels (2401, DFD, DHQ, DHP, DFF, EEC, EED, 017), which were chosen at random to be representative of the four main steel types (i.e. semi-killed, fully-killed, controlled rolled and USA manufactured semi-killed), as well as the three heat-treated samples of 12 inch pipe. The results thus obtained are summarized in Table 6.2, where the values of correlation coefficient and gradient for each plot are listed. It may be seen that, with the exception of Samples A and C, the correlation coefficients are all better than 0.995 and the curve gradients vary from unity by less than 2%, thus confirming the conclusions of the previous section.

A typical plot is shown in Figure 6.5 which indicates the behaviour of both B predicted and (B predicted - B actual) versus B actual for DFD. The latter, referred to as the residual plot, reveals that discrepancies from linear behaviour are less than 0.05 tesla for induction values less than 1.85 T, whereafter significant deviations are observed. This general result holds for all steel types studied and again serves to confirm how well the data is represented by Kneppo's equation. The comparatively large residuals noted about 1.85 T do not give rise to concern because such values of induction are well above the "knee" region of the magnetization characteristic and, for the purposes of modelling the behaviour of the intelligent PIG (see Chapter 1), this curve region is not required as induction levels of this order are unobtainable throughout the pipe wall with current PIG

Steel Code	Correlation Coefficient	Curve gradient
2401	0.997	1.02
DFD	0.998	1.01
DHQ	0.998	0.98
DHP	0.996	1.01
DFF	0.997	1.01
EEC	0.998	0.99
EED	0.998	0.98
017	0.997	0.96
Sample A	0.995	1.06
Sample B	0.998	1.02
Sample C	0.995	1.09

Table 6.2 Values of correlation coefficient and curve gradient for plots of $B_{predicted}$ versus B_{actual} obtained for several pipe-steels. The predicted values are calculated using the known values of k and LnA for each steel.

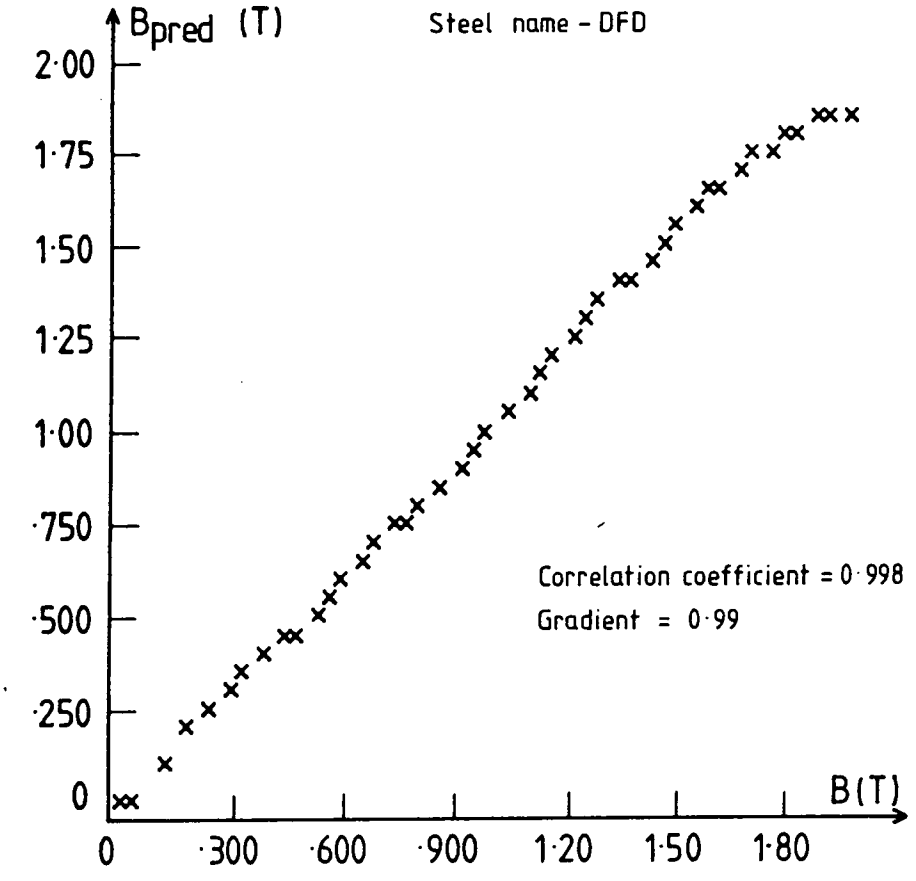

(a) Plot of $B_{predicted}$ versus B_{actual} for steel DFD. $B_{predicted}$ values calculated from known values of k and LnA.

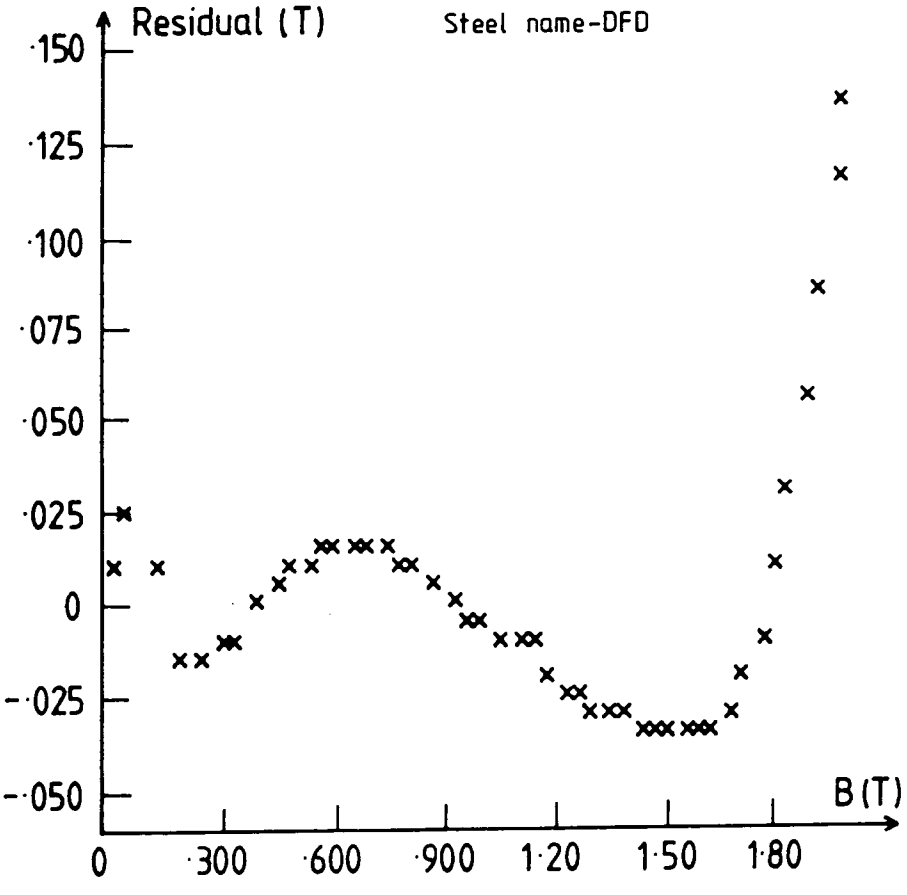

(b) Residual plot for DFD calculated from results presented in (a).

Figure 6.5

design.

6.2(v) Prediction of the magnetization characteristics of pipe-steels from measurements of coercive field

The most significant test of the curve parameterization and correlation work reported above involved the prediction of the initial magnetization characteristics, for the same steel types as above, from a knowledge of the coercive field. Equations (6.4) and (6.15) were used to determine the parameters k and LnA respectively from measured values of H_c, and plots of predicted values versus measured values were generated in a manner identical to that described above.

The results obtained are summarized in Table 6.3 and typical plots, again those found for DFD, are shown in Figure 6.6. With the single exception of Sample A, correlation coefficients for all steels are again better than 0.995 and, with the single exception of Sample B, the average curve gradients vary from unity by approximately 2.5%. It is noted, then, that even the characteristics of the extreme heat-treated samples are well reproduced. The residuals are again seen to increase rapidly for values of induction greater than 1.85T, but below this limit the maximum residuals (at field values near 1.5T) are found to be between 0.08 and 0.1 tesla, thus representing "errors" of approximately 6%.

Steel Code	Correlation coefficient	Curve gradient
2401	0.996	0.99
DFD	0.998	0.97
DHQ	0.998	0.98
DHP	0.996	0.99
DFF	0.996	0.94
EEC	0.998	1.01
EED	0.997	1.00
017	0.998	1.03
Sample A	0.993	0.98
Sample B	0.998	0.89
Sample C	0.996	0.96

Table 6.3 Values of correlation coefficient and curve gradient for plots of $B_{predicted}$ versus B_{actual} obtained for several pipe-steels. The predicted values are calculated using values of k and LnA obtained from a knowledge of the coercivity and the linear relationships between H_c, k and LnA.

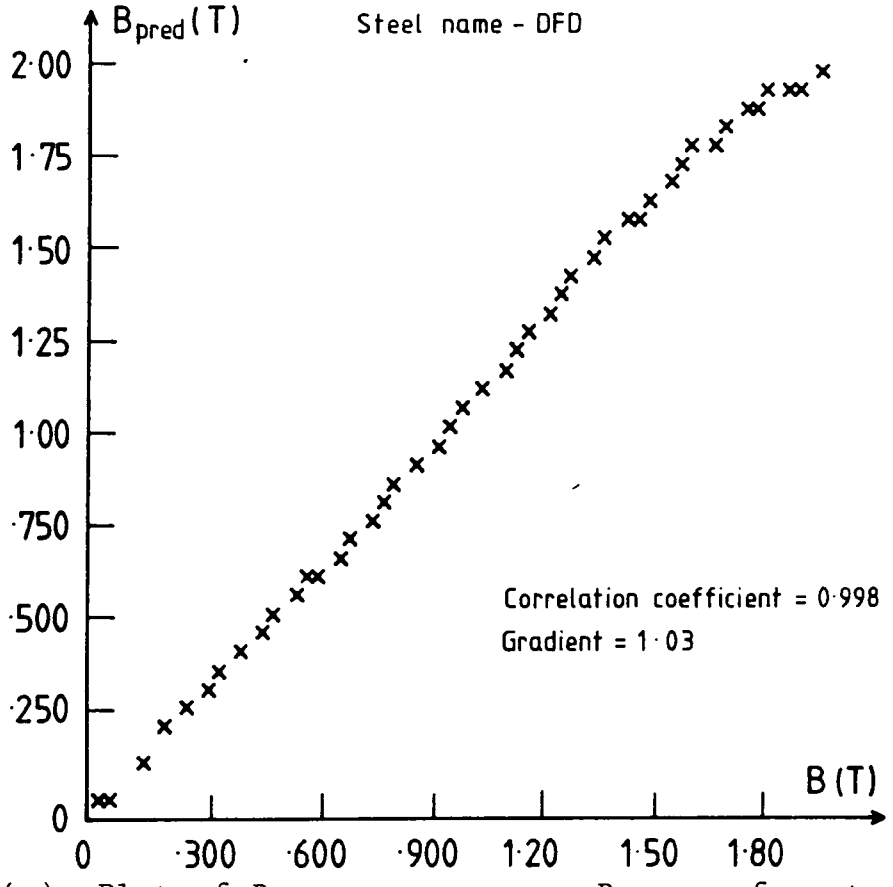

(a) Plot of $B_{predicted}$ versus B_{actual} for steel DFD. $B_{predicted}$ values calculated from values of k and LnA deduced from a knowledge of the coercive field.

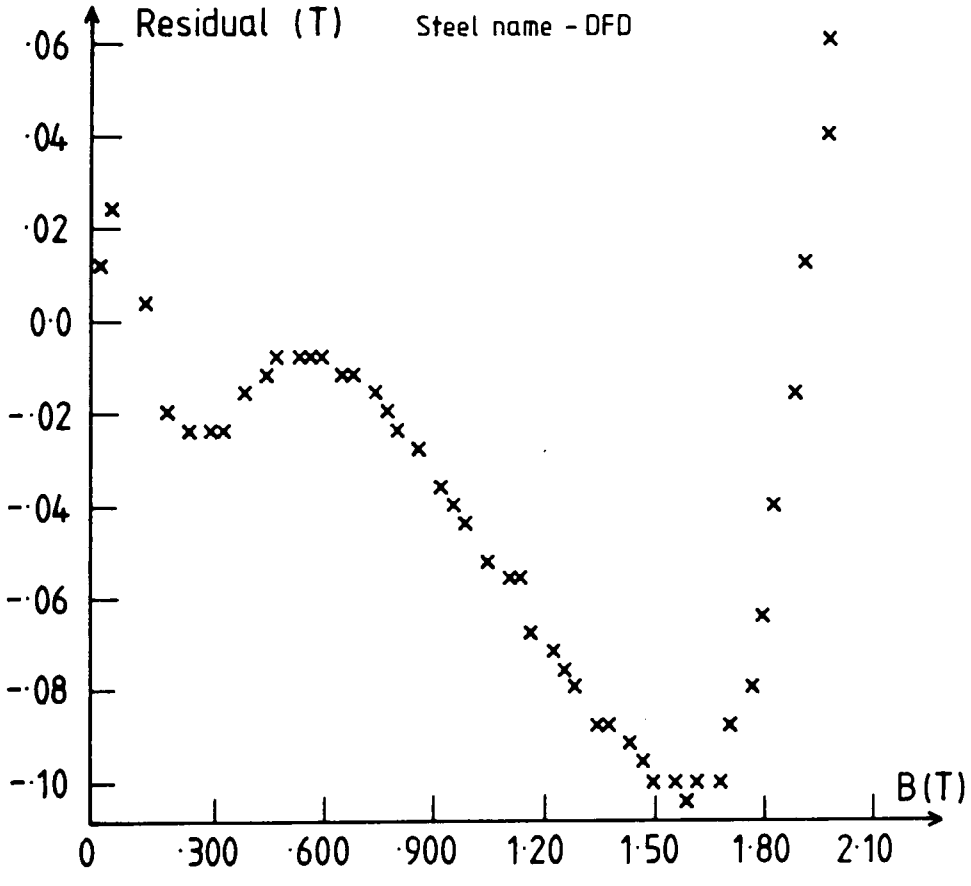

(b) Residual plot for DFD calculated from results presented in (a).

Figure 6.6

The conclusions which can be drawn from this study are, therefore, that, for the purposes of modelling the behaviour of the intelligent PIG, the initial magnetization characteristics of both normal and heat-treated pipe-steels may be predicted with reasonable precision from a knowledge of the coercive field of the material, thus confirming the postulate of section 6.2(ii). The results presented here suggest, for values of induction less than 1.85T, that the error between predicted and measured curves will be below 6%, with the largest deviations occurring at 1.5T. The coercive field may be determined to high precision from small steel samples by using the VSM and, by adopting this approach, the magnetic properties of both previously unstudied steel types, for which large sample quantities are unavailable, and the heat-affected regions around weld sites may be determined.

6.3 FURTHER CORRELATION WORK

6.3(i) Chemical analysis results

The chemical analysis (steel chemistry) of all steel types was obtained by spark emission spectroscopy to a precision of better than $\pm$ 0.03% (see Appendix D), and a visual inspection of this data confirmed the expectation that the semi-killed steels would have low Mn and Si content compared to fully-killed and controlled rolled steels (see Chapter 1). Scatter plots between these parameters and the rest of the data set did not

reveal any correlations of note with any of the magnetic parameters, and only poor relationships between the Mn content and both Ultimate Tensile Stress and (Mean Ferrite Diameter)$^{-1}$ were found, viz:

$$\%Mn = 4.23 \times 10^{-3} UTS - 1.11 \qquad \text{Correlation coefficient } 0.72 \qquad (6.19)$$

$$\%Mn = 8.50(MFD)^{-1} + 0.406 \qquad \text{Correlation coefficient } 0.85 \qquad (6.20)$$

Together they represent qualitatively the refinement of ferrite grain size and the subsequent increase in strength and toughness which is achieved indirectly by additions of manganese during the killing process.

The scatter plots also revealed that, unlike the case for pure iron-carbon steels, the observed variation in carbon concentration did not account for the difference in pearlite fractions found in these pipe-steels. It is suggested that this is due to the presence of the other alloying elements, with the formation of carbides (e.g. vanadium carbonitride and niobium carbide) accounting for significant proportions of the total carbon content.

The failure to find a relationship between any single compositional parameter and the magnetic parameters prompted a wider search using linear combinations of the chemistry data. The multiple linear regression option of the BMDP package made this task more expedient and resulted in the following single relationship between the coercive field and the C and Mn content:

$$H_c = 1.186\%C + 0.237\%Mn \qquad (6.21)$$

Using this relation the coercive field (H_c) may be predicted, therefore, from steel chemistry alone. The confidence in this prediction may be seen from Figure 6.7 where the predicted and experimental values of coercive field are plotted against one another. The correlation coefficient is only 0.81 for this plot, and errors of $\pm$ 20% are found for 99% confidence limits. This, however, is extreme and the probable error in prediction for the majority of steel types will be better than $\pm$ 10%.

The final comment in this section relates to the American semi-killed steels which are found to have anomalously high Cu content and coercive field. Many authors (Kussmann and Scharnov (1929), Kneller (1962) and Dietze (1962)) have presented data on the influence of copper inclusions in both iron and steel on the coercive force, and their results suggest that the above observations must be related. No quantitative estimation of the size of such an effect, however, has been made for these steels.

6.3(ii) Mechanical Properties

Measurements of steel strength (Ultimate Tensile Stress and Yield Stress) and steel hardness (Vickers Hardness) were made on bulk specimens of pipe at the British Gas Engineering Research Station, Killingworth. Whilst toughness data for these steels, currently being measured at ERS, is as yet unavailable, the UTS results show clearly their categorization into the three main classes; semi-killed, fully-killed and controlled rolled

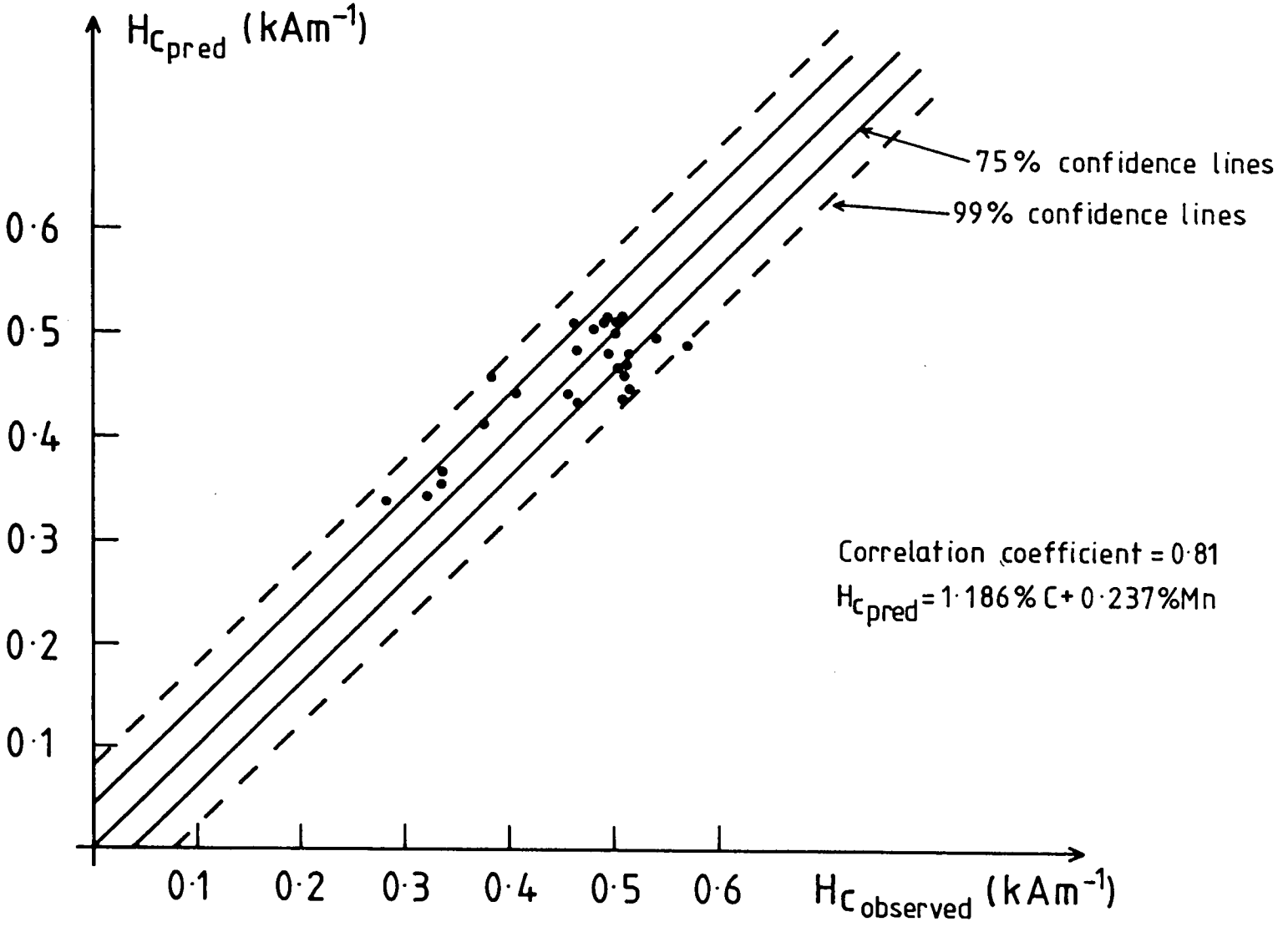

Figure 6.7 Plot of predicted coercive field values versus measured coercive field values. Predicted values calculated from a knowledge of %C and %Mn content.

(see Figure 6.8). By referring to this diagram, it can be seen that controlled-rolled steels generally show the highest UTS, while semi-killed steels exhibit the lowest values. Further, it is seen that the American semi-killed steels also have anomalously high strength. Whereas the first finding is expected from the considerations of Chapter 1, the increased presence of copper inclusion, resulting in a greater lattice friction stress, is suggested to explain the second.

Attempted correlations between the mechanical parameters and all other data groups revealed, apart from the relation between UTS and Mn content already reported, a good correlation between VH and the coercive field which includes the heat-treated data (see Figure 6.9). We have

$$VH = 166H_c + 93 \qquad \begin{matrix}\text{Correlation coefficient} \\ 0.96\end{matrix} \qquad (6.22)$$

and, by referring to Figure 6.9, it may be seen that the normal pipe-steel data clusters about the curve defined by the heat-treated 12 inch pipe-steel results. Such a relationship between coercive field and hardness is commonly observed in low carbon - low alloy steels over the entire range of heat treatment and the measurement of coercive field is often used to assess the heat-treated quality of steel parts non-destructively (Tomilov et al. (1959)).

Inter-dependences between UTS, YS and VH were also found, which may be summarized by:

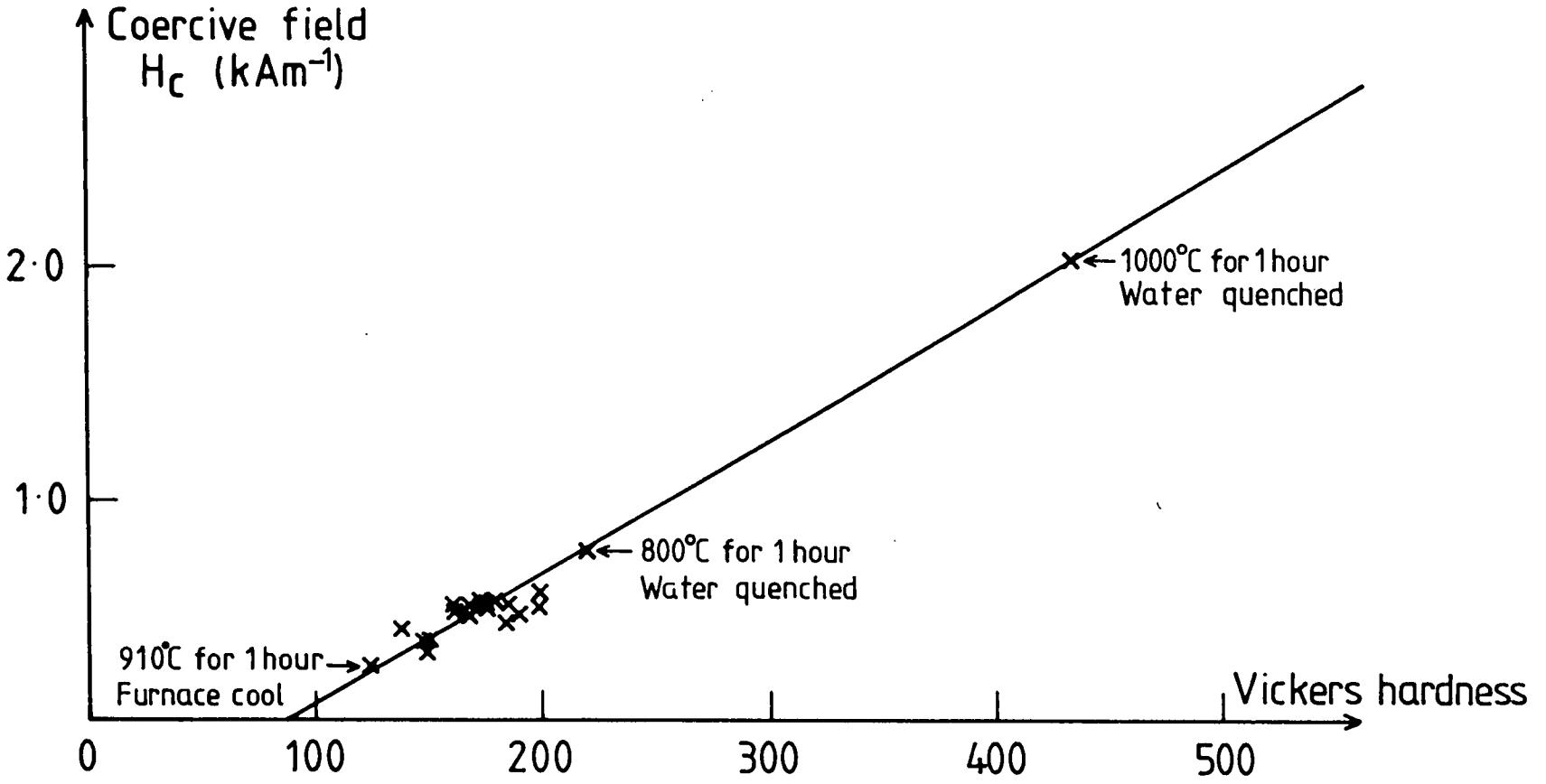

Figure 6.9 Correlation between coercive field and Vickers hardness showing clustering of normal pipe steel values around curve defined by heat treated 12 inch pipe steel values.

		Correlation coefficient	
UTS = 1.93 VH + 206		0.82	(6.23)
UTS = 0.79 YS + 211		Correlation coefficient 0.83	(6.24)

but while these results are generally of interest, no great significance is attached to them.

6.3(iii) Metallography and domain observations

The measurement of grain size and shape for both the ferrite and pearlite phase and an estimation of the relative fractions of both phases were made at Durham by my colleagues Dr. J.A. Szpunar and Mrs. J. Edwards. This work has been reported in detail elsewhere (Tanner and Corner (1985)) and, consequently, only relevant results will be referred to here.

The first correlation to be found, involving the metallography data, related the coercive field to the (mean ferrite grain diamater (d))$^{-1}$, where d is measured in μm. This relationship is illustrated in Figure 6.10 and is represented by:

		Correlation coefficient	
$H_c = 2.39d^{-1} + 0.264$		0.70	(6.25)

Whilst this relationship does not provide an excellent fit to the data, it serves as a description of the qualitative trend observed between the coercive field and d^{-1}. It is noted, however, that, if the anomalous values of the American semi-killed steels are ignored, the fit is much improved (see Figure 6.10) and becomes

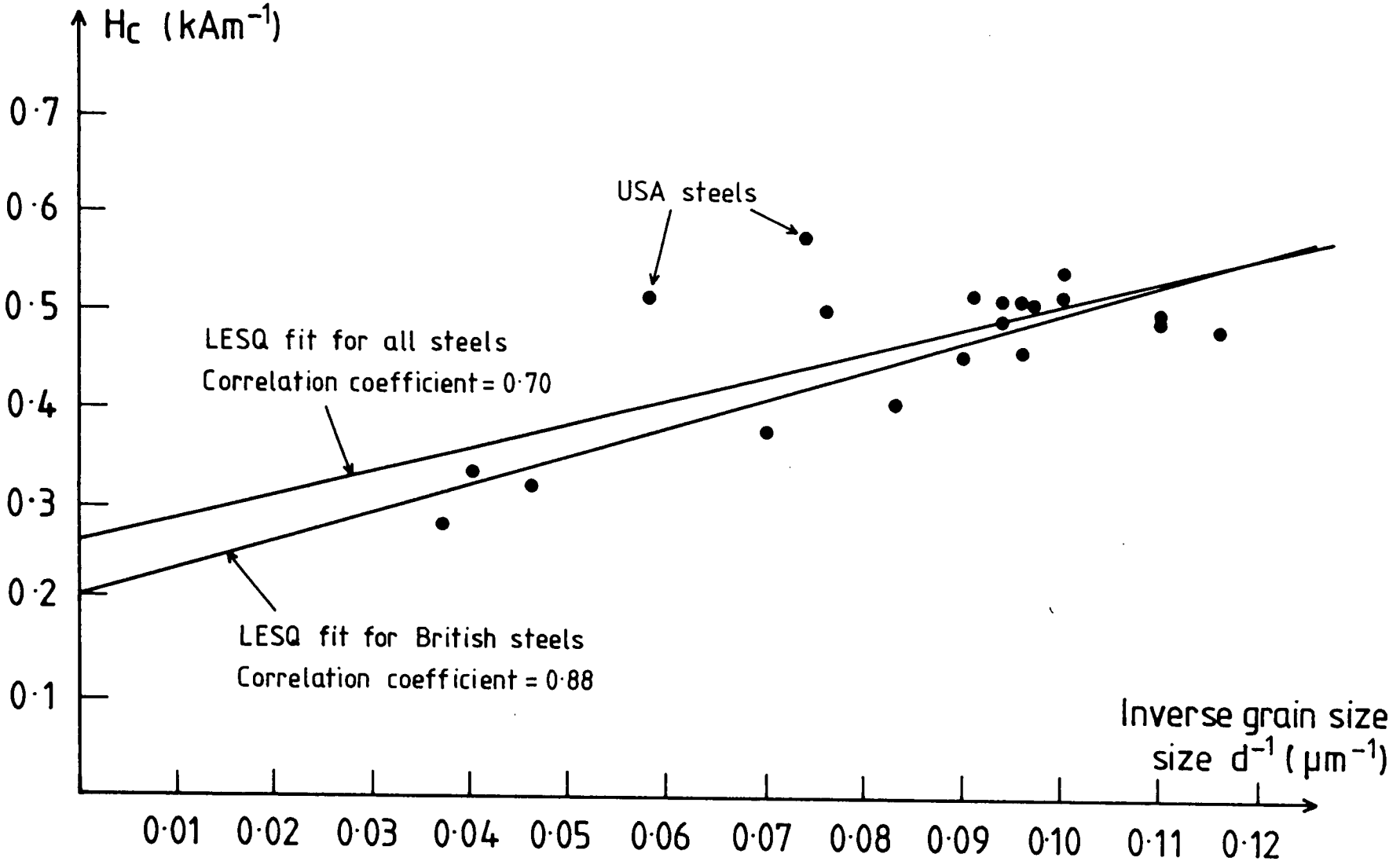

Figure 6.10 Relationship between coercive field and inverse ferrite grain size with and without USA semi-killed steels.

$$H_c = 2.88d^{-1} + 0.208 \qquad \begin{matrix}\text{Correlation coefficient}\\ 0.88\end{matrix} \qquad (6.26)$$

Relationships of the form

$$H_c = Ad^{-1} + B \qquad (6.27)$$

have been observed repeatedly for iron and steel systems (see, for example, Ruder (1934), Yensen and Ziegler (1935) and Mikheev and Gorkunov (1981)), in which the coefficients A and B are found to be non-trivial functions of the degree of alloying and the nature of the alloying elements. Several theoretical treatments (Doring (1938), Mager (1952), and Goodenough (1954)) of the portion of the coercive force dependent on the ferrite grain size also predict an inverse relationship. All authors are agreed that the delay/friction of the domain wall movement, rather than the nucleation of reverse domains, is responsible for the coercive force in iron systems, a hypothesis which is supported by subsequent observations of easy formation of reverse domains at material defects, inclusions and voids commonly found at grain boundaries (DeBlois and Bean (1959), Turner et al. (1969) and Hawkes and Corner (1985)). The approaches differ, however, when considering the mechanism of this "friction" of domain wall motion. Doring and Mager consider the conditions for irreversible growth of strongly elongated ellipsoidal reverse domain nuclei and assume that only one reverse domain is created at each grain boundary. Goodenough, however, considers the surface tension of the domain walls as the resistance to domain growth and allows for the possibility of the creation of more than one

reverse domain per grain boundary.

Table 6.4 shows a comparison of the theoretical expressions, thus obtained, for the parameter A. Here γ is the total energy of a 180^{o} domain wall per unit area, equal to 1.8×10^{-3} Jm^{-2} for iron (Kittel (1949)), and M_s is the saturation magnetization, measured to be 1.6×10^{6} Am^{-1} for pipe-steel. Using the above values, the expressions are evaluated and compared with the experimental value found by Yensen and Ziegler (1935) during their work on iron. It can be seen that the experimental result observed here for pipe-steels (see equation (6.26)) nestles within the range of predicted values and is in good agreement with the values found by Yensen and Ziegler. This suggests, therefore, that a successful qualitative description of the portion of the coercive field dependent on the ferrite grain size in these pipe-steels may be provided by the theories of Doring, Mager and Goodenough.

A further consideration of the friction of domain wall motion reveals that the initial permeability (or reversible permeability) of a material is determined by essentially the same physical conditions as the coercive force. The qualitative dependency this suggests, therefore, is the greater the friction (and hence H_c) the lower the initial permeability (μ_i). More formally we expect

$$H_c \ \mu_i = \text{constant} \qquad (6.28)$$

and such a relationship is indeed found for the range of properties exhibited by the pipe-steels. Figure

Author(s)	Theoretical expression for A	Numerical value (kAm^{-1}(μm))
Doring	$\frac{3\pi\gamma}{4M_s}$	2.12
Mager	$\frac{9\pi\gamma}{8M_s}$	3.18
Goodenough	$\frac{4\gamma}{M_s}$	3.6
Yensen and Ziegler	-	2.96 (experimental result)
Willcock	-	2.88 (experimental result)

Table 6.4 Comparison between expressions obtained both theoretically and experimentally linking the coercive field value H_c(kAm^{-1}) to the mean ferrite grain diameter d (μm)

6.11 shows this data and reveals that

$$\frac{1}{\mu_i} = 6.33H_c + 0.98 \qquad \text{Correlation coefficient } 0.76 \qquad (6.29)$$

Observations of domain wall motion with varying applied field have been made using high voltage Lorentz microscopy on thin steel sections by my colleagues Drs. B.K. Tanner and J.A. Szpunar. This work has yet to be reported in detail, but the results showed that the strongest pinning sites were in the pearlite grains and were assumed to exist at the cementite-ferrite interfaces within this phase (private communication Tanner (1985)). Weaker pinning was also observed at ferrite grain boundaries and a consideration of the number of pinning sites per unit volume within both phases led to the following relationship:

$$H_c = \frac{AC_p}{d_p} + \frac{BC_p}{d_f} \qquad (6.30)$$

where C_p, C_f are the relative proportions of the pearlite and ferrite phases, d_p, d_f are the diameters of pearlite and ferrite grains and A,B are constants.

A best fit to all the data gave

$$H_c = \frac{13.6\ C_p}{d_p} + \frac{1.7\ C_f}{d_f} \qquad (6.31)$$

and, by using this relation, the coercive field may be predicted from metallographs alone. A plot of predicted and measured values of H_c is shown in Figure 6.12 for which the correlation coefficient is 0.75. For 99% confidence it may be seen that an extreme error of

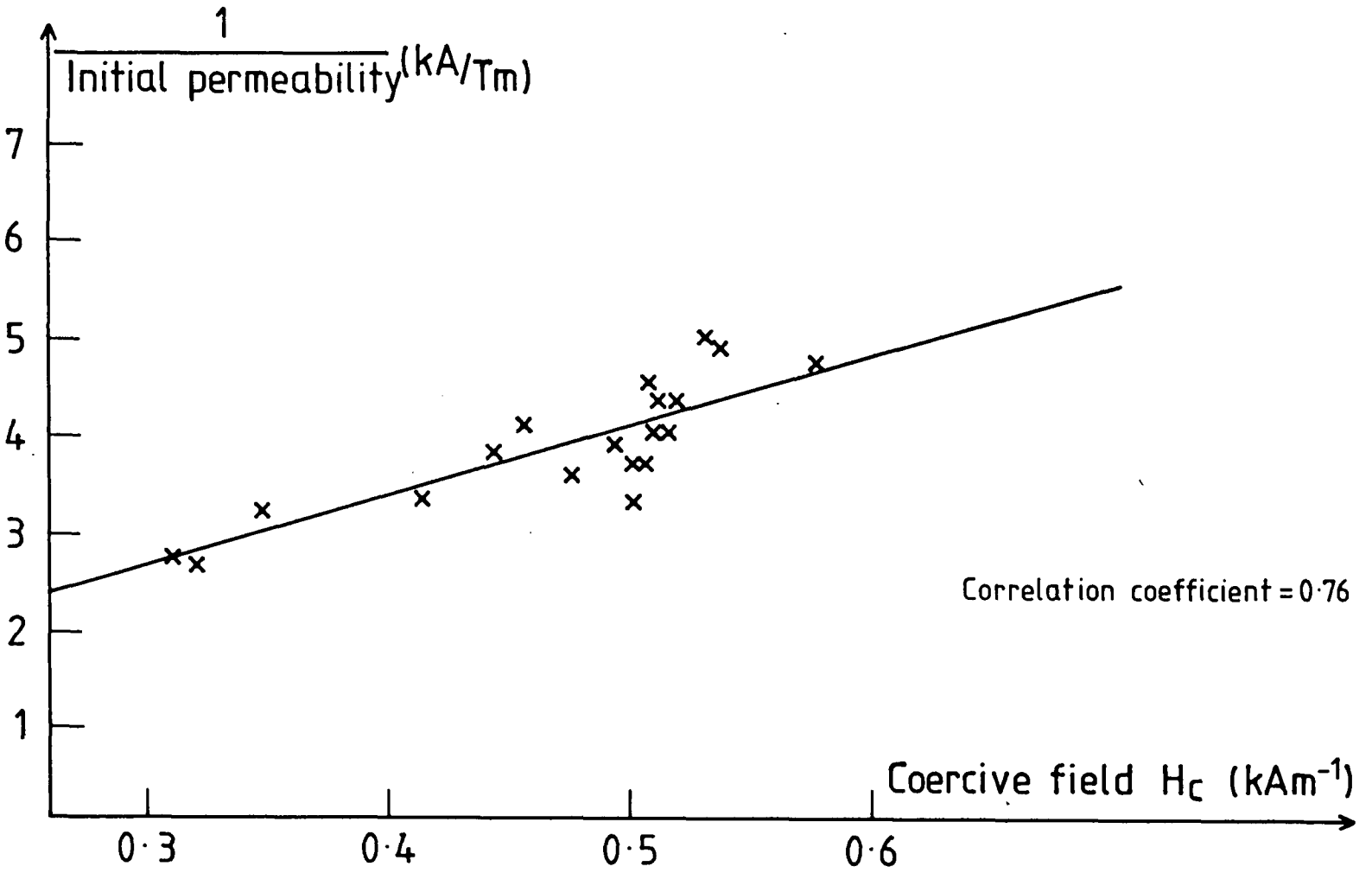

Figure 6.11 Illustration of inverse relationship between initial permeability and coercive field found for pipe steel.

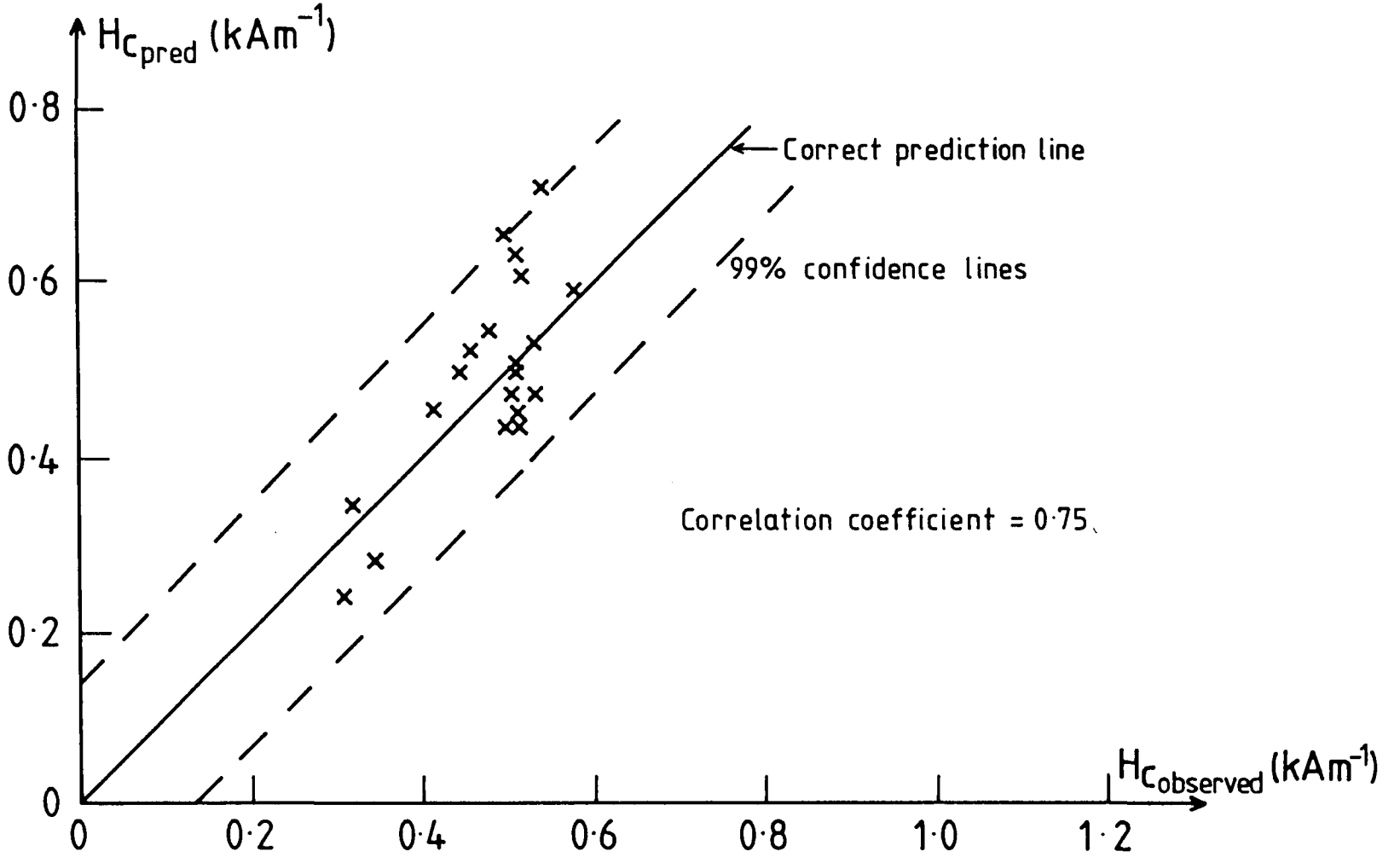

Figure 6.12 Plot of predicted coercive field values versus measured values. Predicted results obtained from knowledge of metallography (see equation (6.31)).

$\pm$ 25% is present, but the probable error in the prediction of H_c using equation (6.31) is thought to be nearer $\pm$ 15% (Tanner and Corner (1985)). A greater level of confidence is obtained, however, from an identical plot which has been calculated using only the grain dimensions perpendicular to the field direction during the measurement of H_c (see Figure 6.13). The reasons for this are not fully understood, at present, but they may be clarified by further domain observation experiments.

6.4 VARIATIONS OF MAGNETIC CHARACTERISTICS AS A FUNCTION OF ORIENTATION AND POSITION WITHINTHE PIPE-WALL

In order to obtain information on the variability of magnetic behaviour of pipe-steels as a function of orientation and position within the pipe-wall, it was decided to measure the coercive field of small steel samples taken from the relevant pipe section in the VSM, and to use the results of Section 6.2 to predict the initial magnetization curve from these measurements. Such an approach avoided the considerable problem of determining accurately the demagnetizing field for large magnetization materials, which normally requires a very high tolerance on sample geometry and a precise knowledge of demagnetizing factor if the sample is non-ellipsoidal (Bozorth and Chapin (1942)).

Calibration experiments with a polycrystalline nickel sample showed that, with care, measurements of H_c using the VSM are reliable to better than $\pm$ 0.08 kAm^{-1}, and a detailed study of the coercive field of three

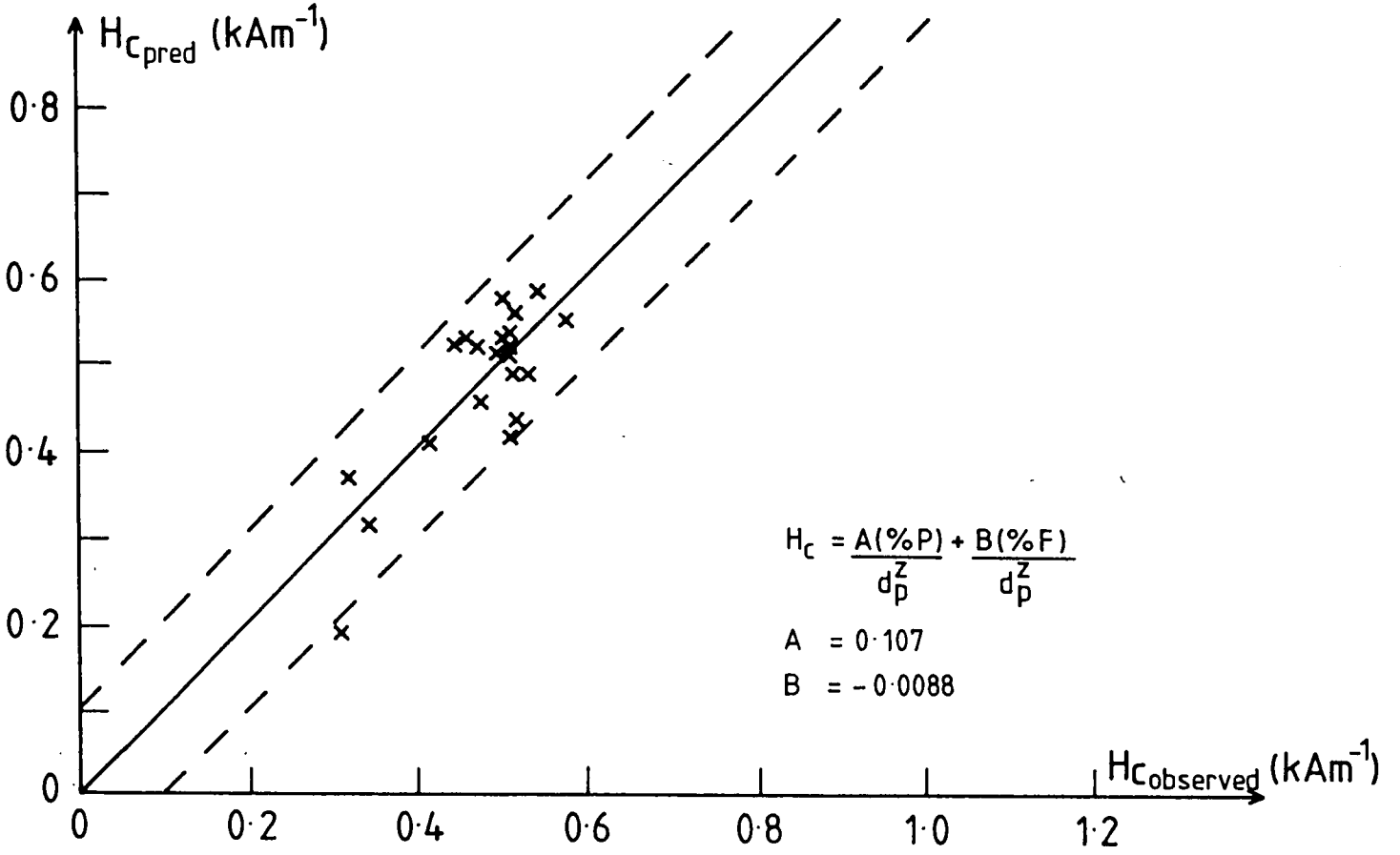

Figure 6.13 Improved plot of predicted coercive field values versus measured values. Predicted results obtained from a knowledge of metallographic parameters in a direction transverse to magnetization direction.

steels was subsequently undertaken. The three steels (DHP, DFD and 017) were selected as being typical of the steel type (semi-killed, fully-killed and controlled-rolled) and disc specimens, nominally 4,5 mm diameter and 1 mm thick, were prepared from bulk sections by machining and grinding. Great care was taken to ensure minimal specimen heating during both operations, which were performed in the presence of copious amounts of coolant. The selection of a mechanical preparative technique in preference to spark cutting, for example, was made after Jansen and Zeedijk had shown that less material damage (dislocations etc.) was observed in similar steels using the former method (Jansen and Zeedijk (1972)).

Five specimens were cut through the thickness of each bulk sample, as indicated in Figure 6.14, and the steel rolling directions was marked on every one. Measurements made as a function of position within the pipe wall were all conducted with the field direction parallel to the rolling direction. Those made as a function of angle with respect to the rolling direction were conducted on the middle specimen.

In addition to the magnetic measurements, metallographic analyses were performed through the pipe wall for the three steels. A 13 mm by 9 mm surface, perpendicular to the pipe surface, was prepared for this study by mechanically polishing down to a 0.25 μm diamond paste and then etching the grain boundaries with nital (0.2%

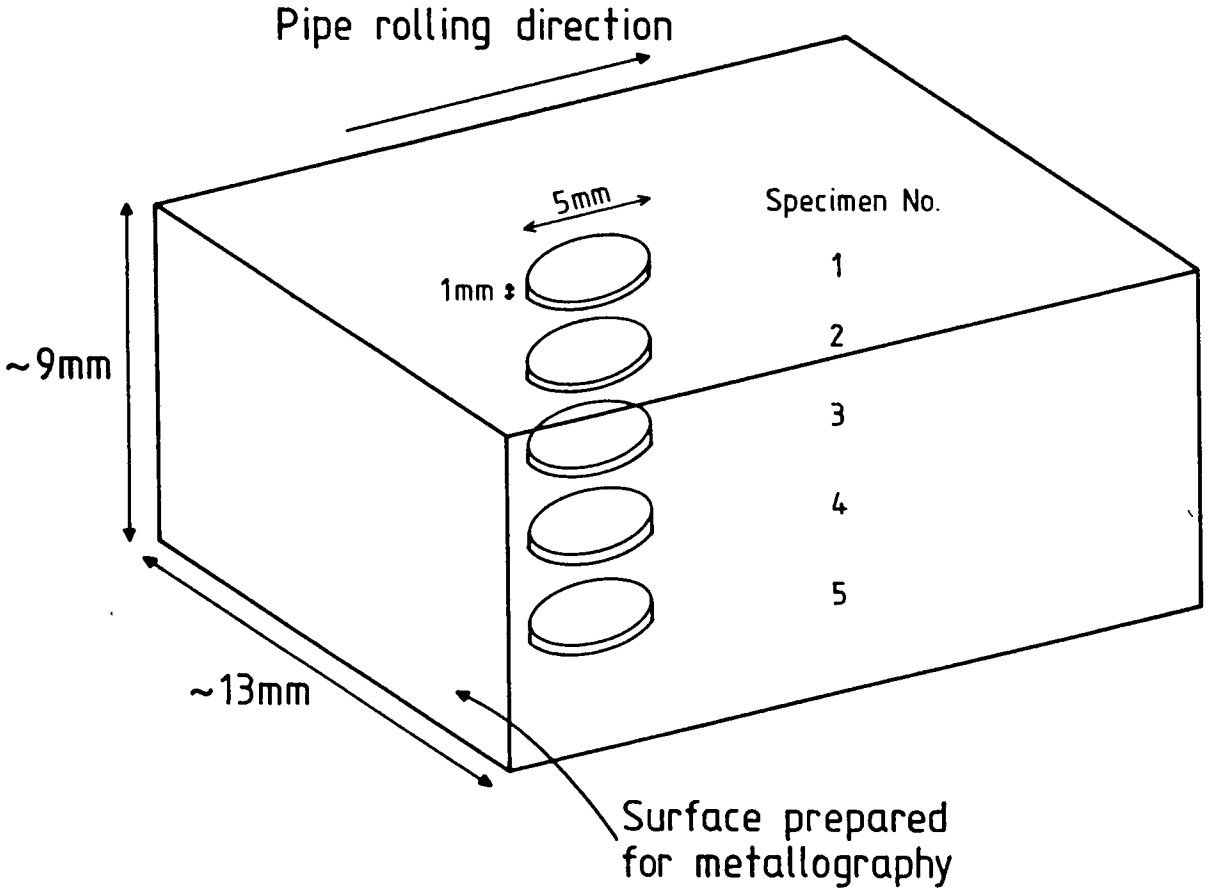

Figure 6.14 Illustration of position of the through wall thickness specimens within the pipe wall.

solution of nitric acid in ethanol). Metallographs were recorded in 1 mm intervals along five rows, corresponding to the different depths through the pipe wall from which the above specimens had been taken, and, in order to obtain statistically sound results, approximately 1800 ferrite and 950 pearlite grains were counted and measured along each row. Vickers hardness measurements were also made along these same rows for one of the steels (DHP).

The results obtained from these studies on DHP, 017 and DFD are shown in Tables 6.5, 6.6 and 6.7 respectively. By referring to Table 6.5 it can be seen that the coercive field of DHP decreases to a minimum at the middle of the pipe wall, with a variation of 13.5% between surface and centre, and a similar increase of 10.7% is observed with respect to angle from the rolling direction. It is noted that the mean ferrite diameter shows clearly the opposite trends, while there is no such trend for the pearlite diameter. The hardness measurements also are seen to vary by 10.8%,with a minimum value at the middle of the pipe wall.

Using the relationships observed between H_c and both (mean ferrite diameter)$^{-1}$ and Vickers Hardness (equations (6.26) and (6.22) respectively), values of coercive field may be predicted from the grain size and hardness measurements. These results are also shown in Table 6.5 where it is seen that reasonable agreement is obtained between the measured values of H_c and those derived from a knowledge of the ferrite grain size,

Specimen/ Row number	Measured H_c (kAm^{-1})	Mean ferrite diameter (μm)	Mean pearlite diameter (μm)	Vickers Hardness	Predicted values (see text) From d^{-1}	From VH
1	0.366	21.8	10.25	154 ± 4	0.340	0.367
2	0.348	24.0	11.2	146 ± 2	-	-
3	0.322	25.5	10.9	139 ± 1	0.321	0.277
4	0.332	23.7	11.6	148 ± 2	-	-
5	0.344	22.25	10.25	155 ± 2	-	-
Average value of H_c = 0.343 kAm^{-1} Bulk measured value = 0.349 kAm^{-1}						
0°	0.322	25.5	10.9	-	0.321	-
45°	0.355	-	-	-	-	-
90°	0.361	19.7	7.5	-	0.354	-

Table 6.5

Through-Wall and Anisotropy data for DHP (semi-killed)

Specimen/ Row number	Measured H_c (kAm^{-1})	Mean ferrite diameter (μm)	Mean pearlite diameter (μm)	Predicted value (see text)
1	0.470	8.5	8.6	0.547
2	0.438	8.8	8.1	-
3	0.474	8.7	8.2	-
4	0.430	9.7	8.5	0.504
5	0.473	9.1	8.1	-
Average value of H_c = 0.457 kAm^{-1} Bulk measured value = 0.479 kAm^{-1}				
0^o	0.474	8.7	8.2	0.539
45^o	0.585	-	-	-
90^o	0.759	7.2	4.8	0.610

Table 6.6

Through-Wall and Anisotropy data for 017 (controlled-rolled)

Specimen/ Row number	Measured H_c (kAm^{-1})	Mean ferrite diameter (μm)	Mean pearlite diameter (μm)	Predicted value (see text)
1	0.488	9.9	12.5	0.385
2	0.496	10.6	10.1	-
3	0.522	11.2	9.1	-
4	0.532	11.6	8.6	-
5	0.535	12.1	8.0	0.397
Average value of H_c = 0.515 kAm^{-1}		Bulk measured value= 0.507 kAm^{-1}		
0^o	0.522	11.2	9.1	0.392
45^o	0.597	-	-	-
90^o	0.672	8.3	5.2	0.589

Table 6.7

Through-Wall and Anisotropy data for DFD (fully-killed)

but that predictions based on hardness measurements are not as reliable. Both sets of data, however, do indicate qualitatively the observed trends in the coercive field measurements.

Tables 6.6 and 6.7 show similar results for 017 and DFD but, while similar arguments to the above may be used to describe the trends observed for 017, this is not the case for DFD. Here it is seen that a systematic increase of 9.6% in the coercive field is accompanied by a similar increase of 22% in ferrite grain size and a decrease of 36% in pearlite grain size. The contribution to the coercive field from the pearlite phase cannot be ignored for this steel and the result indicated by equation (6.31) is invoked to provide a qualitative prediction of the observed trend. The observed anisotropy of the coercive field with respect to the rolling direction is much increased for these steels (60% and 29% variations for 017 and DFD respectively) and is not well fitted by variations in ferrite and pearlite grain sizes or the ferrite grain size alone. The interpretation of this data, therefore, is not clear at the present time, although it has been suggested (Tanner and Corner (1985)) that anisotropy of the cementite and ferrite-pearlite grain boundary pinning sites may be responsible for this. Further observations of domain wall motion in these steels, however, are required to verify this.

It is noted that the average values of coercive field for the five specimens of each steel agree well with the value obtained from the permeametry of bulk

samples. Although the VSM measures the field at which the magnetization is reduced to zero, compared to the yoke permeameter which defines H_c as the field at which the total induction is nulled, good agreement is expected between the two independent measurements because the low coercive field values and the large differential permeability ($\sim$ 8000) of these steels in this field region produces a theoretical difference of less than 0.01 kAm^{-1} between the two results.

In terms of the relevance to the modelling of the behaviour of the intelligent PIG within such pipe-steels the values of coercive field may be used to reconstruct the initial magnetization curve for the five regions within the pipe-wall thickness by using the results of section 6.2. These may then be input to the computer package (PE2D) to provide a more accurate representation of the pipe material's characteristics. By way of example, Figure 6.15 shows the range of behavioural differences predicted by the results obtained for DHP. The two curves presented here are for the surface and middle regions of the pipe wall and they reveal a 10.8% increase in the value of maximum permeability (μ_m) and a corresponding 11.6% decrease in the field value at which maximum permeability ($H_{\mu m}$) is observed. These values could have been determined directly from the relationships revealed in Section 6.2 but, for the purposes of computer modelling, the complete characteristic is required.

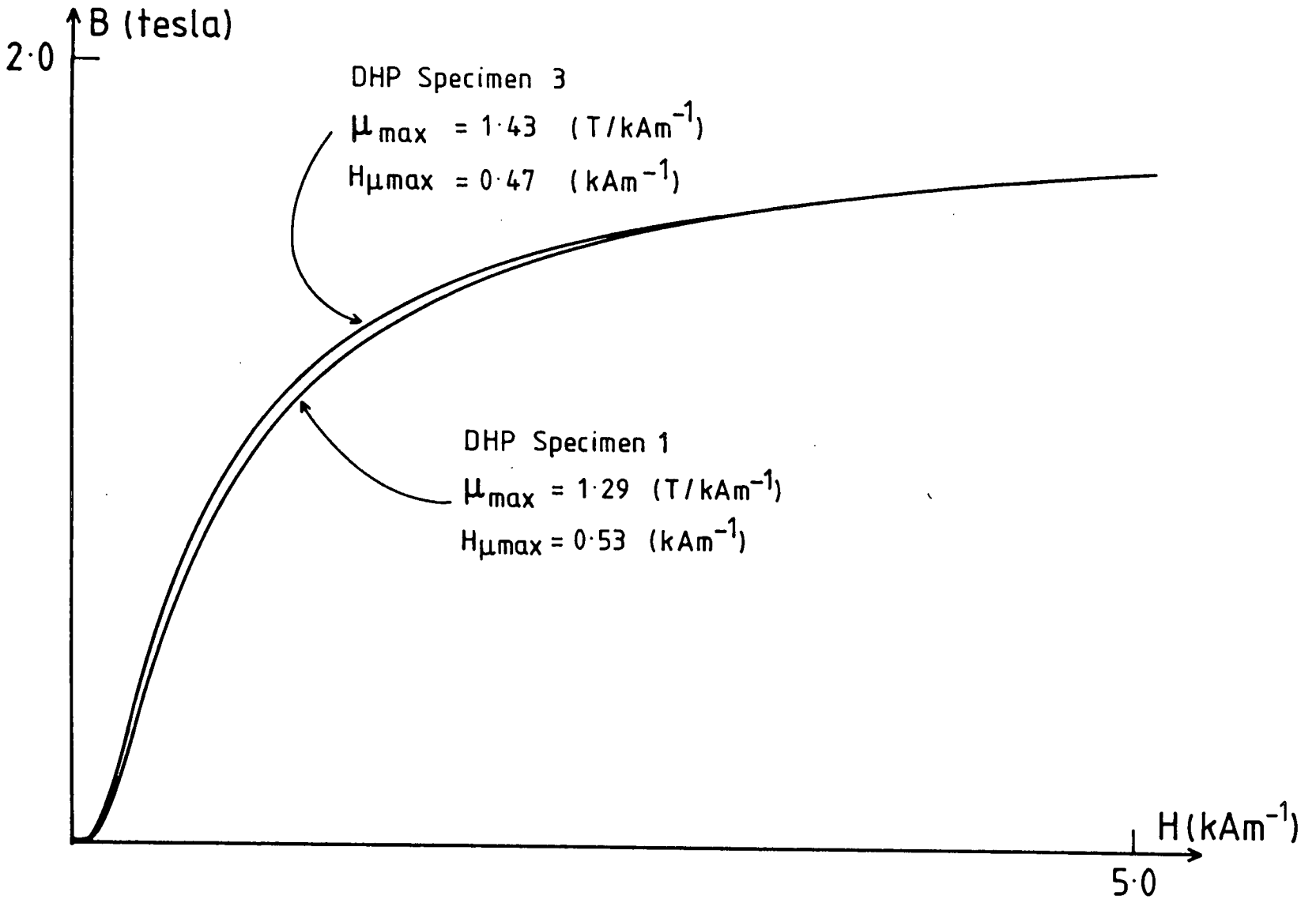

Figure 6.15 Illustration of the range of magnetic characteristics found for through wall thickness specimens of DHP.

CHAPTER 7

SUGGESTIONS FOR FURTHER WORK

Despite the very substantial body of data collected by the Durham research team over the 3 years of the contract with British Gas, there are inevitably many areas which have not been studied in sufficient detail and some areas which have not been studied at all. The results presented in this thesis have highlighted a few of these and they are referred to below as suggestions for further work.

The original objectives of the research contract included the determination of the variations of both magnetic properties and metallography of pipesteels between pipe lengths from different batches. To date, little data has been collected which would reveal such differences and the continuing categorization of these parameters is suggested, therefore, in order to achieve this. Whilst the determination of the magnetic properties requires little manpower investment, the time required to prepare and measure the metallographs is considerable. An investigation into the feasibility of automatic scanning of metallographs would, therefore, be worthwhile.

It has been shown here that predictions of the magnetic properties of both normal and heat-treated pipe-steels may be made to a reasonable tolerance from measurements of the coercive field. This permits the determination of the characteristics in the heat-affected zone near weld sites but does not allow the prediction

of the properties of the weld material. If, however, similar relationships between the parameters required to model the initial magnetization curves of weld material and other parameters, which are easily measurable using small samples, are found, such predictions will be possible. This will require the complete categorization of the properties of weld materials similar to that described here for pipe-steels and, in order to determine accurately the magnetic characteristics of the materials, a permeameter, designed for use with small samples, must be constructed.

Further investigations are also suggested into the various models for the coercive field in these pipe-steels. The initial results presented here indicate a grain size dependent term which is consistent with the theories of Doring (1938), Mager (1952) and Goodenough (1954), but verification of this can be obtained by conducting measurements of coercive field as a function of temperature (Goodenough (1954)). This study will also require a knowledge of the variation of the effective anisotropy and the saturation magnetization of the material as a function of temperature, and a torque magnetometer capable of measurements at both reduced and elevated temperatures will be required.

Magnetic anisotropy measurements made at room temperature, however, will also yield useful data, as suggested by the measurements of coercive field as a function of angle. These results, combined with measurements of steel texture and further observations of domain

wall movement, including an investigation into the possible anisotropy of cementite orientation within the pearlite phase, would help to clarify the anisotropy of magnetic behaviour reported here.

A much more ambitious project would involve an investigation into the effect of the alloying elements present in these steels on the magnetic properties, and the coercive field in particular. This would involve a considerable investment of time and equipment in order to study the behavioural changes to the steel as the inclusion content is increased, but evidence suggests (Yensen and Ziegler (1935)) that the results obtained from this work, although complex in nature, will give invaluable information on the grain size independent term to the coercive field (Goodenough (1954)).

APPENDIX A

Listing of Digitizer and Analysis program

This appendix contains a listing of the program which digitizes a pre-recorded B-H loop and conducts a Fourier analysis of the resulting data. It is written in PET Basic and contains commands for a two channel DAC board (addresses 18 and 19) and an ADC board (address 9) on MINICAM. These are used to provide signals to control the X and Y movement of the plotter's pen carriage and measure the response of the light pen respectively.

```
 1 poke1,0:poke2,148:a%=1:n%=1:t%=1
 2 open4,4,0:print#4,chr$(27);chr$(96);chr$(27);chr$(80);
 3 print#4,chr$(27);chr$(48);chr$(00);
 4 print#4,"                  ";chr$(27);chr$(09)
 5 print#4,"                                                  ";
 6 print#4,"                                                  ";chr$(27);ch
r$(00)
 12 k=1:h=0:p=0:q=0
 13 dimy(300),z(300),b(300)
 15 a%=19:n%=k-1:a=usr(4)
 16 a%=18:n%=p:a=usr(4)
 18 print"S"
 19 print"■■■■■□□□□□hit any key to continue"
 20 geta$: ifa$=""then20
 30 a%=18:n%=p:a=usr(4)
 31 a%=19:n%=k:a=usr(4)
 32 b=ti
 33 ifti-b<100then33
 35 a%=9:x=usr(5):printx;
 40 a%=19:n%=k:a=usr(4)
 50 a%=9:y=usr(5):printy
 55 ifk>800then150
 60 ify<650then100
 66 k=k+1
 70 goto35
 100 print"x="p;"t="p;"y="k
 106 q=p
 107 t=(q+10)/10
 108 y(t)=k
 109 z(t)=p
 120 p=p+10:k=k-15
 130 goto30
 150 k=k-200:h=h+1:ifh=1     goto40
 160 k=k+200:p=p-10:q=p+10
 170 a%=18:n%=p:a=usr(4)
 171 a%=19:n%=k:a=usr(4)
 172 b=ti
 173 ifti-b<100then173
 180 a%=9:x=usr(5):printx;
 190 a%=19:n%=k:a=usr(4)
 200 a%=9:y=usr(5):printy
 210 ifk=0then300
 220 ify<650then250
 230 k=k-1
 240 goto180
 250 print"x="p;"t="q;"y="k
 256 t=(q+10)/10
 257 y(t)=k
 258 z(t)=p
 265 ifp=0then310
 270 p=p-10:q=q+10:k=k+15
 290 goto170
```

```
 300 k=k+800:h=h+1:p=p-10:ifh=3then170
 310 k=0
 320 fori=2to300
 330 b=z(i):a=z(i-1)
 340 ifa=bthen360
 350 nexti
 360 a=(a+10)/10
 370 b=y(a)-y(1):a=z(a)-z(1)
 380 b=b/2:a=a/2
 390 fori=2to300
 400 c=i-1
 410 ify(i)=0then425
 420 nexti
 425 d=y(1)
 430 forj=1toc
 440 y(j)=y(j)-d-b:z(j)=z(j)-z(1)-a
 450 nextj
 460 d=c+1
 470 fori=dto300
 480 y(i)=y(i-c):z(i)=z(i-c)
 490 nexti
 500 fori=1to300
 510 b(i)=y(i)*350/y(a)
 520 nexti
 1035 f=0:x=0:d=0:e=0:a=0
 1040 print"□□□□□fourier analysis starting"
 1050 fori=1to300
 1070 g=f
 1080 ifi=1then1140
 1090 j=i-1
 1100 v=z(i):c=z(j)
 1110 d=sgn(v):e=sgn(c)
 1120 ife=0then1150
 1130 ifd>ethen print"the plot of h against t crosses h=0 at i=";
i:f=i:x=x+1
 1140 ifx=2then1155
 1150 nexti
 1155 t=1000:goto1180
 1160 print"type in the time period(t)"
 1170 inputt
 1180 r=t/(f-g)
 1190 print"the time interval(r)between samples of the flux densi
ty b=";r
 1200 y=f+1-g
 1210 dimc(y),s(y),m(y),n(y),q(y),p(10),r(y),u(10),a(10),pha(10)
 1220 forn=1to10
 1230 fork=1toy
 1240 c(k)=cos(2*n*(k-1)*r*↑/t)
 1250 s(k)=sin(2*n*(k-1)*r*↑/t)
 1255 h=g-1+k
 1260 n(k)=s(k)*b(h)
 1270 m(k)=c(k)*b(h)
 1290 nextk
 1300 m(1)=m(1)/2:m(y)=m(y)/2
```

```
 1310 n(1)=n(1)/2:n(y)=n(y)/2
 1320 for l=1toy
 1321 if l>1goto1325
 1322 q(l)=m(l)
 1323 r(l)=n(l)
 1324 goto1350
 1325 a=l-1
 1330 q(l)=q(a)+m(l)
 1340 r(l)=r(a)+n(l)
 1350 next l
 1360 p(n)=r*q(y)*2/t
 1370 u(n)=r*r(y)*2/t
 1380 a(n)=sqr(p(n)^2+u(n)^2)
 1390 ifp(n)<>0then1430
 1400 ifp(n)=0thenprint"even amplitude=0 for n=";n
 1410 pha(n)=†/2
 1420 goto1440
 1430 pha(n)=atn(u(n)/p(n))
 1440 nextn
 1450 print"fourier coeff.a(n)    phase angles"
 1460 fork=1to10
 1470 printa(k);"         ";pha(k)
 1480 nextk
 1510 print#4,"      ";chr$(27);chr$(01);"SIN COEFF U(N)    ";chr$
(27);chr$(01);
 1511 print#4,"COS COEFF P(N)    ";chr$(27);chr$(01);"TOTAL COEFF
 A(N)"
 1512 fori=1to10:a=u(i):b=p(i):c=a(i)
 1513 print#4,chr$(09);a;chr$(09);b;chr$(09);c
 1514 nexti
 1515 z=z+1
 1516 ifz=2then1550
 1519 print#4,"                        NORMALISED  COEFFICIENTS"
 1520 c=a(1)
 1530 fori=1to10:u(i)=u(i)*100/c:p(i)=p(i)*100/c:a(i)=a(i)*100/c:
nexti
 1540 z=1:goto1512
 1550 end
```

APPENDIX B

Listing of BHLOOP.BAS program

This appendix contains a listing of the program written for the MINC mini-computer to conduct a full magnetization loop study using the peripheral equipment described in Chapter 3.

```
 10 common m%,x(100),y(100),c%(100)
 20 common d7$,a$,x$,y$,s$,s
 25 b$=chr$(7)+chr$(7)+chr$(7)+chr$(7)+chr$(7)
 30 dim r(1),d$(15)
 35 dim b(100),b0(100),b1(100),h(100),h0(100),h1(100)
 36 dim p%(100)
 40 aout(,0)
 70 c%(0)=18 ! rem gaussmeter input channel
 80 c%(1)=16 ! rem integrator input channel
 90 m%=1 ! rem fields evaluated over m%+1/2 cycles
 100 m1%=50 ! rem no of samples at each maximum field
 102 aout(,0,,,0)
 103 print b$,"switch power supply on now"
 105 print "width & thickness of bar cms." ! input l1,l2
 110 t=l1*l2/10000*2*10*99.6 ! rem 2*bar area*no of turns*gain of
 111 rem  integrating amplifier
 115 p7%=1
 120 k=.04 ! rem min b step
 125 k1=1.00000e-03 ! rem max difference in b values for cyclic s
tate
 130 print"check integrating amplifier":
 140 input q$
 150 if q$<>"y" go to 200
 160 set-gain(,4,c%(1))
 165 display-clear
 170 for n=0 to 500
 180 ain('d',r,,,c%(1))
 190 next n
 192 get-char(a$)
 194 if a$="" then 165
 200 display-clear
 220 aout(,0,,,0)
 230 set-gain('r',0,c%(0),2)
 240 wide-line('w',12)
 250 htext('u',12,10,"reset integrating amplifier")
 251 print" gaussmeter scale",
 260 input g% ! g=g%
 270 if int((g%)/3)*3=g% then g=g%/3*sqr(10)
 280 print"maximun current , no of points per quadrant"
 290 input p%,i0%
 300 s%=p%/100
 310 print"max. cur","step","inc"," h "," b "
 320 n%=0
 330 h(0)=0 ! b(0)=0
 340 x(n%)=0 ! y(n%)=0
 345 b1(k%)=0
 350 for n=0 to 2*m%
 370 p7%=-p7%
 380 a%=0 ! b%=p7%*p% ! c%=abs(s%) ! k%=0 ! gosub 6000
 390 gosub 6200
 400 a%=p7%*p% ! b%=0 ! c%=abs(s%)
 410 gosub 6000
```

```
 620 next n
 630 x(n%)=h(k%)/2/m%*g*.04 § y(n%)=b(k%)/m%/2/t
 640 print p%,s%,e%,x(n%),y(n%)
 650 if h(k%)/4/m%<1.3 go to 680 § print"gaussmeter overflow"
 651 print"new gaussmeter scale";
 655 pause(2) § print b$
 660 input g% § g=g%
 670 if int((g%)/3)*3=g% then g=g%/3*sqr(10)
 675 go to 330
 680 if abs(y(n%)+z)<k1 then 700
 690 z=y(n%) § z1=x(n%) § go to 330
 700 y(n%)=abs((y(n%)-z)/2)
 710 x(n%)=abs((x(n%)-z1)/2)
 760 rem
 770 rem          recoil curve
 780 rem
 800 for i%=0 to i0%
 805 i=i% § p=p% § i0=i0%
 806 p1=i*p/i0
 810 p%(i%)=p1 § p%(2*i0%-i%)=p1
 820 next i%
 830 for i%=0 to 2*i0% § b(i%)=0 § b1(i%)=0 § h(i%)=0 § h1(i%)=0
§ next i%
 835 if p7%>0 go to 840
 836 a%=0 § b%=p% § c%=s% § gosub 6000 § pause(2)
 837 a%=p% § b%=0 § c%=s% § gosub 6000
 840 pause(2)
 850 for k%=0 to 2*i0%-1
 855 p%(k%)=-p%(k%)
 860 for n=0 to 2*m%
 865 p%(k%)=-p%(k%) § p%(k%+1)=-p%(k%+1)
 868 print p%(k%)
 870 a%=p%(k%) § b%=p%(k%+1) § c%=s%
 880 gosub 6000
 890 gosub 6200
 900 pause(0.5)
 902 if n=2 go to 910
 905 gosub 6500
 910 next n
 915 pause(.5)
 920 next k%
 930 for k%=0 to 2*i0%-1
 940 x(k%)=h(k%)/2/m%*g*.04 § y(k%)=b(k%)/m%/2/t
 950 next k%
 955 if x(i0%)>0 go to 975
 960 for n=0 to 2*i0%-1 § x(n)=-x(n) § next n
 975 if y(i0%)>0 go to 1000
 980 for n=0 to 2*i0%-1 § y(n)=-y(n) § next n
1000 aout(,0,,,0)
1010 print b$ § pause(2) § print b$
1020 graph-init
1025 text-init
1030 window(,-1,-1,x(i0%),2.2,0)
1040 graph('-g',i0%,x(0),y(0),,,1)
```

```
 1045 graph('-g',i0%,x(i0%),y(i0%),,,2)
 3000 rem beginning of print on lp:
 3005 n%=2*i0%
 3010 print"print file":
 3020 input q2$ ⧵ if seg$(q2$,1,1)<>"y" go to 5000
 3030 open "lp:" for output as file #1
 3040 print #1:
 3050 print #1:,,,"b-h data",dat$,clk$
 3060 print #1:
 3070 print #1:
 3080 print #1:,"gaussmeter scale ",g%;" gauss"
 3090 print #1:
 3100 print #1:,,"  h kA/m"," b tesla","  Mu"," Mu diff"
 3110 print #1:,0,x(0),y(0),y(0)/x(0)*.08
 3120 for o=1 to n%-2
 3130 print #1:,o,x(o),y(o),y(o)/x(o)*.08,(y(o+1)-y(o-1))/(x(o+1)
-x(o-1))*.08
 3140 next o
 3150 print #1:,n%-1,x(n%-1),y(n%-1),y(n%-1)/x(n%-1)*.08
 3160 close #1
 5000 rem beginning of save on disc
 5010 print" save file ":
 5020 input q1$
 5030 if seg$(q1$,1,1)<>"y" then 5140
 5040 print" file name ":
 5050 input f$
 5060 print" title":
 5070 linput t$
 5080 open f$ for output as file #2
 5090 print #2,t$
 5100 for n=0 to n%-1
 5110 print #2,using "######.####'###.####",x(n)*1000;",";y(n)
 5120 next n
 5130 close #2
 5140 go to 10000
 6000 rem current output routine
 6005 if a%>b% then c%=-c%
 6010 for i%=a% to b% step c%
 6030 if i%>2048 then print b$,,"current too large" ⧵ go to 6090
 6070 aout(,i%,,,0)
 6080 next i%
 6090 return
 6200 rem input routine
 6205 r0=0 ⧵ r1=0
 6210 pause(1)
 6220 for j%=1 to m1%
 6230 ain('r',r(),2,,c%(0),2)
 6240 r0=r(0)+r0 ⧵ r1=r(1)+r1
 6250 next j%
 6290 h0(k%)=r0/m1% ⧵ b0(k%)=r1/m1%
 6300 if b1(k%)=0 then 6350
 6310 h(k%)=(h0(k%)-h1(k%))-h(k%)
 6320 b(k%)=(b0(k%)-b1(k%))-b(k%)
 6350 h1(k%)=h0(k%) ⧵ b1(k%)=b0(k%)
```

```
6360 return
6500 rem advance halfway round loop
6510 if k%>=(i0%-1) go to 6590
6520 if n=1 go to 6560
6530 b%=-p% \ a%=p%(k%+1)
6540 go to 6570
6560 b%=p% \ a%=p%(k%+1)
6570 c%=s%
6580 gosub 6000 \ pause(.5)
6590 if k%>=i0% go to 6606
6600 if n=1 go to 6602
6601 a%=-p% \ goto 6603
6602 a%=p%
6603 b%=0 \ c%=s%
6604 gosub 6000 \ pause(.5)
6605 go to 6721
6606 a%=p%(k%+1) \ b%=0 \ c%=s%
6607 gosub 6000 \ pause(.5)
6721 if k%<=i0% go to 6735
6722 if n=1 go to 6725
6723 a%=0 \ b%=p%
6724 go to 6726
6725 a%=0 \ b%=-p%
6726 c%=s%
6727 gosub 6000 \ pause(.5)
6728 if n=1 go to 6731
6729 a%=p% \ b%=-p%(k%)
6730 go to 6732
6731 a%=-p% \ b%=-p%(k%)
6732 c%=s%
6733 gosub 6000 \ pause(.5)
6734 go to 6750
6735 a%=0 \ b%=-p%(k%)\ c%=s%
6740 gosub 6000 \ pause(0.5)
6750 return
10000 end
```

APPENDIX C

TRANSFER OF DATA BETWEEN MINC MINICOMPUTER AND PET MICROCOMPUTER

C.1 Introduction

This appendix contains a brief description and a listing of the complete suite of programs written to transfer disc based data files between a MINC minicomputer at OLIC and a CBM disc drive normally connected to a PET microcomputer at Durham. The user selects the program relevant to the particular task with the aid of a menu of options:

DIRØ - gives directory of PET disc Ø

DIR1 - gives directory of PET disc 1

LIST - allows both program and sequential (data) files on PET disc to be listed

CP2M - copies data files from PET to MINC

CM2P - copies data files from MINC to PET

QUIT - exits program suite.

Non-ambiguous abbreviations of the above commands are allowed.

The subroutine SEQ is called to list either program or sequential files stored on PET disc unless the relevant sequential file has previously been transferred from MINC to PET, in which case the subroutine SEQNEW is called. Subroutine SFTRAN transfers sequential (data) files from MINC disc to PET disc 1, while a transfer in the opposite direction calls subroutine PETCOP.

C.2 The PET address system

In order to communicate with a disc file on a CBM disc drive both a primary and a secondary address is required. The primary address is the device number which is always set equal to 8 for a CBM disc drive, but the secondary address takes on different values depending on the required operation (see Table C.1 and also Fischer and Jensen (1980) and West (1982)).

By referring to Table C.1 it can be seen that the channel no., which corresponds to the four least significant bits of the secondary address, must be equal to 0 or 1 only for loading and saving program files. Any other disc input/output operation, however, can have any channel no. between 2 and 14 inclusive (the value of 15 is reserved for the PET command channel). The secondary addresses used throughout the program suite can, therefore, be explained in terms of this table. For example, the sequence of events required to list a program file stored on PET disc are:

(i) Send LOAD command - secondary address 240_{10}

(ii) Input data bytes (repeat) - secondary address 96_{10}

(iii) Send CLOSE command - secondary address 224_{10}

and by referring to subroutine SEQ it can be seen how these secondary address values are used in conjunction with the necessary instrument bus unlisten and untalk commands (IBUNL and IBUNT) to achieve the program listing.

TABLE C.1

OPERATION	SECONDARY ADDRESS BIT PATTERN
	MSB LSB
LOAD	1 1 1 1 Ø Ø Ø Ø
SAVE	1 1 1 1 Ø Ø Ø 1
CLOSE	1 1 1 Ø b b b b
OPEN (with file name)	1 1 1 1 b b b b b = Ø or 1
OPEN (no file name)	Ø 1 1 Ø b b b b
PRINT #	Ø 1 1 Ø b b b b
INPUT #	Ø 1 1 Ø b b b b
	channel no.

C.3 The format of sequential and program files stored on PET disc

The retrieval of data from PET sequential files is straightforward. Once the relevant OPEN command has been sent the PET disc drive responds by allowing the data bytes contained in the file to be INPUT to the controller until the end of file is reached. These data bytes are sent down the GPIB as the normal ASCII character set and decoding is trivial. When no more data bytes are received by the MINC the PET file is CLOSED.

The listing of PET program files, however, is made more complicated by the manner in which the program is stored on disc by the CBM microcomputer. All data bytes are still stored and sent as ASCII characters but the decoding is no longer trivial due to the fact that Basic commands (e.g. END, FOR, NEXT, DATA, INPUT# etc.) are stored as single bytes called TOKENS. The tokens can be recognized immediately as the value of the byte containing the token is negative (bit 8 is set to 1). Once bit 8 has been reset to 0 the token bytes then have values from 0 to 74 and they have a one to one correspondence with the Basic commands. For example:

0 = END

1 = FOR

and 2 = NEXT etcetera.

Having written a byte handling routine to deal with the tokens the decoding of the PET program file can proceed byte by byte as it is passed from PET disc drive to MINC

minicomputer via the GPIB. The PET Basic line consists of:

(i) 2 bytes containing memory location information for the CBM microcomputer,

(ii) 2 bytes containing the Basic line number

(iii) A string of single bytes containing the Basic line (+ TOKENS).

(iv) A null byte at the end of the line.

The end of file condition is designated by three consecutive null bytes.

```
C
C               THIS PROGRAM ENABLES YOU TO:
C                1) LOOK AT PROGRAM AND SEQUENTIAL FILES
C               ON PET DISK
C                2) TRANSFER SEQUENTIAL (DATA) FILES FROM
C               MINC TO PET
C                3) TRANSFER SEQUENTIAL FILES FROM PET
C               TO MINC
C
50              TYPE 1000
                ACCEPT 1001,I1,I2,I3,I4
                IF (I1.EQ.'H') GOTO 500
                IF (I1.EQ.'L') GOTO 400
                IF (I1.EQ.'C') GOTO 300
                IF (I1.EQ.'D') GOTO 200
                IF (I1.EQ.'Q') CALL EXIT
                GOTO 500
200             IF (I4.EQ.'0') GOTO 250
                NCHAR=1
                CALL SEQ(NCHAR)
                GOTO 50
250             NCHAR=0
                CALL SEQ(NCHAR)
                GOTO 50
300             IF (I2.EQ.'M') CALL SFTRAN
                IF (I2.EQ.'P') CALL PETCOP
                GOTO 50
400             NCHAR=2
                CALL SEQ(NCHAR)
                GOTO 50
500             TYPE 1007
                TYPE 1002
                TYPE 1003
                TYPE 1004
                TYPE 1005
                TYPE 1006
                TYPE 1008
                GOTO 50
C
C               FORMAT STATEMENTS
C
1000            FORMAT(1H ,/,'0OPTION? (H FOR HELP)...'.$)
1001            FORMAT(4A1)
1002            FORMAT('0DIR0 - DIRECTORY OF PET DISK 0')
1003            FORMAT(' DIR1 - DIRECTORY OF PET DISK 1')
1004            FORMAT(' LIST - LISTS SEQUENTIAL OR PROGRAM FILE
     C ON PET DISK')
1005            FORMAT(' CM2P - COPIES SEQUENTIAL FILE FROM MINC TO PET')
1006            FORMAT(' CP2M - COPIES SEQUENTIAL FILE FROM PET TO MINC ')
1007            FORMAT('0THE OPTIONS ARE AS FOLLOWS:')
1008            FORMAT(' QUIT - TO LEAVE PROGRAM')
                END
```

```
      SUBROUTINE SEQ(NCHAR
C           FORTRAN PROG . TO LOOK AT PET 8050 DISK
C           AND DECODE DIRECTORIES
C
      BYTE LADDR(3),TADDR(3),DD(8,75),FILNAM(20),RMESS(132),J
      BYTE DATA(10)
      DOUBLE PRECISION TK(75)
      COMMON TK
      EQUIVALENCE (TK,DD)
      DATA TK/'END','FOR','NEXT','DATA','INPUT#','INPUT','DIM
     1     ,'READ','LET','GOTO','RUN','IF','RESTORE','GOSUB
     2     ,'RETURN','REM','STOP','ON','WAIT','LOAD','SAVE'
     3     ,'VERIFY','DEF','POKE','PRINT#','PRINT','CONT','LIST
     4     ,'CLR','CMD','SYS','OPEN','CLOSE','GET','NEW','TAB('
     5     ,'TO','FN','SPC(','THEN','NOT','STEP','+','-','*','/
     6     ,'^','AND','OR','>','=','<','SGN','INT','ABS','USR'
     7     ,'FRE','POS','SQR','RND','LOG','EXP','COS','SIN','TAN
     8     ,'ATN','PEEK','LEN','STR$','VAL','ASC','CHR$'
     9     ,'LEFT$','RIGHT$','MID$'/
      DO 10 J1=1,75
      DD(8,J1)=0
10    CONTINUE
      LADDR(1)=8
      TADDR(1)=8
      LADDR(3)=0
      TADDR(3)=0
      CALL IBTERM(
      CALL IBSTER(1,0)
      CALL IBTIMO(300)
      CALL IBREN
      IF (NCHAR.GT.1) GOTO 50
      FILNAM(1)='$'
      IF (NCHAR.EQ.1) GOTO 40
      FILNAM(2)='0'
      GOTO 45
40    FILNAM(2)='1'
45    NCHAR=2
      GOTO 70
50    TYPE 1000
      ACCEPT 1005,IFTYPE
      IF (IFTYPE.EQ.'@') GOTO 5000
      IF (IFTYPE.EQ.'S') GOTO 500
      TYPE 1001
      ACCEPT 1002,NCHAR,FILNAM
70    LADDR(2)=240
      CALL IBSEOI(FILNAM,NCHAR,LADDR)
      CALL IBUNL
      TADDR(2)=96
      NUM=IBRECV(RMESS,132,TADDR)
      ENCODE(2,99,IDAT) RMESS(5),RMESS(6)
99    FORMAT(2A1)
      TYPE 1004,IDAT
      I=7
      GO TO 130
100   NUM=IBRECV(RMESS,128)
            I=1
120   DO 125,J1=132,11,-1
      RMESS(J1)=RMESS(J1-10)
125   CONTINUE
      DO 126, J1=1,10
      RMESS(J1)=DATA(J1)
126   CONTINUE
128   NUM1=NUM
```

```
                GOTO 131
130             NUM1=NUM-10
131             DO 132,I1=1,10
132             DATA(I1)=RMESS(NUM1+I1)
140                     IF (RMESS(I)) 4000,2000,150
150                     IF (RMESS(I).LT."40)GO TO 200
160                     TYPE 1003,RMESS(I)
200                     I=I+1
                        IF(I.LE.NUM1)GO TO 140
                IF(NUM1.EQ.122)GO TO 100
                IF (I.GE.(NUM1+11)) GOTO 300
                GOTO 140
300             CALL IBUNT
                LADDR(2)=224
                CALL IBSEND('',0,LADDR)
                CALL IBUNL
                IF (FILNAM(1).EQ.'$') GO TO 5000
                GO TO 50
500             TYPE 1007
                ACCEPT 1005,IFTYPE
                IF (IFTYPE.EQ.'Y') CALL SEGNEW
                IF (IFTYPE.EQ.'Y') GOTO 50
                TYPE 1006
                ACCEPT 1002,NCHAR,FILNAM
                FILNAM(NCHAR+1)='.'
                FILNAM(NCHAR+2)='S'
                FILNAM(NCHAR+3)='.'
                FILNAM(NCHAR+4)='R'
                NCHAR=NCHAR+4
                LADDR(2)=242
                CALL IBSEDI(FILNAM,NCHAR,LADDR)
                CALL IBUNL
                TADDR(2)=98
600             NUM=IBRECV(RMESS,132,TADDR)
                        I=1
640                     IF (RMESS(I)) 700,700,650
650                     IF (RMESS(I).LT."40)GO TO 700
660                     TYPE 1003,RMESS(I)
700                     I=I+1
                        IF(I.LE.NUM)GO TO 640
                IF(NUM.EQ.132) GO TO 600
                CALL IBUNT
                LADDR(2)=226
                CALL IBSEND('',0,LADDR)
                CALL IBUNL
                GO TO 50
800             GOTO 700
1000            FORMAT(1H ,//,'0FILE TYPE  S OR P  (OR Q TO QUIT)... ',$)
1001            FORMAT('0LOAD FILE OR MESSAGE... ',$)
1002            FORMAT(Q,20A1)
1003            FORMAT( ' ',A1,$)
1004            FORMAT (1H ,/,I7,'     ',$)
1005            FORMAT (A1)
1006            FORMAT('0FILE NAME...',$)
1007            FORMAT('0HAS SEQ. FILE BEEN
     C COPIED FROM MINC FILE? (Y OR N).....',$)
C
C               NULL BYTE HERE !!!
C
2000            IF (RMESS(I+1).EQ.0.AND.RMESS(I+2).EQ.0) GO TO 200
                ENCODE(2,99,IDAT) RMESS(I+3),RMESS(I+4)
                TYPE 1004,IDAT
2010            I=I+4
```

```
                IF (NUM1.LT.122) GOTO 200
                IF ((I+1).GT.NUM1) GOTO 2025
2020            GO TO 200
2025            I1=I-NUM1+1
                I=I1
                NUM=IBRECV(RMESS,122)
                GOTO 120
C
C               BIT EIGHT SET HERE !
C
4000            RMESS(I)=(RMESS(I).AND."177)+1
                CALL TOKEN(RMESS(I))
                GO TO 200
5000            RETURN
9999            END
C
C
C               THIS WILL DECODE BASIC TOKENS
C
C
                SUBROUTINE TOKEN(I)
                BYTE I,DD(8,75)
                DOUBLE PRECISION TK(75)
                COMMON TK
                EQUIVALENCE (TK,DD)
C
C
                CALL TRIM(TK(I))
                K=LEN(TK(I))
                DO 100 L=1,K
                TYPE 1000,DD(L,I)
100             CONTINUE
1000            FORMAT(' ',A1,$)
                RETURN
                END
```

```
                SUBROUTINE SEGNEW
C                       LISTS SEQUENTIAL FILES COPIED
C                       FROM MINC TO PET
C
                BYTE LADDR(3),TADDR(3),FILNAM(20),RMESS(152),J
                LADDR(1)=6
                TADDR(1)=8
                LADDR(3)=0
                TADDR(3)=0
                CALL IBTERM()
                CALL IBSTER(1,0)
                CALL IBTIMO(300)
                CALL IBREN
510             TYPE 1006
                ACCEPT 1002,NCHAR,FILNAM
                FILNAM(NCHAR+1)='.'
                FILNAM(NCHAR+2)='S'
                FILNAM(NCHAR+3)='.'
                FILNAM(NCHAR+4)='R'
                NCHAR=NCHAR+4
                LADDR(2)=242
                CALL IBSEDI(FILNAM,NCHAR,LADDR)
                CALL IBUNL
                TADDR(2)=98
600             NUM=IBRECV(RMESS,132,TADDR)
                        I=1
640                     IF (RMESS(I)) 700,700,650
650             IF (RMESS(I).EQ."15) GOTO 3000
                        IF (RMESS(I).LT."40)GO TO 700
660                     TYPE 1003,RMESS(I)
700                     I=I+1
                        IF(I.LE.NUM)GO TO 640
                IF(NUM.EQ.132) GO TO 600
                CALL IBUNT
                LADDR(2)=226
                CALL IBSEND(' ',0,LADDR)
                CALL IBUNL
                GO TO 5000
800             GOTO 700
1000            FORMAT(1H ,//,'OFILE TYPE  S OR P  (OR Q TO QUIT)... ',$)
1001            FORMAT('OLOAD FILE OR MESSAGE... ',$
1002            FORMAT(Q,20A1)
1003            FORMAT(' ',A1,$)
1004            FORMAT (1H ,/,I7,'     ',$)
1005            FORMAT (A1)
1006            FORMAT('OFILE NAME...',$)
1007            FORMAT(1H,/,A1,$)
C
C               CARRIAGE RETURN HERE
C
3000            IF ((I+1).GT.NUM) GOTO 3100
                I=I+1
                TYPE 1007, RMESS(I)
                GOTO 700
3100            IF (NUM.LT.132) GOTO 700
                I=I+1-NUM
                NUM=IBRECV(RMESS,132)
                TYPE 1007,RMESS(I)
                GOTO 700
5000            RETURN
9999            END
```

```
                SUBROUTINE SFTRAN
C
C               THIS PROGRAM TRANSFERS A SEQUENTIAL FILE
C               FROM MINC DISK 1 TO PET DISK 1
C
                BYTE LADDR(3),FILNAM(20),RMESS(132),CL(2),NAMOFIL(20)
                DATA CL /"15,"12/
                LADDR(1)=8
                LADDR(3)=0
                CALL IBTERM()
                CALL IBSTER(1,0)
                CALL IBTIMO(150)
                CALL IBREN
                GOTO 50
40              TYPE 1004
                ACCEPT 1003, IFTYPE
                IF (IFTYPE.EQ.'N') GOTO 6000
C
C               TYPE NAME OF NEW SEQUENTIAL FILE TO BE
C                    CREATED ON PET DISK
C
50              TYPE 1000
60              ACCEPT 1002,NCHAR,FILNAM
                FILNAM(NCHAR+1)=','
                FILNAM(NCHAR+2)='S'
                FILNAM(NCHAR+3)=','
                FILNAM(NCHAR+4)='W'
                NCHAR=NCHAR+4
                DO70, I1=20,3,-1
                FILNAM(I1)=FILNAM(I1-2)
70              CONTINUE
                FILNAM(1)='1'
                FILNAM(2)=':'
                NCHAR=NCHAR+2
C
C               TYPE IN NAME OF FILE TO BE COPIED
C                  (E.G.   TEST.DAT   )
C
                TYPE 1001
                ACCEPT 1002,MCHAR,NAMOFIL
                DO 75,J1=20,5,-1
                NAMOFIL(J1)=NAMOFIL(J1-4)
75              CONTINUE
                NAMOFIL(1)='D'
                NAMOFIL(2)='Y'
                NAMOFIL(3)='1'
                NAMOFIL(4)=':'
                MCHAR=MCHAR+4
                LADDR(2)=242
C
C               CREATE NEW FILE ON PET AND OPEN EXISTING
C               FILE ON MINC
C
                CALL IBSEDI(FILNAM,NCHAR,LADDR)
                CALL IBUNL
                LADDR(2)=98
80              OPEN(UNIT=3,NAME=NAMOFIL,TYPE='OLD',READONLY,ERR=4000)
                DO 100, I1=1,10000
                DO 90, I2=1,132
                RMESS(I2)=0
90              CONTINUE
C
C               READ DATA FROM FILE
```

```
C
                READ(3,1008,END=150,ERR=3000) LCHAR,RMESS
91              IF (LCHAR.EQ.132) GOTO 95
                RMESS(LCHAR+1)= "15
                LCHAR=LCHAR+1
95              CALL IBSEND(RMESS,LCHAR,LADDR)
100             CONTINUE
C
C               CLOSE BOTH MINC AND PET FILES
C
150             CLOSE (UNIT=3,ERR=5000)
                CALL IBSEND(RMESS,LCHAR,LADDR)
                CALL IBSEOI(CL,2,LADDR)
                CALL IBUNL
                LADDR(2)=226
                CALL IBSEND('',0,LADDR)
                CALL IBUNL
                GOTO 40
C
C               FORMAT STATEMENTS
C
1000            FORMAT('0TYPE NAME OF SEQUENTIAL FILE TO BE CREATED ON
     C PET DISK 1.....',$)
1002            FORMAT(Q,20A1)
1001            FORMAT('0TYPE NAME OF THE SEQUENTIAL FILE TO BE COPIED
     C FROM MINC DISK 1.....',$)
1003            FORMAT(A1)
1004            FORMAT('0DO YOU WISH TO COPY MORE FILES ONTO PET DISK?
     C (Y OR N).....',$)
1005            FORMAT('0ERROR OCCURED IN OPENING FILE - TRY AGAIN?
     C (Y OR N).....',$)
1006            FORMAT('0ERROR OCCURED IN CLOSING FILE - TRY AGAIN?
     C (Y OR N).....',$)
1007            FORMAT('0ERROR OCCURED IN READING FILE - TRY AGAIN?
     C (Y OR N).....',$)
1008            FORMAT(Q,132A1)
1009            FORMAT('0TYPE DIFFERENT SEQUENTIAL FILE NAME TO BE
     C CREATED ON PET DISK.....',$)
C
C               ERROR IN READING MINC FILE
C
3000            TYPE 1007
                ACCEPT 1003,IFTYPE
                IF (IFTYPE.EQ.'Y') GOTO 5500
                GOTO 6000
C
C               ERROR IN OPENING MINC FILE
C
4000            TYPE 1005
                ACCEPT 1003,IFTYPE
                IF (IFTYPE.EQ.'Y') GOTO 80
                GOTO 6000
C
C               ERROR IN CLOSING MINC FILE
C
5000            TYPE 1006
                ACCEPT 1003,IFTYPE
                IF (IFTYPE.EQ.'Y') GOTO 150
                GOTO 6000
C
C               ERROR IN READING FILE CAUSES FILE
C               TO BE READ FROM START (NEW PET FILE NAME NEEDED.
C


5500            CLOSE(UNIT=3)
                TYPE 1009
                GOTO 60
6000            RETURN
                END
```

```
      SUBROUTINE PETCOP
C
C     THIS PROGRAM TRANSFERS A SEQUENTIAL FILE
C     FROM PET DISK TO MINC DISK 1
C
      BYTE LADDR(3),TADDR(3),FILNAM(20),RMESS(132)
      BYTE NAMOFIL(20)
      LOGICAL*1 ERR
      TADDR(1)=8
      TADDR(3)=0
      LADDR(1)=8
      LADDR(3)=0
      CALL IBTERM(15)
      CALL IBSTER(1,0)
      CALL IBTIMO(150)
      CALL IBREN
      GOTO 50
40    TYPE 1004
      ACCEPT 1003, IFTYPE
      IF (IFTYPE.EQ.'N') GOTO 6000
C
C     TYPE NAME OF SEQUENTIAL FILE TO BE
C          COPIED FROM PET DISK
C
50    TYPE 1000
60    ACCEPT 1002,NCHAR,FILNAM
      FILNAM(NCHAR+1)=','
      FILNAM(NCHAR+2)='S'
      FILNAM(NCHAR+3)=','
      FILNAM(NCHAR+4)='R'
      NCHAR=NCHAR+4
C
C     TYPE IN NAME OF FILE TO BE CREATED
C     ON MINC DISK (E.G.   TEST.DAT   )
C
      TYPE 1001
      ACCEPT 1002,MCHAR,NAMOFIL
      DO 75,J1=20,5,-1
      NAMOFIL(J1)=NAMOFIL(J1-4)
75    CONTINUE
      NAMOFIL(1)='D'
      NAMOFIL(2)='Y'
      NAMOFIL(3)='1'
      NAMOFIL(4)=':'
      MCHAR=MCHAR+4
      LADDR(2)=242
C
C     CREATE NEW FILE ON MINC AND OPEN EXISTING
C     FILE ON PET
C
      CALL IBSEOI(FILNAM,NCHAR,LADDR)
      CALL IBUNL
      TADDR(2)=98
80    OPEN(UNIT=3,NAME=NAMOFIL,ERR=4000)
      DO 100, I1=1,10000
      DO 90, I2=1,132
      RMESS(I2)=0
90    CONTINUE
C
C     READ DATA FROM FILE
C
      NUM=IBRECV(RMESS,132,TADDR)
      IF (NUM.EQ.0) GOTO 120
```

```
                RMESS(NUM+1)="15
                CALL PUTSTR(3,RMESS,0,ERR)
95              A=1
100             CONTINUE
C
C               CLOSE BOTH MINC AND PET FILES
C
120             IF (A.EQ.0) GOTO 150
                A=0
                GOTO 100
150             CLOSE (UNIT=3,ERR=5000)
                TYPE 1009
                CALL IBUNT
                LADDR(2)=226
                CALL IBSEND('',0,LADDR)
                CALL IBUNL
                GOTO 40
C
C               FORMAT STATEMENTS
C
1000            FORMAT('0TYPE NAME OF SEQUENTIAL FILE TO BE COPIED FROM
     C PET DISK.....',$)
1002            FORMAT(Q,20A1)
1001            FORMAT('0TYPE NAME OF THE DATA FILE TO BE CREATEI
     C ON MINC DISK 1.....',$)
1003            FORMAT(A1)
1004            FORMAT('0DO YOU WISH TO COPY MORE FILES ONTO MINC DISK?
     C (Y OR N).....',$)
1005            FORMAT('0ERROR OCCURED IN OPENING FILE - TRY AGAIN?
     C (Y OR N).....',$)
1006            FORMAT('0ERROR OCCURED IN CLOSING FILE - TRY AGAIN?
     C (Y OR N).....',$)
1007            FORMAT('0ERROR OCCURED IN WRITING FILE - TRY AGAIN?
     C (Y OR N).....',$)
1009            FORMAT('0THE TIME-OUT ERROR HERE SHOWS THAT ALL
     C DATA HAS BEEN RECEIVED')
C
C               ERROR IN WRITING MINC FILE
C
3000            TYPE 1007
                ACCEPT 1003,IFTYPE
                IF (IFTYPE.EQ.'Y') GOTO 5500
                GOTO 6000
C
C               ERROR IN OPENING MINC FILE
C
4000            TYPE 1005
                ACCEPT 1003,IFTYPE
                IF (IFTYPE.EQ.'Y') GOTO 80
                GOTO 6000
C
C               ERROR IN CLOSING MINC FILE
C
5000            TYPE 1006
                ACCEPT 1003,IFTYPE
                IF (IFTYPE.EQ.'Y') GOTO 150
                GOTO 6000
C
C               ERROR IN WRITING FILE CAUSES FILE
C               TO BE REWRITTEN FROM START
C
5500            CLOSE(UNIT=3)
                GOTO 50


6000            RETURN
                END
```

APPENDIX D

TABLE OF RESULTS

This appendix contains a compilation of most of the data obtained by the Durham research team and British Gas staff at both OLIC and ERS during the extensive investigations into the properties of pipe steels described above.

Steel code	Steel type	Widger polynomial coefficients							
		a_o^1	$-b_1^1$	$-a_1^1$	b_2^1	a_2^1	a_o	b_1	a_1
DFB	FK	0.333	0.931	0.111	0.220	0.058	0.285	0.819	2.196
DFF	FK	0.320	0.943	0.185	0.226	0.109	0.333	1.244	2.567
DFE	FK	0.311	0.934	0.094	0.221	0.067	0.289	1.020	2.188
EEC	CR	0.332	0.935	0.087	0.221	0.036	0.304	1.018	2.209
DME	SK	0.333	0.938	0.299	0.223	0.156	0.374	1.541	3.171
EEB	FK	0.247	0.961	0.006	0.233	0.001	0.307	1.207	2.545
OLI-030	USA SK	0.347	0.934	0.159	0.221	0.095	0.310	1.042	2.204
OLI-015	FK	0.402	0.944	0.344	0.226	0.161	0.393	1.258	2.732
OLI-010	FK	0.381	0.934	0.352	0.221	0.173	0.400	1.435	3.004
EED	CR	0.351	0.926	0.177	0.217	0.082	0.354	1.121	2.447
DHP	SK	0.273	0.934	0.180	0.221	0.122	0.315	1.029	2.367
OLI-013	FK	0.362	0.962	0.219	0.234	0.086	0.389	1.207	2.597
DWA	FK	0.362	0.945	0.242	0.226	0.116	0.348	1.181	2.521
DHQ	USA SK	0.367	0.927	0,143	0.218	0.087	0.311	0.932	2.014
2401	SK	0.246	0.956	0.173	0.232	0.104	0.357	1.839	3.607
EEE	CR	0.273	0.957	0.000	0.231	0.010	0.277	1.354	2.832
OLI-017	CR	0.354	0.935	0.151	0.221	0.063	0.342	1.067	2.323
DFD	FK	0.283	0.957	0.008	0.231	0.003	0.296	1.038	2.247
DLR	SK	0.296	0.933	0.339	0.221	0.198	0.376	2.042	3.995
OLI-012	FK	0.385	0.946	0.314	0.227	0.144	0.401	1.325	2.800
EAO	CR	-	-	-	-	-	-	-	-
DEQ	FK	-	-	-	-	-	-	-	-
DEZ	FK	-	-	-	-	-	-	-	-
EER	SK	-	-	-	-	-	-	-	-
OLI-009	FK	-	-	-	-	-	-	-	-
OLI-011	CR	-	-	-	-	-	-	-	-
Sample A	HT	-	-	-	-	-	-	-	-
Sample B	HT	-	-	-	-	-	-	-	-
Sample C	HT	-	-	-	-	-	-	-	-

Steel code	Continued $-b_2$	$-a_2$	Full loop harmonic amplitudes 1st odd	3rd odd	5th odd	7th odd	1st even (-)	3rd even (-)
DFB	0.215	0.445	1.941	0.407	0.173	0.069	0.293	0.205
DFF	0.049	0.097	1.892	0.413	0.185	0.078	0.290	0.212
DFE	0.051	0.105	2.001	0.443	0.197	0.081	0.311	0.228
EEC	0.046	0.095	2.000	0.440	0.197	0.085	0.286	0.210
DME	0.061	0.121	2.014	0.479	0.226	0.106	0.269	0.206
EEB	0.056	0.113	2.000	0.460	0.216	0.103	0.250	0.186
OLI-030	0.043	0.086	1.932	0.414	0.179	0.069	0.297	0.212
OLI-015	0.085	0.175	1.988	0.455	0.202	0.082	0.313	0.241
OLI-010	0.058	0.117	2.028	0.483	0.226	0.104	0.281	0.218
EED	0.053	0.111	2.005	0.435	0.188	0.074	0.305	0.222
DHP	0.123	0.253	1.981	0.456	0.217	0.108	0.217	0.156
OLI-013	0.058	0.120	1.999	0.456	0.198	0.075	0.335	0.258
DWA	0.058	0.118	1.972	0.440	0.189	0.073	0.325	0.243
DHQ	0.041	0.084	1.917	0.395	0.162	0.053	0.328	0.234
2401	0.058	0.108	2.021	0.496	0.248	0.131	0.207	0.157
EEE	0.082	0.165	2.028	0.465	0.216	0.101	0.275	0.206
OLI-017	0.049	0.102	1.977	0.420	0.174	0.061	0.331	0.242
DFD	0.052	0.107	1.962	0.423	0.184	0.074	0.307	0.223
DLR	0.066	0.123	2.020	0.497	0.247	0.130	0.211	0.161
OLI-012	0.055	0.112	2.005	0.468	0.211	0.088	0.305	0.236
EAO	-	-	2.003	0.441	0.190	0.075	0.296	0.223
DEQ	-	-	2.051	0.490	0.220	0.092	0.304	0.244
DEZ	-	-	-	-	-	-	-	-
EER	-	-	1.996	0.467	0.226	0.114	0.215	0.156
OLI-009	-	-	1.984	0.451	0.205	0.089	0.279	0.210
OLI-011	-	-	2.003	0.438	0.193	0.082	0.283	0.209
Sample A	-	-	-	-	-	-	-	
Sample B	-	-	-	-	-	-	-	
Sample C	-	-	-	-	-	-	-	

Steel code	continued 5th even (-)	7th even (-)	Kneppos parameters LnA	kLnA	Coercive field (kAm^{-1})	B_s (T) at 25kAm^{-1}	Initial permeability (T/kAm^{-1})	UTS (MNm^{-2}
DFB	0.148	0.110	0.714	0.663	0.492	2.028	0.278	551
DFF	0.161	0.126	0.649	0.664	0.490	2.008	0.303	540
DFE	0.174	0.133	0.712	0.661	0.502	2.014	0.270	558
EEC	0.157	0.125	0.739	0.686	0.460	2.028	0.230	586
DME	0.161	0.128	0.536	0.664	0.377	2.035	0.299	484
EEB	0.142	0.115	0.614	0.655	0.404	2.021	0.260	548
OLI-030	0.158	0.118	0.746	0.674	0.512	2.019	0.230	545
OLI-015	0.187	0.147	0.697	0.713	0.516	2.025	0.250	524
OLI-010	0.171	0.137	0.611	0.693	0.456	2.042	0.244	507
EED	0.166	0.127	0.722	0.710	0.512	2.042	0.230	576
DHP	0.118	0.093	0.520	0.629	0.334	2.035	0.313	490
OLI-013	0.200	0.154	0.734	0.721	0.538	2.028	0.204	530
DWA	0.184	0.140	0.689	0.688	0.510	2.008	0.250	548
DHQ	0.172	0.128	0.829	0.688	0.577	2.014	0.211	556
2401	0.123	0.100	0.462	0.635	0.321	2.031	0.377	462
EEE	0.160	0.128	0.677	0.694	0.495	2.028	0.256	577
OLI-017	0.180	0.136	0.765	0.713	0.479	2.035	0.200	581
DFD	0.167	0.128	0.707	0.672	0.507	2.035	0.270	541
DLR	0.127	0.102	0.417	0.630	0.281	2.035	0.364	458
OLI-012	0.184	0.145	0.672	0.706	0.509	2.028	0.220	507
EAO	0.169	0.131	0.848	0.747	0.510	2.063	-	592
DEQ	0.192	0.149	0.841	0.789	0.500	2.049	-	466
DEZ	-	-	0.608	0.666	0.379	2.049	-	538
EER	0.120	0.094	0.551	0.643	0.336	2.042	-	476
OLI-009	0.161	0.126	0.705	0.705	0.465	2.035	-	520
OLI-011	0.155	0.120	0.718	0.708	0.467	2.049	-	576
Sample A	-	-	0.309	0.597	0.240	-	-	-
Sample B	-	-	1.065	0.591	0.770	-	-	-
Sample C	-	-	2.567	0.664	2.020		-	-

Steel Code	YS (MNm^{-2})	Steel chemical composition								
		% C	% Mn	% Si	% S	% P	% Al	% V	% Nb	% Ni
DFB	385	0.19	1.20	0.26	0.013	0.011	0.049	-	-	-
DFF	381	0.19	1.22	0.22	0.013	0.007	0.017	0.007	-	-
DFE	404	0.19	1.25	0.23	0.011	0.009	0.044	0.005	-	-
EEC	462	0.14	1.45	0.35	0.010	0.014	0.044	0.015	0.042	0.018
DME	368	0.15	1.00	0.03	0.025	0.022	0.006	-	0.013	0.017
EEB	458	0.12	1.28	0.31	0.012	0.017	0.027	-	-	0.011
OLI-030	404	0.24	0.82	0.06	0.020	0.011	0.005	-	-	0.047
OLI-015	399	0.16	1.08	0.29	0.023	0.008	0.020	0.006	0.018	0.015
OLI-010	384	0.16	1.07	0.29	0.020	0.008	0.022	-	0.015	0.015
EED	479	0.12	1.38	0.34	0.012	0.012	0.020	0.006	0.031	0.014
DHP	397	0.14	0.80	0.07	0.031	0.037	-	-	-	0.052
OLI-013	388	0.17	1.24	0.23	0.019	0.007	0.030	0.010	0.022	0.020
DWA	412	0.18	1.04	0.29	0.018	0.014	0.048	0.006	0.020	0.015
DHQ	406	0.21	0.98	0.09	0.024	0.013	0.007	0.006	-	0.060
2401	371	0.15	0.70	0.07	0.020	0.018	0.005	-	-	0.034
EEE	447	0.13	1.37	0.33	0.008	0.011	0.043	-	0.029	0.012
OLI-017	464	0.14	1.43	0.34	0.012	0.013	0.045	0.013	0.036	0.017
DFD	378	0.19	1.22	0.26	0.012	0.008	0.050	0.007	-	-
DLR	369	0.15	0.68	0.06	0.027	0.022	-	-	-	0.015
OLI-012	385	0.16	1.16	0.21	0.018	0.009	0.034	0.008	0.021	0.018
EAO	482	-	-	-	-	-	-	-	-	-
DEQ	311	-	-	-	-	-	-	-	-	-
DEZ	423	-	-	-	-	-	-	-	-	-
EER	370	-	-	-	-	-	-	-	-	-
OLI-009	386	-	-	-	-	-	-	-	-	-
OLI-011	478	-	-	-	-	-	-	-	-	-
Sample A	-	-	-	-	-	-	-	-	-	-
Sample B	-	-	-	-	-	-	-	-	-	-
Sample C	-	-	-	-	-	-	-	-	-	-

Steel code	continued % Cu	% Co	% Cr	% Mo	Vickers Hardness	B_r (T)	μ_{max} (Tm/kA)	H at μ_{max} (kAm^{-1})
DFB	0.010	-	-	0.007	169	0.97	1.01	0.69
DFF	0.011	-	-	0.008	162	1.07	1.16	0.67
DFE	0.010	-	-	0.007	176	1.13	1.04	0.71
EEC	0.023	0.010	0.018	0.010	198	1.06	1.04	0.73
DME	0.017	0.011	0.006	0.008	140	1.10	1.38	0.58
EEB	0.016	0.009	0.020	0.007	184	1.02	1.19	0.61
OLI-030	0.132	0.026	0.015	0.011	172	1.02	1.01	0.76
OLI-015	0.013	0.010	0.008	0.088	161	1.16	1.17	0.75
OLI-010	0.012	0.010	0.007	0.007	151	1.15	1.27	0.66
EED	0.015	0.010	0.020	0.008	185	1.07	1.11	0.73
DHP	0.059	0.012	0.036	0.014	148	0.91	1.38	0.48
OLI-013	0.024	0.011	0.006	0.009	173	1.21	1.13	0.76
DWA	0.021	0.009	0.012	0.009	169	1.14	1.12	0.72
DHQ	0.079	0.029	-	0.008	200	1.09	0.93	0.84
2401	0.042	0.011	0.010	0.010	150	0.98	1.56	0.46
EEE	0.018	0.009	0.013	0.007	189	1.11	1.14	0.68
OLI-017	0.021	0.010	0.017	0.009	180	1.11	1.06	0.77
DFD	0.010	-	-	0.008	174	1.09	1.07	0.69
DLR	0.021	0.009	0.006	0.009	-	0.99	1.64	0.43
OLI-012	0.015	0.011	0.020	0.008	174	0.94	1.19	0.73
EAO	-	-	-	-	179	1.07	1.00	0.85
DEQ	-	-	-	-	140	1.18	1.09	0.90
DEZ	-	-	-	-	164	0.98	1.23	0.62
EER	-	-	-	-	168	0.91	1.30	0.55
OLI-009	-	-	-	-	170	1.06	1.14	0.74
OLI-011	-	-	-	-	188	1.04	1.13	0.73
Sample A	-	-	-	-	125	-	-	-
Sample B	-	-	-	-	210	-	-	-
Sample C	-	-	-	-	432	-	-	-

Steel code	Percentage pearlite content	Mean ferrite diameter (μm)	Mean pearlite diameter (μm)
DFB	21.9	8.91	7.66
DFF	22.4	11.25	8.75
DFE	20.4	13.13	8.44
EEC	21.9	10.47	8.75
DME	18.0	14.38	6.88
EEB	18.2	12.03	6.56
OLI-030	30.5	17.19	10.94
OLI-015	18.7	10.00	5.47
OLI-010	17.0	11.09	5.94
EED	19.8	10.94	8.75
DHP	16.6	24.84	10.16
OLI-013	22.4	9.84	5.31
DWA	23.0	10.47	8.44
DHQ	33.0	13.59	8.91
2401	16.0	21.88	7.81
EEE	17.6	9.06	4.84
OLI-017	18.5	8.59	6.72
DFD	20.5	10.31	5.63
DLR	12.1	27.34	8.75
OLI-012	17.5	10.63	6.41
EAO	-	-	-
DEQ	-	-	-
DEZ	-	-	-
EER	-	-	-
OLI-009	-	-	-
OLI-011	-	-	-
Sample A	-	—	-
Sample B	-	—	-
Sample C	-	-	-

APPENDIX E

Description of Location and Listing of Machine-Code Serial Poll Routine

E.1 The PET microcomputer and the IEEE-488 instrument bus

The IEEE 488-1978* standard defines a bit-parallel byte-serial bus structure designed to allow communications between intelligent devices. The standard defines all voltage and current levels, pinouts, connector specifications, timing and handshake requirements (see IEEE Standard Digital Interface for Programmable Instrumentation**). It should, therefore, be possible to connect two or more devices equipped with a GPIB port and expect that they will be able to communicate on the bus. The PET microcomputers, however, do not have a full IEEE bus capability as defined by the standard and this makes communication via the bus more difficult. This Appendix contains an outline to most of the concepts related to the bus structure and points out some of the failings of the PET in meeting the standard's requirements. In particular, a machine-code routine written to conduct a serial poll of any IEEE device, is described.

---

*IEEE Standard Digital Interface for Programmable Instrumentation (The Institute of Electrical and Electronic Engineers Inc., New York, N.Y., November 30th 1978), IEEE Std. 488-1978 (Revision of ANSI/IEEE Std. 488-1975).

** IEEE Standard Digital Interface for Programmable Instrumentation (The Institute of Electrical and Electronic Engineers Inc., New York, N.Y., April 4th, 1975), IEEE Std. 488-1975-ANSI MC 1.1-1975.

E.2 The Bus Structure

The basic bus structure is illustrated in Figure E.1 and a maximum of 15 devices, of four types, can be connected to this bus system. The four device types are:

(1) The controller (i.e. microcomputer)

(2) Devices that talk only (e.g. voltmeter)

(3) Devices that listen only (e.g. printer)

(4) Devices that talk or listen (e.g. EGeG 5206 Lock-in Analyser).

These device types have already implied the three operating states on the bus: controller, talker and listener. The controller coordinates communications on the bus by commanding the other devices connected to it. In a PET system there can only be one, the PET itself. Talkers can only put information on the bus and listeners can only accept messages that have been placed on the bus. The controller, clearly, must be able to do all three. A non-PET system may have more than one controller but only one can be active at a time. Similarly, only one talker can be active at a time. Listening, however, is a passive activity so all devices that can may listen all the time. The IEEE devices are given address (GPIB addresses) for identification and the controller activates the appropriate device by placing its address on the bus. Once "alerted", the appropriate commands/data can be sent to it.

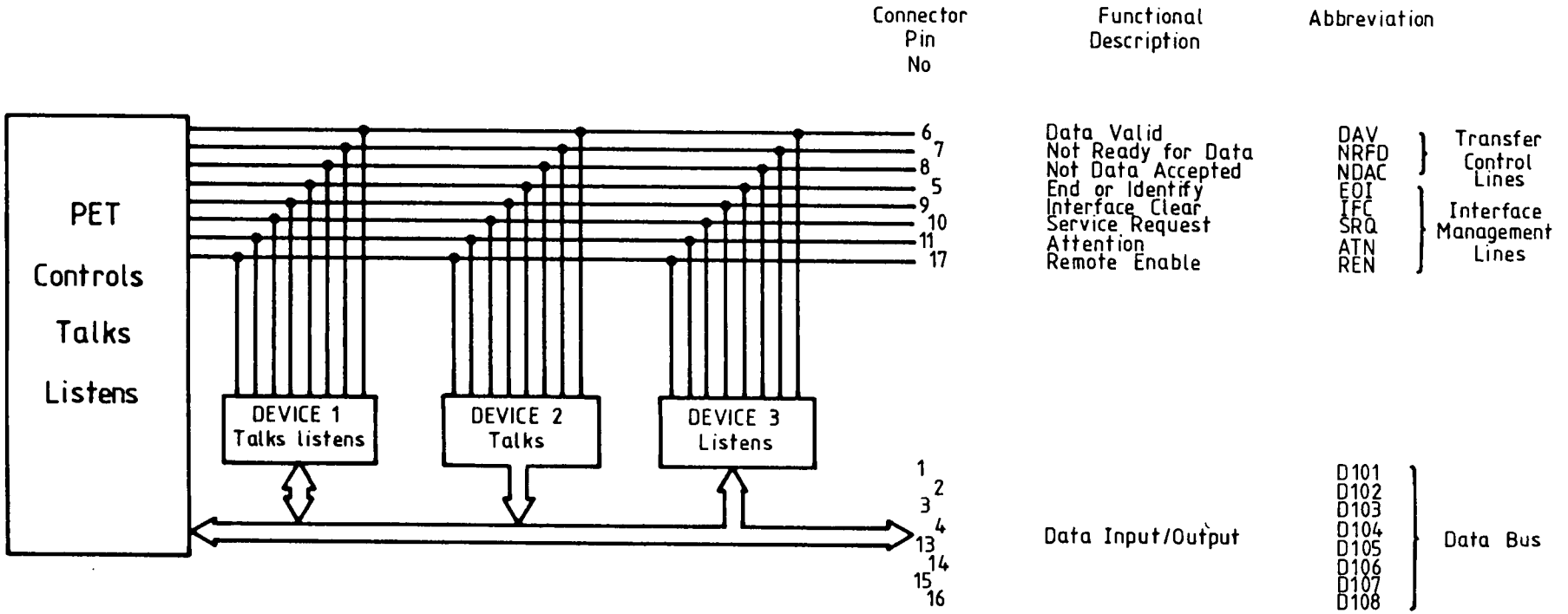

Figure E.1 Schematic representation of basic IEEE-488 GPIB structure

By referring to Figure E.1 it can be seen that the bus operates with sixteen lines. Eight of these are the parallel bi-directional DIO lines that connect all instruments and the controller, which carry both data and commands. They form the data bus. To process the data flow on the data bus up to eight control and status signals are required, which can be split into two groups, called "Interface Management Lines" and "Transfer Control Lines" respectively. Not all of these lines take part in every data transaction, but all are important to the complete operation of the standard bus. The transfer control lines control and perform the handshake required to transmit a data byte. The others are used for single-line commands and status messages and function independently from the handshake requirement. A brief description of each of these lines follows:

(i) DAV (Data Valid) - asserted low (true) by a talker after it places data on the DIO lines. It informs the listener that the information on these lines is valid.

(ii) NRFD (Not Ready for Data) - asserted low (true) to indicate that not all devices are ready to receive data. Each instrument releases this line when ready.

(iii) NDAC (Not Data Accepted) - asserted low (true) by all listeners until data byte or address information is received, then it is set high.

(iv) ATN (attention) - when asserted low (true) by the controller it indicates to the devices on the bus

that some address or command information is about to be sent to them. When ATN is returned high, only the devices that are addressed take part in the subsequent data exchange.

(v) IFC (Interface Clear) - asserted low to override all bus activity and return the bus to a known "clear" state. Its use is reserved for situations where something has gone wrong and any data on the bus may be lost when IFC is pulled low

(vi) REN (Remote Enable) - asserted low to transfer devices on the bus from local to remote control. The PET controller holds this line permanently to ground.

(vii) SRQ (Service Request) - asserted low by any device on the bus to request service from the controller. This can be initiated, for example, by a digital meter having data available, or a bus device having an internal error which has been detected. This is not implemented in PET BASIC and neither are the serial or parallel polls which are normally sent by the controller to determine which device sent the SRQ.

(viii) EOI (End Or Identify) - asserted low by any talker including the controller to indicate the last byte of a multibyte message.

E.3 The Handshake Procedure

The three lines that do the communication handshaking between the controller/talker and the listener are DAV, NRFD and NDAC. A simplified handshake timing diagram

for these three lines is shown in Figure E.2, and is described as follows:

(i) The talker may or may not have relevant data on the eight data bus lines. This does not affect the upcoming transfer.

(ii) The talker continuously monitors the NRFD line. Once all active listeners are ready, NRFD goes high and the transfer begins.

(iii) The talker places data on the bus and after a short delay asserts DAV low to inform the active listeners that they can read the first byte of information.

(iv) The active listeners become "busy" reading the data and assert NRFD low. When every listener is ready to receive more data, NRFD is set high.

(v) The listeners also control the NDAC line which is asserted low until every listener has accepted the data byte whereupon NDAC goes high. This informs the talker that the data byte has been read.

(vi) The talker releases DAV to the high state and the listeners respond by asserting NDAC low again.

Thus the bus is returned to its quiescent state ready for its next data transfer, and the process outlined above is repeated every time a data or command byte is sent. All characters, whether numbers or letters, are represented in hexadecimal code and they are transmitted down the data bus in this format.

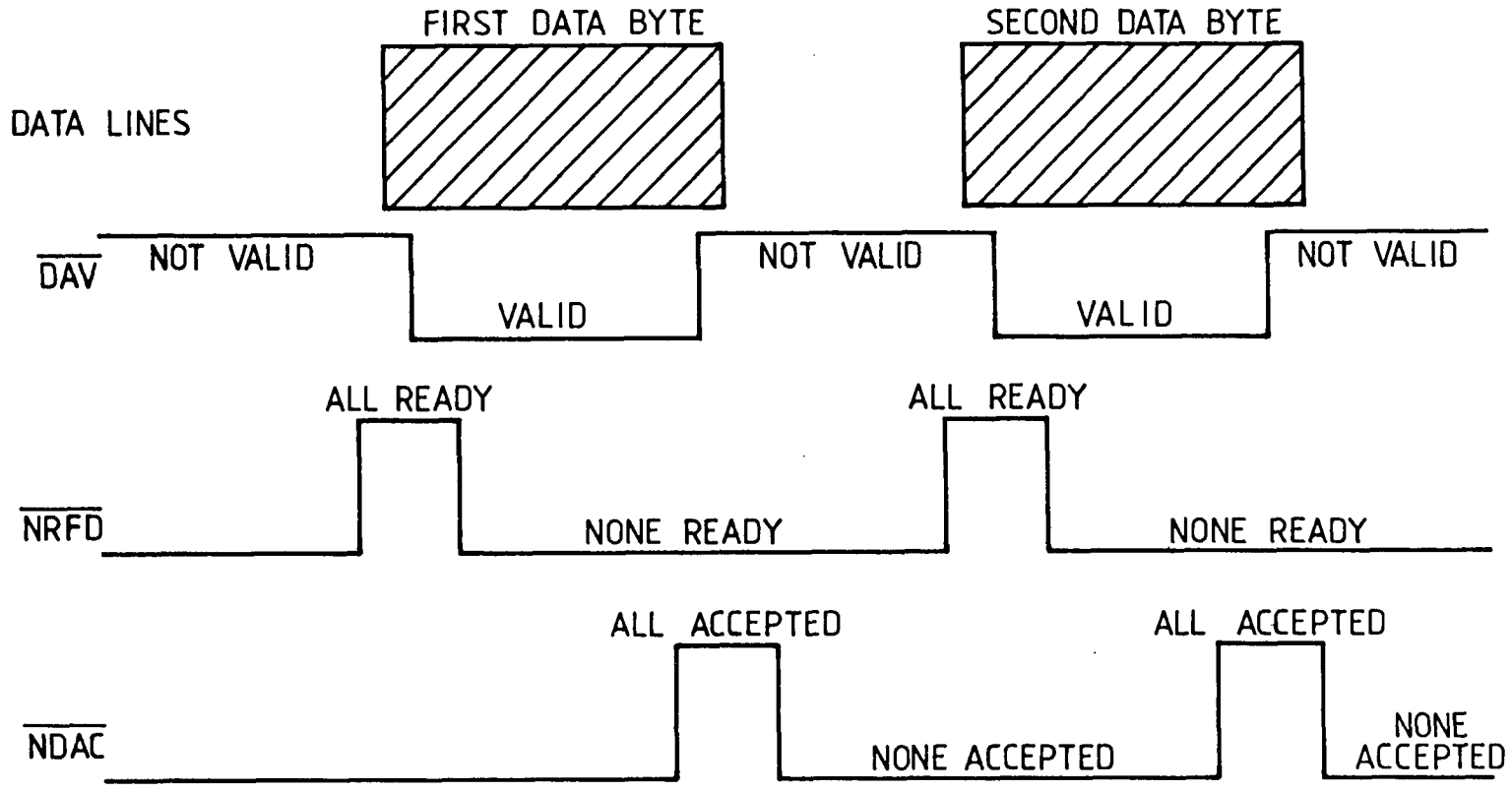

Figure E.2 Simplified handshake timing diagram for IEEE-488 data bus.

E.4 Communication problems between the PET and the VSM peripherals

The PET's handshake sequences, both as a talker and a listener, are slightly different from that described above and are shown by flow diagrams in Figures E.3 and E.4 respectively. It can be seen from these that the PET only allows the IEEE device it is communicating with 65 milliseconds to complete the data transfer otherwise the PET defaults to a "timeout". This has caused severe problems when the PET is communicating as a listener with both the Brookdeal Lock-In Analyser and the Fluke Multimeter. Both these devices sometimes take longer than 65 milliseconds to respond and the data transferred is either lost or corrupted as a result of the PET's timeout.

Attempts were made to overcome this problem by making use of the PET's internal bus status indication (ST). By referring to Figure E.4 it can be seen that the value of ST is set equal to 64 or 0 at the conclusion of a successful listening sequence, depending on whether EOI has been set or not. The simplest solution involved the straightforward repetition of the PET's INPUT statement to the device until the value of ST indicated a successful transfer. Even this, however, did not prove to be 100% reliable and much experimentation on the VSM was wasted as a result of bus hang-ups. It was decided, therefore, to write a machine-code routine to conduct a serial poll of the device in order that the PET could determine

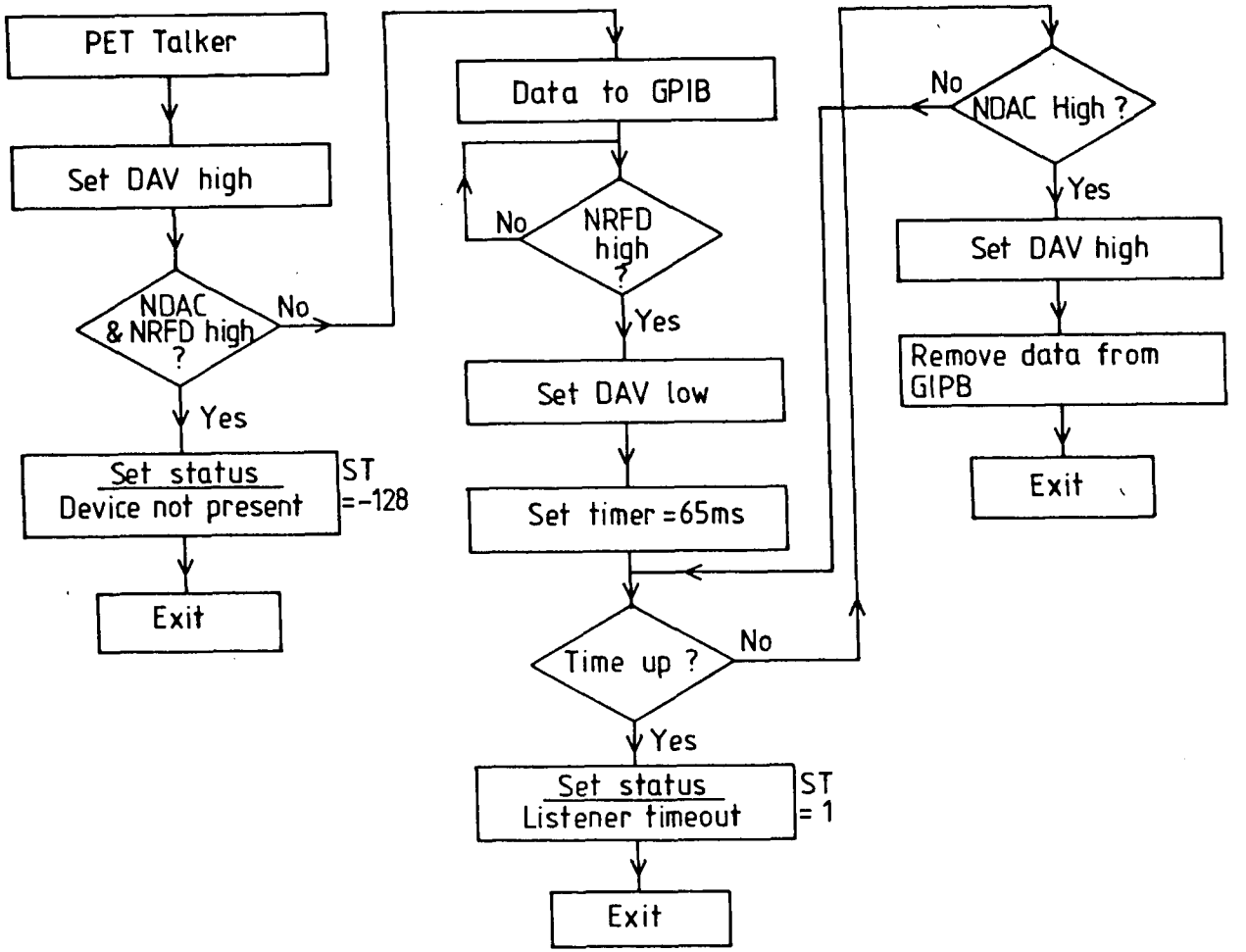

Figure E.3 The PET'S IEEE-488 handshake sequence as a "talker".

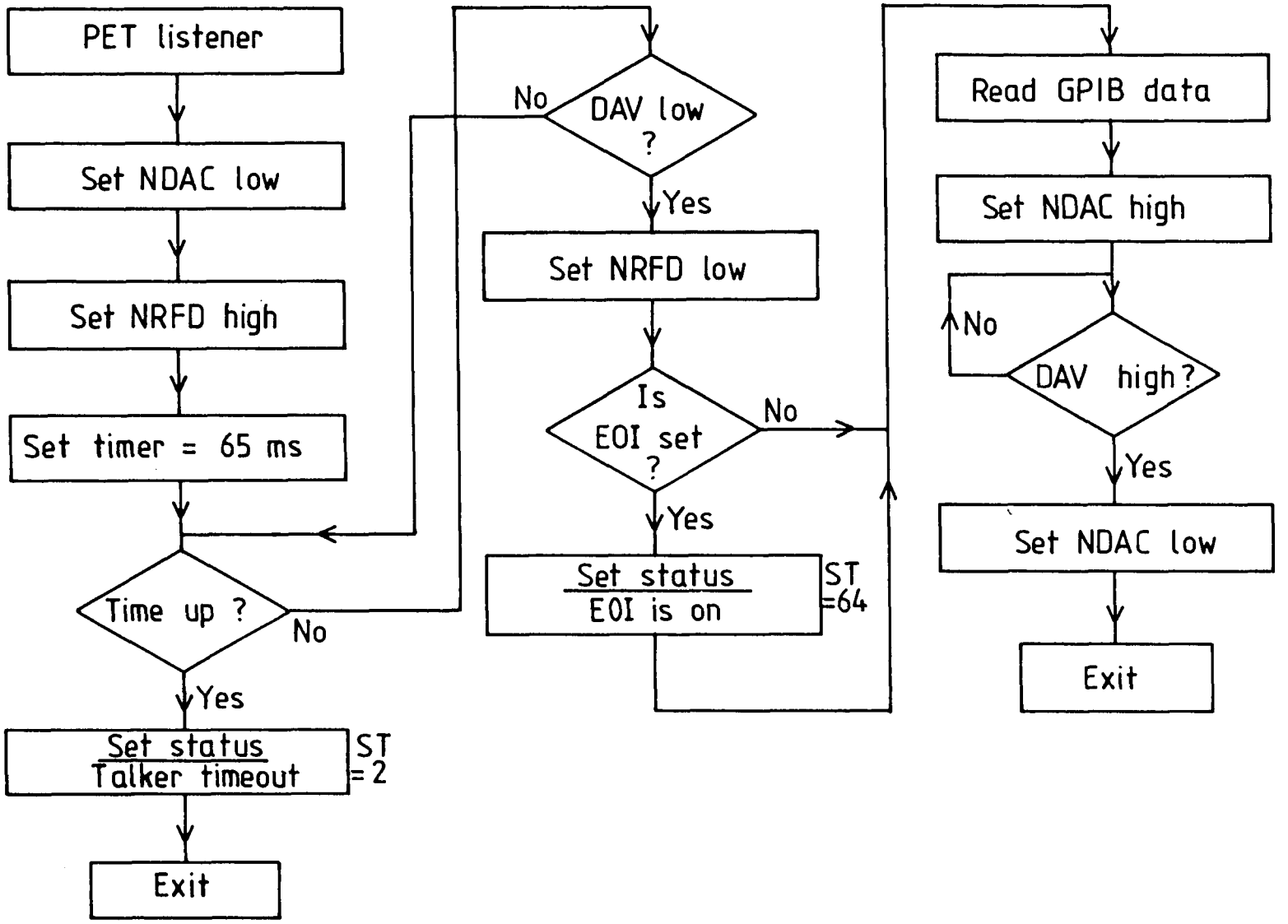

Figure E.4 The PET's IEEE-488 handshake sequence as a "listener".

precisely when the device was ready to transmit data thus avoiding the above problems.

With reference to the publications by Fischer and Jensen (1980) and Skier (1981) such a routine was written and the code was blown into an EPROM which was then placed in a spare socket inside the PET. The code starts at location 40714 dec. (9F0A hex.), ends at 40925 dec. (9FDD hex.) and uses three locations (700 - 702 dec.) in the PET's first cassette buffer to transfer the device address and the result of the poll to and from the main BASIC program. The following pages contain a listing of the routine both in machine-code and assembly language, as well as a detailed explanation of the assembly language listing. By following this it will be seen that the handshakes implemented during the poll follow exactly the same procedure as that described earlier.

Appendix F gives examples of the use of this routine and how it has ensured the complete reliability of communication between the PET and the Brookdeal/Fluke.

PET memory locations Dec.	Hex	Machine code listing			Assembly language listing	
40714	9FOA	A9	FB		LDAIM	251
40716	9FOC	20	40	E8	AND	59456
40719	9FOF	8D	40	E8	STA	59456
40722	9F12	A9	18		LDAIM	24
40724	0F14	8D	BD	02	STA	701
40727	9F17	20	72	9F	JSR	40818
40730	9F1A	AD	BC	02	LDA	700
40733	9F1D	09	40		ORAIM	64
40735	9FIF	8D	BD	02	STA	701
40738	9F22	20	72	9F	JSR	40818
40741	9F25	A9	FD		LDAIM	253
40743	9F27	2D	40	E8	AND	59456
40746	9F2A	8D	40	E8	STA	59456
40749	9F2D	A9	F7		LDAIM	247
40751	9F2F	2D	21	E8	AND	59425
40754	9F32	8D	21	E8	STA	59425
40757	9F35	A9	04		LDAIM	4
40759	9F37	OD	40	E8	ORA	59456
40762	9F3A	8 D	40	E8	STA	59456
40765	9F3D	20	A2	9F	JSR	40866
40768	9F40	A9	08		LDAIM	8
40770	9F42	OD	21	E8	ORA	59425
40773	9F45	8D	21	E8	STA	59425
40776	9F48	A9	02		LDAIM	2
40778	9F4A	OD	40	E8	ORA	59456
40781	9F4D	8D	40	E8	STA	59456
40784	9F50	A9	FB		LDAIM	251
40786	9F52	2D	40	E8	AND	59456
40789	9F55	8D	40	E8	STA	59456
40792	9F58	A9	5F		LDAIM	95
40794	9F5A	8D	BD	02	STA	701
40797	9F5D	20	72	9F	JSR	40818
40800	9F60	A9	19		LDAIM	25
40802	9F62	8D	BD	02	STA	701
40805	9F65	20	72	9F	JSR	40818
40808	9F68	A9	04		LDAIM	4
40810	9F6A	OD	40	E8	ORA	59456

PET memory locations Dec.	Hex	Machine code listing			Assembly language listing	
40813	9F6D	8D	40	E8	STA	59456
40816	9F70	60			RTS	
40817	9F71	EA			NOP	
40818	9F72	AD	40	E8	LDA	59456
40821	9F75	29	40		ANDIM	64
40823	9F77	FO	F9		BEQ	249
40825	9F79	AD	BD	02	LDA	701
40828	9F7C	49	FF		EORIM	255
40830	9F7E	8D	22	E8	STA	59426
40833	9F81	A9	F7		LDAIM	247
40835	9F83	2D	23	E8	AND	59427
40838	9F86	8D	23	E8	STA	59427
40841	9F89	AD	40	E8	LDA	59456
40844	9F8C	29	01		ANDIM	1
40846	9F8E	FO	F9		BEQ	249
40848	9F90	A9	08		LDAIM	8
40850	9F92	OD	23	E8	ORA	59427
40853	9F95	8D	23	E8	STA	59427
40856	9F98	A9	FF		LDAIM	255
40858	9F9A	8D	22	E8	STA	59426
40861	9F9D	60			RTS	
40862	9F9E	EA			NOP	
40863	9F9F	EA			NOP	
40864	9FAO	EA			NOP	
40865	9FA1	EA			NOP	
40866	9FA2	A9	02		LDAIM	2
40868	9FA4	OD	40	E8	ORA	59456
40871	9FA7	8D	40	E8	STA	59456
40874	9FAA	AD	40	E8	LDA	59456
40877	9FAD	29	80		ANDIM	128
40879	9FAF	DO	F9		BNE	249
40881	9FB1	AD	20	E8	LDA	59424
40884	9FB4	49	FF		EORIM	255
40886	9FB6	8D	BE	02	STA	702
40889	9FB9	A9	FD		LDAIM	253
40891	9FBB	2D	40	E8	AND	59456
40894	9FBE	8D	40	E8	STA	59456
40897	9FC1	A9	08		LDAIM	8
40899	9FC3	0D	21	E8	ORA	59425

PET memory locations		Machine code listing			Assembly language listing	
Dec.	Hex					
40902	9FC6	8D	21	E8	STA	59425
40905	9FC9	AD	40	E8	LDA	59456
40908	9FCC	29	80		ANDIM	128
40910	9FCE	FO	F9		BEQ	249
40912	9FDO	A9	F7		LDAIM	247
40914	9FD2	2D	21	E8	AND	59425
40917	9FD5	8D	21	E8	STA	59425
40920	9FD8	A9	FF		LDAIM	255
40922	9FDA	8D	22	E8	STA	59426
40925	9FDD	60			RTS	

MAIN ROUTINE

```
LDAIM 251    Load accumulator with 251 immediately (251
             is two's complement of 4 (255-4)).
AND 59456    Logical AND operation between accumulator
             and contents of location 59456.  Accumulator
             becomes contents of 59456 except bit 2 = 0
             regardless.  Bit 2 of 59456 = ATN output.
STA 59456    Store accumulator at 59456 .'. ATN set LOW.
LDAIM 24     Load accumulator with 24 immediately.
STA 701      Store accumulator at 701 (1st cassette buffer).
JSR 40818    Jump to subroutine at 40818 - transmits
             byte stored at 701.  This invokes serial
             poll response.
LDA 700      Load accumulator with contents of 700.
             Location 700 holds device address.
ORAIM 64     Logical OR operation on accumulator adds
             64 to device address to give IEEE talk address.
STA 701      Store accumulator at 701.
JSR 40818    Transmit byte - send IEEE talk address.
LDAIM 253    Load accumulator with 253 immediately.
AND 59456    Accumulator becomes contents of location
             59456 except bit 1 = 0 regardless.  Bit
             1 of 59456 = NRFD output.
STA 59456    Store accumulator at 59456 .'. NRFD set
             LOW.
LDAIM 247    Load accumulator with 247 immediately.
AND 59425    Accumulator becomes contents of location
             59425 except bit 3 = 0 regardless.  Bit
             3 of 59425 = NDAC output.
STA 59425    Store accumulator at 59425 .'. NDAC set
             LOW.
LDAIM 4      Load accumulator with 4 immediately.
ORA 59456    Logical OR operation on accumulator adds
             contents of 59456 to accumulator.  Bit 2
             = 1 regardless.  Bit 2 of 59456 = ATN output.
STA 59456    Store accumulator at 59456 .'. ATN set HIGH
             (i.e. released).
JSR 40866    Jump to subroutine at 40866 - receives byte
             and stores result at location 702.
LDAIM 8      Load accumulator with 8 immediately.
ORA 59425    Accumulator becomes 59425 contents with
             bit 3 = 1 regardless. Bit 3 of 59425 = NDAC
             output.
STA 59425    NDAC set HIGH
LDAIM 2   ┐
ORA 59456 ├─   similarly NRFD set HIGH
STA 59456 ┘    (Bit 1 of 59456).
LDAIM 251 ┐
AND 59456 ├─   Sets ATN i.e. ATN set LOW
STA 59456 ┘
LDAIM 95     Load accumulator with 95 immediately.  95
             is IEEE untalk command.
```

```
STA 701
JSR 40818     Transmit untalk command byte
LDAIM 25
STA 701       Transmit serial poll disable byte
JSR 40818     (25 disables poll)
LDAIM 4
ORA 59456     Releases ATN i.e. ATN set HIGH
STA 59456
RTS           Return to caller (i.e. BASIC)
```

Subroutine at 40818

```
LDA 59456     This loop looks to see if bit 6 (64) of
ANDIM 64      location 59456 is set.  This is NRFD
BEQ 249       input.  If bit 6 = 1 then NRFD = HIGH and
              device ready to receive data.  BEQ 249
              causes code to jump back 7 locations if
              NRFD = LOW still.
LDA 701       Load accumulator with data to transmit.
EORIM 255     Take complement of data because PET "1"
              state corresponds to bus low state and vice-
              versa.
STA 59426     Store complemented data at 59426.  This
              is data bus output location.
LDAIM 247
AND 59427     Sets bit 3 of location 59427 to 0.  This
STA 59427     is DAV output, i.e. DAV set LOW
LDA 59456     This loop looks to see if bit 0 (1) of
ANDIM 1       location 59456 is set.  This is NDAC input.
BEQ 249       If bit 0 = 1 then NDAC = HIGH and data
              has been accepted.
LDAIM 8
ORA 59427     Resets DAV i.e. DAV set HIGH
STA 59427
LDAIM 255     Clears data bus output location (59426)
STA 59426     with nulls.
RTS           Return to call in main routine.
```

Subroutine at 40866

```
LDAIM 2
ORA 59456     Sets bit 1 of location 59456 = 1.  This
STA 59456     is NRFD output location i.e. NRFD set HIGH.
LDA 59456     This loop looks to see if bit 7 (128)
ANDIM 128     of location 59456 = 1.  If it is DAV is
BNE 249       HIGH and BNE loops back until DAV set LOW.
LDA 59424
EORIM 255     Location 59424 is data bus input.  Result
STA 702       is complemented and stored at 702.
LDAIM 253
AND 59456     Sets bit 1 of location 59456 = 0.  This
STA 59456     is NRFD output location i.e. NRFD set LOW.
LDAIM 8
ORA 59425     Sets bit 3 of location 59425 = 1.  This
STA 59425     is NDAC output location i.e. NDAC set HIGH.
```

```
LDA 59456 ┐   This loop looks to see if bit 7 (128) of
ANDIM 128 ├-  location 59456 is set.  This is DAV input.
BEQ 249   ┘   When bit 7 is set DAV = HIGH otherwise
              DAV still LOW.

LDAIM 247 ┐
AND 59425 ├-  Sets bit 3 of 59425 = 0, i.e. NDAC set
STA 59425 ┘   LOW

LDAIM 255 ┐   Clears data bus output location (59426)
STA 59426 ┘   with nulls.
RTS           Return to call in main routine.
```

APPENDIX F

The VSM Control Program

F.1 Introduction

This appendix contains a complete listing of the VSM control program which is capable of conducting both full magnetization loop and detailed coercive field studies. The scope of the software is unfortunately limited by the PET's available RAM for BASIC storage. Indeed, the program as shown here is too long to even be loaded into the PET 4032 and several REM statements (comments) have to be excluded in order for this to be possible. A similar program, therefore, has had to be written to conduct initial magnetization studies. This is not included here.

Although the listing contains many comments throughout, to aid the reading of the same, these are not in sufficient abundance as to make the program intelligible to anyone unfamiliar with the system. To this end, therefore, there is a short section providing additional guidance to the listing immediately after the listing itself. By way of a further example, the procedure followed by the program when conducting a full magnetization loop or a detailed study of the coercive field is shown in flow diagram form in Figures F.1 and F.2.

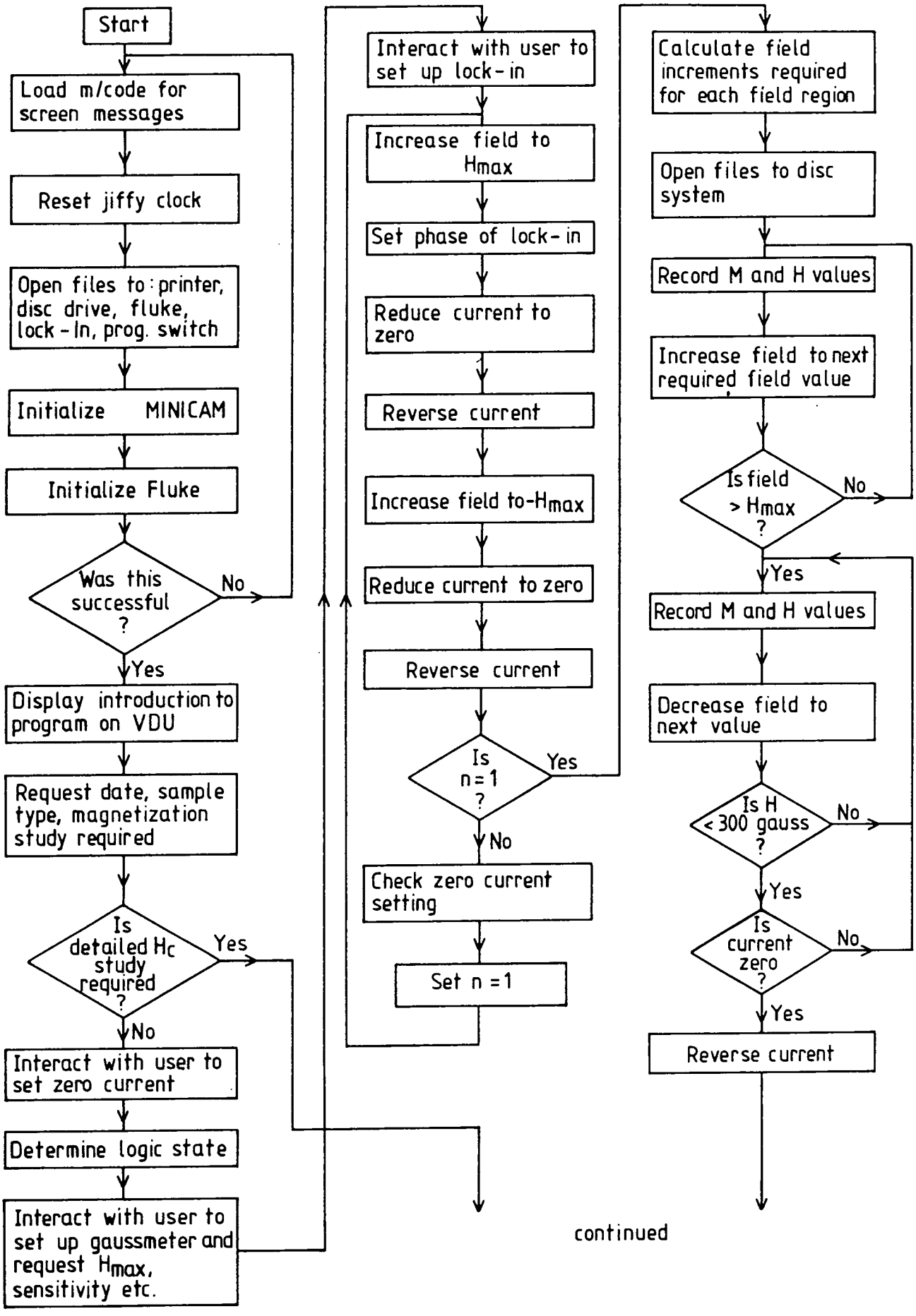

Figure F.1 Part of flow diagram for VSM control program conducting full loop or detailed coercivity study.

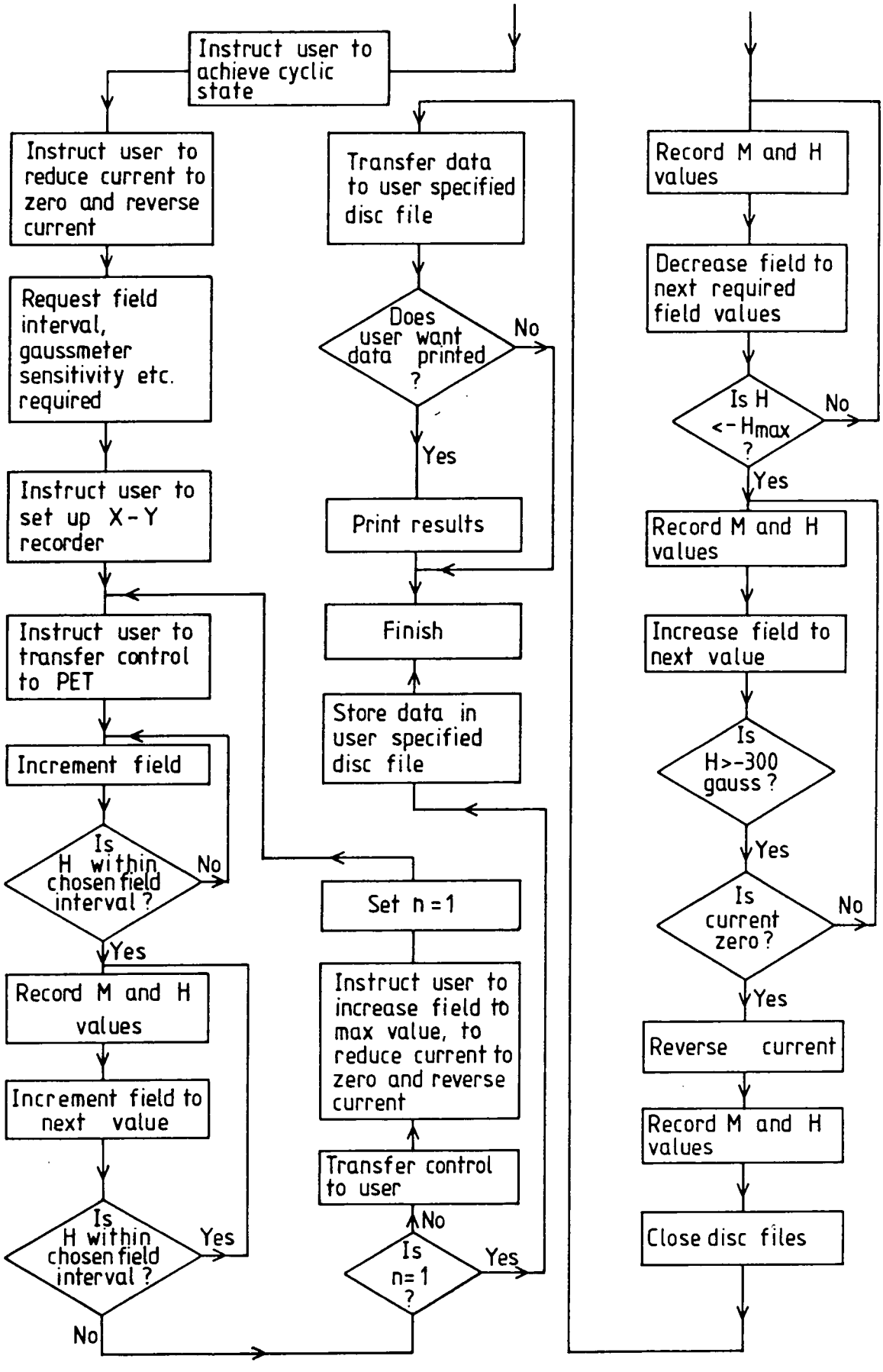

Figure F.2 Part of flow diagram for VSM control program conducting full loop or detailed coercivity study.

```
 1 s%=1:n%=1:t%=1:data 169,5,141,122,2,160,0,140,123,2,162,0,189,
194,2,240
 2 data 7,153,10,128,232,200,208,244,173,123,2,105,40,141,123,2,1
68,232,206,122
 3 data 2,173,122,2,208,226,96:rem machine code routine to displa
y messages
 4 fori=636to678:readab:pokei,ab:next:rem data for screen message
s follows
 5 data*1,160,160,160,160,160,160,160,160,160,160,160,160,160,160
,160,160,160
 6 data160,160,160,0,160,160,160,160,160,210,197,195,207,210,196,
201,206,199,160
 7 data 160,160,160,160,160,00,160,160,160,160,160,160,160,160,16
0,160,160,160,160
 8 data 160,160,160,160,160,160,160,00,160,160,160,205,160,193,20
6,196,160,200,160
 9 data214,193,204,213,197,211,160,160,160,00,160,160,160,160,160
,160,160,160,160
 10 data160,160,160,160,160,160,160,160,160,160,160,00,*2,160,160
,160,160,160,160
 11 data160,160,160,160,160,160,160,160,160,160,160,160,160,160,0
,160,204,207,199
 12 data201,195,160,198,207,210,215,193,210,196,160,160,160,160,1
60,160,0,160,160
 13 data160,160,160,160,160,160,160,160,160,160,160,160,160,160,1
60,160,160,160,0
 14 data160,195,213,210,210,197,206,212,160,201,206,195,210,197,1
93,211,201,206
 15 data199,160,0,160,160,160,160,160,160,160,160,160,160,160,160
,160,160,160,160
 16 data160,160,160,160,0,*3,160,160,160,160,160,160,160,160,160,
160,160,160,160
 17 data160,160,160,160,160,160,160,0,160,204,207,199,201,195,160
,210,197,214,197
 18 data210,211,197,196,160,160,160,160,160,0,160,160,160,160,160
,160,160,160,160
 19 data160,160,160,160,160,160,160,160,160,160,160,0,160,195,213
,210,210,197,206
 20 data212,160,201,206,195,210,197,193,211,201,206,199,160,0,160
,160,160,160,160
 21 data160,160,160,160,160,160,160,160,160,160,160,160,160,160,1
60,0,*4,160,160
 22 data160,160,160,160,160,160,160,160,160,160,160,160,160,160,1
60,160,160,160,0
 23 data160,204,207,199,201,195,160,198,207,210,215,193,210,196,1
60,160,160,160,160
 24 data160,160,0,160,160,160,160,160,160,160,160,160,160,160,160
,160,160,160,160
 25 data160,160,160,160,0,160,195,213,210,210,197,206,212,160,196
,197,195,210,197
 26 data193,211,201,206,199,160,0,160,160,160,160,160,160,160,160
,160,160,160,160
```

```
 27 data160,160,160,160,160,160,160,160,0,*5,160,160,160,160,160,
160,160,160,160,160
 28 data160,160,160,160,160,160,160,160,160,160,160,0,160,204,207
,199,201,195,160
 29 data210,197,214,197,210,211,197,196,160,160,160,160,160,0,160
,160,160,160,160,160
 30 data160,160,160,160,160,160,160,160,160,160,160,160,160,160,1
60,0,160,195,213
 31 data210,210,197,206,212,160,196,197,195,210,197,193,211,201,2
06,199,160,0,160
 32 data160,160,160,160,160,160,160,160,160,160,160,160,160,160,1
60,160,160,160
 33 data160,0
 34 poke141,0:poke142,0:poke143,0:rem setting jiffy clock to zero
 35 open4,4,0:print#4,chr$(27);chr$(96);chr$(27);chr$(48);chr$(00
);
 36 print#4,chr$(27);chr$(80);"                    ";chr$(27);chr$(09)
;
 37 print#4,"                                        ";
 38 print#4,"                                            ";chr$(
27);chr$(00)
 40 open9,9:open10,10:open16,16
 41 rem 4=printer 8=disk drive 9=switch 10=lock-in 16=fluke
 42 poke1,0:poke2,148:a%=1:n%=1:t%=1:rem initialising minicam
 44 poke59468,14
 46 a%=40:n%=0:a=usr(4)
 47 a%=40:n%=8:a=usr(4)
 48 print#16,"*w6t2":rem device clear,suppress eoi+lf,disarms con
tinuous trigger
 50 print"■■■■■■■■■■■■Is the Fluke multimeter showing all     zero
s (y or n)";:inputa$
 51 ifa$="n"thenend
 70 gosub1500:rem "INITIAL WRITTEN INTRODUCTION"
 80 print"■■■■■WELCOME TO THE MAIN PROGRAM"
 90 print"■■■■■■■■■Please enter:"
 100 print"■■■■■■■■■■■■Todays date:";:inputda$
 110 print"■■■■■■■■■■■■Sample type:";:inputsa$
 120 print"■■Coercivity study required (y or n):";:inputa$
 125 ifa$="n"then130
 126 gosub9500
 127 print"■■■Program finished":end
 130 gosub2000:rem "SETTING ZERO CURRENT"
 140 gosub2500:rem "SETTING UP BELL GAUSSMETER"
 150 gosub3000:rem "SETTING UP 5206 LOCK-IN"
 160 gosub4000:rem "CHECKING CYCLIC STATE,PHASE AND ZERO CURRENT"
 170 g1=h2/n1:g2=(h3-h2)/n2:g3=(hm-h3)/n3
 180 s1=int(g1/3/10):s2=int(g2/3/10):s3=int(g3/3/10)
 181 rem allows at least 10 steps between each required field val
ue
 182 ifg1<3theng1=3:rem smallest field increment possible
 183 ifg2<3theng2=3
 184 ifg3<3theng3=3
 190 ifs1<1thens1=1
 191 ifs2<1thens2=1
```

```
192 ifs3<1thens3=1
200 tn=(n1+n2+n3)*4:tn=tn+n1+50:rem tn=total no. of readings
210 open11,8,11,"@1:M Values,s,w":open12,8,12,"@1:H Values,s,w"
211 open13,8,13,"@1:EM Values,s,w":open14,8,14,"@1:EH Values,s,w
"
212 rem em and eh are errors in m & h
220 h1=g1:ss=s1
224 gosub7000:rem taking readings
226 h=h9
228 goto240
230 gosub7000:rem taking readings
240 ifh9>h2then280
250 h=h+h1
260 gosub5000
270 goto230
280 h1=g2:ss=s2
290 h=h+h1
300 gosub5000
310 gosub7000
320 ifh9>h3then340
330 goto290
340 h1=g3:ss=s3
350 h=h+h1
360 gosub5000
370 gosub7000
380 ifh9>hmthen400
390 goto350
400 h=h-h1
410 gosub6000
420 gosub7000
425 ifb$="Changeover needed"then570
430 ifh9<h3then450
440 goto400
450 h1=g2:ss=s2
460 h=h-h1
470 gosub6000
480 gosub7000
485 ifb$="Changeover needed"then570
490 ifh9<h2then510
500 goto460
510 h1=g1:ss=s1
520 h=h-h1
530 gosub6000
540 gosub7000
550 ifb$="Changeover needed"then570
560 goto520
570 b$="":h1=g1:ss=s1:gosub9000
580 gosub7000
590 ifh9<-h2then630
600 h=h-h1
610 gosub5500
620 goto580
630 h1=g2:ss=s2
640 h=h-h1
```

```
 650 gosub5500
 660 gosub7000
 670 ifh9<-h3then690
 680 goto640
 690 h1=g3:ss=s3
 700 h=h-h1
 710 gosub5500
 720 gosub7000
 730 ifh9<-hmthen750
 740 goto700
 750 h=h+h1
 760 gosub6500
 770 gosub7000
 775 ifb$="Changeover needed"then920
 780 ifh9>-h3then800
 790 goto750
 800 h1=g2:ss=s2
 810 h=h+h1
 820 gosub6500
 830 gosub7000
 835 ifb$="Changeover needed"then920
 840 ifh9>-h2then860
 850 goto810
 860 h1=g1:ss=s1
 870 h=h+h1
 880 gosub6500
 890 gosub7000
 900 ifb$="Changeover needed"then920
 910 goto870
 920 b$="":h1=g1:ss=s1:gosub9000
 930 gosub7000
 940 ifh9>100then980
 950 h=h+h1
 960 gosub5000
 970 goto930
 980 print"■■■■■M-H data taking finished"
 990 print"■■■■■■■■■■■■■■■■■■■■■■■■■■( hit space bar to continue )"
 1000 print#4,chr$(07);:b=ti
 1010 ifti-b<60then1010
 1020 geta$:ifa$=""then1000
 1025 close11:close12:close13:close14
 1026 open11,8,11,"1:M Values,s,r":open12,8,12,"1:H Values,s,r"
 1027 open13,8,13,"1:EM Values,s,r":open14,8,14,"1:EH Values,s,r"
 1030 print"■■■■■■■Enter name of file to be created■■■■■■■■ on dis
k 1:";:inputf$
 1035 print"■■■■■Do you wish to store the standard errors ( y or n
 ):";:inputa$
 1036 ifa$="y"then1092
 1040 open8,8,8,"1:"+f$+",s,w"
 1050 rd$=sa$+" M-H loop data: "+da$
 1060 print#8,rd$chr$(13)y
 1070 fori=1toy
 1075 input#11,m:input#12,h:input#13,em:input#14,eh
 1080 print#8,hchr$(13)m
```

```
 1090 nexti
 1091 goto1098
 1092 open8,8,8,"1:"+f$+",s,w"
 1093 rd$=sa$+" M-H loop data & std. errors: "+da$
 1094 print#8,rd$chr$(13)y
 1095 fori=1toy:input#11,m:input#12,h:input#13,em:input#14,eh
 1096 print#8,hchr$(13)ehchr$(13)mchr$(13)em
 1097 nexti
 1098 close11:close12:close13:close14
 1100 print#10,"w 0":rem returns lock-in to local mode
 1110 b=ti
 1120 ifti-b<60then1120
 1130 print"■■Do you wish to list results on printer  ( y or n )
:";:inputa$
 1140 ifa$="n"then1230
 1141 open11,8,11,"1:M Values,s,r":open12,8,12,"1:H Values,s,r"
 1142 open13,8,13,"1:EM Values,s,r":open14,8,14,"1:EH Values,s,r"
 1145 print#4,"                ";rd$:print#4,"":print#4,""
 1150 print#4,"      ";chr$(27);chr$(01);"H values (gauss)  ";chr$
(27);chr$(01);
 1160 print#4,"Std. error eh       ";chr$(27);chr$(01);"M values (
volts)  ";
 1170 print#4,chr$(27);chr$(01);"Std. error em  "
 1180 print#4,"-----------------------------------------";
 1190 print#4,"-----------------------------------------"
 1191 print#4,"":print#4,""
 1200 fori=1toy
 1205 input#11,m:input#12,h:input#13,em:input#14,eh
 1210 print#4,chr$(09);h;chr$(09);eh;chr$(09);m;chr$(09);em
 1220 nexti
 1230 print#16,"*":close4:close8:close9:close10:close16
 1235 close11:close12:close13:close14
 1240 print"■■■■Program finished"
 1250 end
 1500 rem
 1501 rem*****************************************************************
****************
 1502 rem
 1503 rem
 1505 rem "INITIAL WRITTEN INTRODUCTION"
 1506 rem
 1507 rem
 1508 rem*****************************************************************
****************
 1509 rem
 1511 print"■■*******************************************";
 1512 print"*                                             *";
 1513 print"*   PROGRAM FOR AUTOMATED DATA TAKING         *";
 1514 print"*                 ON THE VSM                  *";
 1515 print"*                                             *";
 1516 print"*  copyright S.N.M.WILLCOCK July 1983          *";
 1517 print"*                                             *";
 1518 print"*********************************************"
 1520 print"■■This program will control the operationof and take
```

```
data from the ";
 1530 print"VSM and        Newport Power Supply system."
 1535 print""
 1540 print"■■■Before continuing please make sure    that you are
fully familiar ";
 1550 print"with the    operation of the Newport Power Supply   a
nd the other ";
 1560 print"items of apparatus         associated with the VSM."
 1570 print"■IMPORTANT: PLEASE NOTE THAT THE MAIN    REVERSING RE
LAY WILL NOT TAKE ";
 1580 print"A CURRENT OF 20 AMPS FOR MORE THAN HALF AN HOUR."
 1590 print"■■■(hit space bar to continue)";
 1600 geta$:ifa$=""then1600
 1601 ifasc(a$)<>32then1600
 1610 print"■■■The program assumes that the Bell     gaussmeter i
s set initially ";
 1620 print"and remains unaltered throughout the experiment. Allo
ther peripherals ";
 1630 print"are under computer    control."
 1640 print"■■■The operator must decide the maximum  external fie
ld ( Hext ) ";
 1650 print"that he/she     wishes to obtain and must select the
   appropriate ";
 1660 print"scale on the gaussmeter."
 1670 print"■■■The program will allow the operator tosplit the ra
nge from 0 ";
 1680 print"to Hext gauss    into three regions and to specify th
e   density at ";
 1690 print"which readings are taken in  each of these regions. T
he smallest ";
 1700 print"stepin field available with the present     system is
 3 gauss."
 1710 print"■■■The function settings on the 5206 Lock-In amplifie
r as selected ";
 1720 print"by the program can be displayed and altered if
 required."
 1730 print"■■■■■(hit space bar to continue)";
 1740 geta$:ifa$=""then1740
 1741 ifasc(a$)<>32then1740
 1750 print"■■■The M-H data will be stored on disk atthe end of t
he program,";
 1760 print" so please ensurethat a suitable disk is placed in dr
ive 1 of the ";
 1761 print"disk drive."
 1770 print"■■■The values of M are taken to be the   value of Cha
nnel 1 of the ";
 1780 print"5206 and thesereadings are stored on disk in units of
 volts."
 1790 print"■■■Before launching into the MAIN PROGRAMallow the Be
ll gaussmeter,";
 1800 print" the 5206 Lock-In and the Newport Power Supply ( with
 generator ";
 1810 print"running under manual control )at least half an hour t
o warm up."
```

```
 1815 print"■■■Make sure that the gaussmeter is on   centre zero
scale and is set ";
 1816 print"to the NOR setting. Also please ensure that the    Ha
ll probe is always ";
 1817 print"inserted with the +marking facing the coil connected
to    the BLACK ";
 1818 print"supply lead."
 1820 print"■K hit space bar to launch into MAIN     PROGRAM )";
 1830 geta$:ifa$=""then1830
 1840 ifasc(a$)<>32then1830
 1850 return
 2000 rem
 2001 rem*****************************************************************
****************
 2002 rem
 2003 rem
 2005 rem "SETTING ZERO CURRENT"
 2006 rem
 2007 rem
 2008 rem*****************************************************************
****************
 2009 rem
 2010 print"■■■■SETTING ZERO CURRENT"
 2011 print#9,"+1":rem +1 means fluke reads voltage across shunt
resistor
 2020 print"■■■■Adjust the lockable potentiometer on the Newport
 Supply until ";
 2030 print"a reading of    less than 0.005 mV is obtained on the
  Fluke ";
 2040 print"Multimeter."
 2050 print"■■■Make sure that the Logic and Current  are in the F
ORWARD state and ";
 2060 print"that all   connections from the Newport Control    Un
it to the Minicam ";
 2070 print"are made."
 2080 print"■■■SWITCH TO COMPUTER CONTROL"
 2090 print"■■■■K hit space bar to continue )"
 2095 gosub8000:rem trigger fluke externally
 2100 geta$:ifa$=""then2095
 2200 ifasc(a$)<>32then2095
 2201 b=ti:print"■"
 2202 ifti-b<60then2202
 2210 print#9,"-1":rem -1 means fluke reads voltage o/p from bell
gaussmeter
 2220 a%=12:c=usr(5):ifabs(c)>1000thenlo$="Forward":goto2300
 2230 lo$="Reversed"
 2300 return
 2500 rem
 2501 rem*****************************************************************
****************
 2502 rem
 2503 rem
 2505 rem "SETTING UP BELL GAUSSMETER"
 2506 rem
```

```
 2507 rem
 2508 rem*****************************************************************
**************
 2509 rem
 2510 print"SCC■■■SETTING UP BELL GAUSSMETER"
 2511 print#9,"-1"
 2520 print"CC■■Adjust the calibration of the          gaussmeter
until a reading ";
 2530 print"of 1.000 V isobtained on the Fluke."
 2540 print"C■■Place the Hall probe into the zero    gauss chambe
r and set the ";
 2550 print"output to zerousing the zero adjust controls. Make
 sure that the";
 2560 print" coarse zero suppression   switch is OFF."
 2565 print"C■■Turn coarse zero suppression switch to0 position a
nd note reading on";
 2566 print" Fluke."
 2570 print"C■Does reading equal zero volts (y or n)?":rem antici
pating zero offset
 2575 gosub8000
 2580 geta$:ifa$=""then2575
 2590 ifa$="y"then2610
 2600 print"C■Enter zero offset of                    gaussmete
r (volts):";:inputx1
 2610 print"SC■Please enter:"
 2620 print"CC■■Selected range of gaussmeter
  ( in gauss ):";
 2630 inputg0
 2640 ifint(g0/3)*3=g0theng0=g0/3*sqr(10)
 2650 print"CC■■Maximum Hext required:";:inputhm
 2660 print"CCValues for boundaries between field   regions 1 &
 2 and 2 & 3:";
 2670 inputh2,h3
 2680 print"CCNo. of equally spaced readings to be    taken in re
gions 1,2 & 3:";
 2690 inputn1,n2,n3
 2700 print"CCCC■■Do you wish to check this data
( y or n ):";
 2710 inputa$:ifa$="n"then2850
 2720 print"SCC■■Maximum Hext  :"
 2725 print"C■■■■■■■■■"hm"gauss
 2730 print"CC■■Values for boundaries:"
 2735 print"C■■■■■■■■■"h2"&"h3"gauss"
 2740 print"CC■■No. of readings in regions:"
 2745 print"C■■■■■■■■■"n1","n2"&"n3
 2750 print"CCCCCCCC■■Any alterations ( y or n ):";
 2780 inputa$:ifa$="y"then2610
 2850 return
 3000 rem
 3001 rem*****************************************************************
**************
 3002 rem
 3003 rem
 3005 rem "SETTING UP 5206 LOCK-IN AMPLIFIER"
```

```
 3006 rem
 3007 rem
 3008 rem*****************************************************************
****************
 3009 rem
 3010 print"■■■SETTING UP 5206 LOCK-IN AMPLIFIER"
 3020 print"■■■■■Please press the SENSITIVITY key      briefly whi
le the SELECT key ";
 3030 print"is pressed to perform a device clear."
 3040 print"■■■■■( hit space bar to continue )"
 3050 geta$:ifa$=""then3050
 3060 ifasc(a$)<>32then3050
 3070 print"■■■■The front panel keys have now been     disabled"
 3080 print"■■The 5206 is being initialised and set to predeterm
ined function ";
 3085 print"settings."
 3090 print#10,"c 13":b=ti:rem defining carriage return as termin
ator
 3095 ifti-b<60then3095
 3100 print#10,"t 5,0":b=ti:rem setting time constant & db/octave
 3105 ifti-b<60then3105
 3110 print#10,"a1 1":b=ti:rem auto-range on
 3111 ifti-b<60then3111
 3112 print#10,"l 17":b=ti:rem setting auto-limit
 3113 ifti-b<60then3113
 3114 print#10,"w 1":b=ti:rem disabling front key controls
 3115 ifti-b<60then3115
 3121  l0$="CH1":l1$="Zero and off":l2$="High stab":l3$="Audio":l4
$="Ext. F"
 3122  l5$="0 degrees":l6$="300 ms":l7$="12":l8$="any":l9$="Autora
nge":i0$="X,Y"
 3123 i1$="Off":i2$="10 microvolts"
 3130 print"■■■■Do you wish to inspect these
    ( y or n ):";
 3131  l0$="CH1":l1$="Zero and off":l2$="High stab":l3$="Audio":l4
$="Ext. F"
 3132  l5$="0 degrees":l6$="300 ms":l7$="12":l8$="any":l9$="Autora
nge":i0$="X,Y"
 3133 i1$="Off":i2$="10 microvolts"
 3135 inputa$:ifa$="n"then3999
 3140 print"■■■Display          : ";l0$
 3150 print"■■CH1 Offset       : ";l1$
 3160 print"■■Reserve          : ";l2$
 3170 print"■■Fband            : ";l3$
 3180 print"■■Reference        : ";l4$
 3190 print"■■Phase            : ";l5$
 3200 print"■■Time constant    : ";l6$
 3210 print"■■dB/octave        : ";l7$
 3220 print"■■Sensitivity      : ";l8$
 3230 print"■■Auto-Functions   : ";l9$
 3240 print"■■Output mode      : ";i0$
 3250 print"■■Expand           : ";i1$
 3260 print"■■Auto-limit       : ";i2$
 3270 print"■■■■How many of these functions do you    wish to al
```

```
ter ( 0-13 ):";
 3280 inputn:ifn=0then3999
 3290 fori=1ton
 3300 print"S■■(1) Display          : ";l0$
 3301 print"■■(2) CH1 Offset       : ";l1$
 3302 print"■■(3) Reserve          : ";l2$
 3303 print"■■(4) Fband            : ";l3$
 3304 print"■■(5) Reference        : ";l4$
 3305 print"■■(6) Phase            : ";l5$
 3306 print"■■(7) Time constant    : ";l6$
 3307 print"■■(8) dB/octave        : ";l7$
 3308 print"■■(9) Auto-Functions   : ";l9$
 3309 print"■■(10) Sensitivity     : ";l8$
 3310 print"■■(11) Output mode     : ";i0$
 3311 print"■■(12) Expand          : ";i1$
 3312 print"■■(13) Auto-limit      : ";i2$
 3320 print"■■■■■Which of these do you wish to alter    ( 1-13 ):
";:inputn4
 3321 rem possible options for each function follow
 3322 ifn4>1then3326
 3324 a0$(0)="CH1":a0$(1)="CH2":a0$(2)="PHASE":a0$(3)="CH1 Offset
"
 3325 a0$(4)="Int. freq":a0$(5)="Aux":n5=5:goto3380
 3326 ifn4>2then3330
 3328 a0$(0)="0-1000 for N1                                    and 0-2 fo
r N2":n5=0
 3329 goto3380
 3330 ifn4>3then3334
 3332 a0$(0)="High res":a0$(1)="Normal":a0$(2)="High stab":n5=2:g
oto3380
 3334 ifn4>4then3338
 3336 a0$(0)="Broad band":a0$(1)="Audio":a0$(2)="Low":n5=2:goto33
80
 3338 ifn4>5then3342
 3340 a0$(0)="100-1000 for N1                                  and 0-7 fo
r N2":n5=0
 3341 goto3380
 3342 ifn4>6then3346
 3344 a0$(0)="0-3 for N1 and                                   100-3900 f
or N2":n5=0
 3345 goto3380
 3346 ifn4>7then3350
 3348 a0$(0)="0-10 for N1 and                                  0-1 for N2
":n5=0:goto3380
 3350 ifn4>8then3354
 3352 a0$(0)="0-10 for N1 and                                  0-1 for N2
":n5=0:goto3380
 3354 ifn4>9then3358
 3356 a0$(0)="Autoset":a0$(1)="Auto-offset":a0$(2)="Autonormalise
"
 3357 a0$(3)="Autophase":a0$(4)="All off":n5=4:goto3380
 3358 ifn4>10then3362
 3360 a0$(0)="0-20 for N":n5=0:goto3380
 3362 ifn4>11then3366
```

```
 3364 a0$(0)="X,Y":a0$(1)="R,Theta":a0$(2)="logR,Theta"
 3365 a0$(3)="X,Y ( phase locked )":n5=3:goto3380
 3366 ifn4>12then3370
 3368 a0$(0)="Off":a0$(1)="On":n5=1:goto3380
 3370 a0$(0)="0-20 for N":n5=0
 3380 print"S■■■■■■■Options are:■■■"
 3390 ifn5=0then3410
 3400 print"■■■■■N■■■■■■■■■■■■Option■■"
 3410 forj=0ton5
 3420 print"■■■j"■■■■■■■■■■"a0$(j)
 3430 nextj
 3440 ifn4=2then3450
 3441 ifn4=5then3450
 3442 ifn4=6then3447
 3443 ifn4=7then3450
 3444 ifn4=8then3450
 3446 print"■■■Enter required value for N:";:inputn6$:goto3460
 3447 print"■■■Enter required phase in degrees:";:inputp$
 3448 n6$=str$(int(val(p$)/90)):n7$=str$((40*val(p$))-(3600*val(n
6$))+200)
 3449 goto3460
 3450 print"■■■Enter required values for N1                    and
 N2:";:inputn6$,n7$
 3455 rem selecting correct message to send to lock-in for requir
ed setting
 3460 ifn4<>9then3470
 3461 ifn6$="0"thenn6=val(n6$):l9$=a0$(n6):n6$="a2 1":goto3470
 3462 ifn6$="1"thenn6=val(n6$):l9$=a0$(n6):n6$="a3":goto3470
 3463 ifn6$="2"thenn6=val(n6$):l9$=a0$(n6):n6$="a4 1":goto3470
 3464 ifn6$="3"thenn6=val(n6$):l9$=a0$(n6):n6$="a7":goto3470
 3465 ifn6$="4"thenn6=val(n6$):l9$=a0$(n6):n6$="a1 0"
 3470 ifn4>1then3480
 3475 n6=val(n6$):l0$=a0$(n6):n6$="d "+n6$:goto3900
 3480 ifn4>2then3490
 3485 l1$="Ranges "+n6$+" and "+n7$:n6$="o "+n6$+","+n7$:goto3900
 3490 ifn4>3then3500
 3495 n6=val(n6$):l2$=a0$(n6):n6$="r "+n6$:goto3900
 3500 ifn4>4then3510
 3505 n6=val(n6$):l3$=a0$(n6):n6$="f "+n6$:goto3900
 3510 ifn4>5then3520
 3515 l4$="Ranges "+n6$+" and "+n7$:n6$="j "+n6$+","+n7$:goto3900
 3520 ifn4>6then3530
 3525 l5$=" "+p$:n6$="p "+n6$+","+n7$:goto3900
 3530 ifn4>7then3540
 3535 l6$="Range "+n6$:n6$="t "+n6$+","+n7$:goto3900
 3540 ifn4>8then3550
 3545 l7$="Range "+n7$:n6$="t "+n6$+","+n7$:goto3900
 3550 ifn4>9then3560
 3555 goto3900
 3560 ifn4>10then3570
 3565 l8$="Range "+n6$:n6$="s "+n6$:goto3900
 3570 ifn4>11then3580
 3575 n6=val(n6$):i0$=a0$(n6):n6$="m "+n6$:goto3900
 3580 ifn4>12then3590
```

```
 3585 n6=val(n6$):i1$=a0$(n6):n6$="x "+n6$:goto3900
 3590 i2$="Range "+n6$:n6$="l "+n6$
 3900 print#10,n6$:rem sending correct setting message
 3910 nexti
 3920 print"■■Are the function settings                    now co
rrect ( y or n ):";
 3930 inputa$:ifa$="n"then3140
 3999 return
 4000 rem
 4001 rem*****************************************************************
****************
 4002 rem
 4003 rem
 4005 rem "CHECKING CYCLIC STATE AND PHASE OF 5206"
 4006 rem
 4007 rem
 4008 rem*****************************************************************
****************
 4009 rem
 4010 print"■■CHECKING CYCLIC STATE AND PHASE OF 5206"
 4020 print"■■■■Place Hall probe in field gap."
 4030 print"■■■■Place sample in VSM and switch motor on."
 4040 print"■■■■■( hit space bar to continue )"
 4050 geta$:ifa$=""then4050
 4060 ifasc(a$)<>32then4050
 4070 print"■■■■The program is checking for a cyclic  state and
reducing CH2 ";
 4080 print"output to zero byaltering the phase."
 4090 print#9,"-1"
 4091 b=ti
 4092 gosub8000
 4093 ifti-b<120then4092
 4100 a%=46:n%=150:t%=1:a=usr(1):rem increasing current
 4110 b=ti
 4120 ifti-b<60then4120
 4140 gosub8000
 4150 h0=(val(a$)-x1)*g0:rem h0=field value (gauss)
 4160 ifh0<hmthen4100
 4170 print#10,"d 1":rem display channel 2
 4180 b=ti
 4190 ifti-b<600then4190
 4200 poke700,10:rem device address
 4202 print#10,"z":rem request for status - reply = 32 if lock-in
 settled
 4204 sys40714:ifpeek(702)=160then4208:rem m/code serial poll + r
esponse
 4205 ifpeek(702)=144then4208
 4206 ifpeek(702)=176then4208
 4207 ifpeek(702)<>128then4204:rem serial poll result
 4208 input#10,a$:ifst<>64then4208
 4220 ifval(a$)=32then4230
 4222 if19$="Autorange"then4180
 4223 print#10,"a2 0":b=ti:rem autoset off
 4224 ifti-b<60then4224
```

```
 4225 print#10,"a4 0":b=ti:rem autonormalise off
 4226 ifti-b<60then4226
 4227 print#10,"a1 1":rem autorange on
 4228 goto4180
 4230 print#10,"a1 0":rem autorange off
 4240 b=ti
 4250 ifti-b<60then4250
 4255 print"■■Autophasing required:";:inputph$:ifph$="n"then4380
 4260 fori=1to20
 4270 poke700,10:rem device address
 4272 print#10,"q2":rem reading channel 2
 4274 sys40714:ifpeek(702)=160then4278:rem m/code serial poll + r
esponse
 4275 ifpeek(702)=144then4278
 4276 ifpeek(702)=176then4278
 4277 ifpeek(702)<>128then4274:rem serial poll result
 4278 input#10,a$:ifst<>64then4278
 4290 q2=q2+val(a$)
 4300 nexti
 4305 goto4380
 4310 q2=q2/20:ifabs(q2)<5then4380
 4320 q2=0:b=ti
 4330 ifti-b<60then4330
 4340 print#10,"a7":rem autophasing
 4350 b=ti
 4360 ifti-b<360then4360
 4370 goto4260
 4380 b=ti
 4390 ifti-b<60then4390
 4430 print#10,"d 0":rem display channel 1
 4440 a%=47:n%=150:t%=1:a=usr(1):rem decreasing current
 4450 b=ti
 4460 ifti-b<60then4460
 4480 gosub8000
 4490 h0=(val(a$)-x1)*g0
 4500 ifh0>g0/10then4440
 4510 print#9,"+1"
 4515 b=ti
 4520 gosub8000
 4530 ifti-b<120then4520
 4550 gosub8000
 4560 ifval(a$)>0.05e-3then4440
 4570 gosub9000
 4575 print"■■CHECKING CYCLIC STATE AND PHASE OF 5206"
 4580 ifph=1then4890
 4590 fori=1to1
 4600 print#9,"-1"
 4610 b=ti
 4620 gosub8000
 4630 ifti-b<120then4620
 4640 a%=46:n%=150:t%=1:a=usr(1):rem increasing current
 4650 b=ti
 4660 ifti-b<60then4660
 4680 gosub8000
```

```
 4690 h0=(val(a$)-x1)*g0
 4700 ifabs(h0)<hmthen4640
 4710 a%=47:n%=150:t%=1:a=usr(1):rem decreasing current
 4720 b=ti
 4730 ifti-b<60then4730
 4750 gosub8000
 4760 h0=(val(a$)-x1)*g0
 4770 ifabs(h0)>g0/10then4710
 4780 print#9,"+1"
 4790 b=ti
 4800 gosub8000
 4810 ifti-b<120then4800
 4830 gosub8000
 4840 ifval(a$)>0.05e-3then4710
 4850 gosub9000
 4855 print"■■CHECKING CYCLIC STATE AND PHASE OF 5206"
 4860 nexti
 4870 ifph=2then4986
 4880 ph=1:goto4090
 4890 print"■■■■CHECKING ZERO CURRENT"
 4900 print"■■■■■■■Readjust the set zero potentiometeruntil a rea
ding of less ";
 4910 print"than 0.005 mV isobtained on the Fluke Multimeter."
 4915 print"■■■■■■■■( hit space bar to continue )"
 4920 print#9,"+1"
 4955 print#4,chr$(07);:gosub8000
 4965 geta$:ifa$=""then4955
 4970 ifasc(a$)<>32then4955
 4975 print"■■■■■■Readings of M and H will be taken      after anot
her couple of ";
 4980 print"cycles."
 4985 ph=2:goto4590
 4986 if19$<>"Autorange"then4988
 4987 print#10,"a1 1":rem autorange on if required
 4988 b=ti
 4989 ifti-b<60then4989
 4990 return
 5000 rem
 5001 rem*****************************************************************
****************
 5002 rem
 5003 rem
 5005 rem increasing current to known h value
 5006 rem
 5007 rem
 5008 rem*****************************************************************
****************
 5009 rem
 5010 print#9,"-1"
 5011 print"■■■■■■■■■■■"
 5012 restore
 5015 fori=1to1e6:reada$:ifa$<>"*2"thennext
 5017 fori=706to706+104:readab:pokei,ab:next
 5018 sys636:rem screen message
```

```
 5020 b=ti
 5025 gosub8000
 5030 ifti-b<120then5025
 5040 a%=46:n%=ss:t%=1:a=usr(1):rem increasing current
 5041 b=ti
 5042 ifti-b<5then5042
 5050 gosub8000
 5060 h0=(val(a$)-x1)*g0:printh0:sys636
 5070 ifabs(h0)>g0*1.3thengosub10000:rem failure protection
 5075 ifabs(h0)>12500thengosub10000:rem failure protection
 5076 ifh0-h<0then5040
 5080 return
 5500 rem
 5501 rem************************************************************
***************
 5502 rem
 5503 rem
 5505 rem increasing current to known h value after changeover
 5506 rem
 5507 rem
 5508 rem************************************************************
***************
 5509 rem
 5510 print#9,"-1"
 5511 print"S[10 cursor-right]"
 5512 restore
 5515 fori=1to1e6:reada$:ifa$<>"*3"thennext
 5517 fori=706to706+104:readab:pokei,ab:next
 5518 sys636:rem screen message
 5520 b=ti
 5525 gosub8000
 5530 ifti-b<120then5525
 5540 a%=46:n%=ss:t%=1:a=usr(1):rem increasing current
 5541 b=ti
 5542 ifti-b<5then5542
 5550 gosub8000
 5560 h0=(val(a$)-x1)*g0:printh0:sys636
 5570 ifabs(h0)>g0*1.3thengosub10000:rem failure protection
 5575 ifabs(h0)>12500thengosub10000:rem failure protection
 5576 ifh0-h>0then5540
 5580 return
 6000 rem
 6001 rem************************************************************
***************
 6002 rem
 6003 rem
 6005 rem decreasing current to known h value
 6006 rem
 6007 rem
 6008 rem************************************************************
***************
 6009 rem
 6010 print#9,"-1"
 6011 print"S[10 cursor-right]"
```

```
 6012 restore
 6015 fori=1to1e6:reada$:ifa$<>"*4"thennext
 6017 fori=706to706+104:readab:pokei,ab:next
 6018 sys636:rem screen message
 6020 b=ti
 6025 gosub8000
 6030 ifti-b<120then6025
 6040 a%=47:n%=ss:t%=1:a=usr(1):rem decreasing current
 6041 b=ti
 6042 ifti-b<5then6042
 6050 gosub8000
 6060 h0=(val(a$)-x1)*g0:printh0:sys636
 6065 rem lines 6070-6160 test to see if changeover likely or nec
essary
 6070 n0=n0+1:ifn0=10then6086
 6080 ifabs(h0)>g0*1.3thengosub10000:rem failure protection
 6081 ifabs(h0)>12500thengosub10000:rem failure protection
 6082 ifh0>hthen6040
 6085 goto6170
 6086 ifabs(h0)<300then6090
 6087 n0=0:ifh0>hthen6040
 6088 goto6170
 6090 print#9,"+1":n0=0
 6100 b=ti
 6105 gosub8000
 6110 ifti-b<120then6105
 6120 gosub8000
 6130 printa$:sys636:ifval(a$)<0.05e-3then6160:rem condition for
changeover
 6140 ifh0>hthen6010
 6150 goto6170
 6160 b$="Changeover needed"
 6170 return
 6500 rem
 6501 rem*****************************************************************
***************
 6502 rem
 6503 rem
 6505 rem decreasing current to known h value after changeover
 6506 rem
 6507 rem
 6508 rem*****************************************************************
***************
 6509 rem
 6510 print#9,"-1"
 6511 print"S[redacted]"
 6512 restore
 6515 fori=1to1e6:reada$:ifa$<>"*5"thennext
 6517 fori=706to706+104:readab:pokei,ab:next
 6518 sys636:rem screen message
 6520 b=ti
 6525 gosub8000
 6530 ifti-b<120then6525
 6540 a%=47:n%=ss:t%=1:a=usr(1):rem decreasing current
```

```
 6541 b=ti
 6542 ifti-b<5then6542
 6550 gosub8000
 6560 h0=(val(a$)-x1)*g0:printh0:sys636
 6565 rem lines 6570-6660 test to see if changeover likely or nec
essary
 6570 n0=n0+1:ifn0=10then6586
 6580 ifabs(h0)>g0*1.3thengosub10000:rem failure protection
 6581 ifabs(h0)>12500thengosub10000:rem failure protection
 6582 ifh0<hthen6540
 6585 goto6670
 6586 ifabs(h0)<300then6590
 6587 n0=0:ifh0<hthen6540
 6588 goto6670
 6590 print#9,"+1":n0=0
 6600 b=ti
 6605 gosub8000
 6610 ifti-b<120then6605
 6620 gosub8000
 6630 printa$:sys636:ifval(a$)<0.05e-3then6660:rem condition for
changeover
 6640 ifh0<hthen6510
 6650 goto6670
 6660 b$="Changeover needed"
 6670 return
 7000 rem
 7001 rem*****************************************************************
****************
 7002 rem
 7003 rem
 7005 rem recording m and h values
 7006 rem
 7007 rem
 7008 rem*****************************************************************
****************
 7009 rem
 7010 print#9,"-1":y=y+1:q1=0:h9=0:em=0:eh=0:rem y=no. of reading
s so far
 7011 print"ssssssssssss"
 7012 restore
 7013 fori=1to10:h9(i)=0:q1(i)=0:next
 7015 fori=1to1e6:reada$:ifa$<>"*1"thennext
 7017 fori=706to706+104:readab:pokei,ab:next
 7018 sys636:rem screen message
 7020 b=ti
 7025 gosub8000
 7030 ifti-b<300then7025
 7040 poke700,10:rem device address
 7042 print#10,"z"
 7044 sys40714:rem m/code serial poll
 7045 ifpeek(702)=160then7050
 7046 ifpeek(702)=144then7050
 7047 ifpeek(702)=176then7050
 7048 ifpeek(702)<>128then7044:rem serial poll result
```

```
 7050 input#10,a$:ifst<>64then7050
 7060 ifval(a$)<>32then7020
 7070 poke700,10:rem device address
 7072 print#10,"s":rem request for sensitivity setting
 7074 sys40714:ifpeek(702)=160then7078:rem m/code serial poll + r
esponse
 7075 ifpeek(702)=144then7078
 7076 ifpeek(702)=176then7078
 7077 ifpeek(702)<>128then7074:rem serial poll result
 7078 input#10,a$:ifst<>64then7078
 7085 rem lines 7090-7094 calculate sensitivity
 7090 x2=val(a$)
 7091 z4=x2-(int(x2/3)*3)+1
 7092 ifz4=1thenz4=5
 7093 ifz4=3thenz4=1
 7094 z4=(10^(-(int(x2/3))))*z4
 7095 b=ti
 7096 ifti-b<60then7096
 7100 fori=1to10
 7110 gosub8000
 7120 h9(i)=(val(a$)-x1)*g0:printh9(i):sys636:rem h9(i)=field val
ue
 7125 poke700,10:rem device address
 7130 print#10,"q1":rem reading channel 1
 7135 sys40714:rem m/code serial poll
 7136 ifpeek(702)=160then7140:rem serial poll result
 7137 ifpeek(702)=144then7140
 7138 ifpeek(702)=176then7140
 7139 ifpeek(702)<>128then7135
 7140 input#10,a$:ifst<>64then7140
 7145 q1(i)=val(a$)/2000*z4:printq1(i):sys636:rem q1(i)=channel 1
 reading
 7150 nexti
 7155 forj=1to10
 7158 h9=h9(j)+h9:q1=q1(j)+q1
 7160 nextj
 7165 z5=z4
 7170 poke700,10:rem device address
 7171 print#10,"s":rem checking to make sure sensitivity unaltere
d
 7172 sys40714:rem m/code serial poll
 7173 ifpeek(702)=160then7179:rem serial poll result
 7174 ifpeek(702)=144then7179
 7175 ifpeek(702)=176then7179
 7178 ifpeek(702)<>128then7172
 7179 input#10,a$:ifst<>64then7179
 7180 x2=val(a$)
 7181 z4=x2-(int(x2/3)*3)+1
 7182 ifz4=1thenz4=5
 7183 ifz4=3thenz4=1
 7184 z4=(10^(-(int(x2/3))))*z4
 7185 ifz4=z5then7200
 7190 y=y-1:goto7001
 7200 q1=q1/10:h9=h9/10
```

```
 7205 fori=1to10:em=(q1-q1(i))^2+em:eh=(h9-h9(i))^2+eh:next:rem s
tandard errors
 7206 em=(sqr(em/9))/3:eh=(sqr(eh/9))/3
 7210 print#11,q1:print#12,h9:print#13,em:print#14,eh
 7211 rem storing m & h values & standard errors
 7220 return
 8000 rem
 8001 rem*****************************************************************
***************
 8002 rem
 8003 rem
 8005 rem serial poll routine + reading of fluke
 8006 rem
 8007 rem
 8008 rem*****************************************************************
***************
 8009 rem
 8010 a%=40:n%=0:a=usr(4)
 8020 bb=ti
 8030 ifti-bb<5then8030
 8040 a%=40:n%=8:a=usr(4)
 8050 poke700,16:bb=ti
 8060 sys40714:ifti-bb>120then8010
 8070 ifpeek(702)<>144then8060
 8080 input#16,a$:ifst<>0then8080
 8090 return
 9000 rem
 9001 rem*****************************************************************
***************
 9002 rem
 9003 rem
 9005 rem current reversal
 9006 rem
 9007 rem
 9008 rem*****************************************************************
***************
 9009 rem
 9010 rem lines 9019-9090 change logic
 9014 print"■■■REVERSING CURRENT DIRECTION"
 9015 ifabs(c)>1000thenlo$="FORWARD":goto9017
 9016 lo$="REVERSE"
 9017 print"■■■Logic and current in "lo$" direction":b=ti
 9018 ifti-b<300then9018
 9019 a%=40:n%=10:a=usr(4)
 9020 b=ti
 9030 ifti-b<20then9030
 9040 a%=40:n%=12:a=usr(4)
 9050 b=ti
 9060 ifti-b<20then9060
 9070 a%=40:n%=8:a=usr(4)
 9080 b=ti
 9090 ifti-b<30then9090
 9100 a%=12:d=usr(5):rem checking logic reversal
 9110 ifabs(d-c)<10then9010
```

```
 9120 c=d
 9130 a%=40:n%=9:a=usr(4):rem activate main relay
 9140 b=ti
 9150 ifti-b<20then9150
 9160 a%=40:n%=8:a=usr(4)
 9170 a%=12:d=usr(5):ifabs(d-c)<10then9280:rem checking logic is
unaltered
 9175 rem lines 9180-9270 resets logic if necessary
 9180 a%=40:n%=10:a=usr(4)
 9190 b=ti
 9200 ifti-b<20then9200
 9210 a%=40:n%=12:a=usr(4)
 9220 b=ti
 9230 ifti-b<20then9230
 9240 a%=40:n%=8:a=usr(4)
 9250 b=ti
 9260 ifti-b<30then9260
 9270 a%=12:d=usr(5):ifabs(d-c)>10then9180
 9280 ifabs(c)>1000thenlo$="FORWARD":goto9300
 9290 lo$="REVERSE"
 9300 print"■■■Now changed to "lo$" direction":b=ti
 9310 ifti-b<300then9310
 9320 return
 9500 rem
 9501 rem*****************************************************************
*****************
 9502 rem
 9503 rem
 9505 rem detailed coercivity study
 9506 rem
 9507 rem
 9508 rem*****************************************************************
*****************
 9509 rem
 9510 print"■■■DETAILED COERCIVITY STUDY :-■■■■■■■■■■■■■■■This pa
rt of the program ";
 9511 a%=12:c=usr(5):ifabs(c)>1000thenlo$="forward":goto9520
 9512 lo$="reversed"
 9520 print"will conduct adetailed study of the coercivity region
 once the ";
 9530 print"operator has ramped the field  up & down two and a ha
lf times for both";
 9540 print" calibration and test samples. The       program will
 then take over and";
 9550 print" completethe experiment. The operator should noteboth
 calibration & ";
 9560 print"max. magnetization   voltage readings. Before the ope
rator   hands over";
 9570 print" the control to the micro boththe gaussmeter & 5206 r
anges for the ";
 9580 print"   detailed study must be established."
 9590 print"■■■Hit space bar when above criteria havebeen estabLi
shed."
 9591 print#9,"-1"
```

```
 9595 dimm(30),h(30):ff$=" fc"
 9600 b=ti
 9610 gosub8000:getb$:ifb$=""then9620
 9615 ifasc(b$)=32then9630
 9620 ifti-b<120then9610
 9625 goto9600
 9630 print"■Range of gaussmeter";:inputg0
 9640 print"■■Range of 5206";:inputz4
 9650 print"■■Type range of detailed study about zero gauss (<150
)";:inputhr
 9660 print"■■Type field intervals";:inpuths
 9665 print"■■Type file name required";:input#$
 9670 ns=int(hs/3):ifns=0thenns=1
 9680 print"■Set gaussmeter to 10K range."
 9681 print"■■Connect all leads from computer to powersupply."
 9682 print"■■■Hit space bar to continue."
 9700 b=ti
 9710 gosub8000:getb$:ifb$=""then9720
 9715 ifasc(b$)=32then9740
 9720 ifti-b<120then9710
 9725 goto9700
 9740 print"■Program running"
 9750 b=ti
 9760 ifti-b<120then9760
 9770 gosub9000
 9775 gosub8000
 9776 ifabs(val(a$)*10000)<0.9*hrthen9800
 9780 a%=46:n%=3:t%=1:a=usr(1)
 9781 b=ti
 9782 ifti-b<120then9782
 9790 goto9775
 9800 print"■Change gaussmeter range to required     range. Make
sure probe set up";
 9801 print" and        positioned properly. Ensure 5206 also onco
rrect ranges. Place";
 9802 print" paper on plotter  and connect plotter."
 9810 b=ti
 9820 gosub8000:getb$:ifb$=""then9830
 9825 ifasc(b$)=32then9840
 9830 ifti-b<120then9820
 9835 goto9810
 9840 print"■Program continuing and taking readings."
 9845 z=1
 9850 b=ti
 9860 ifti-b<1800then9860
 9870 m=0:h=0
 9880 fori=1to10:print#10,"q1"
 9890 input#10,m$:ifst<>64then9890
 9900 m=m+val(m$):gosub8000
 9910 h=h+val(a$):nexti
 9920 m(z)=m/2000*z4/10:h(z)=h/10*g0
 9930 z=z+1:print#9,"+2":b=ti
 9940 ifti-b<15then9940
 9950 print#9,"-2":ifabs(h(z-1))>hrthen9980
```

```
 9960 a%=46:n%=ns:t%=1:a=usr(1)
 9970 goto9850
 9980 open8,8,8,"1:"+ff$+ff$+",s,w":print#8,z-1
 9981 fori=1toz-1:print#8,m(i)chr$(13)h(i):nexti
 9982 close8:iffff$=" rc"then9996
 9983 print"■Disconnect leads to computer to supply.■ Set gaussme
ter to 10K range, ";
 9984 print"ramp field to 1.2 tesla and back."
 9985 print"■Hit space bar.":print#4,chr$(09);chr$(09);
 9990 b=ti
 9991 gosub8000:getb$:ifb$=""then9993
 9992 ifasc(b$)=32then9995
 9993 ifti-b<120then9991
 9994 goto9990
 9995 ff$=" rc":goto9680
 9996 return
 10000 rem
 10001 rem*****************************************************************
*****************
 10002 rem
 10003 rem
 10005 rem error occurred - ramping field down
 10006 rem
 10007 rem
 10008 rem*****************************************************************
*****************
 10009 rem
 10010 print"■■■ERROR OCCURRED - RAMPING FIELD DOWN"
 10020 print"■■■■■■■K hit space bar to end )"
 10030 print#4,chr$(07);
 10040 a%=47:n%=150:t%=1:a=usr(1):rem current decreasing
 10050 geta$:ifa$=""then10030
 10060 ifasc(a$)=32thenend
 10070 goto10030
```

```
 11000 rem
 11001 rem*****************************************************************
***************
 11002 rem
 11003 rem
 11005 rem list of variables used
 11006 rem
 11007 rem
 11008 rem*****************************************************************
***************
 11009 rem
 11010 rem h1 = step in external field
 11020 rem h = next field value required
 11030 rem h9 = last measured field value
 11040 rem c = measure of logic state
 11050 rem x1 = offset of gaussmeter
 11060 rem m,h = values of m & h
 11070 rem em,eh = std. errors of m & h values
 11080 rem b$ = changeover flag
 11090 rem f$ = filename
 11100 rem b = time ti
 11110 rem a & a$ used
 11120 rem a%,n% & t% used for minicam
 11130 rem h0 = field at each step
 11140 rem n0 = flag used in decreasing current
 11150 rem q1 = value of channel 1
 11160 rem x2 = response to request for sensitivity setting
 11170 rem y = no. of readings taken
 11180 rem z4 = sensitivity in volts
 11190 rem z5 = sensitivity in volts
 11200 rem da$ = date
 11210 rem sa$ = sample type
 11220 rem x0 & y0 = dimensions of sample
 11230 rem g0 = range of gaussmeter
 11240 rem hm = max. ext. h required
 11250 rem h2 & h3 = values of boundaries between field regions
 11260 rem n1,n2 & n3 = no. of readings in regions
 11270 rem n used to set up lock-in
 11280 rem l0$ to l9$ used for lock-in commands
 11290 rem i0$ to i2$ used for lock-in commands
 11300 rem n4 & n5 used for lock-in commands
 11310 rem a0$() used for lock-in commands
 11320 rem n6$ & n7$ used for lock-in commands
 11330 rem n6 used for lock-in commands
 11340 rem q2 = value of channel 2
 11350 rem ph used as flag to see how often zeroing of ch2 has oc
cured
 11360 rem l0$ = logic state "Forward" or "Reversed"
 11370 rem g1,g2 & g3 = steps in gauss in the three fields
 11380 rem s1,s2 & s3 = step sizes for the stepper motor
 11390 rem tn = total no. of readings required
 11400 rem ss = step size used in stepper motor statement
```

```
11410 rem rd$ = first record to file
11420 rem aa used for screen messages
11430 rem cc used for screen messages
11440 rem ab used for m/code routine
11450 rem nn used of reading fluke
11460 rem q1() = values of m
11470 rem h9() = field values
11480 rem bb = time ti
```

F.2 Further comments on the program

1. Line 1 : The a%, n% and t% parameters are required for MINICAM's operation and must be the first variables declared.

2. Lines 1-4 : The data statements here form a machine-code routine to display messages on the VDU during the program. The code is located in memory locations 636 to 678 (decimal) which is part of the first cassette buffer (unused because of disc drive).
   An assembly language version of the code and interpretation follows:

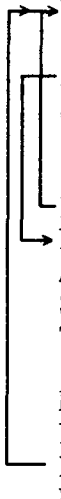

```
LDAIM 05     Load accumulator with 5 immediately
STA 634      Store acc. at location 634.
LDYIM 00     Load y register with 0 immediately.
STY 635      Store y at location 635.
LDXIM 00     Load x register with 0 immediately.
LDA 706,x    Load accumulator with value of location
             (706 + x) - message data stored here.
BEQ 660      Branch on result zero to location 660
STA 32778,y  Store acc. at location (32778 + y) - PET screen.
INX          Increment x
INY          Increment y
BNE 648      Branch on result not zero to location 648.
LDA 635      Load acc. with value of location 635.
ADC 40       Add 40 to accumulator immediately.
STA 635      Store acc. at location 635.
TAY          Transfer acc. to register y.
INX          Increment x.
DEC 634      Decrement location 634.
LDA 634      Load acc. with value of location 634.
BNE 648      Branch on result not zero to location 648.
RTS          Return to caller (i.e. BASIC).
```

By following the above it will be seen that a five line message is displayed at the top of the PET VDU (location 32768 is top left hand corner of PET screen). The message data is stored from locations 706 to 810 and the length of each message line (20 characters)

is determined by null characters in this data.

3. Lines 5-33 : These data statements contain the data required for the five screen messages and are separated by string variables (e.g. *3 denotes start of message 3 data). The five messages are:

   * 1 - Recording M and H values.
   * 2 - Logic Forward Current Increasing
   * 3 - Logic Reversed Current Increasing
   * 4 - Logic Forward Current Decreasing
   * 5 - Logic Reversed Current Decreasing

and all are displayed as reverse field characters within a solid white box 20 characters wide and 5 lines deep.

4. Line 34 : The jiffy clock (TI) is used extensively throughout the program for timing events (one jiffy = 1/60th second). Resetting the jiffy clock at the start ensures that any timing procedures are not ruined by an automatic reset of the jiffy clock during the experiment.

5. Line 44 : Converts PET VDU to lower case characters.

6. Lines 46 and 47 : a% = 40 is the address for MINICAM's GPOB and setting n% = 0 initializes all the outputs to a TTL "1" state. Output bit 3 is connected to the Fluke's external trigger and needs to remain at a "0" state until a reading is required. This is achieved by sending n% = 8.

The USR function passes the bracketed parameter into floating point accumulator #1 and then jumps to the user written code which starts at the location defined by contents of locations 1 and 2 (see line 42). This

MINICAM code is contained in an EPROM inside the PET and starts at location 37888 (decimal). The parameter in the bracket defines the relevant section of code required for each board type.

For example : USR(1) is required for stepper motors
USR(4) is DAC's and GPOB
USR(5) for ADC's.

7. Subroutine 2000 : The voltage potential across the 2.5 mΩ resistor is observed and the supply is adjusted to achieve zero current.

In line 2220 the logic level analog voltage indication from the latching relay control circuitry is read by an ADC with address a% = 12. The result (c) indicates whether the logic is forward or reversed.

8. Subroutine 2500 : The gaussmeter is set up and all information required (e.g. Max. Field, gaussmeter range etc.) is requested by the PET.

9. Subroutine 3000 : This is the most extensive subroutine which allows the user to set up and observe any of the function settings on the lock-in analyser from the keyboard. For a full explanation of all the functions and the codes required to adjust them via the IEEE bus the reader is referred to the 5206 manual.

10. Subroutine 4000 : This subroutine cycles the field twice, during which time it sets the phase setting of the lock-in analyser, checks the zero current setting of the supply and re-checks the lock-in phase setting. The phase setting is set and checked by observing the channel 2 output of the lock-in at one extreme of the

magnetization loop and reducing this value to near zero using the auto-phase function.

Lines 4100 and 4440 give the first example of increasing and decreasing the current using MINICAM's stepper motor. The number of steps is determined by the parameter n% and the direction of motion by the value of a%. The parameter t% can be used to control the time interval between each step but it is set to its minimum interval throughout the program.

Lines 4204 - 4207 give the first example of the use of the machine-code serial poll routine with the lock-in analyser. Sys 40714 calls the routine and the replies from the instrument are made up as follows:

128 means output ready

32 means device settled (i.e. not autoranging)

16 means overload indication

Thus the result of the serial poll can be 128, 144, 160 or 176 and all indicate that data is ready and this data must be removed before the lock-in will correct itself.

Before any data readings are taken from the lock-in the PET always checks that the device is settled. When it is, the response to the PET's request for the lock-in status is 32. Until it receives this reply, the program will not continue.

Lines 4560 and 4840 give the first example of the PET checking the voltage output across the 2.5 mΩ resistor to see if zero current has been reached.

Line 4955 sounds a bell on the PET printer to indicate to the operator that the zero current setting requires checking.

11. Subroutine 5000 : This subroutine shows the first example of the PET screen message routine. The correct data set for the message is located in line 5015 and then stored in the correct locations in line 5017. The sys 636 call in line 5018 invokes the code which displays the messages on the screen.

Lines 5070 and 5075 provide protection against the possibility of the gaussmeter overranging and the PET trying to achieve field values not possible with the electromagnet respectively.

Subroutine 5500 is almost identical to subroutine 5000 except that the field increment logic is reversed because increasing the current decreases the field once changeover has occurred.

12. Subroutine 6000 (and 6500) : Similar to subroutine 5000 (and 5500) but contains an additional section (lines 6070 - 6160) to test if a current reversal is required.

The current is decreased ten times, at the end of which the voltage output across the 2.5 mΩ is tested if and only if the field reading is less than 300 gauss (i.e. nearing the magnet's remanent field). If the current is below 0.01 amps then a request for current reversal is made, otherwise the current is decreased further until either the required field value is reached

or the current does fall below this limit.

13. Subroutine 7000 : This subroutine records ten values of the magnetization (once the lock-in is settled) and field. It then calculates the mean values and the standard errors and stores the results in the appropriate disc files.

The subroutine checks that the lock-in is settled (lines 7040 - 7060), it then finds the sensitivity setting (lines 7070 - 7094) after which it records ten values of the samples magnetization and the field (lines 7100 - 7150). It then checks that the sensitivity of the lock-in hasn't altered, calculates the mean and standard errors (lines 7200 - 7206) and stores the results in the four separate disc files (line 7210). If the sensitivity of the lock-in has changed while the readings were recorded the results are ignored and the whole subroutine is repeated.

14. Subroutine 8000 : This subroutine triggers the Fluke into taking a reading and conducts a serial poll to determine when the data is ready.

The TTL "1" state pulse required for the external trigger to the Fluke is supplied from bit 3 of MINICAM's GPOB by lines 8010 - 8040. The Fluke is then serial polled until the only response signalling data ready (144) is received. The data is then input to the PET.

15. Subroutine 9000 : This subroutine reverses the logic on the latching relay control circuitry, checks that this has been successful and then activates the

latching relay itself. It then checks to see if the logic is still in the correct state and , if not, alters it. It then remembers the state of the logic until the next current reversal so that it can detect whether the logic has been corrupted in the meantime. If it has been it will be corrected.

The two relays which provide the signal required to reverse the logic are activated in turn by lines 9019 and 9040 respectively. Relay A is connected to bit 1 and relay B is connected to bit 2 of the GPOB and are activated when these bits are sent low. (Note that bit 3 must always be kept low).

Line 9100 checks, via the ADC and the logic level analog voltage indication, that the operation has been successful. If not is is repeated.

The switch controlling the power to the energizing coils of the latching relay is activated by sending bit 0 of the GPOB low (line 9130).

The logic state on the control circuitry is then checked (line 9170) and altered if necessary (lines 9180 - 9270).

16. Subroutine 9500 : This subroutine will conduct a detailed study of the coercive field of a sample material if this value is less than 150 gauss (the magnet remanence field). The results are stored on disc and can also be plotted out as they are recorded on an X-Y plotter.

The subroutine relies on the operator to perform all large changes in the field and to provide information about the region of interest, and change gaussmeter ranges etc. By connecting the analog output of both lock-in and gaussmeter to an X-Y recorder, and using the programmable switch to operate the pen lift (lines 9930 - 9950), a plot can be obtained as the data is recorded. Once again ten values of magnetization and field values are recorded and the average values calculated and stored. For the purposes of this study, however, the lock-in must not be allowed to autorange.

17. Subroutine 10,000 : This subroutine decreases the current in the magnet whilst sounding the bell on the PET's printer. It is only called if the gaussmeter is overranging or the field is approaching the maximum field possible with the electromagnet.

18. The remaining section of software not described so far (lines 170 - 1240) controls the whole VSM apparatus while conducting a full M-H loop study.

Lines 170-192 calculate the field steps, and hence the stepper motor step intervals, required for each field interval chosen by the user. Files are then opened to the disc system to store the values of magnetization and field etc. as they are recorded (lines 210 and 211).

Lines 220 - 980 control the field ramping, data taking, current reversal etc. for the whole loop study by calling the subroutines described earlier in the correct sequence.

The bell on the PET printer is sounded (lines 1000 - 1020) to indicate the end of the run after which the user can store the results in a disc file of his choosing (lines 1026 - 1098). The user can also choose to store just the magnetization and field values or a combination of these values together with the relevant standard errors.

The results can then be listed on the printer if required (lines 1130 - 1220).

The program then ends.

APPENDIX G

Listing of PLOTTER program

This appendix contains a listing of the PET Basic program written to plot either full or initial magnetization curves on an X-Y recorder. The B-H data is assumed to reside on disc and the use of a two channel DAC board (addresses 18 and 19) to control the X-Y motion of pen is also assumed.

The program will allow the user to apply a correction for the demagnetizing field (if required). It will also permit an enlargement of a region of the curve (centred on the origin) to be produced.

```
 5 sys(38366)
 6 poke15,2
 8 dima(500),b(500)
 10 poke1,0:poke2,148:a%=0:n%=0:t%=0:poke59468,14
 15 open9,9
 20 print"■■■■■■Set X-Y plotter sensitivity to 20mV/cm"
 25 a%=18:n%=2000:t%=2000:a=usr(7)
 30 print"■■Position pen at exact middle of chart   bed"
 40 print"■■Do you wish to plot axes? (y or n)"
 50 print"■■":inputa$
 51 ifa$="y"thengosub500
 60 print"■■■Type name of file to be plotted"
 70 print"■■":inputf$
 80 g$="1:"+f$+",s,r"
 100 print"■■Is first record a title? (y or n)"
 110 inputb$
 111 print"■■Is second record no. of data points          (y or n)"
;:inputz$
 115 print"■■Does file contain std errors?"
 117 inputd$
 120 print"■■Are you sure? (y or n)"
 130 inputc$:ifc$="n"then600
 140 open8,8,8,g$
 150 ifb$="n"then161
 160 input#8,a1$:printa1$:print"■■"
 161 ifz$="n"then180
 162 input#8,a1
 163 ifd$="y"then167
 165 fori=1toa1:input#8,a(i),b(i):printa(i)"   ,   "b(i):nexti
 166 goto170
 167 fori=1toa1:input#8,a(i),xx,b(i),yy:printa(i)"   ,   "b(i):next
i
 170 goto260
 180 fori=1to500
 185 ifd$="y"then195
 190 input#8,a2$,a3$
 191 goto200
 195 input#8,a2$,a4$,a3$,a5$
 200 ifa2$+a3$=a2$then260
 210 ifa2$+a3$="the end"then260
 220 a(i)=val(a2$):b(i)=val(a3$)
 230 printa(i)" , "b(i)
 235 a1=i
 240 a2$="the ":a3$="end"
 250 nexti
 260 close8
 261 print"■■Is the file an initial curve"
 262 inputa$:ifa$="y"then2000
 270 print"■■Is the file a complete B-H loop? (y or n)"
 280 inputa$:ifa$="n"thengosub800
 285 print"Demag. correction required? (y or n)":inputa$:ifa$="y"
thengosub1500
```

```
290 fori=2toa1
300 ifa(i)>h1thenh1=a(i)
310 ifb(i)>h2thenh2=b(i)
320 nexti
330 print"■■Max. X value ="h1
340 print"■■Max. Y value ="h2
350 print"■■Type full scale values for X and Y axes"
360 inputx,y
370 a=int(a(1)/x*2000)+2000:b=int(b(1)/y*1600)+2000
380 a%=18:n%=a:t%=b:a=usr(7)
390 print#9,"+2"
400 fori=2to500
410 a=int(a(i)/x*2000)+2000
420 b=int(b(i)/y*1600)+2000
430 a%=18:n%=a:t%=b:a=usr(6)
435 ifa(i)>a(1)then438
436 ifa(i)<a(1)thenp=2
437 goto440
438 ifp=2then445
440 nexti
445 print#9,"-2"
450 print"■■■Blow-up required?";:inputa$
460 ifa$<>"y"then490
470 gosub1000
480 goto450
490 end
500 rem "PLOTTING AXES"
501 print#9,"+2"
505 fori=0to20
510 a%=18:n%=4000-(i*200):t%=2000:a=usr(6)
515 a%=18:n%=4000-(i*200):t%=1970:a=usr(6)
520 a%=18:n%=4000-(i*200):t%=2000:a=usr(6)
525 nexti
530 a%=18:n%=2000:t%=2000:a=usr(6)
535 forj=0to20
540 a%=18:n%=2000:t%=3600-(j*160):a=usr(6)
545 a%=18:n%=1970:t%=3600-(j*160):a=usr(6)
550 a%=18:n%=2000:t%=3600-(j*160):a=usr(6)
555 nextj
560 a%=18:n%=2000:t%=2000:a=usr(6)
565 print#9,"-2"
570 return
600 rem "DISPLAY FILE CONTENTS"
605 print"■■"
610 open8,8,8,g$
620 input#8,a1$:printa1$:print"■■"
625 b=ti
626 ifti-b<60then626
630 fori=1to500
640 input#8,a2$,a3$
650 ifa2$+a3$=a2$then710
660 ifa2$+a3$="the end"then710
670 a=val(a2$):b=val(a3$)
680 printa" , "b
```

```
690 a2$="the ":a3$="end"
700 nexti
710 close8
720 goto100
800 rem "COMPLETING B-H LOOP"
810 fori=1toa1
820 a(a1+i)=-a(i):b(a1+i)=-b(i)
830 nexti
840 d=2*a1+1
850 fori=dto300:b(i)=b(i-2*a1):a(i)=a(i-2*a1):nexti
855 a1=300
860 return
1000 rem blow-up
1005 z=0:zz=0:s$="":ss$=""
1010 print"[CR]Type max X & Y values";:inputx,y
1015 a%=18:n%=2000:t%=2000:a=usr(6)
1030 gosub500
1040 fori=1toa1
1045 ifs$="this"then1060
1050 ifa(i)>.9*h1then1105
1055 goto1110
1060 if(a(i)>x)or(b(i)>y)then1110
1070 z=z+1:a=int(a(i)/x*2000)+2000:b=int(b(i)/y*1600)+2000
1075 printa(i),b(i)
1076 if(a(i)<-x)or(b(i)<-y)then1120
1080 a%=18:n%=a:t%=b:a=usr(6)
1090 ifz=1thenprint#9,"+2"
1105 s$="this"
1110 nexti
1120 a2=i:print#9,"-2"
1130 fori=a2toa1
1135 ifss$="off"then1150
1140 ifa(i)<-.9*h1then1195
1145 goto1200
1150 if(a(i)<-x)or(b(i)<-y)then1200
1160 zz=zz+1:a=int(a(i)/x*2000)+2000:b=(b(i)/y*1600)+2000
1165 if(a(i)>x)or(b(i)>y)then1210
1170 a%=18:n%=a:t%=b:a=usr(6)
1175 printa(i),b(i)
1180 ifzz=1thenprint#9,"+2"
1195 ss$="off"
1200 nexti
1210 print#9,"-2"
1220 return
1500 rem demagnetizing field correction
1510 print"Type demag. factor N";:inputn
1520 mo=↑*4e-7
1530 fori=1toa1
1540 a(i)=a(i)/mo/1e4:rem converts oersted to a/m
1550 a(i)=a(i)-n*b(i):rem ext to int field
1560 b(i)=mo*(a(i)+b(i)):rem b value in tesla
1570 nexti
1580 return
2000 rem plotting initial curve and axes
```

```
2010 a%=18:n%=90:t%=90:a=usr(7)
2020 b=ti
2030 ifti-b<60then2030
2040 print#9,"+2"
2050 a%=18:n%=4090:t%=90:a=usr(6)
2060 a%=18:n%=90:t%=90:a=usr(6)
2070 a%=18:n%=90:t%=3090:a=usr(6)
2080 a%=18:n%=90:t%=90:a=usr(6)
2085 print#9,"-2"
2090 fori=2toa1:ifa(i)>h1thenh1=a(i)
2095 ifb(i)>h2thenh2=b(i)
2100 nexti
2110 print"■■Max H value ="h1
2120 print"■■Max B value ="h2
2130 print"■■Type full scale values for H and B axes"
2140 inputx,y
2150 print#9,"+2"
2160 fori=1toa1
2170 a=int(a(i)/x*4000)+90:ifa<0then2210
2180 b=int(b(i)/y*3000)+90:ifb<0then2210
2190 a%=18:n%=a:t%=b:a=usr(6)
2200 nexti
2210 print#9,"-2"
2220 end
```

APPENDIX H

Predicted relationships arising from a consideration of Kneppo's equation

Kneppo's equation is written as

$$B = A^{(k - \frac{1}{H})} \qquad (H.1)$$

which, on taking logarithms of both sides, becomes

$$LnB = kLnA - \frac{1}{H} LnA \qquad (H.2)$$

Differentiation with respect to H then gives

$$\frac{1}{B}\frac{dB}{dH} = \frac{1}{H^2} LnA \qquad (H.3)$$

and hence

$$\frac{dB}{dH} = LnA \left(\frac{B}{H^2}\right) \qquad (H.4)$$

the result for differential permeability. Further differentiation of (H.4) w.r.t. H gives

$$\frac{d^2B}{dH^2} = LnA \left(\frac{B}{H^3}\right) \left(\frac{LnA}{H} - 2\right) \qquad (H.5)$$

which indicates that the differential permeability will have its maximum value when $H = \frac{LnA}{2}$.

The absolute permeability, $\mu (= B/H)$, is given by:-

$$\mu = \frac{A^{(k - \frac{1}{H})}}{H} \qquad (H.6)$$

whence

$$\frac{d\mu}{dH} = \frac{1}{H}\frac{dB}{dH} - \frac{B}{H^2} = \frac{B}{H^2}\left(\frac{LnA}{H} - 1\right) \qquad (H.7)$$

Equating (H.7) to zero gives the field at which the maximum permeability ($H_{\mu m}$) is observed, thus

$$H_{\mu m} = LnA \qquad (H.8)$$

The maximum permeability (μ_m) is then given by:

$$\mu_m = \frac{A^{(k - \frac{1}{H_{\mu m}})}}{H_{\mu m}} \qquad (H.9)$$

and hence, using equation (H.8), we have

$$Ln(\mu_m H_{\mu m}) = kLnA - 1 \qquad (H.10)$$

This may be rewritten as

$$Ln(\mu_m H_{\mu m} e) = kLnA \qquad (H.11)$$

and, since $LnB_s = kLnA$ (equation (6.9)), we have:

$$LnB_s = Ln(\mu_m H_{\mu m} e) \qquad (H.12)$$

and, therefore, that

$$\mu_m = \frac{B_s}{eH_{\mu m}} \qquad (H.13)$$

Alternatively

$$\mu_m = \frac{B_s e^{-1}}{LnA} \qquad (H.14)$$

and use of equation (6.9) yields

$$\mu_m = \left(\frac{B_s e^{-1}}{LnB_s}\right)^k \qquad (H.15)$$

The above equations (H.4), (H.8), (H.13) and (H.15) are the relationships expressed in Chapter 6 of this thesis as equations (6.12), (6.11), (6.14) and (6.13) respectively.

REFERENCES

ANDERSON, M., Dept. of Energy Report OT/R/8034 (1980).

ATKINSON, P., and THOMAS, P.J., "Improved describing function for hysteresis", Electron Lett., 11, 141, (1975).

BAILEY, F.W.J., "Fundamentals of engineering metallurgy and materials" (5th Edition), Cassell, London (1973).

BASAK, A., and MOSES, A.J., "Harmonic losses in a three phase transformer core", IEEE Trans. Magn. MAG-14, 990 (1978).

BATES, L.F., "Modern Magnetism", (4th Edition), Cambridge, University Press, London (1963).

BATES, L.F. "The Introduction of SI in Magnetism", Contemp. Phys. 11, 301, (1970).

BIOMEDICAL DATA PROGRAMS STATISTICAL SOFTWARE, University of California Press (1981).

BITTER, F., "On Inhomogeneities in the Magnetization of Ferromagnetic Materials", Phys. Rev. 38, 1903, (1931).

BLACKBURN, J.A., and SMITH, H.J.T., "Automatic curve digitizer", Rev. Sci. Instrum., 52, 1586, (1981).

BLACKETT, P.M.S., "Lectures on Rock Magnetism", The Weizmann Scientific Press of Israel, Rehovot, (1956).

BLOCH, F., "Zur Theorie des Austauschproblems und der Remanenzersheining der Ferromagnetika", Z. Physik. 74, 295, (1932).

BOWDEN, G.J., "Detection coil systems for vibrating sample magnetometers", J. Phys. E : Sci. Instrum. 5, 1115, (1972).

BOZORTH, R.M., "Ferromagnetism", Van Nostrand (1951).

BOZORTH, R.M., and CHAPIN, D.M., "Demagnetizing factors of rods", J. Appl. Phys. 13, 320 (1942).

BRAGG, E.E., and SEEHRA, M.S., "Analysis of induced EMF in vibrating sample magnetometers", J. Phys. E: Sci. Instrum., 9, 216, (1976).

BRAILSFORD, F., and MAZZA, V.R., "The alternating magnetic flux distribution in right-angled corners of transformer laminations", Inst. Elect. Eng. 173, (1962).

BUNGE, H.J., "Texture Analysis in Materials Science", Butterworths, London (1982).

CAHN, J.W., "The Kinetics of Grain Boundary Nucleated Reactions", Acta Metallurgica 4, 449 (1956).

CAHN, J.W., "On the Kinetics of the Pearlite Reaction", J. Metals 9, 140 (1957).

CASE, W.E., and HARRINGTON, R.D., "Calibration of Vibrating Sample Magnetometers", J. Res. Nat. Bur. Stand. 70C, 255, (1966).

CHANTRELL, R.W., POPPLEWELL, J., and CHARLES, S.W., "Measurements of Particle Size Distribution in Ferrofluids", IEEE Trans. Magn. MAG-14, 975 (1978).

CHIKAZUMI, S., "Physics of Magnetism", Wiley, New York (1964).

DAVIS, N., "Derivation and application of an equation to the B-H Loop", J. Phys. D : Appl. Phys., 4, 1034, (1971).

DAVIS, N., "Research Techniques in Non destructive Testing", (R.S. Sharpe, Ed.), Academic, London, vol. 2, (1973).

DeBLOIS, R.W., and BEAN, C.P., "Nucleation of Ferromagnetic Domains in Iron Whiskers", J. Appl. Phys. 30, 225S, (1959).

DIETZE, H.D., "Statistical Theory of Coercive Field", J. Phys. Soc. Jpn. Suppl. 17-B1, 663, (1962).

DOMENICALI, C.A., "A Null-Coil Pendulum Magnetometer", Rev. Sci. Instrum. 21, 327 (1950).

DORING, W., "Uber das Anwachsen der Unmagnetisierungs Keime bei grossen Barkhausen-Sprungen", Z. Phys., 108, 137, (1938).

DWIGHT, K., "Experimental Techniques with General Applicability for the Study of Magnetic Phenomena", J. Appl. Phys. 38, 1505, (1967).

FEARNEHOUGH, G.D., JUDE, D.W., and WEINER, R.T., "The Arrest of Brittle Fracture in Pipelines", Institution of Mechanical Engineers Conference on Practical Applications of Fracture Mechanics to Pressure Vessel Technology, London, p.156, (1971).

FISCHER, E., and JENSEN, C.W., "Pet and the IEEE 488 Bus (GPIB)", Osborne/McGraw-Hill (1980).

FLANDERS, P.J., and DOYLE, W.D., "Motor driven Magnetometer for Thin Magnetic Films", Rev. Sci. Instrum. 33, 691, (1962).

FOILES, C.L., and McDANIEL, T.W., "Dipole approximation for vibrating sample magnetometers", Rev. Sci. Instrum. 45, 756, (1974).

FONER, S., "Vibrating sample magnetometer", Rev. Sci. Instrum. 27, 548, (1956).

FONER, S., "Versatile and sensitive vibrating sample magnetometer", Rev. Sci. Instrum. 30, 548 (1959).

FONER, S., "Special Magnetic Measurement Techniques", J. Appl. Phys. 38, 1510, (1967).

FONER, S., "Sensitivity of vibrating sample magnetometers and how to increase sensitivity if needed", Rev. Sci. Instrum., 45, 1181 (1974).

FONER, S., "Further improvements in vibrating sample magnetometer sensitivity", Rev. Sci. Instrum. 46, 1425, (1975).

FONER, S., "Review of magnetometry", IEEE Trans. Magn. MAG-17, 3358, (1981).

FORSTER, F., "Non-destructive Inspection by the method of magnetic leakage fields. Theoretical and experimental foundations of the detection of surface cracks of finite and infinite depth", Defektoskopiya No. 11, 3, (1982).

FRANKFURT, V.I., ZATSEPIN, N.N., and GUSLITSER, B.G., "Inspecting the heat-treatment quality of ShKh15 and ShKh15SG balls by the method of higher harmonics", Defektoskopiya No. 7, 12, (1981).

FRIDMAN, L.A., TABACHNIK, V.P., and CHERNOVA, G.S., "Features of the operation of ferroprobes with low permeability and the shape of cores, with excitation fields of low intensity", Defektoskopiya No. 5, 11, (1971).

GERBER, J.A., BURMESTE, W.L., and SELLMYER, D.J., "Simple Vibrating Sample Magnetometer", Rev. Sci. Instrum. 53, 691, (1982).

GONDA, P., MARCELY, P., MACKO, J., and PAVLOVIC, M., "Computerized evaluation of magnetic properties", J. Magn. Magn. Mater, 41, 241 (1984).

GOODENOUGH, J.B., "A theory of domain creation and coercive force in polycrystalline ferromagnetics", Phys. Rev. 95, 917, (1954).

GRAHAM, C.D., "Iron and nickel as magnetization standards", J. Appl. Phys. 53, 2032 (1982).

GUTNOV, R.B., SUKHOTIN, B.N., SOKOL, I. YA, et al. "The Production of Low-Carbon Iron", Metallurgiya, Moscow 7, (1973).

GUY, C.N., "Frequency doubling - a new approach to vibrating sample magnetometers", J. Phys. E : Sci. Instrum. 9, 433, (1976a).

GUY, C.N., "A simple approach to coil design for vibrating sample magnetometers", J. Phys. E : Sci. Instrum. 9, 790, (1976b).

HAWKES, S., and CORNER, W.D., "Optical Observations of Domains in Constructional Steels", submitted to J. Magn. Magn. Mater. (1985).

HAWKINS, R.D., "The Magnetocrystalline Anisotropy of Gadolinium/Terbium Alloys", Ph.D. Thesis, University of Durham, (1982).

HEISENBERG, W., "Zur Theorie des Ferromagnetismus", Zeitschrift fuer Physik, 49, 619 (1928).

HICKLEY, C.M., and WOODHEAD, J.H., "Formation of Ferrite in Hypo-Eutectoid Plain Carbon Steels", J. Iron and Steel Inst. 176, 129, (1954).

HIGGINS, R.A., "Engineering Metallurgy (Part 1)", The English Universities Press Ltd., London (1965).

HOON, S.R., "An inexpensive, sensitive vibrating sample magnetometer", Eur. J. Phys. 4, 61 (1983).

HOON, S.R., KILNER, M., RUSSELL, G.J., and TANNER, B.K., "Preparation and properties of Nickel Ferrofluids", J. Magn. Magn. Mater. 39, 107 (1983).

HOON, S.R., LAMBRICK, D.B., and PAIGE, D.M., "An automated micrograph image size analyser", J. Phys. E : Sci. Instrum. 18, 389 (1985).

HOON, S.R., and WILLCOCK, S.N.M., "The Design and Operation of an Automated Double-Crank VSM", submitted to J. Phys. E : Sci. Instrum. (1985).

HUME-ROTHERY, W., "The Structures of Alloys of Iron", Pergamon Press Ltd., London (1966).

HUMPHREY, F.B., "Magnetic measurement Techniques for Thin Films and Small particles", J. Appl. Phys. 38, 1520, (1967).

JANSEN, J., and ZEEDIJK, H.B., "Deformation layers in Spark-machined and Mechanically Sectioned specimens of 0.2%C Mild Steel", J. Phys. E, 5, 973 (1972).

JOHNSON, C.S., and WEEKS, W.R., "Metallurgy (4th Edition)" The Technical Press Ltd., London, (1964).

JONES, C.L., "Material Requirements for British Gas Transmission pipelines", British Gas Internal report ERS E.322 (1982).

KAESER, R.S., AMBLER, E., and SCHOOLEY, J.F., "Vibrating coil magnetometer for use at very low temperatures", Rev. Sci. Instrum. 37, 173, (1966).

KELLY, P.M., and NUTTING, J., "The martensite transformation in carbon steels", Proc. Roy. Soc. A259, 45 (1960).

KEMPSTER, M.H.A., "Materials for Engineers (3rd Edition)", Hodder and Stoughton, London (1976).

KIRKALDY, J.S., and WARD, R.G., "Aspects of Modern Ferrous Metallurgy", Blackie, London (1964).

KITTEL, C., "Physical Theory of Ferromagnetic Domains", Rev. Mod. Phys. 21, 541 (1949).

KITTEL, C., "Introduction to Solid State Physics, (5th Edition)", Wiley, New York (1976).

KNELLER, E., "Ferromagnetismus", Publ. Berlin, 522 (1962).

KONOVALOV, O.S., GOLOVKO, A.S., and ROITMAN, V.I., "Magnetic Inspection of the Mechanical Properties of Steel Pipes", Defektoskopiya, No. 8, 82 (1982).

KURDJUMOV, G.V., "Phenomena occurring in the quenching and tempering of steels", J. Iron and Steel Inst. 195, 26, (1960).

KUSSMANN, A., and SCHARNOV, B., "Uber die Koerzitivkraft, 1. Teil Koerzitivraft und Mechanische Harte", Z. Phys. 54, 1, (1929).

KUZNETSOV, I.A., and MIKHEEV, M.N., "Magnetic and Electrical Properties of Steels viewed in connection with electromagnetic methods of inspection", Fiz. Met. Metalloved. 17, 201, (1964).

LANDAU, L., and LIFSHITZ, E., "Theory of the Dispersion of Magnetic Permeability in Ferromagnetic Bodies", Phys. Zeits. d. Sowjetunion, 82, 153 (1935).

LIM, K.K., and HAMMOND, P., "Universal loss chart for the calculation of eddy-current losses in thick steel plates", Proc. IEE 117, 857, (1970).

LIPSON, H., and PETCH, N.J., "The crystal structure of cementite Fe_3C", J. Iron and Steel Inst. 142, 95, (1940).

McFARLANE, J., and HARRIS, M.J.,"The control of flux waveforms in iron testing by the application of feedback amplifier techniques", Proc. IEE Paper No. 2554M (105A p. 395) (1958).

McMULKIN, F.J., "Oxygen Steel Produced at Dofasco can compete with Open Hearth". J. Metals 7, 530 (1955).

MACFADYEN, W.K., SIMPSON, R.R.S., SLATER, R.D., and WOOD, W.S., "Representation of magnetization curves by exponential series", Proc. IEE, 120, 902, (1973).

MAGER, A., "Uber der Einfluss der Korngrosse auf die Koerzitvikraft", Annalen der Physik, 11, 15, (1952).

MALLINSON, J., "Magnetometer coils and reciprocity", J. Appl. Phys. 37, 2514, (1966).

MANGUM, B.W., and THORNTON, D.D., "Vibrating Sample Magnetometer for Use at Very Low Temperatures and in High Magnetic fields", Rev. Sci. Instrum. 41, 1764, (1970).

MAPPS, D.J., and WHITE, C.E., "Phase Shifted flux harmonics and magnetostriction in (110) (001) Si-Fe", IEEE Trans. Magn. MAG-18, 1505 (1982).

MEHL, R.F., and HAGEL, W.C., "The Austenite : Pearlite Reaction", Prog. Metal Phys. 6, 74 (1956).

MEYER, L., HEISTERKAMP, F., and MUESCHENBORN, W., "Columbium, Titanium, and Vanadium in Normalized Thermo-Mechanically Treated and Controlled Rolled Steels", Microalloying 75, Washington, October 1975.

MIKHAILOVSKII, V.N., and SPEKTOR, Y.I., "Some problems of the theory of magnetic amplifiers and of ferroprobes type 'second harmonic'", Automat. Telemekh, 18, 716, (1957).

MIKHEEV, M.N., and GORKUNOV, E.S., "Correlation between the magnetic properties and the structural state of a substance, the physical foundation of magnetic structural analysis", Defektoskopiya No. 8, 5, (1981).

MIKHEEV, M.N., ZHUKOVA, P.N., and TOMILOV, G.S., "The magnetic and electrical properties of alloy steels after various heat treatments", Proceedings of the Institute of Metal Physics Academy of Science of the USSR, 15, 90 (1954).

MOROZOVA, V.M., MIKHEEV, M.N., ZAKHAROVA, G.N., and POMORTSEVA, L.V., "The magnetic and electrical properties of 17KhN2, 30Kh3A and 17N3MA steels and of carburized layers of a base of them", Defektoskopiya No. 5, 7, (1966).

MORRISH, A.H., "The Physical Principles of Magnetism", Wiley, New York (1965).

MOSES, A.J., and THOMAS, B., "The spatial variation of localized power loss in two practical transformer T-joints", IEEE Trans. Magn. 9, 655, (1973).

NOAKES, J.E., ARROTT, A., and HAAKANA, C., "Vibrating Sample Magnetometers", Rev. Sci. Inst. 39, 1436 (1968).

O'KELLY, D., "Hysteresis and eddy-current losses in steel plates with non-linear magnetization characteristics", Proc. IEE, 119, 1675, (1972).

O'KELLY, D., "Losses in cylindrical ferromagnetic cores including hysteresis and eddy-current effects", J. Phys. D. 8, 568, (1975a).

O'KELLY, D., "Flux penetration and core loss in solid iron", IEEE Trans. Magn. MAG-11, 56, (1975b).

O'KELLY, D., "Fundamental and Harmonic flux estimation in steel plate with sinsuisoidal applied field", J. Phys. D. 10, 2107 (1977).

OMAR, M.A., "Elementary Solid State Physics", Addison-Wesley, Reading, Massachusetts, (1975).

OSBORN, J.A., "Demagnetizing factors of the general ellipsoid", Phys. Rev. 67, 351, (1945).

PACYNA, A.W., "General theory of the signal induced in a vibrating sample magnetometer", J. Phys. E : Sci. Instrum. 15, 663, (1982).

PACYNA, A.W., and RUEBENBAUER, K., "General theory of a vibrating magnetometer with extended coils", J. Phys. E : Sci. Instrum., 17, 141, (1984).

PAIN, H.J., "The Physics of Vibrations and Waves (2nd Edition)", Wiley, London (1976).

PAUTHENET, R., "Variation thermique de l'aimantation spontanee des ferrites de nickel, cobalt, fer et manganese", Comptes Rendus Acadamie de Sciences (Paris), 230 1842, (1950).

PAUTHENET, R., "Spin-waves in nickel, iron and yttrium-iron garnet", J. Appl. Phys. 53, 2029, (1982a).

PAUTHENET, R., "Experimental verification of spin-wave theory in high fields", J. Appl. Phys. 53, 8187, (1982b).

PETCH, N.J., "The Cleavage Strength of Polycrystals", J. Iron Steel Inst. (London), 173. 25, (1953).

PETCH, N.J., "The Fracture of Metals", Prog. Metal Phys. 5, 1, (1954).

PLOTKIN, H., "Quarterly Progress Report", Massachusetts Institute of Technology, Research Laboratory Electronics, 28, (October 15, 1951).

PONOMAREV, Y.F., "Calculation of the harmonics of emf of ferrosondes with longitudinal excitation in case of high intensity of the measured fields", Defektoskopiya No. 1, 68 (1970).

PONOMAREV, YU.F., "Oscillations of harmonic components of magnetization of cyclically remagnetized ferromagnetic cores. I. Short review and experiments", Defektoskopiya No. 4, 3 (1983a).

PONOMAREV, Y.F., "Oscillations of the harmonic components of magnetization of cyclically remagnetized ferromagnetic cores. II. Causes of the appearance of oscillations", Defektoskopiya, No. 4, 11, (1983b).

PONOMAREV, Y.F., "Regularities of the harmonic components of magnetization of cyclically remagnetized ferromagnetic cores and possibility of their utilization. I. Criteria of physical similarity", Defektoskopiya No. 9, 52, (1983c).

PONOMAREV, Y.F., "Regularities of the harmonic components of magnetization of cyclically remagnetized ferromagnetic cores and the possibilities of their use. II. Review of the fundamental analytical calculations", Defektoskopiya No. 12, 34, (1983d).

POYNTON, W.A., SHANNON, R.W.E., and FEARNEHOUGH, G.D., "The Design and Application of Shear Fracture Propagation Studies", Trans. ASME, J. Eng. Mat. & Tech. October 1974.

REDFIELD, A.G., and MOLESKI, C., "Vibrating sample magnetometer for protein research", Rev. Sci. Instrum. 43, 760 (1972).

RODGERSON, P., and JONES, C.L., "Strength and toughness in line pipe steels", British Gas Internal report ERS C. 146 (1980).

ROGACHEVSKII, B.M., and SHTAMBERGER, G.A., "Approximations of the characteristics of nonlinear inductive and capacitive elements of electrical circuits by the arctangent and the piecewise linear approximations", Avtometriya No. 4, 327, (1967).

ROLLASON, F.C., "Metallurgy for Engineers (3rd Edition)", Arnold, London (1964).

RUDER, W.E., "The Influence of Grain-Size on Magnetic Properties", Trans. ASM 22, 1120 (1934).

SAMPLE, H.H., and RUBIN, L.G., "Instrumentation and methods for low temperature measurements in high magnetic fields", Cryogenics, 597, November (1977).

SANDOVSKII, V.A., and SYROCHKIN, V.P., "Investigation of the harmonic composition of the emf of a feedthrough coil with a ferromagnetic plate", Defektoskopiya No. 5, 125, (1971).

SHTURKIN, D.A., and STOINSKAYA, E.E., "Operation of a ferroelement with longitudinal excitation in a broad range of measured field intensities", Defektoskopiya, No. 5, 623, (1969).

SKIER, K., "Beyond games : System Software for Your 6502 Personal Computer", BYTE/McGraw-Hill (Peterborough) (1981).

SLATER, J.C., "The Ferromagnetism of Nickel", Phys. Rev. 49, 537, (1936a).

SLATER, J.C., "The Ferromagnetism of Nickel. II. Temperature Effects", Phys. Rev. 49, 931, (1936b).

SLATER, J.C., "The Theory of Ferromagnetism : Lowest Energy Levels", Phys. Rev. 52, 198, (1937).

SMITH, D.O., "Development of a vibrating coil magnetometer", Rev. Sci. Instrum. 27, 261, (1956).

SOULANT, H.A., and BRISKER, H.C., "Methods for magnetically measuring stress using the linear relationship of the third harmonic to stress", U.S. Patent No. 3,636,437 (1972).

SPRINGFORD, M., STOCKTON, J.R., and WAMPLER, W.R., "A vibrating sample magnetometer for use with a superconducting magnet", J. Phys. E : Sci. Instrum. 4, 1036, (1971).

STARRATT, F.W., "L.D ... in the beginning", J. Metals 12, 528 (1960).

STONER, E.C., "Atomic Moments in Ferromagnetic Metals and Alloys with Non-Ferromagnetic Elements", Phil. Mag. 15, 1018, (1933).

STONER, E.C., "Collective electron ferromagnetism", Proc. Roy. Soc. (London) A-165, 372 (1938a).

STONER, E.C., "Collective Electron Energy and Specific Heat", Phil. Mag. 25, 899, (1938b).

STONER, E.C., "Collective electron ferromagnetism. II. Energy and Specific Heat", Proc. Roy. Soc. (London) A-169, 339, (1939).

STONER, E.C., "The Demagnetizing factors for ellipsoids", Phil. Mag., 36, 803, (1945).

STONER, E.C., "Ferromagnetism", Rep. Prog. Phys. 11, 43, (1947).

STONER, R.E., HERBERT, R.H., and SILL, L.R., "Image effects in Vibrating Sample Magnetometer systems", J. Appl. Phys., 41, 3706, (1970).

SZPUNAR, J.A., "Texture studies using neutron diffraction", J. Mater, Sci. 19, 3467, (1984).

SZPUNAR, J.A., and TANNER, B.K., "Grain shape and distribution of the grain-boundary density in polycrystalline materials", J. Mater. Sci. 19, 3249, (1984).

TANNER, B.K., and CORNER, W.D., "Magnetic Properties of Construction Steels", Final Report of Contract with British Gas, Ref. LLM/DP/Q5/P/10/39 OLI 2104-52531.

TOMILOV, G.S., MIKHEEV, M.N., and POMUKHIN, M.F., "Magnetic properties of steels as a basis of magnetic structure analysis", Fiz. Met. Metalloved. 8, 176, (1959).

TRUTT, F.C., ERDELYI, E.A., and HOPKINS, R.E., "Representation of the Magnetization characteristic of DC Machines for Computer use", IEEE Trans. PAS 87, 665 (1968).

TURNER, P.A., STOCKBRIDGE, C.D., and THEUERER, H.C., "Magnetic domain nucleation and propagation in fine wires", J. Appl. Phys. 40 , 1864, (1969).

VAN OOSTERHOUT, "A rapid method for measuring coercive force and other ferromagnetic properties of very small samples", Appl. Sci. Res. Section B 6, 101, (1956).

WEISS, P., "Hypothesis of the Molecular Field", J. Physique 6, 661 (1907).

WEISS, P., and FORRER, R., "Aimantation et Phenomene Magnetocalorique du Nickel", Annales de Physique (Paris) 5, 153 (1926).

WEST, R., "Programming the PET/CBM", Level Limited (1982).

WIDGER, G.F.T., "Representation of magnetization curve over extensive range by rational fraction approximations", Proc. IEE 116, 156 (1969).

WILKINS, F.J., and DRAKE, A.E., "Measurements and interpretation of power losses in electrical sheet steel", Proc. IEE, 112, 771, (1965).

WILLCOCK, S.N.M., and TANNER, B.K., "Harmonic Analysis of B-H loops, IEEE Trans. Magn. MAG-19, 2265 (1983a).

WILLCOCK, S.N.M., and TANNER, B.K.,"Harmonic Analysis of B-H loops of Constructional Steel", IEEE Trans. Magn. MAG-19, 2145, (1983b).

WILLIAMS, H.J., BOZORTH, R.M., and SHOCKLEY, W., "Magnetic domain patterns on single crystals of Silicon Iron", Phys. Rev. 75, 155-178, (1949).

WOLF, W.P., "Force on an Anisotropic Paramagnetic Crystal in an Inhomogeneous Magnetic Field", J. Appl. Phys. 28, 780, (1957).

WURM, M., "Beitrage zur Theorie und Praxis des Feldstarke-differenzmesses fur magnetische Felder nach Forster", Z. Angew. Phys. 11, 210 (1950).

YENSEN, T.D., and ZIEGLER, N.A., "Magnetic Properties of Iron as affected by Carbon, Oxygen and Grain-size". Trans. ASM 23, 556, (1935).

ZAHREWSKI , H., and PIETRAS, F., "Method of calculating the electro-mag. field and power losses in ferromagnetic materials, taking into account magnetic hysteresis", Proc. IEE, 118, 1679, (1971).

ZENER, C., "Kinetics of the Decomposition of Austenite", Trans. AIMME 167, 550, (1946).

ZIEBA, A., and FONER, S., "Detection coil, sensitivity function and sample geometry effects for vibrating sample magnetometers", Rev. Sci. Instrum. 53, 1344, (1982).

ZIEBA, A., and FONER, S., "Superconducting magnet image effects observed with a VSM", Rev. Sci. Instrum. 54, 137, (1983).

ZIJLSTRA, H., "Experimental Methods in Magnetism, 1. Generation and Computation of Magnetic Fields", (E.P. Wohlforth Ed.), North-Holland, Amsterdam (1967a).

ZIJLSTRA, H., "Experimental Methods in Magnetism, 2. Measurement of Magnetic Quantities", (E.P. Wohlforth Ed.), North-Holland, Amsterdam (1967b).